THÈSE

Pour obtenir le grade de

DOCTEUR DE L'UNIVERSITÉ DE GRENOBLE

Spécialité : **Mathématiques Appliquées**

Arrêté ministérial : 7 août 2006

Présentée par

Beniamin Bogosel

Thèse dirigée par **M. Dorin Bucur**
et codirigée par **M. Édouard Oudet**

préparée au sein de **LAMA, Université Savoie Mont Blanc**
et de **École Doctorale MSTII**

Optimisation de formes et problèmes spectraux

Thèse soutenue publiquement le **8 Décembre 2015**,
devant le jury composé de :

Mme. Maïtine Bergounioux
Professeur, MAPMO, Université d'Orleans, Présidente
Mme. Virginie, Bonnaillie-Noël
Directrice de recherche CNRS, DMA, ENS Paris, Rapporteur
M. Antoine, Henrot
Professeur, IECN, École des Mines de Nancy, Rapporteur
M. Gérard, Besson
Directeur de recherche CNRS, Institut Fourier, Examinateur
M. Marc Dambrine
Professeur, IPRA-LMAP, Université de Pau et des Pays de l'Adour, Examinateur
M. Dorin Bucur
Professeur, LAMA, Université Savoie Mont Blanc, Directeur de thèse
M. Édouard Oudet
Professeur, LJK, Université Joseph Fourier, Directeur de thèse

Contents

3 Multiphase spectral problems   77

4 Boundary eigenvalue problems   115

Introduction

Dans ce projet de thèse, nous étudions du point de vue qualitatif et numérique quelques problèmes d'optimisation de formes associés à des fonctionnelles spectrales et/ou géométriques. De façon générique, un problème de ce type peut être formulé comme

$$\min\{J(\Omega) : \Omega \in \mathcal{U}_{ad}\},$$

où J est une fonctionnelle coût définie sur une classe d'ensembles (ouverts, quasi-ouverts ou mesurables) notée $\mathcal{U}_{ad}$.

Nous avons organisé la présentation de ce mémoire, suivant les problèmes étudiés :

- optimisation de la k-ème valeur propre du Laplacien avec des conditions de Dirichlet au bord, sous contrainte de périmètre (chapitre 1),

- partitions d'un domaine donné en cellules d'aire prescrite minimisant une longueur anisotrope des contours (chapitre 2),

- un problème d'optimisation de formes multiphasique pour des fonctionnelles spectrales (chapitre 3),

- optimisation de fonctionnelles associées au spectre de Steklov et Wentzell (chapitre 4),

- partitions optimales de surfaces dans $\mathbb{R}^3$, pour des fonctionnelles associées au spectre de l'opérateur Laplace-Beltrami avec conditions de Dirichlet, ainsi que pour des fonctionnelles purement géométriques (chapitre 5).

Concernant l'analyse qualitative de ces problèmes, mes contributions portent sur l'étude des conditions d'optimalité dans le cadre des valeurs propres multiples sous contrainte de périmètre, l'analyse de la stabilité du spectre de Steklov pour des perturbations géométriques du domaine, l'analyse des points de jonction des cellules dans une partition optimale, l'estimation de l'erreur dans le calcul du spectre de Steklov par une méthode de type solutions fondamentales.

Dans tout ce travail, un point commun des méthodes numériques mises en œuvre est l'absence de maillage spécifique associé aux domaines variables. En effet, on utilise l'une des deux approches suivantes :

1. Pour des problèmes de partitionnement optimal, il convient d'identifier un ensemble Ω par sa fonction caractéristique et ensuite de l'approcher par une fonction de champ de phase. Ceci nous permet à la fois de travailler sur un maillage et un domaine fixe et de transformer la condition géométrique de partition en une condition algébrique, plus facile à appréhender numériquement.

2. Pour des problèmes d'optimisation de formes associés aux fonctionnelles spectrales, nous utiliserons systématiquement une approche basée sur des solutions fondamentales. Le développement de cette méthode dans le contexte de l'optimisation de formes a été initié par Antunes, Freitas, Osting, qui se sont concentrés sur des conditions au bord de type Dirichlet, Robin ou Neumann. Cette méthode s'avère à la fois très rapide et très précise. Dans ce mémoire, nous l'avons étendue à des problèmes de Steklov et Wentzell, mais aussi pour l'opérateur Laplace-Beltrami associé aux surfaces bi-dimensionnelles de $\mathbb{R}^3$ (voir chapitres 4 et 5)

Le manuscrit est divisé en cinq chapitres qui traitent de problèmes distincts. On peut identifier des connexions entre certains chapitres, mais chaque chapitre peut être lu indépendamment des autres. Les chapitres 1, 3 et 4 font l'objet d'articles soumis pour publication.

Dans la suite de l'introduction, on présente plus en détail les problèmes considérés ainsi que les principaux résultats.

Chapitre 1

Dans ce chapitre on étudie le problème de la minimisation de la k-ème valeur propre du laplacien Dirichlet sous contrainte de périmètre. Ce problème a été étudié pour la première fois par D. Bucur, G. Buttazzo et A. Henrot dans [28] dans le cas particulier $k = 2$ en dimension deux. C'est le premier cas intéressant car pour $k = 1$ la forme optimale est connue : c'est une boule en toute dimension. Les auteurs ont prouvé que la forme optimale (notée dans la suite Ω_2) existe et est de classe C^∞. De plus, $\partial\Omega_2$ ne contient pas de segments ou d'arcs de cercles. G. de Philippis et B. Velichkov ont prouvé dans [44] un résultat général d'existence pour le problème

$$\min_{\mathrm{Per}(\Omega)=c} \lambda_k(\Omega), \Omega \subset \mathbb{R}^n \tag{1}$$

et le fait que les formes optimales sont de classe $C^{1,\alpha}$ en dehors d'un ensemble de mesure $\mathcal{H}^{n-8}$ nulle.

Pour $k \geq 2$ on ne connaît pas avec exactitude les formes optimales solutions de ce problème, ce qui motive une recherche numérique de ces formes. Une première étape a été d'utiliser une méthode développée par B. Osting [78] et P. Antunes, P. Freitas [9], qui consiste à représenter la frontière de la forme Ω par sa fonction radiale. Évidement, cette procédure n'est possible

que si Ω est étoilé, mais dans le cas du problème (1) on peut voir facilement qu'en dimension deux la forme optimale est nécessairement convexe, et est par conséquent étoilée. La fonction radiale est approchée par une série de Fourier tronquée. Ainsi cette discrétisation fournit une approximation de $\lambda_k(\Omega)$ par une fonction qui ne dépend que d'un nombre fini de paramètres. Un algorithme d'optimisation basé sur le gradient nous permet alors de trouver de bonnes approximations numériques des formes optimales.

Il n'est pas difficile de voir que le problème (1) est équivalent, à une homothétie près, à la minimisation de $\lambda_k(\Omega) + \mathrm{Per}(\Omega)$. Récemment, chacune des deux composantes de cette expression a été étudiée numériquement en utilisant une procédure de relaxation. Dans chacune de ces deux procédures, on remplace la forme Ω par une fonction $\varphi : D \to [0,1]$. Ici φ est destinée à représenter une approximation de χ_Ω (la fonction caractéristique de Ω). Le domaine ouvert et borné D est simplement une boîte choisie assez large pour que la forme optimale y soit contenue. Il est important de remarquer que le problème (1) admet une solution sans imposer une contrainte de boîte et que les solutions ont un diamètre borné. Par conséquent, si la boîte D est assez large, les problèmes avec ou sans contrainte de boîte sont équivalents.

La valeur propre $\lambda_k(\Omega)$ a été approchée en utilisant une formulation avec pénalisation du type

$$-\Delta u + C(1 - \varphi)u = \lambda_k u, \ u \in H_0^1(D). \tag{2}$$

Cette formulation a été utilisée dans [18] pour étudier numériquement un problème de partitionnement spectral. La même formulation nous a permis d'étudier un problème d'optimisation multiphase pour des valeurs propres décrites plus loin dans le chapitre 3. Le périmètre admet une relaxation classique par Γ-convergence, en utilisant un théorème dû à Modica et Mortola,

$$c\,\mathrm{Per}(\Omega) \approx \varepsilon \int_D |\nabla\varphi|^2 + \frac{1}{\varepsilon} \int_D \varphi^2(1-\varphi)^2 \tag{3}$$

Cette approximation du périmètre a été utilisée par É. Oudet dans l'étude des partitions en cellules de même aire qui minimisent la somme des périmètres en deux et trois dimensions. La question est à présent de savoir si on peut combiner ces deux approches pour trouver une approximation de la fonctionnelle $\lambda_k(\Omega) + \mathrm{Per}(\Omega)$. La réponse est ici positive, et un résultat d'approximation par Γ-convergence est proposé dans le chapitre 1. Ce résultat de Γ-convergence nous suggère une approche numérique que nous avons mise en œuvre, avec des résultats très satisfaisants en dimension deux et trois.

Les résultats qualitatifs de [28] ne peuvent, *a priori*, pas être généralisés pour k quelconque car on ne sait pas si la valeur propre optimale $\lambda_k(\Omega)$ est simple. En effet, les calculs numériques effectués suggèrent qu'à quelques exceptions près, la valeur propre optimale $\lambda_k(\Omega)$ est multiple. Il est important de noter qu'une valeur propre λ_k est différentiable si et seulement si elle est simple. Comme conséquence, on ne peut utiliser les propriétés de différentiabilité pour trouver une condition d'optimalité dans le cas où λ_k est multiple. Pour pouvoir déduire des propriétés qualitatives que dans le cas général, on aurait besoin d'une condition d'optimalité qui peut être

écrite même dans ce type de situation. Une telle condition a été trouvée en [47] pour le problème avec contrainte de volume. En utilisant des outils similaires, nous avons réussi à montrer que si Ω est un minimiseur local pour le problème (1), de classe C^3, alors il existe une famille de fonctions propres $(u_i)_{i=1}^m$ associées aux λ_k telle que

$$\sum_{i=1}^m (\partial_n u_i)^2 = \mathcal{H},$$

où $\mathcal{H}$ est la courbure moyenne du bord de Ω. Ce résultat nous permet de trouver quelques propriétés qualitatives des minimiseurs :

1. Un minimiseur ne peut pas contenir de parties plates dans sa frontière.

2. En utilisant un processus de bootstrap similaire à celui de [28], on peut déduire que les minimiseurs sont de classe C^∞ s'ils sont de classe C^3. Ainsi pour déduire la régularité des solutions du problème (1), il suffit de prouver qu'un minimiseur de classe $C^{1,\alpha}$ est C^3.

La fin du chapitre présente deux autres études numériques concernant les valeurs propres du Laplacien Dirichlet. La première concerne la minimisation de $\lambda_k(\Omega)$ sous contrainte d'aire en dimension deux. On améliore les résultats de [9] en faisant les calculs pour $k \in [5, 21]$. La deuxième est une étude numérique de la conjecture de Polya. Cette conjecture affirme que la première valeur propre d'un polygone d'aire fixée à nombre de côtés donné est minimisée par le polygone régulier. On vérifie cette conjecture pour les polygones avec au plus 15 côtés. Pour calculer les premières valeurs propres des polygones réguliers on utilise une méthode basée sur des solutions fondamentales de l'équation elliptique associée.

Resumé et originalité : On montre un résultat d'approximation par Γ-convergence de λ_k + Per, qui nous permet de formuler et d'implémenter une méthode nouvelle pour calculer numériquement les optimiseurs de (1). On montre une condition d'optimalité pour (1), qui est valide même dans le cas où la valeur propre optimale est multiple. Cette condition d'optimalité nous permet de trouver quelques propriétés concernant la structure et la régularité des ensembles optimaux et d'évaluer la qualité des résultats numériques.

Chapitre 2

Dans ce chapitre on étudie un problème de partitionnement optimal. Le coût associé à chaque ensemble de la partition est un périmètre anisotrope. On pourra considérer, pour un ensemble assez régulier, la définition suivante du périmètre classique :

$$\text{Per}(\Omega) = \int_{\partial\Omega} d\sigma = \int_{\partial\Omega} \|\vec{n}\| d\sigma.$$

On voit que dans cette formulation on mesure toute partie de $\partial\Omega$ avec le même poids, sans tenir compte de son orientation. Si à la place de la norme euclidienne on considère une autre norme φ qui privilégie certaines directions, on définit alors un périmètre qualifié de anisotrope associé

à φ pour la quantité :

$$\mathrm{Per}_\varphi(\Omega) = \int_{\partial\Omega} \varphi(\vec{n})d\sigma.$$

Ainsi, le problème consiste à trouver la partition d'un domaine D en un nombre fixe de sous parties de même aire telles que la somme des périmètres anisotropes est minimisée.

Pour étudier ce problème, on utilise une relaxation du périmètre anisotrope en utilisant la Γ-convergence: pour $\varepsilon \to 0$ les minimiseurs des fonctionnelles

$$\varepsilon \int_D \varphi(\nabla u)^2 + \frac{1}{\varepsilon}\int_D u^2(1-u)^2 \tag{4}$$

convergent dans la topologie $L^1(D)$ vers un minimiseur de $\frac{1}{3}\mathrm{Per}_\varphi(\cdot)$. L'avantage de cette représentation est qu'en étudiant des problèmes de partitionnement optimal, la condition "(Ω_i) est une partition de D" devient

$$\varphi_1 + \varphi_2 + ... + \varphi_N = 1 \text{ sur } D.$$

Cette dernière condition est plus facile à implémenter numériquement. L'approximation du périmètre total d'une partition est simplement la somme des approximations du périmètre anisotrope de chaque cellule de la partition. La preuve du résultat théorique de Γ-convergence n'est pas immédiate, car si on a deux suites $F_\varepsilon, G_\varepsilon$ qui Γ-convergent vers F et G, respectivement, il n'est pas vrai que $F_\varepsilon + G_\varepsilon \xrightarrow{\Gamma} F + G$. Un algorithme de minimisation et des résultats numériques sont présentés.

Nous terminons ce chapitre en montrant une extension de l'étude présentée dans [80] dans le cas isotrope, en considérant des domaines généraux et une formulation utilisant des éléments finis. Cette nouvelle formulation nous permet d'améliorer certains des résultats de [80]. Par ailleurs, en considérant des aires fixées qui ne sont pas toutes égales, on peut étudier le problème des configurations d'équilibre des bulles de savon.

Resumé et originalité : On prouve un résultat de Γ-convergence qui nous permet d'étudier numériquement les partitions optimales pour certains périmètres anisotropes. On présente une formulation basée sur des éléments finis qui nous permet d'étudier les partitions optimales sur des ensembles 2D généraux.

Chapitre 3

Ce chapitre traite quelques aspects qualitatifs et numériques d'un problème multiphase spectral. Il s'agit de l'étude du problème

$$\min_{(\Omega_i)\in\mathcal{A}} \sum_{i=1}^{h} \left(\lambda_1(\Omega_i) + \alpha|\Omega_i|\right), \tag{5}$$

où $\mathcal{A}$ est l'ensemble des ouverts $(\Omega_i)_{i=1}^{h}$ contenus dans un ouvert borné D. On note que pour $\alpha = 0$ on retrouve le problème de partition spectrale étudié dans [18]. Le cas $\alpha > 0$ a été étudié dans [31], le but ici est d'étudier si on observe numériquement les propriétés qualitatives obtenues dans [31]. Une des propriétés intéressante dans le cas $\alpha > 0$ est le fait que (Ω_i) n'est

plus une partition de D. Par ailleurs, on ne peut pas avoir des points triples $x \in \partial\Omega_i \cap \partial\Omega_j \cap \partial\Omega_k$ (i, j, k distincts). Les tests numériques fournissent des informations complémentaires : les formes optimales ne présentent pas d'angles et on ne peut pas avoir de points triples sur ∂D. En fait l'ensemble de ces observations peut être déduit des résultats prouvés en [31] si ∂D a la propriété du disque extérieur. On établit aussi dans ce chapitre une formule de monotonie pour deux phases qui nous permet de prouver le résultat suivant : si ∂D est Lipschitz, alors on ne peut pas avoir des points triples sur la frontière.

Concernant la partie numérique on utilise l'approche de [18], où on calcule les valeurs propres à l'aide de la formulation pénalisée (2). Le point clé est de pouvoir gérer la condition de non-intersection. Une manière astucieuse de faire ça est de considérer une phase supplémentaire pour modéliser l'espace vide. Ce processus transforme le problème multiphase en un problème de partition optimale, avec une phase dont la fonction coût n'apparaît pas.

On réalise une étude numérique et théorique de l'erreur du calcul des valeurs propres fait en utilisant la formulation (2). On compare les dix premières valeurs propres obtenues avec celles données par MpsPack [14]. En utilisant des résultats de [29], on trouve aussi une borne théorique pour l'erreur relative obtenue en calculant les valeurs propres par (2). On observe qu'il y a une concordance intéressante entre les erreurs observées numériquement et ce résultat théorique. On calcule quelques configurations optimales sur des régions rectangulaires en utilisant des différences finies et on propose un cadre pour étudier des régions plus générales, par éléments finis ou différences finies.

Resumé et originalité : On prouve une estimation quantitative de l'erreur faite en utilisant la formulation (2). On ajoute une phase supplémentaire pour transformer le problème multiphase en un problème de partition. On étudie le problème sur des domaines généraux, et on montre que la méthode peut être étendue aux surfaces tridimensionnelles.

Chapitre 4

Ce chapitre traite de quelques aspects théoriques et numériques concernant des problèmes aux valeurs propres définis sur le bord d'un ensemble régulier. On appelle valeur propre de Wentzell correspondant au $\beta > 0$, une valeur σ pour laquelle l'équation suivante admet une solution non-triviale :

$$\begin{cases} -\Delta u = 0 & \text{dans } \Omega, \\ -\beta\Delta_\tau u + \partial_n u = \sigma u & \text{sur } \partial\Omega, \end{cases} \tag{6}$$

où Δ_τ est le Laplacien Beltrami associé à $\partial\Omega$. Dans le cas $\beta = 0$, on retrouve le problème de Steklov. Les valeurs pour lesquelles le problème (6) admet des solutions non triviales forment une suite croissante divergente

$$0 = \sigma_0 \leq \sigma_1 \leq \sigma_2 \leq \cdots \to \infty.$$

La première partie de ce chapitre étudie le comportement du spectre de l'opérateur de Steklov associé à différents types de convergences d'ensembles. Ce comportement est important quand on regarde des problèmes d'existence d'ensembles optimaux pour des problèmes

d'optimisation de fonctionnelles qui dépendent du spectre de l'opérateur Steklov. À ce jour, seuls des résultats d'existence pour l'optimisation d'une fonctionnelle qui dépend du spectre de Steklov sont connus en identifiant précisément la forme optimale (par exemple le disque). En général, trouver la forme optimale explicitement n'est pas possible, ce qui rend ce type d'approche essentielle. On peut observer ce fait dans la partie numérique de ce chapitre pour le problème $\max_{|\Omega|=1} \sigma_2(\Omega)$. Le résultat de continuité/semicontinuité supérieure prouvé dans cette première partie nous permet de montrer que sous certaines contraintes de régularité sur Ω (convexité ou propriété de ε-cone) on peut déduire des résultats généraux d'existence pour des problèmes d'optimisation associés à des éléments du spectre de Steklov.

Le résultat clé qui nous permet de déduire ces propriétés de continuité/semincontinuité est un résultat de convergence des traces des fonctions Sobolev sur des frontières variables. On observe en plus, qu'une condition suffisante pour que le spectre de Steklov d'une suite (Ω_n) converge vers le spectre de Steklov du domaine Ω est le fait que les périmètres des ensembles (Ω_n) convergent vers le périmètre de Ω.

La deuxième partie de ce chapitre traite de l'étude numérique des problèmes d'optimisation pour les problèmes de Steklov et de Wentzell. Un premier aspect est le calcul des valeurs propres Steklov/Wentzell de manière efficace et précise. Une méthode qui a suscité beaucoup d'intérêt récemment consiste à utiliser des solutions fondamentales. Étant donne que l'on cherche des fonctions qui sont harmoniques à l'intérieur de Ω, on peut travailler directement avec des fonctions harmoniques fondamentales. Si on choisit des points *source* $(y_i)_{i=1}^n$ à l'extérieur de Ω et que l'on considère les fonctions harmoniques $\phi_i = \log|x - y_i|$, alors toute combinaison linéaire,

$$u = \alpha_1 \phi_i + ... + \alpha_n \phi_n$$

est harmonique dans Ω. Pour trouver une solution il reste ainsi à imposer la condition au bord du domaine. On impose cette condition au bord sur un nombre fini de points sur Ω, et on se retrouve avec un problème aux valeurs propres généralisé.

On observe dans des cas particuliers, pour lesquels les valeurs propres sont connues, comme le disque, que la méthode est très précise. Dans le cas général, on fait une comparaison avec des méthodes avec maillage en utilisant FreeFem++. On observe qu'en raffinant le maillage, les valeurs données par FreeFem++ s'approchent des valeurs obtenus avec notre methode utilisant les solutions fondamentales. Il est possible de donner une borne théorique de l'erreur en utilisant une méthode similaire à celle présenté par Moler et Payne en [73]. L'idée est de considérer le problème aux valeurs propres approchées

$$\begin{cases} -\Delta u_\varepsilon = 0 & \text{dans } \Omega \\ -\beta \Delta_\tau u_\varepsilon + \partial_n u_\varepsilon - \sigma_\varepsilon u_\varepsilon = f_\varepsilon & \text{sur } \partial\Omega \end{cases} \tag{7}$$

et de remarquer que si $\|u_\varepsilon\| = 1$ et $\|f_\varepsilon\|_{L^2(\partial\Omega)}(= \delta)$ est petit, alors σ_ε est proche d'une vraie valeur propre de l'opérateur de Steklov/Wentzell, avec une erreur relative d'ordre $O(\delta)$. Grâce

à cette observation, on déduit numériquement que la precision de notre méthode peut atteindre 10^{-6}.

Une fois convaincu que la méthode fournit de bonnes estimations des valeurs propres, nous avons mené à bien des calculs d'optimisation en utilisant les formules de dérivées de forme données de [42]. On travaille, dans un premier temps, dans le cas des formes simplement-connexes étoilées, pour s'appuyer sur une représentation radiale. On retrouve les résultats classiques en faisant des tests concernant la minimisation ou maximisation de certaines quantités dépendant du spectre Steklov/Wentzell. On vérifie plusieurs conjectures proposées par Hersch, Payne et Schiffer [67], et on observe les comportements qualitatifs des optimiseurs.

Pour traiter les ensembles simplement connexes en général, et ne pas restreindre l'étude aux formes étoilées, on propose une méthode légèrement différente, qui consiste à paramétrer la courbe en coordonnées cartésiennes $t \in [0, 2\pi], t \mapsto (x(t), y(t))$ et de représenter x, y par des séries de Fourier.

Resumé et originalité : On présente un résultat théorique de (semi-)continuité du spectre de l'opérateur de Steklov, qui permet d'établir l'existence de formes optimales. On propose une méthode numérique pour calculer de manière rapide et efficace les premières valeurs propres de Steklov/Wentzell, et on mène à bien plusieurs expériences d'optimisation qui nous permettent de tester et de proposer un certain nombre de conjectures. On propose une approche nouvelle en optimisation numérique, qui consiste à paramétrer séparément les deux coordonnées du bord du domaine. Cette méthode permet de traiter des problèmes généraux dans le cas de formes simplement connexes.

Chapitre 5

Ce chapitre traite du problème des partitions optimales sur des surfaces tridimensionnelles. On utilise la méthode générale présentée aux chapitres 2 et 3 : on représente chaque cellule de la partition par une fonction à valeurs dans $[0, 1]$. Ainsi, la condition de partition est simplement le fait que la somme des fonctions représentatives est égale à 1.

Dans la première partie du chapitre on étudie les partitions en cellules de même aire qui minimisent la somme des périmètres géodésiques. Le cas bidimensionnel a été étudié par Cox et Flikkema [39] en utilisant le logiciel Evolver [21] et par Oudet [80] en utilisant une relaxation par Γ-convergence. L'avantage d'une méthode de relaxation est le fait qu'on ne doit pas prescrire la topologie de la configuration optimale. Les points triples/multiples sont gérés de manière naturelle sans poser de problèmes d'implémentation. Pour étudier le cas des surfaces, on propose dans un premier temps un résultat de relaxation pour le périmètre géodésique en généralisant le résultat de Modica et Mortola [72]. Ensuite on décrit un algorithme qui nous permet de raffiner l'optimisation en faisant des calculs exacts pour l'aire et le périmètre dans le cas particulier de la sphère. Ces calculs nous permettent de voir que nos résultats sont comparables a ceux connus dans la littérature.

Le deuxième problème étudié dans ce chapitre traite des partitions d'une surface qui minimisent leur somme des premières valeurs propres de l'opérateur de Laplace-Beltrami. Ce problème a été étudié récemment par Elliott et Ranner [48] avec une méthode de pénalisation

développée dans [33]. Le premier obstacle à franchir concerne le calcul du spectre de Laplace-Beltrami pour un ensemble contenu dans une surface. Une méthode directe consisterait à mailler la surface et à utiliser des espaces d'éléments finis. Une autre méthode, plus précise et plus rapide dans certains cas, est donnée en utilisant des solutions fondamentales. Au lieu de considérer des fonctions qui sont définies seulement sur la surface, on peut considérer leur extension harmonique en dimension trois. On analyse la précision de cette méthode en étudiant quelques sous domaines de la sphère unité pour lesquels les valeurs propres ont une expression analytique.

Afin d'étudier les partitions optimales, on utilise une formulation pénalisée similaire à (2). Après avoir trouvé les fonctions densités qui sont proches de la partition optimale, on regarde l'interface entre deux phases et on observe que les frontières sont proches d'arcs géodésiques. Dans le cas de la sphère on extrait la structure topologique, et on fait une optimisation raffinée en supposant que les ensembles sont des polygones géodésiques. Pour calculer la valeur propre de chaque polygone, on considère le maillage de chaque polygone et on utilise successivement la méthode des solutions fondamentales et la méthode des éléments finis.

Resumé et originalité : On justifie et on propose une méthode pour trouver les partitions minimales pour le périmètre et pour des fonctionnelles spectrales sur des surfaces. On propose une méthode basée sur les solutions fondamentales pour calculer le spectre de Laplace-Beltrami d'un sous ensemble d'une variété.

Optimization of the Dirichlet Laplacian eigenvalues - perimeter constraint

Résumé

Dans ce chapitre on étudie le problème de minimisation de la première valeur propre du Laplacien Dirichlet sous contrainte de périmètre: $\min\limits_{\mathrm{Per}(\Omega)=1} \lambda_k(\Omega)$. Le problème d'optimisation sous contrainte de volume: $\min\limits_{|\Omega|=1} \lambda_k(\Omega)$ a été très largement étudié, et malgré les travaux intensifs qui ont été faits, on sait très peu des choses concernant les minimiseurs de cet problème pour $k \geq 3$. Le problème sous contrainte de périmètre a été étudié que très récemment. Le cas $k = 2$ en dimension deux a été étudié par D. Bucur, G. Buttazzo and A. Henrot [28]. Les auteurs ont prouvé que la forme optimale existe et qu'elle est de classe C^∞. En plus, un résultat qualitatif a été donné: la forme optimale ne contient ni segments ni arcs des cercles sur son bord. Le cas général a été étudié par G. Philippis et B. Velichkov en [44]. Ils ont prouvé que la solution existe pour tout k et toute dimension. De plus, la solution est bornée, connexe et son bord est de classe $C^{1,\alpha}$ en dehors d'un ensemble de mesure $d - 8$. Le contenu de ce chapitre est un article écrit en collaboration avec Édouard Oudet, soumis pour publication dans SIAM Journal on Control and Optimization.

Les résultats qualitatifs prouvés pour $k = 2, d = 2$ montrent que les minimiseurs n'ont pas une structure simple et les trouver analytiquement n'est pas envisageable. Il y a ainsi un réel intérêt de trouver numériquement les ensembles optimaux. Des études similaires ont été faites pour l'optimisation sous contrainte de volume par É. Oudet [79] et P. Antunes, P. Freitas [9].

La première contribution originale de ce chapitre est un résultat théorique de Γ-convergence pour approximer la fonctionnelle $\lambda_k(\Omega) + \mathrm{Per}(\Omega)$. La recherche de ce résultat de Γ-convergence a été motivée par quelques calculs numériques.

- É. Oudet a étudié dans [80] les partitions optimales en cellules de même aire qui minimisent la somme des périmètres en utilisant l'approximation par Γ-convergence du périmètre

(le théorème de Modica et Mortola)

- B. Bourdin, D. Bucur et É. Oudet ont étudié le problème de partitionnement spectral en dimension deux, en utilisant une relaxation pour calculer les valeurs propres.

L'idée principale est de connecter ces deux résultats pour retrouver l'approximation désirée. On souligne le fait que notre résultat de Γ-convergence n'est pas trivial, car la Γ-convergence n'est pas stable pour la somme.

La deuxième contribution originale est la construction d'une méthode numérique à partir de ce résultat de Γ-convergence. On utilise cette méthode pour étudier les minimiseurs pour $k \leq 20$ en dimension deux et $k \leq 10$ en dimension trois. Pour vérifier les résultats on utilise une méthode de paramétrisation radiale et le logiciel MpsPack [14] pour trouver une approximation assez précise des ensembles optimaux. On extrait ensuite les ensembles de niveaux égal à 0.5 des densités optimales obtenues grace à la la méthode basée sur la Γ-convergence. En comparant les résultats obtenus par ces deux méthodes on voit que la méthode basée sur la Γ-convergence est très précise. On mentionne le fait que la méthode basée sur MpsPack permet de faire des calculs d'optimisation pour $k \in [1, 50]$ (et peut être plus). Les résultats obtenus ont été comparés avec ceux obtenus par P. Antunes et P. Freitas récemment en [10]. En dimension deux on trouve quelques formes optimales qui ont une valeur optimale plus basse que celles d'Antunes et Freitas. En dimension trois la situation est inversée. Antunes et Freitas ont étudié les formes optimales pour $k \in [1, 20]$ et nos formes optimales sont proches pour $k \in [1, 6]$. Pour $k \geq 7$ leurs résultats sont meilleurs. Cet effet est dû au manque de précision en dimension trois de la méthode basée sur la Γ-convergence.

La troisième contribution originale consiste à trouver une condition d'optimalité générale, qui peut être écrite même quand les valeurs propres optimales sont multiples. Un résultat classique nous dit qu'une valeur propre d'un ensemble Ω est différentiable par rapport à une perturbation régulière si et seulement si elle est simple. Les résultats numériques obtenus nous montrent que c'est n'est pourtant pas toujours le cas. On utilise des méthodes similaires à celles utilisées par El-Soufi et Ilias [47] pour déduire que si Ω est un minimiseur local du λ_k sous contrainte de périmètre et si Ω est de classe C^3, alors il existe une famille de fonctions propres $(u_i)_{i=1}^m$ telle que

$$(\partial_n u_1)^2 + ... + (\partial_n u_m)^2 = \mathcal{H},$$

où $\mathcal{H}$ est la courbure moyenne du bord de Ω. Cette condition d'optimalité nous permet de prouver les résultats qualitatifs suivants :

- La frontière d'un ensemble optimal ne contient pas des parties plates ;

- Cette condition d'optimalité permet d'utiliser un processus de bootstrap similaire à celui qui a été utilisé dans [28] pour conclure que Ω est de classe C^∞.

Pour conclure la question de régularité pour le problème sous contrainte de périmètre, il est suffisant de pouvoir passer de $C^{1,\alpha}$ à C^3. Afin de vérifier les résultats numériques, on cherche nu-

mériquement les fonctions propres qui donnent l'erreur minimale dans la condition d'optimalité. Pour $k \leq 15$ on trouve des erreurs d'ordre inférieur à 10^{-4}, ce qui signifie qu'il est très probable que les solutions numériques sont des minimas locaux.

En fin de ce chapitre on utilise quelques outils développés au cours de l'étude précédente pour étudier deux problèmes spectraux.

1. On continue l'étude du problème sous contrainte d'aire en dimension deux pour $k \in [5, 21]$. L'étude de Freitas et Antunes [9] s'arrêtant à $k = 15$.

2. On vérifie numériquement la conjecture de Polya pour des polygones ayant n arêtes avec $n \in [5, 15]$. Les résultats numériques confirment le fait que les polygones réguliers minimisent la première valeur propre sous contrainte d'aire. Ces tests numériques sont faits a l'aide de deux ingrédients:

   - en utilisant la méthode des solutions fondamentales on construit un algorithme inspiré de [4] pour calculer les valeurs propres d'un polygone.

   - on déduit l'expression de la dérivée de la première valeur propre par rapport aux coordonnées des sommets du polygone.

1.1 Introduction and previous results

Given a measurable set $\Omega \subset \mathbb{R}^d$ such that the injection $H_0^1(\Omega) \hookrightarrow L^2(\Omega)$ is compact, it is possible to define the eigenvalues of the Dirichlet Laplace operator associated to Ω. These eigenvalues satisfy

$$\begin{cases} -\Delta u = \lambda u & \text{in } \Omega \\ u \in H_0^1(\Omega). \end{cases}$$

It is possible to write a variational characterization using the Rayleigh quotients in the following way:

$$\lambda_k(\Omega) = \min_{S_k \subset H_0^1(\Omega)} \max_{u \in S_k} \frac{\int_\Omega |\nabla u|^2}{\int_\Omega u^2},$$

where the minimum is taken over all k-dimensional subspaces $S_k \subset H_0^1(\Omega)$. This variational characterization allows an immediate proof of the following two important properties of λ_k:

(i) If $\Omega_1 \subset \Omega_2$ then $\lambda_k(\Omega_1) \geq \lambda_k(\Omega_2)$.

(ii) If $t > 0$ then $\lambda_k(t\Omega) = \dfrac{1}{t^2}\lambda_k(\Omega)$.

It is a natural shape optimization problem to consider the minimization of $\lambda_k(\Omega)$ under certain constraints. The first reference to such a problem can be found in the book *The Theory of Sound* authored by lord Rayleigh [82]. The optimization problem

$$\min_{|\Omega|=c} \lambda_k(\Omega) \tag{1.1.1}$$

has been extensively studied in the past decades. Despite the large amount of progress made in this field of study there are still many open questions concerning the optimization of the low eigenvalues of the Dirichlet Laplacian.

The first notable result is due to Faber and Krahn. They proved that $\lambda_1(\Omega)$ is minimized by a ball under volume constraint. Polya and Szego proved that $\lambda_2(\Omega)$ is minimised by two balls under volume constraint. For the case $k \geq 3$ the shapes of the minimizers are unknown. Numerical studies of the optimal shapes were performed, initially by É. Oudet in [79] for $k = 3, ..., 10$, and more recently by P. Antunes, P. Freitas [9] for $k \leq 15$. An extension of these computations up to $k = 21$ can be found in Section 1.8.1.

In recent articles [28],[44] authors considered a different problem, where the measure constraint was replaced by a perimeter constraint:

$$\min\{\lambda_k(\Omega) : \Omega \subset \mathbb{R}^d, \Omega \text{ open}, \operatorname{Per}(\Omega) = c\}. \tag{1.1.2}$$

It is not difficult to see that problem (1.1.2) is equivalent to

$$\min\{\lambda_k(\Omega) + \operatorname{Per}(\Omega) : \Omega \subset \mathbb{R}^d, \Omega \text{ open}\} \tag{1.1.3}$$

in the sense that any solution of (1.1.2) is homothetic to a solution of (1.1.3) and conversely. We give a proof in the following proposition.

Proposition 1.1.1. *The problems* (1.1.2) *and* (1.1.3) *have homothetic solutions.*

Proof: We know that the above problems have solutions in $\mathbb{R}^d$ and moreover, for (1.1.2) if we change the value of the parameter c the optimal forms change only homothetically.

Consider Ω_c^* a solution for (1.1.2). Then we can find t_0 for which

$$f(t) = \lambda_k(t\Omega_c^*) + \operatorname{Per}(t\Omega_c^*) = \frac{\lambda_k(\Omega_c^*)}{t^2} + t^{d-1}\operatorname{Per}(\Omega_c^*)$$

is minimal. Denote $\Omega_0 = t_0\Omega_c^*$. We claim that Ω_0 does not depend on c. Indeed, if $f'(t) = 0$ then we have

$$-\frac{2}{t^3}\lambda_k(\Omega_c^*) + (d-1)t^{d-2}\operatorname{Per}(\Omega_c^*) = 0$$

so $t_0 = {}^{d+1}\!\sqrt{\dfrac{2\lambda_k(\Omega_c^*)}{(d-1)\operatorname{Per}(\Omega_c^*)}}$. This means that

$$\operatorname{Per}(\Omega_0) = t_0^{d-1}\operatorname{Per}(\Omega_c^*) = {}^{d+1}\!\sqrt{2\lambda_k(\Omega_c^*)\operatorname{Per}(\Omega_c^*)^2}$$

and we note that the last term is scale invariant. Therefore Ω_0 is the same no matter what c we choose.

Pick now $\Omega \in \mathbb{R}^d$ arbitrary and consider $\Omega_1 = \alpha\Omega_0$ a solution of

$$\min_{\operatorname{Per}(S)=\operatorname{Per}(\Omega)} \lambda_k(S).$$

Then we have

$$\lambda_k(\Omega) + \mathrm{Per}(\Omega) \geq \lambda_k(\Omega_1) + \mathrm{Per}(\Omega_1) \geq \lambda_k(\Omega_0) + \mathrm{Per}(\Omega_0)$$

where in the last inequality we have used the fact that Ω_0 is optimal for $\lambda_k() + \mathrm{Per}()$ among all its homothetic transforms. Thus we have proved that a solution of (1.1.2) produces a homothetic solution of (1.1.3).

Conversely, if we have a solution Ω_0 of (2) then it is obvious that Ω_0 is a solution for

$$\min_{\mathrm{Per}(\Omega) = \mathrm{Per}(\Omega_0)} \lambda_k(\Omega).$$

$\square$

In the case $k = 1$, the solution to problem (1.1.2) is obviously a ball as a consequence of the isoperimetric inequality and the Faber-Krahn inequality (using the formulation (1.1.3)). The case $k = 2, d = 2$ was considered by D. Bucur, G. Buttazzo and A. Henrot in [28]. The authors provided that the optimal shape exists and it has C^∞ regularity. Further qualitative results are given:

- The optimal shape does not contain segments or arcs of circles in its boundary.

- There are exactly two points on the boundary of the optimal shape where the curvature vanishes.

A numerical computation of the optimizer, provided by É. Oudet, is also presented. Recently G. De Philippis and B. Velichkov [44] proved that the shape optimization problem (1.1.2) has a solution for any $k \in \mathbb{N}$ and for any dimension d. They also proved that the solution is bounded, connected, open with boundary which is $C^{1,\alpha}$ outside a closed set of Hausdorff dimension $d-8$.

The numerical studies performed by É. Oudet [79] and P. Antunes, P. Freitas [9] for problem (1.1.1) show that the expected minimizers do not have an obvious geometric structure for $k \geq 5$. In [28] it is proved that the optimal shape Ω^* for $k = 2, d = 2$ does not contain any segment or any arc of circle in its boundary. This suggests that we cannot hope to find a simple geometric description of the solution of (1.1.2) even in the case of $k = 2$.

In this context it is relevant to introduce new numerical approaches which provide a precise description of optimal candidates in two and three dimensions.

One numerical approach which has been successfully used in the last few years is the following Fourier parametric method. Considering the formulation (1.1.3) we note that the monotonicity of λ_k and the fact that in $\mathbb{R}^2$ convexification decreases perimeter imply that every solution of the problem (1.1.2) in the plane is convex. Thus we can represent any optimal candidate in the plane using its radial function $r(\theta)$. Furthermore, we can approximate the radial function r by its truncated Fourier series r_n (n sine and cosine coefficients). Doing this truncation, we don't perturb the eigenvalues too much. B. Osting gives an estimate of this error in [78]. In this way we can represent a good approximation of the boundary of a star convex shape by a finite

number of parameters. It is possible to find the partial derivatives of $\lambda_k(\Omega_{r_n})$ with respect to the Fourier coefficients. Then a gradient descent algorithm can be used in order to find the optimal shape candidate in terms of first $2n + 1$ Fourier coefficients. This method is very precise and gives reliable estimates of computed eigenvalues. The same method is used in [9]. The method also works in three dimensions and P. Antunes and P. Freitas announced a result in this direction [10]. A possible drawback of using this method in three or more dimensions is the fact that we do not know *a priori* that the solutions of (1.1.2) are star-convex in dimension greater than two. Moreover, the implementation of this method in dimensions $d \geq 3$ is not straightforward.

A different approach consists of representing the shape Ω as a density function $\varphi : D \rightarrow [0, 1]$ (where D is a bounded, open set of $\mathbb{R}^2$). In recent works of É. Oudet [80] and B. Bourdin, D. Bucur, É. Oudet [18], some Γ-convergence results are used in order to approximate the perimeter of Ω and the eigenvalue $\lambda_k(\Omega)$ by relaxed functionals calculated on a density approximation of Ω. As stated above, choosing a large enough bounding box D, does not modify the optimizer. In the case of the Γ-convergence approximation presented in Section 1.3, considering a bounding box D simplifies the proofs.

The first main contribution of this chapter is to prove that we can combine the two results above in order to produce a relaxation by Γ-convergence of $\lambda_k(\Omega) + \text{Per}(\Omega)$. We implement this method for $d = 2$ and $d = 3$ and we obtain comparable results with the Fourier parametrization approach, in the two dimensional case. The advantage of our method is the fact that we do not make any topological assumptions on the optimal shape. Moreover, the numerical implementation in dimension three or greater is very similar to the one in dimension two.

The second contribution is to provide new optimality conditions (Corollary 1.5.4) for this spectral shape optimization problem which are also relevant in a non differentiable context. As a matter of fact, the difficulty that arises very often in problem (1.1.2) is the fact that the cost function is not differentiable anymore when the optimizer does not have a simple k^{th} eigenvalue. This fact was observed in our computations presented in Section 1.4. Notice that the question of finding the multiplicity at the optimum is still open even for problem (1.1.1). Thanks to these new optimality conditions, we are able to generalize the qualitative results obtained in [28] in our general setting: for every k and any d, the optimal shape does not contain flat parts in its boundary. The optimality condition is obtained under the hypothesis that Ω is of class C^3, which is stronger than the result proved in [44]. The optimality relation allows us to use a bootstrap argument, similar to the one used in [28], in order to prove that if Ω is of class C^3, then Ω is of class C^∞. Thus, in order to completely solve the regularity issue for problem 1.1.2, it only remains to fill the gap between $C^{1,\alpha}$ and C^3.

1.2 Preliminaries

In the proof of our results we will need different theoretical tools, which are recalled below.

1.2.1 Spectrum of a measurable set

For well posedness reasons, it is convenient to extend the notion of Sobolev space to any measurable set $\Omega \subset \mathbb{R}^d$ by defining

$$\widetilde{H}_0^1(\Omega) = \{u \in H^1(\mathbb{R}^d) : u = 0 \text{ a.e. on } \Omega^c\}.$$

In general we have $H_0^1(\Omega) \subset \widetilde{H}_0^1(\Omega)$ and we have equality if, for instance, Ω has Lipschitz boundary. Furthermore, it is proved in [66, Chapter 4] that there exists a quasi-open set $\omega \subset \Omega$ such that $\widetilde{H}_0^1(\Omega) = H_0^1(\omega)$. More technical details about the choice of this space, and why is it suitable in the study of problem (1.1.2), can be found in [28] and [44].

For any $\Omega \subset \mathbb{R}^d$ of finite measure and any $f \in L^2(\mathbb{R}^d)$ we define $R_\Omega(f) \in \widetilde{H}_0^1(\Omega)$ as the weak solution in $\widetilde{H}_0^1(\Omega)$ of the equation

$$-\Delta u = f, \ u \in \widetilde{H}_0^1(\Omega)$$

or equivalently as the unique minimizer in $\widetilde{H}_0^1(\Omega)$ of

$$u \mapsto \frac{1}{2} \int_\Omega |\nabla u|^2 - \int_\Omega fu.$$

Then $R_\Omega : L^2(\Omega) \to \tilde{H}_0^1(\Omega)$ is a positive, self-adjoint and compact operator. As a consequence, its spectrum is discrete and its eigenvalues form a sequence converging to zero. Thus we can set

$$\lambda_k(\Omega) = \frac{1}{\Lambda_k(R_\Omega)}$$

where $0 < ... \leq \Lambda_k(R_\Omega) \leq ... \leq \Lambda_1(R_\Omega)$ are the eigenvalues of R_Ω.

If μ is a capacitary measure (i.e. $\mu(A) = 0$ if $\mathrm{cap}(A) = 0$) then $\lambda_k(\mu)$ is defined as the kth eigenvalue of the operator $-\Delta + \mu I$. The corresponding Rayleigh formulas are

$$\lambda_k(\mu) = \min_{E \in S_k} \max_{u \in E \setminus \{0\}} \frac{\int_D |\nabla u|^2 dx + \int_D u^2 d\mu}{\int_D u^2 dx},$$

where the minimum is taken over n dimensional subspaces of $H_0^1(D) \cap L^2(D; \mu)$. Using this formula we immediately deduce the following monotonicity property: if $\mu \leq \nu$ then $\lambda_k(\mu) \leq \lambda_k(\nu)$. We note that the eigenvalues of a shape Ω correspond to the eigenvalues of the measure $+\infty_{\Omega^c}$.

The notion which is well suited to the study of the convergence of Dirichlet eigenvalues is the γ-convergence. If $(\mu_n), \mu$ are capacitary measures we say that μ_n γ-converges to μ if

$$|\mathcal{R}_{\mu_n} - \mathcal{R}_\mu|_{\mathcal{L}(L^2(D))} \to 0.$$

We have denoted $\mathcal{R}_\mu$ the resolvent of the operator $-\Delta + \mu I$. In particular, if μ_n γ-converges to μ, then

$$\lambda_k(\mu_n) \to \lambda_k(\mu).$$

A useful characterization of the γ-convergence of a sequence of sets (Ω_n) to another set Ω is the Mosco convergence of the spaces $H_0^1(\Omega_n)$ to $H_0^1(\Omega)$. We suppose that Ω_n, Ω are contained in a bounded open set D. We say that $H_0^1(\Omega_n)$ converges to $H_0^1(\Omega)$ in the sense of Mosco if the two following conditions are satisfied:

(M1) For all $u \in H_0^1(\Omega)$ there exists a sequence $u_n \in H_0^1(\Omega_n)$ such that u_n converges strongly in $H_0^1(D)$ to u.

(M2) For every sequence $u_{n_k} \in H_0^1(\Omega_{n_k})$ weakly convergent in $H_0^1(D)$ to a function u we have $u \in H_0^1(\Omega)$.

For more details we refer to [27, Chapter 6] and [66].

For every measurable set Ω of finite measure we denote w_Ω the weak solution of the equation

$$-\Delta w_\Omega = 1, \ w_\Omega \in \widetilde{H}_0^1(\Omega).$$

We have $w_U \leq w_\Omega$ whenever $U \subset \Omega$ and

$$H_0^1(\{w_\Omega > 0\}) = \widetilde{H}_0^1(\{w_\Omega > 0\}) = \widetilde{H}_0^1(\Omega).$$

We refer to [28], [44] for further details.

1.2.2 Γ-convergence and Modica Mortola Theorem

In shape optimization, many numerical methods replace the shape variable by some unknown function. One main difficulty in our context is to associate to this kind of functional framework a way to compute the perimeter of the set. To achieve this goal, the characteristic function χ_Ω will be approximated by a regular function $u \in H^1(\Omega)$ and the perimeter of Ω will be replaced by some smooth functional. This smooth functional is chosen from a sequence of functionals which Γ-converges to the perimeter.

The notion of Γ-convergence, introduced by de Giorgi, is a suitable tool for the study of the convergence of variational problems. For the sake of completeness, we present its definition and some of its main properties.

Definition 1.2.1. *Let X be a metric space and $F_\varepsilon, F : X \rightarrow [0, +\infty]$ a sequence of functionals on X (defined for $\varepsilon > 0$). We say that F_ε Γ-converges to F and we denote $F_\varepsilon \xrightarrow{\Gamma} F$ if the following two properties hold:*

(LI) For every $x \in X$ and every $(x_\varepsilon) \subset X$ with $x_\varepsilon \rightarrow x$ we have

$$F(x) \leq \liminf_{\varepsilon \to 0} F_\varepsilon(x_\varepsilon) \tag{1.2.1}$$

(LS) For every $x \in X$ there exists $(x_\varepsilon) \subset X$ such that $(x_\varepsilon) \rightarrow x$ and

$$F(x) \geq \limsup_{\varepsilon \to 0} F_\varepsilon(x_\varepsilon). \tag{1.2.2}$$

Given $x_0 \in X$ we will call *recovery sequence* a sequence (x_ε), which satisfies property (1.2.2). This sequence satisfies, in particular, the relation

$$\lim_{\varepsilon \to 0} F_\varepsilon(x_\varepsilon) = F(x).$$

Here are three main properties of the Γ-convergence.

Proposition 1.2.2. *If $F_\varepsilon \xrightarrow{\Gamma} F$ in X then the following properties hold:*

  (i) F is lower semicontinuous;

  (ii) If $G : X \to [0, \infty)$ is a continuous functional then

$$F_\varepsilon + G \xrightarrow{\Gamma} F + G.$$

  (iii) Suppose x_ε minimizes F_ε over X. Then every limit point of (x_ε) is a minimizer for F.

The last property suggests that we could approximate a minimizer of F by a minimizer of F_ε for ε small enough. This method was successfully used in [18, 80].

Sometimes it is difficult to prove the (LS) property (1.2.2) for every $x \in X$. Having an element x with some good regularity properties may aid in constructing the recovery sequence. The following procedure, of reducing the class of elements x for which we prove (1.2.2) to a dense subset of $\{F < +\infty\}$, is classical (see for example [19],[20]).

Proposition 1.2.3. *Let $\mathcal{D} \subset \{F < +\infty\}$ be a dense subset of X, such that for every $x \in \{F < +\infty\}$ and $(u_n) \subset \mathcal{D}$, with $(u_n) \to x$ we have*

$$\limsup_{n \to \infty} F(u_n) \le F(x).$$

Suppose that for every $x \in \mathcal{D}$, the property (1.2.2) is verified. Then (1.2.2) is verified in general.

The result stated below is due to Modica and Mortola [72], and it provides an approximation of the perimeter using Γ-convergence.

Theorem 1.2.4. *Let D be a bounded open set and let $W : \mathbb{R} \to [0, \infty)$ be a continuous function such that $W(z) = 0$ if and only if $z \in \{0, 1\}$. Denote $c = 2 \int_0^1 \sqrt{W(s)} ds$. We define $F_\varepsilon, F : L^1(D) \to [0, +\infty]$ by*

$$F_\varepsilon(u) = \begin{cases} \varepsilon \int_D |\nabla u|^2 + \frac{1}{\varepsilon} \int_D W(u) & u \in H^1(D) \\ +\infty & \text{otherwise} \end{cases}$$

and

$$F(u) = \begin{cases} c \operatorname{Per}(u^{-1}(1)) & u \in BV(D; \{0, 1\}) \\ +\infty & \text{otherwise} \end{cases}$$

then

$$F_\varepsilon \xrightarrow{\ \Gamma\ } F$$

in the $L^1(D)$ topology.

For a proof we refer to [1] or [32]. In the numerical simulations we fix the potential

$$W(s) = s^2(1-s)^2$$

which imposes the corresponding constant $c = 1/3$.

Remark 1.2.5. In general if $F_\varepsilon \xrightarrow{\ \Gamma\ } F$ and $G_\varepsilon \xrightarrow{\ \Gamma\ } G$ we cannot conclude that $F_\varepsilon + G_\varepsilon \xrightarrow{\ \Gamma\ } F + G$. Thus, the result proved in Section 1.3 is not trivial. One sufficient condition for the above implication to hold would be that for each u we could find the same recovery sequence for F and G. For more details and examples see [19].

1.2.3 Perturbation theory for eigenvalues

Let (f_ε) be a family of diffeomorphisms of $\mathbb{R}^d$ which depend analytically of ε, such that f_0 is the identity. Each such family of diffeomorphisms determines a sequence of perturbations $(\Omega_\varepsilon) = (f_\varepsilon(\Omega))$ of Ω. The vector field $V = \frac{d}{d\varepsilon} f_\varepsilon|_{\varepsilon=0}$ is called the direction of the perturbation. One natural question is to see whether the map

$$\varepsilon \mapsto \lambda_k(\Omega_\varepsilon) \tag{1.2.3}$$

is differentiable at $\varepsilon = 0$. It is known that the above map is differentiable if and only if $\lambda_k(\Omega)$ is simple. Nevertheless, it is possible to prove that if $\lambda_k(\Omega)$ has multiplicity $p > 1$ and if we consider an analytic perturbation $\Omega_\varepsilon = f_\varepsilon(\Omega)$, then the p corresponding eigenvalues move on p smooth curves as ε varies. The differentiability is lost because the p eigenvalues change their places on the p smooth curves as ε passes through zero, due to their ordering. We could recover some informations on differentiability if we relabel them. This method has been used in [47]. We present below some of the results needed to derive our optimality conditions.

Consider Ω a bounded, open set of class C^3 in $\mathbb{R}^d$; therefore the mean curvature $\mathcal{H}$ is well defined and continuous. We denote by n the outer normal to Ω. Any perimeter preserving perturbation $\Omega_\varepsilon = f_\varepsilon(\Omega)$ induces a function $v = \langle \frac{d}{d\varepsilon} f_\varepsilon|_{\varepsilon=0}, n \rangle$ on $\partial\Omega$ satisfying $\int_{\partial\Omega} \mathcal{H}\, v\, d\sigma = 0$. We denote by $\mathcal{P}_0(\partial\Omega)$ the set of C^1 functions on $\partial\Omega$ such that $\int_{\partial\Omega} \mathcal{H}\, v\, d\sigma = 0$. We denote by $\operatorname{div}_\Gamma$ the tangential divergence with respect to Γ. We refer to [66, Section 5.4.3], for a precise description of $\operatorname{div}_\Gamma$.

Lemma 1.2.6. *Let $v \in \mathcal{P}_0(\partial\Omega)$. Then there exists an analytic perimeter preserving deformation $\Omega_\varepsilon = f_\varepsilon(\Omega)$ such that $v = \langle \frac{d}{d\varepsilon} f_\varepsilon|_{\varepsilon=0}, n \rangle$.*

Proof: Let U be an open neighborhood of $\overline{\Omega}$ and $\tilde{v}, \tilde{n}$ be C^1 extensions of v, n to U. For ε sufficiently small, the map $\varphi_\varepsilon(x) = x + \varepsilon\tilde{v}(x)\tilde{n}(x)$ is a diffeomorphism from Ω to $\varphi_\varepsilon(\Omega)$

(local inversion theorem). This deformation is analytic in ε, but is not necessarily perimeter-preserving.

Let X be an analytic vector field on U such that $\int_{\partial\Omega} \operatorname{div}_{\partial\Omega} X \neq 0$ and let u_t be the one parameter group of diffeomorphisms associated to X. Define $(t, \varepsilon) \mapsto G(t, \varepsilon) = \operatorname{Per}(u_t \circ \varphi_\varepsilon(\Omega))$. Using the fact that $\frac{du_t}{dt}|_{t=0} = X$ and Proposition 5.4.18 from [66] we obtain

$$\frac{\partial G}{\partial t}(0,0) = \frac{d}{dt}\operatorname{Per}(u_t(\Omega)) = \int_{\partial\Omega} \operatorname{div}_{\partial\Omega} X d\sigma \neq 0.$$

Therefore we can apply the implicit function theorem around $(0, 0)$ to see that there exists an analytic function $\varepsilon \mapsto t(\varepsilon)$ defined on a neighborhood $(-\eta, \eta)$ of 0 such that

$$G(t(\varepsilon), \varepsilon) = G(0, 0) = \operatorname{Per}(\Omega).$$

Thus the deformation $g_\varepsilon = u_{t(\varepsilon)} \circ \varphi_\varepsilon$ is perimeter preserving. Moreover, using Propositions 5.4.9 and 5.4.18 from [66], we have

$$t'(0) = -\frac{\frac{d}{d\varepsilon}\operatorname{Per}(\varphi_\varepsilon(\Omega))|_{\varepsilon=0}}{\frac{d}{dt}\operatorname{Per}(u_t(\Omega))|_{t=0}} = -\frac{\int_{\partial\Omega} \operatorname{div}_{\partial\Omega} \tilde{v}\tilde{n}d\sigma}{\int_{\partial\Omega} \operatorname{div}_{\partial\Omega} Xd\sigma} = -\frac{\int_{\partial\Omega} \mathcal{H} v \, d\sigma}{\int_{\partial\Omega} \operatorname{div}_{\partial\Omega} Xd\sigma} = 0.$$

Therefore, if we set $H(t, \varepsilon) = u_t \circ \varphi_\varepsilon$ then

$$\frac{d}{d\varepsilon}g_\varepsilon(x)|_{\varepsilon=0} = \frac{d}{dt}H(t(0), 0)t'(0) + \frac{d}{d\varepsilon}H(t(0), 0) = \frac{d\varphi_\varepsilon}{d\varepsilon}|_{\varepsilon=0} = \tilde{v}(x)\tilde{n}(x) = v(x)n(x)$$

for $x \in \partial\Omega$. In conclusion, g_ε is the desired perturbation. $\square$

Below we present two results from [47], which will be used freely in the rest of the article. We omit the proofs, as they can be found in the cited article.

Lemma 1.2.7. *Let λ be an eigenvalue of multiplicity p of the Dirichlet Laplacian on Ω. For any analytic deformation Ω_ε of Ω there exist p families of real numbers $(\Lambda_{i,\varepsilon})_{i\leq p}$ and p families of functions $(u_{i,\varepsilon})_{i\leq p} \subset C^\infty(\Omega_\varepsilon)$, depending analytically on ε, satisfying for all $\varepsilon \in (-\varepsilon_0, \varepsilon_0)$ and for all $i \in \{1, ..., p\}$:*

(a) $\Lambda_{i,0} = \lambda$.

(b) The family $\{u_{1,\varepsilon}, ..., u_{p,\varepsilon}\}$ is orthonormal in $L^2(\Omega_\varepsilon)$.

(c) We have $\begin{cases} -\Delta u_{i,\varepsilon} = \Lambda_{i,\varepsilon}u_{i,\varepsilon} \text{ in } \Omega_\varepsilon \\ u_{i,\varepsilon} = 0 \text{ on } \partial\Omega_\varepsilon. \end{cases}$

Lemma 1.2.8. *Let λ be an eigenvalue of multiplicity p of the Dirichlet Laplace operator and denote E_λ the corresponding eigenspace. Let $\Omega_\varepsilon = f_\varepsilon(\Omega)$ be an analytic deformation of Ω. Let $(\Lambda_{i,\varepsilon})_{i\leq p}$ and $(u_{i,\varepsilon})_{i\leq p}$ be like in Lemma 1.2.7. Then $\Lambda'_i = \frac{d}{d\varepsilon}\Lambda_{i,\varepsilon}|_{\varepsilon=0}$ are the eigenvalues of the quadratic form q_v defined on $E_\lambda \subset L^2(\Omega)$ by*

$$q_v(u) = -\int_{\partial\Omega} \left(\frac{\partial u}{\partial n}\right)^2 v \, d\sigma,$$

where $v = \langle\frac{d}{d\varepsilon}f_\varepsilon, n\rangle$. Moreover, the L^2-orthonormal basis $u_{1,0}, ..., u_{p,0}$ diagonalizes q_v on E_λ.

In the rest of the chapter we use $\lambda_{k,\varepsilon}$ to denote $\lambda_k(\Omega_\varepsilon)$. We define the following notion of critical domain for the eigenvalues of the Dirichlet Laplacian, which generalizes the notion of local minimum or local maximum.

Definition 1.2.9. *The domain Ω is said to be* critical *for the kth eigenvalue of the Dirichlet problem if, for any analytic perimeter-preserving deformation Ω_ε of Ω, the right-sided and left-sided derivatives of $\lambda_{k,\varepsilon}$ (see Lemma 1.2.7) at $\varepsilon = 0$ have opposite signs, that is*

$$\frac{d}{d\varepsilon}\lambda_{k,\varepsilon}\Big|_{\varepsilon=0^+} \times \frac{d}{d\varepsilon}\lambda_{k,\varepsilon}\Big|_{\varepsilon=0^-} \le 0.$$

1.3 The Γ-convergence result

In this section we construct a Γ-convergence approximation for $\lambda_k(\Omega) + \mathrm{Per}(\Omega)$. This result allows us to construct a numerical method for the study of problem (1.1.2), which will be presented in the next section. Consider $F : \mathbb{R}^k \to \mathbb{R}_+$ a continuous function which is increasing in each variable. Let $D \subset \mathbb{R}^d$ be a bounded, open set. For every $\varphi : D \to \mathbb{R}_+$, measurable we define $\lambda_k(\varphi) = \lambda_k(\varphi\, dx)$, where $\varphi\, dx$ is seen as a capacitary measure. In the following, q will be a fixed positive real parameter.

Theorem 1.3.1. *Define $J_\varepsilon : L^1(D; [0,1]) \to \mathbb{R}_+ \cup \{+\infty\}$ by*

$$J_\varepsilon(\varphi) = F\left(\lambda_1\left(\frac{1-\varphi}{\varepsilon^q}dx\right), ..., \lambda_k\left(\frac{1-\varphi}{\varepsilon^q}dx\right)\right) + \varepsilon\int_D |\nabla\varphi|^2 + \frac{1}{\varepsilon}\int_D \varphi^2(1-\varphi)^2$$

if $\varphi \in H^1(D)$ and $+\infty$ otherwise. Then $J_\varepsilon \xrightarrow{\Gamma} J$ in the $L^1(D)$ topology, where

$$J(\varphi) = \begin{cases} F(\lambda_1(\Omega), ..., \lambda_k(\Omega)) + \frac{1}{3}\mathrm{Per}(\Omega), & \text{if } \varphi = \chi_\Omega \in BV(D) \\ +\infty & \text{otherwise} \end{cases}$$

Proof: For simplicity, in the rest of the proof we denote the quantity $F(\lambda_1(\Omega), .., \lambda_k(\Omega))$ by $F(\Omega)$. With this notation, F becomes decreasing for the inclusion, as a function of Ω. We make the same convention when instead of Ω we have a measure μ. Let us begin by proving the $\Gamma - \limsup$ part of our result.

1. Reduction to regular domains. This part of the proof is a standard step in the proof of the $\Gamma - \limsup$ property (see Proposition 1.2.3). We refer to [19],[20] for more details and examples. If Ω is regular, the construction of a recovery sequence is straightforward (see Part 2 of the proof). We are left to prove that regular sets are a dense subset $\mathcal{D}$ of $\{F < +\infty\}$ and that they satisfy the following property: for each $\Omega \in \{F < +\infty\}$ we can find $(\Omega_n) \subset \mathcal{D}$ such that $\chi_{\Omega_n} \to \chi_\Omega$ in $L^1(D)$ topology and $\limsup\limits_{n\to\infty} J(\chi_{\Omega_n}) \le J(\chi_\Omega)$.

In [7], Thm 3.4.2 it is proved that the sets with boundary of class C^∞ are dense in the class of finite perimeter sets, when considering the L^1 topology. Thus we can choose our dense set $\mathcal{D}$ to be the family of subsets of D with finite perimeter and smooth boundary. If φ is the characteristic function χ_Ω of Ω and it belongs to $BV(D)$ then Ω is a set of finite perimeter. The theorem we cited above says that each finite perimeter Ω set can be approximated in the $L^1(D)$ topology with a sequence (Ω_n) of finite perimeter sets having smooth boundaries such that $\mathrm{Per}(\Omega_n) \to \mathrm{Per}(\Omega)$. At this point it is not clear if we have $\limsup_{n\to\infty} F(\Omega_n) \leq F(\Omega)$. The objective of the following paragraphs is to construct (Ω_n) in such a way that the previous inequality holds.

If we denote (ρ_k) a sequence of mollifiers, we have

$$\mathrm{Per}(\Omega) = \int_{\mathbb{R}^d} |\mathrm{D}\chi_\Omega| = \lim_{k\to\infty} \int_{\mathbb{R}^d} |\nabla\chi_\Omega * \rho_k| =$$
$$= \lim_{k\to\infty} \int_0^1 \mathrm{Per}(\{\chi_\Omega * \rho_k > t\})dt \geq \int_0^1 \liminf_{k\to\infty} \mathrm{Per}(\{\chi_\Omega * \rho_k > t\})dt \qquad (1.3.1)$$

where we have applied the co-area formula and Fatou's lemma. Here and in the sequel we denote by $\mathrm{D}\chi_\Omega$ the gradient of χ_Ω in the sense of distributions. By applying Chebyshev's inequality we obtain that

$$|\{\chi_\Omega * \rho_k > t\} \setminus \Omega| = |\{\chi_\Omega * \rho_k - \chi_\Omega \geq t\}| \leq \frac{1}{t}\int_{\mathbb{R}^d} |\chi_\Omega * \rho_k - \chi_\Omega|$$

and

$$|\Omega \setminus \{\chi_\Omega * \rho_k > t\}| = |\{\chi_\Omega - \chi_\Omega * \rho_k \geq 1-t\}| \leq \frac{1}{1-t}\int_{\mathbb{R}^d} |\chi_\Omega * \rho_k - \chi_\Omega|.$$

Therefore $\chi_{\{\chi_\Omega * \rho_k > t\}}$ converges to χ_Ω in the $L^1(D)$ topology for almost every $t \in (0,1)$. By the lower semicontinuity of the perimeter we deduce that

$$\liminf_{k\to\infty} \mathrm{Per}(\{\chi_\Omega * \rho_k > t\}) \geq \mathrm{Per}(\Omega),$$

Combining this with (1.3.1) we obtain

$$\liminf_{k\to\infty} \mathrm{Per}(\{\chi_\Omega * \rho_k > t\}) = \mathrm{Per}(\Omega).$$

for almost every $t \in (0,1)$. Sard's theorem tells us that the level sets of $\chi_\Omega * \rho_k$ are smooth for almost every t. Moreover, Lemma 2.95 from [7] tells us that almost all level sets of $\chi_\Omega * \rho_k$ are transversal, i.e. $\mathcal{H}^{n-1}(\partial\{\chi_\Omega * \rho_k\} \cap \partial D) = 0$. In this way, we can choose the smooth, transversal approximating sets at almost every level $t \in (0,1)$.

Denote $w = R_\Omega(1) = R_\omega(1)$ where $\omega \subset \Omega$ is a quasi open set with the property that $H_0^1(\omega) = \widetilde{H}_0^1(\Omega)$. We can assume that $\|w\|_\infty \leq 1$ (or otherwise rescale it) so that we get $w \leq \chi_\Omega$ which implies that $w*\rho_k \leq \chi_\Omega*\rho_k$ and as a consequence $\{w*\rho_k > t\} \subseteq \{\chi_\Omega*\rho_k > t\}$.

We want to prove that $\limsup_{k\to\infty} F(\{w * \rho_k > t\}) \leq F(\{w > t\})$. Denote $A_k = \{w * \rho_k > t\} \cap \{w > t\}$. It is enough to prove that (A_k) γ-converges to $\{w > t\}$. Indeed, if this holds, then

$$\limsup_{k\to\infty} F(\{w * \rho_k > t\}) \leq \lim_{k\to\infty} F(A_k) = F(\{w > t\})$$

To prove this γ-convergence result it suffices to prove the first Mosco condition, since the second one comes from $A_k \subset \{w > t\}$. For more details we refer to [27, Section 4.5]. To prove the first Mosco condition it is enough to prove it on a dense subset of $H_0^1(\{w > t\})$. One such dense subset is given in [41] Prop 5.5 and is $\{C_c^\infty(\mathbb{R}^d) \cdot (w - t)^+\}$. Let $\varphi \in C_c^\infty(\mathbb{R}^d)$. Then if $\varphi_k = \varphi \cdot \min\{(w * \rho_k - t)^+, (w - t)^+\}$ we have $\varphi_k \to \varphi \cdot (w - t)^+$ in $H_0^1(D)$ and $\varphi_k \in H_0^1(A_k)$. This concludes the proof of the fact that A_k γ-converges to $\{w > t\}$.

Therefore we have found a sequence

$$B_k^t = \{w * \rho_k > t\} \subseteq C_k^t = \{\chi_M * \rho_k > t\}$$

with $C_k^t \to \chi_\Omega$ in $L^1(D)$, $\liminf_{k\to\infty} \mathrm{Per}(C_k^t) = \mathrm{Per}(\Omega)$ for almost every t, $F(C_k^t) \leq F(B_k^t)$ and

$$\limsup_{k\to\infty} F(B_k^t) \leq F(\{w > t\}).$$

Thus, we can choose a diagonal sequence $E_k = C_k^{t_k}$ with $t_k \to 0$ such that $\chi_{E_k} \to \chi_\Omega$ in $L^1(D)$, $\mathrm{Per}(E_k) \to \mathrm{Per}(\Omega)$ in order to obtain

$$\limsup_{k\to\infty} F(E_k) \leq F(\{w > 0\}) = F(\omega) = F(\Omega).$$

2. Proof of the $\Gamma - \limsup$ part. Using the previous density result, it suffices to prove the $\Gamma - \limsup$ only for characteristic functions of smooth sets with finite perimeter. Let $\varphi \in L^1(D; [0, 1])$ with $J(\varphi) < +\infty$. Then φ is the characteristic function of a set Ω with finite perimeter. We assume, as mentioned above, that Ω has smooth boundary and that $\mathcal{H}^{n-1}(\partial\Omega \cap \partial D) = 0$.

We take $(\varphi_\varepsilon) \subset H^1(D)$ to be a recovery sequence associated to the Modica-Mortola approximation (see Theorem 1.2.4). We recall that this sequence can be chosen to satisfy $\chi_\Omega(x) = \varphi_\varepsilon(x)$ for $d_\Omega(x) \notin [0, \varepsilon]$ (see [32]; here d_Ω represents the signed distance from a point to $\partial\Omega$). We have $\varphi_\varepsilon \to \varphi$ in $L^1(D)$ and

$$\lim_{\varepsilon \to 0} \left[\varepsilon \int_D |\nabla\varphi_\varepsilon|^2 dx + \frac{1}{\varepsilon} \int_D \varphi_\varepsilon^2(1 - \varphi_\varepsilon^2) dx \right] = \frac{1}{3} \mathrm{Per}(\Omega).$$

Since for every $x \in \Omega$ we have $\varphi_\varepsilon(x) = 1$, we observe that $+\infty_{D\backslash\Omega} \geq \dfrac{1 - \varphi_\varepsilon}{\varepsilon^q}$. By the monotonicity of λ_j we have

$$\lambda_j(\Omega) = \lambda_j(+\infty_{D\backslash\Omega}) \geq \lambda_j\left(\frac{1 - \varphi_\varepsilon}{\varepsilon^q} dx \right).$$

Using the monotonicity of F we obtain

$$\limsup_{\varepsilon \to 0} F\left(\frac{1 - \varphi_\varepsilon}{\varepsilon^q} dx\right) \leq F(\Omega).$$

3. Proof of the $\Gamma - \liminf$ **part.** Let $\varphi \in L^1(D; [0, 1])$ and $(\varphi_\varepsilon) \in L^1(D; [0, 1])$ such that $\varphi_\varepsilon \to \varphi$ in $L^1(D)$. We assume that $\liminf_{\varepsilon \to 0} J_\varepsilon(\varphi_\varepsilon) < +\infty$ since otherwise the result is obvious. The $\Gamma - \liminf$ part of the Modica-Mortola theorem tells us that

$$+\infty > \liminf_{\varepsilon \to 0} \varepsilon \int_D |\nabla \varphi_\varepsilon|^2 + \frac{1}{\varepsilon} \int_D \varphi_\varepsilon^2 (1 - \varphi_\varepsilon)^2 \geq \frac{1}{3} \int_D |D\varphi|.$$

Thus φ has is a characteristic function with bounded variation. This implies that $\Omega = \varphi^{-1}(1)$ is a set of finite perimeter relative to D, and

$$\liminf_{\varepsilon \to 0} \varepsilon \int_D |\nabla \varphi_\varepsilon|^2 + \frac{1}{\varepsilon} \int_D \varphi_\varepsilon^2 (1 - \varphi_\varepsilon)^2 \geq \frac{1}{3} \operatorname{Per}(\Omega).$$

It remains to prove that

$$\liminf_{\varepsilon \to 0} F\left(\frac{1 - \varphi_\varepsilon}{\varepsilon^q} dx\right) \geq F(\Omega).$$

Since F is increasing in each variable, it is enough to prove that

$$\liminf_{\varepsilon \to 0} \lambda_i\left(\frac{1 - \varphi_\varepsilon}{\varepsilon^q} dx\right) \geq \lambda_i(\Omega).$$

Let w_ε be the solution of

$$\begin{cases} -\Delta w_\varepsilon + \frac{1 - \varphi_\varepsilon}{\varepsilon^q} w_\varepsilon = 1 & \text{in } D \\ w_\varepsilon \in H_0^1(D). \end{cases}$$

Without loss of generality we can replace $\liminf$ with $\lim$ by taking a sequence ε_k which realizes the $\liminf$. Denoting $\varphi_k = \varphi_{\varepsilon_k}$, we have to prove that

$$\lim_{n \to \infty} \lambda_i\left(\frac{1 - \varphi_k}{\varepsilon_k^q} dx\right) \geq \lambda_i(\Omega).$$

By compactness there is a subsequence of (w_{n_k}) converging weakly in $H_0^1(D)$ to w. We can choose a subsequence of this sequence which converges almost everywhere to w. For simplicity we relabel this subsequence (w_k). It is enough to prove the inequality for (φ_k) (the corresponding functions for this new sequence (w_k)).

Taking w_k as test functions in the weak form of the partial differential equation we get

$$\int_D \frac{1 - \varphi_k}{\varepsilon_k^q} w_k^2 = \int_D w_k - \int_D |\nabla w_k|^2 \leq \int_D w_k \leq \int_D w_D,$$

where w_D is the solution of

$$\begin{cases} -\Delta w_D = 1 & \text{in } D \\ w_D \in H_0^1(D). \end{cases}$$

We know that

$$\liminf_{k\to\infty} \frac{1 - \varphi_k(x)}{\varepsilon_k^q} = +\infty$$

for $x \in \Omega^c$ since $1 - \varphi_k(x) \to 1$ a.e. on Ω^c and $\varepsilon_k \to 0^+$. Therefore since $w_k \to w$ almost everywhere, if $w(x) > 0$, $x \notin \Omega$ and $w_k(x) \to w(x)$ then

$$\liminf_{k\to\infty} \frac{1 - \varphi_k(x)}{\varepsilon_k^q} w_k^2(x) = +\infty.$$

Fatou's Lemma tells us that

$$+\infty > \liminf_{k\to\infty} \int_D \frac{1 - \varphi_k}{\varepsilon_k^q} w_k^2 \geq \int_D \liminf_{k\to\infty} \frac{1 - \varphi_k}{\varepsilon_k^q} w_k^2 \geq \int_{\Omega^c} \liminf_{k\to\infty} \frac{1 - \varphi_k}{\varepsilon_k^q} w_k^2$$

This inequality and the previous remarks impliy that the set $\Omega^c \cap \{w > 0\}$ is of measure zero, and therefore $w \in \widetilde{H}_0^1(\Omega)$. Since the γ-convergence is compact, up to a subsequence we have

$$\mu_\varepsilon = \frac{1 - \varphi_k}{\varepsilon_k^q} \xrightarrow{\gamma} \mu \geq +\infty_{\Omega^c}.$$

As a consequence, we have

$$\lim_{k\to\infty} \lambda_i \left(\frac{1 - \varphi_k}{\varepsilon_k^q} dx \right) = \lambda_i(\mu) \geq \lambda_i(\Omega),$$

which finishes the proof of the $\Gamma - \liminf$ part. $\qquad\square$

1.4   **Numerical study of problem** (1.1.2)

The method we developed for studying problem (1.1.2) combines the Γ-convergence methods used in approximating the perimeter (used in [80]) and the eigenvalues of the Laplace operator (used in [18]). The combination of the two cited methods is made possible by the Γ-convergence result proved in the previous section. As it has been underlined, our Γ-convergence method is very flexible with respect to both the dimension and the topology of the shapes. In order to evaluate the quality of our solution we recall in subsection 1.4.2 the method used successfully by B. Osting [78] and P. Antunes, P. Freitas [9]. In Table 1.1 we illustrate that both methods give the same results in the easy context of the two dimensional case. Finally, we extend previous results in the three dimensional case, where we notice that some of the optimal shapes found seem to be non-convex. This behaviour has been conjectured in [28].

1.4.1   **Method based on the Γ-convergence result**

We relax our shape optimization problem with respect to Ω by an optimization problem of an unknown function $\varphi : D \to [0, 1]$. In our computations we choose $D = [0, a]^2$ and impose periodic boundary conditions (so that the perimeter of Ω is not influenced by the boundary of D). We consider a $N \times N$ uniform grid and we represent the function φ by its values $(\varphi_{i,j})_{i,j=1}^N$

on this grid. Note that the main Γ-convergence result stated in Theorem 1.3.1 holds for any exponent q positive. In our computations we choose $q = 2$, because we observed a good numerical behaviour with this parameter. This good behavior could be explained by a well balanced effect of the cost values for $q = 2$ in the scale of our discretization.

We approximate

$$\varphi \mapsto \varepsilon \int_D |\nabla \varphi|^2 + \frac{1}{\varepsilon} \int_D \varphi^2 (1 - \varphi)^2$$

by using centred finite differences on the considered grid. This approximation is equivalent to considering a piecewise linear function associated to the grid values.

For the eigenvalue approximation we consider the discrete form of

$$-\Delta u_k + \frac{1 - \varphi}{\varepsilon^2} u_k = \lambda_k u_k.$$

In order to obtain a matrix formulation, we fix an ordering on the $N \times N$ grid. We denote by $\bar{\psi}$ the vector which contains the values on the grid of the function ψ with respect to this fixed ordering. We define A to be the $N^2 \times N^2$ matrix associated to the discrete Laplacian on the considered grid, with respect to the fixed ordering. The discretized eigenvalue problem becomes

$$\left[A + \frac{1 - \bar{\varphi}}{\varepsilon^2} I \right] \bar{u}_k = \lambda_k \bar{u}_k.$$

We used the Matlab solver `eigs` to solve this matrix eigenvalue problem. The expression of the discrete gradient of our functional with respect to each component of $\bar{\varphi}$ is

$$-\frac{1}{\varepsilon^2} \bar{u}_k^2.$$

We refer to [18] for more details.

We can compute the gradient of $\varphi \mapsto \varepsilon \int_D |\nabla \varphi|^2 + \frac{1}{\varepsilon} \int_D \varphi^2 (1 - \varphi)^2$ with respect to a perturbation θ of $\varphi \in H^1(D)$ as follows:

$$\frac{d}{dt} \left[\varepsilon \int_D |\nabla(\varphi + t\theta)|^2 + \frac{1}{\varepsilon} \int_D (\varphi + t\theta)^2 (1 - (\varphi + t\theta))^2 \right]_{t=0} =$$

$$= 2\varepsilon \int_D \langle \nabla\varphi, \nabla\theta \rangle + \frac{1}{\varepsilon} \int_D (2\varphi - 6\varphi^2 + 4\varphi^3)\theta$$

$$= \int_D \left[-2\varepsilon \Delta\varphi + \frac{1}{\varepsilon}(2\varphi - 6\varphi^2 + 4\varphi^3) \right] \theta$$

Thus the discrete gradient of $\varphi \mapsto \varepsilon \int_D |\nabla \varphi|^2 + \frac{1}{\varepsilon} \int_D \varphi^2 (1 - \varphi)^2$ with respect to φ is given by

$$2\varepsilon(4\bar{\varphi}_{i,j} - \bar{\varphi}_{i+i,j} - \bar{\varphi}_{i-1,j} - \bar{\varphi}_{i,j+1} - \bar{\varphi}_{i,j-1}) + \frac{1}{\varepsilon}(2\bar{\varphi}_{i,j} - 6\bar{\varphi}_{i,j}^2 + 4\bar{\varphi}_{i,j}^3). \qquad (1.4.1)$$

To obtain a solution φ_0 of the problem

$$\min \left[\varepsilon_0 \int_D |\nabla \varphi|^2 + \frac{1}{\varepsilon_0} \int_D \varphi^2 (1 - \varphi)^2 + \lambda_k \left(\frac{1 - \varphi}{\varepsilon_0^2} dx \right) \right]$$

we start from a random configuration with a concentration around the center of the grid. Numerical experiments have shown that starting from a totally random configuration tends to lead to a shape consisting of k disks. This configuration is a local minimum, but not the global one, since we know that the optimal shape is connected [44]. We think this behaviour is due to the fact that when we approximate Ω by density functions, the optimization of λ_k tends to separate Ω into nodal domains. Then the perimeter, which is optimized locally, transforms those domains into disks. This observation motivates our previous initialization. For the optimization part, we used the quasi-Newton algorithm LBFGS implemented in [84],[86].

The choice of the initial parameter ε_0 is important for the algorithm to converge. Numerical experiments have shown that $\varepsilon_0 \in [\frac{1}{N}, \frac{4}{N}]$ are suitable for obtaining the expected results. This observation is well known in the phase-field community. The parameter ω was chosen equal to 0.5 which means that after each optimization we divide ε by 2. In the case ε is smaller than the discretization step we refine the grid and interpolate the density functions to this new grid.

Algorithm 1 General form of optimization algorithm for $\min_\varphi J_\varepsilon(\varphi)$

Require: $k \in \mathbb{N}, \varepsilon_0 > 0, p_{max} \in \mathbb{N}, N \in \mathbb{N}, \omega \in (0, 1), \text{tol} \in (0, 1)$
 1: $\varepsilon = \varepsilon_0$;
 2: Choose a random initial shape φ concentrated around the center of D;
 3: **repeat**
 4:     $p = 1$;
 5:     **repeat**
 6:         Compute the eigenpair $(\lambda_k, \overline{u}_k)$ of $A + \frac{1-\bar{\varphi}}{\varepsilon^2}I$ and the gradient $\nabla\lambda_k(\varphi) = -\frac{1}{\varepsilon^2}\bar{u}_k$;
 7:         Compute the gradient of $\varphi \mapsto \varepsilon\int_D |\nabla\varphi|^2 + \frac{1}{\varepsilon}\int_D \varphi^2(1-\varphi)^2$ with respect to the components of $\bar{\varphi}$ on the grid using formula (1.4.1);
 8:         Do a step of the LBFGS algorithm: update descent direction and do a linesearch;
 9:         $\varphi \leftarrow \varphi - d_p$;
10:         $p \leftarrow p + 1$;
11:     **until** $p = p_{max}$ or $|d_p| < \text{tol}$;
12:     $\varepsilon = (1-\omega)\varepsilon$;
13: **until** $\varepsilon < 1/N$.

1.4.2 Parametrization using Fourier coefficients

In order to verify our results, we compare them with the ones obtained using the Fourier boundary parametrization method mentioned in the introduction. This method is well known, and was applied in [9],[78] and [**?**]. We present it below for the sake of completeness.

We know that the solutions to problem (1.1.2) in $\mathbb{R}^2$ are convex shapes, so every such shape is uniquely defined by its radial function $r(\theta)$, $\theta \in [0, 2\pi)$. B. Osting proved in [78, Prop. 3.1] that the error $|\lambda_k(\Omega_r) - \lambda_k(\Omega_{r_n})|$ can be made arbitrarily small if we choose n big enough, where r_n is the truncation of the Fourier series representation of r to $2n + 1$ coefficients:

$$r_n(\theta) = a_0 + \sum_{k=1}^n a_k \cos(k\theta) + \sum_{k=1}^n b_k \sin(k\theta).$$

This allows us to write $\lambda_k(\Omega)$ as a function of $2n + 1$ variables $\lambda_k(a_0, a_1, ..., a_n, b_1, ..., b_n)$. Furthermore, using the fact that the derivative of $\lambda_k(\Omega)$ with respect to a perturbation V of the boundary is

$$\frac{d\lambda_k(\Omega)}{dV} = -\int_{\partial\Omega} \left(\frac{\partial u_k}{\partial n}\right)^2 (V.n)d\sigma$$

(proofs and other references can be found in [65, 66]) we can find that

$$\frac{\partial \lambda_k}{\partial a_k} = -\int_0^{2\pi} r(\theta)\cos(k\theta)\left(\frac{\partial u_k}{\partial n}(r(\theta),\theta)\right)^2 d\theta$$

$$\frac{\partial \lambda_k}{\partial b_k} = -\int_0^{2\pi} r(\theta)\sin(k\theta)\left(\frac{\partial u_k}{\partial n}(r(\theta),\theta)\right)^2 d\theta.$$

We can find similar formulas for the derivatives of the perimeter in terms of Fourier coefficients. For computing the eigenvalues and normal derivatives of the eigenfunctions it is possible to use the publicly available software MpsPack [14].

1.4.3 Our numerical results

In order to solve numerically problem (1.1.2), in its equivalent form (1.1.3), we search the solutions of the relaxed problem

$$\min\left[\varepsilon_0 \int_D |\nabla\varphi|^2 + \frac{1}{\varepsilon_0}\int_D \varphi^2(1-\varphi)^2 + \lambda_k\left(\frac{1-\varphi}{\varepsilon_0^2}dx\right)\right]$$

We use the method presented in subsection 1.4.1 on the square $D = [0, a]^2$ (where a is chosen such that the solution of (1.1.3) fits inside D).

Since the method presented in subsection 1.4.2 was used successfully in the study of the problem (1.1.1), we employ it to find the numerical solutions of (1.1.2). These solutions are a benchmark to which we compare the results we found using our Γ-convergence methods.

The optimal shapes obtained with the Γ-convergence method coincide with the ones found using the Fourier boundary parametrization method. The numerical results can be seen in Figure 1.1. To compare the accuracy of the results, we took the optimal shapes obtained with the Γ-convergence method and we isolated the 0.5 level set. We choose a point in its convex hull, the centroid G of a discretization $\{x_1, ..., x_l\}$ of the boundary, and computed the distances from that point to the contour, denoted by $\{\rho_1, ..., \rho_l\}$ as well as the angles made by Gx_i with the positive x-axis, denoted by $\{\theta_1, ..., \theta_l\}$. This procedure gives us a radial parametrization of our domain. Using a least squares fit

$$\min_{(a_j)_{j=0}^n, (b_j)_{j=0}^n} \sum_{i=1}^l \left(a_0 + \sum_{j=1}^n a_j\cos(j\theta_i) + \sum_{j=1}^n \sin(j\theta_i) - \rho_i\right)^2$$

we are able to find the first $2n + 1$ Fourier coefficients of this radial function. We use these coefficients to construct the radial function of our shape Ω^*. We use MpsPack to compute

$\lambda_k(\Omega^*) + \mathrm{Per}(\Omega^*)$ and we compare the results, which can be seen in Table 1.1. We can see that the results agree, and in general the ones obtained with the Γ-convergence method are a bit weaker, in the sense that the minimal value is higher. Still, the fact that we obtain the same shapes, with small errors, shows that the Γ-convergence method is a suitable tool for the study of problem (1.1.2). Furthermore, it gets close enough to the optimizer without imposing any topological constraints.

One interesting question that has been addressed in several papers ([9],[79]) is the multiplicity of λ_k at the optimum. We noticed in our computations that the optimal shape for (1.1.3) does not always have multiple k^{th} eigenvalue. This was already proved for $k = 2$ in [28] and our computations have shown that for $k = 6, 9, 13, 15$ the optimal eigenvalues should be simple. This behaviour is different from the one observed for problem (1.1.1). It is known that if a local minimizer of problem (1.1.1) would have simple eigenvalue then its eigenfunction would satisfy the overdetermined problem

$$\begin{cases} -\Delta u = \lambda u & \text{in } \Omega \\ \quad u = 0 & \text{on } \partial\Omega \\ \frac{\partial u}{\partial n} = c & \text{on } \partial\Omega, \end{cases} \qquad (1.4.2)$$

where $c > 0$ is a constant. There is a conjecture due to Schiffer concerning the above overdetermined problem. For more details we refer to [15] and [94].

Conjecture 1.4.1. If problem (1.4.2) has a solution, then Ω is a disk.

This is true in the case of λ_1, but the arguments used in the proof rely essentially on the fact that the first eigenfunction can be chosen positive. In the case $k \geq 2$, the eigenfunctions corresponding to λ_k are not positive, so the argument used for $k = 1$ does not work here. Still, to our knowledge, no counter-example of this conjecture is known.

A recent result by A. Berger [16] says that in two dimensions, the only positive integers k for which the ball is a local minimizer for λ_k under volume constraint are $k = 1, 3$. Thus, we have the following interesting fact:

- Suppose that for some $k \notin \{1, 3\}$ the shape for which Ω is solution to (1.1.1) has simple k^{th} eigenvalue. Then the kth corresponding eigenfunction u_k satisfies an overdetermined problem of the type (1.4.2). The result of A. Berger says that Ω cannot be a disk. Thus Conjecture 1.4.1 is contradicted.

Thus, Conjecture 1.4.1 together with the result of [16], imply that in the case of problem (1.1.1), if $k \geq 2$ the multiplicity is greater than one at the optimum.

In the case of the perimeter constraint, the situation is different. We can find shapes Ω, which are not disks, such that the overdetermined problem

$$\begin{cases} -\Delta u = \lambda u & \text{in } \Omega \\ \quad u = 0 & \text{on } \partial\Omega \\ \quad \frac{\partial u}{\partial n} = \mathcal{H} & \text{on } \partial\Omega \end{cases}$$

has a non-trivial solution. Such examples are the shape described in [28] as well as the shapes we found numerically for $k = 6, 9, 13, 15$.

We notice that the numerical optimal shape obtained for $k = 3$ is the disk. This is to be expected, since it is a direct consequence of the conjecture that the disk minimizes $\lambda_3(\Omega)$ under volume constraint. This is still an open problem.

We observe that all the optimal shapes computed have one or more axes of symmetry, while this is not the case for the volume constraint where the optimal shape for $k = 13$ is suspected to be non-symmetric [9].

The fact that we can immediately generalize the method in three dimensions is a big advantage. One drawback is the fact that we were not able to obtain very high resolution due to the fact that the matrices involved have extremely large dimensions. The shapes presented in Figure 1.2 were obtained using a $40 \times 40 \times 40$ grid on $D = [0, a]^3$. As previously, the initial shape was concentrated around the center of the cube D. In the paper [28] a few conjectures were stated regarding the minimizers in higher dimensions. The first conjecture was that the optimal shape for $\lambda_2(\Omega) + \text{Per}(\Omega)$ has cylindrical symmetry and is not convex in the three dimensional case. This can be observed in our results. To conclude that a shape is convex or not we simply apply the following procedure: we first compute a discretization of the isosurface $\{\varphi = 1/2\}$ and estimate the exact measure of its volume (up to roundoff error). Then, in a second step we compute the convexhull of this discretized isosurface and again estimate its volume. When the volume of the convex hull is 5% greater than the volume of the original isosurface we conclude that the computed optimal profile is not convex. We have obtained non-convex shapes for $k = 2, 5, 6, 7$. Cylindrical symmetry can be observed for $k = 2, 3, 4, 5$. For $k = 8$ we observe a symmetry by a rotation of angle $\pi/2$ and for $k = 10$ we observe a tetrahedral symmetry. We notice that the numerical optimal shape for $k = 4$ is approximately a ball. This is a direct consequence of the conjecture that the ball minimizes $\lambda_4(\Omega)$ under volume constraint in three dimensions. The optimal computed value of λ_4, in this case, is 255.56, while the actual eigenvalue of a ball of same surface area is approximately 253.72. We provide for each shape the value of the scale invariant expression $\lambda_k(\Omega) \text{Per}(\Omega)$, calculated using a finite element method.

We discussed our results with P. Antunes and P. Freitas, who made computations for problem (1.1.2) for $k \leq 50$ in two dimensions and $k \leq 20$ in three dimensions. In two dimensions we obtained similar results with the exception of a few shapes which are significantly better in terms of cost function. Our results, for $k \leq 20$ can be seen in Figure 1.1 and the results for $k \in [21, 50]$ can be seen in Figure 1.4. We emphasize the fact that the computations done for

k	mult.	Γ-conv	Fourier		k	mult.	Γ-conv	Fourier
1	1	11.5523	11.5507		11	2	24.6262	24.5966
2	1	15.2819	15.2806		12	3	24.7578	24.7430
3	2	15.7597	15.7573		13	1	25.9891	25.9823
4	2	18.3511	18.3485		14	2	26.4375	26.4325
5	2	19.1168	19.1087		15	1	26.9151	26.9123
6	1	20.0919	20.0908		16	3	27.2753	27.2525
7	2	21.5097	21.5009		17	3	27.3730	27.3600
8	2	22.0686	22.0262		18	2	28.6634	28.6279
9	1	23.2096	23.2073		19	2	29.0940	29.0796
10	2	23.5833	23.5500		20	3	29.5341	29.5136

Table 1.1: Comparative results - 2D

$k \geq 21$ use exclusively the software MpsPack. A detailed comparison of the cost function with the results of Antunes and Freitas is presented in Table 1.3. In the three dimensional case, for $k \leq 6$ our results coincide with theirs, but for $k \geq 7$ their optimal shapes have better cost values than ours. We believe this is due to the limitation on the discretization parameter for our method in three dimensions. A detailed comparation between the optimal costs is presented in Table 1.4.

We observe that in the three dimensional case, the optimal shapes we obtained numerically do not have *holes*. We may ask ourselves if this behaviour can be justified. In order to do this, we can analyse the, so called, topological derivative, which for a point $x \in \Omega$ and a general functional F is defined as

$$T(x) = \lim_{r \to 0} \frac{F(\Omega \setminus B(x,r)) - F(\Omega)}{\varepsilon(r)},$$

where $\varepsilon(r)$ is positive and $\varepsilon(r) \to 0$ as $r \to 0$. For more details see [76]. A negative topological derivative would mean that making a small hole decreases the value of F. In our particular case $F(\Omega) = \lambda_k(\Omega) + \mathrm{Per}(\Omega)$, and for $x \in \Omega$ and r small enough, we have $F(\Omega \setminus B(x,r)) > F(\Omega)$, since the eigenvalue is decreasing with respect to set inclusion, and for small r, we have $\mathrm{Per}(\Omega \setminus B(x,r)) = \mathrm{Per}(\Omega) + \mathrm{Per}(B(x,r))$. Thus, in our case, the topological derivative is always positive, and there is no interest in creating holes in order to decrease the value of the functional.

1.5 Optimality conditions and qualitative results

Once we know that a shape optimization problem has a solution, we would like to write some optimality conditions which could allow us to find further qualitative properties. An eigenvalue of the Dirichlet Laplacian associated to a shape Ω is differentiable with respect to perturbations only if it is simple. Unfortunately, solutions of (1.1.1) and (1.1.2) are conjectured to have multiple k^{th} eigenvalue at the optimum (with a few exceptions in the case of the perimeter
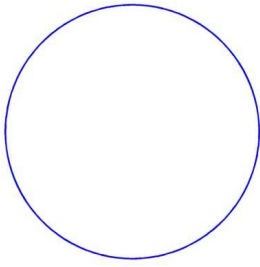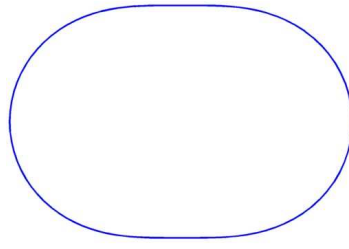
$\lambda_1 = 11.55$, simple $\qquad$ $\lambda_2 = 15.28$, simple $\qquad$ $\lambda_3 = 15.76$, double
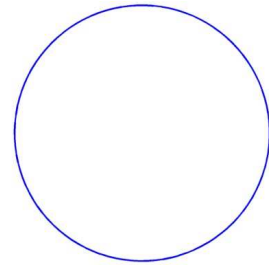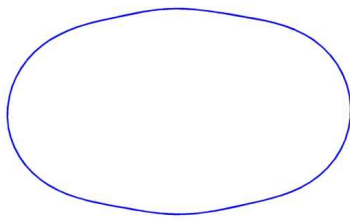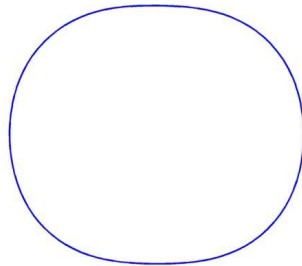
$\lambda_4 = 18.35$, double $\qquad$ $\lambda_5 = 19.11$, double $\qquad$ $\lambda_6 = 20.09$, simple
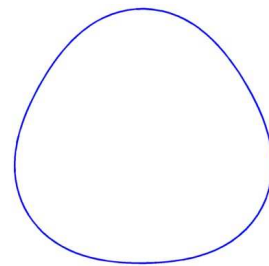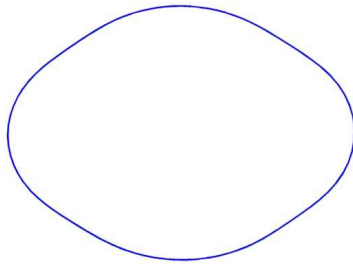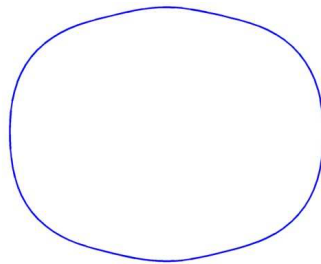
$\lambda_7 = 21.50$, double $\qquad$ $\lambda_8 = 22.03$, double $\qquad$ $\lambda_9 = 23.21$, simple
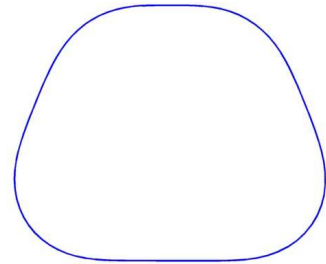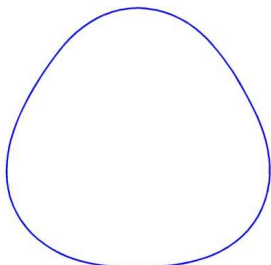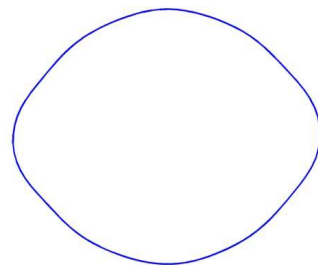
$\lambda_{10} = 23.55$, double $\qquad$ $\lambda_{11} = 24.60$, double $\qquad$ $\lambda_{12} = 24.74$, triple
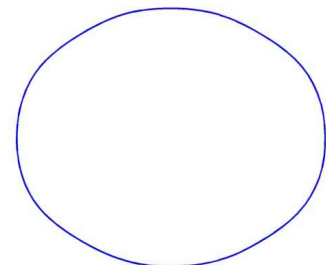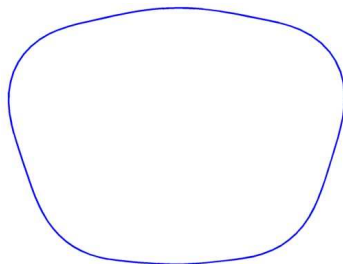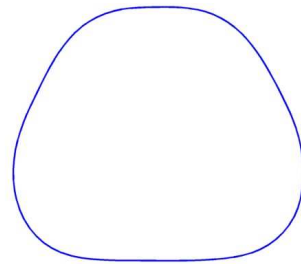
$\lambda_{13} = 25.98$, simple $\qquad$ $\lambda_{14} = 26.43$, double $\qquad$ $\lambda_{15} = 26.91$, simple

$$\lambda_{16} = 27.25, \text{triple} \qquad \lambda_{17} = 27.36, \text{triple} \qquad \lambda_{18} = 28.63, \text{double}$$
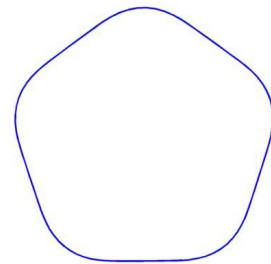
$$\lambda_{19} = 29.08, \text{double} \qquad \lambda_{20} = 29.51, \text{triple}$$
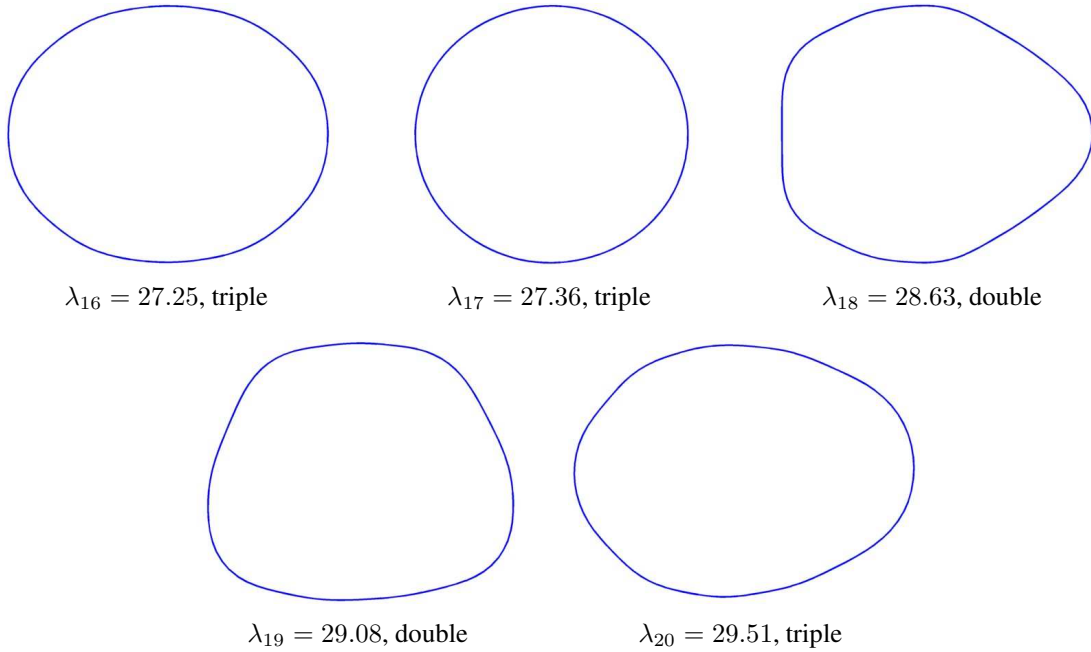
Figure 1.1: Numerical optimizers for problem 1.1.3 in 2D

constraint). Thus, classical optimality conditions, like the one exploited in [28], cannot be written for every k. In our case, we observed that for $d = 2$, $k = 2, 6, 9, 13, 15$ optimal shapes probably have simple eigenvalues. Thus we can apply the method described in [28] to deduce the fact that the boundary of these shapes does not contain any flat parts or any arcs of circles. We may wonder if this is true in the general case. To study this question in the case of multiple eigenvalues it is possible to use methods inspired by [47], [46] and [75]. In the previously cited article [47], the authors provided an optimality condition for problem (1.1.1), which treats the case when the eigenvalue is multiple at the optimum. The results of this section are dedicated to find a similar optimality condition for problem (1.1.2).

The following theorem is a result similar to Theorem 2.5.10 in [65] where it is said that if an optimizer Ω^* for problem (1.1.1) is such that the kth eigenvalue is multiple, then the multiplicity cluster ends at λ_k, i.e. $\lambda_k(\Omega^*) < \lambda_{k+1}(\Omega^*)$. Throughout this section we assume that Ω has boundary of class C^3. In particular, this implies that its curvature, $\mathcal{H}$ is of class C^1. This assumption is stronger than the results obtained in [44], where it is proved that the optimizer has regularity $C^{1,\alpha}$. To our knowledge, this regularity assumption cannot be easily deduced from [44], and it is an open question, though it is natural to expect it.

Theorem 1.5.1. *Let $k \geq 2$ such that $\lambda_k > \lambda_{k-1}$ and assume that Ω is a minimizer for the kth eigenvalue of the Dirichlet Laplacian with a perimeter constraint (i.e. a solution of the problem*

$$\lambda_2(\Omega)\operatorname{Per}(\Omega) = 223.63 \qquad \lambda_3(\Omega)\operatorname{Per}(\Omega) = 251.91 \qquad \lambda_4(\Omega)\operatorname{Per}(\Omega) = 260.98$$

$$\lambda_5(\Omega)\operatorname{Per}(\Omega) = 343.75 \qquad \lambda_6(\Omega)\operatorname{Per}(\Omega) = 394.77 \qquad \lambda_7(\Omega)\operatorname{Per}(\Omega) = 421.20$$

$$\lambda_8(\Omega)\operatorname{Per}(\Omega) = 439.80 \qquad \lambda_9(\Omega)\operatorname{Per}(\Omega) = 446.58 \qquad \lambda_{10}(\Omega)\operatorname{Per}(\Omega) = 510.00$$
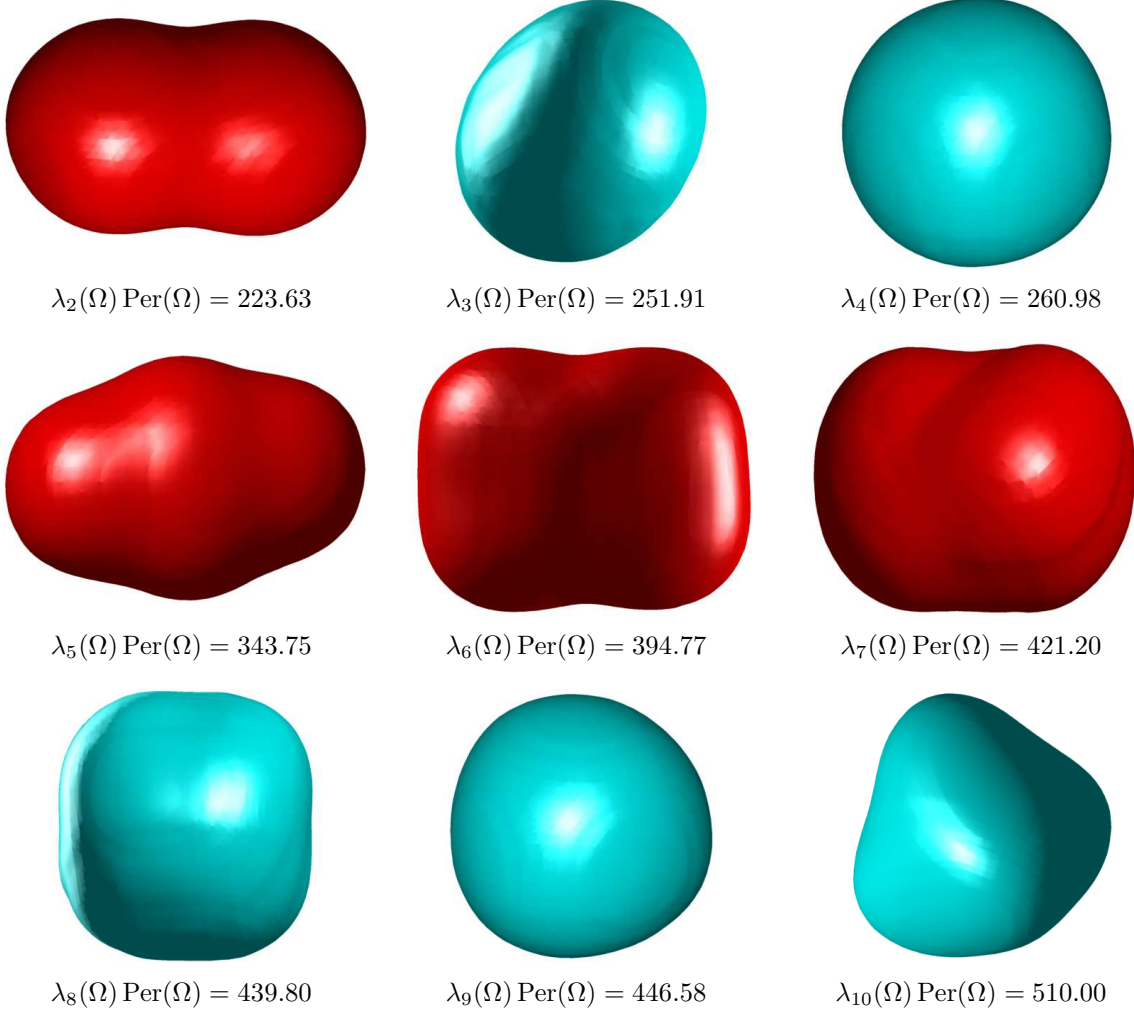
Figure 1.2: Numerical optimizers for problem 1.1.3 in 3D

(1.1.2)*). Then λ_k is simple and there exists a unique (up to sign) eigenfunction u satisfying*

$$\begin{cases} -\Delta u = \lambda_k(\Omega)u & in \ \Omega \\ u = 0 & on \ \partial\Omega \\ \left(\frac{\partial u}{\partial n}\right)^2 = \mathcal{H} & on \ \partial\Omega \end{cases}$$

Proof: Let $\Omega_\varepsilon = f_\varepsilon(\Omega)$ be a perimeter preserving analytic deformation of Ω and denote $(\Lambda_{i,\varepsilon})_{i\le p}$ and $(u_{i,\varepsilon})_{i\le p}$ the families of eigenfunctions and eigenvectors associated to λ_k according to Lemma 1.2.7. We use the notation $\lambda_{k,\varepsilon}(\Omega) = \lambda_k(\Omega_\varepsilon)$. Since $\lambda_k = \Lambda_{i,0} > \lambda_{k-1}$, by continuity, for sufficiently small ε we have

$$\Lambda_{i,\varepsilon} > \lambda_{k-1,\varepsilon}.$$

We know that Ω is a local minimizer for the Dirichlet Laplacian under the considered perturbation, which means that

$$\Lambda_{i,\varepsilon} \ge \lambda_{k,\varepsilon}.$$

The differentiable function $\varepsilon \mapsto \Lambda_{i,\varepsilon}$ achieves a local minimum at $\varepsilon = 0$ and this implies $\frac{d}{d\varepsilon}\Lambda_{i,\varepsilon} = 0$.

As a consequence, the quadratic form q_v defined in Lemma 1.2.8 is identically zero on E_k, where $v = \langle \frac{d}{d\varepsilon} f_\varepsilon, n \rangle$. The perimeter preserving deformation is arbitrary, so by Lemma 1.2.6 we have that q_v vanishes on E_k for every $v \in \mathcal{P}_0(\partial\Omega)$. This means that

$$\int_{\partial\Omega} \left(\frac{\partial u}{\partial n}\right)^2 v d\sigma = 0$$

for every $v \in \mathcal{P}_0(\partial\Omega)$ and for every $u \in E_k$.

Hence, for every function $u \in E_k$ there exists a constant $c > 0$ such that $\left(\frac{\partial u}{\partial n}\right)^2 = c\mathcal{H}$ on $\partial\Omega$. Since Ω is bounded, it is a classical result that the curvature of Ω is non-negative at at least one point. Thus, since $c\mathcal{H}$ is non-negative, it follows that $c \geq 0$. We cannot have $c = 0$, because otherwise $\frac{\partial u}{\partial n} = 0$ on $\partial\Omega$, and we could extend u with $u = 0$ outside Ω. Thus this extension would be an eigenfunction on any set Ω' containing Ω, contradicting the uniqueness of the analytic extension.

Thus, we have $\left|\frac{\partial u}{\partial n}\right| = \sqrt{c\mathcal{H}}$ on $\partial\Omega$. Since $\mathcal{H}$ is continuous, there exists an open set U such that $\mathcal{H} > 0$ on $U \cap \partial\Omega$. Thus, on $\partial\Omega \cap U$, $\frac{\partial u}{\partial n}$ keeps constant sign, so in this set we can only have $\frac{\partial u}{\partial n} = \sqrt{c\mathcal{H}}$ or $\frac{\partial u}{\partial n} = -\sqrt{c\mathcal{H}}$. If we have two eigenfunctions u_1, u_2 then there exists a linear combination $u = \alpha u_1 + \beta u_2$ such that $\frac{\partial u}{\partial n}$ vanishes on $\partial\Omega \cap U$. We apply Holmgren uniqueness theorem to conclude that $u = 0$ and λ_k is simple. $\qquad \square$

The following result connects the criticality of a domain Ω with the definiteness of the quadratic form q_v. This will allow us later to state our optimality result.

Theorem 1.5.2. *Let $k \geq 1$ be a positive integer.*

(1) If Ω is a critical domain for the kth eigenvalue of the Dirichlet Laplacian, then, for all $v \in \mathcal{P}_0(\partial\Omega)$, the quadratic form $q_v(u) = -\int_{\partial\Omega} \left(\frac{\partial u}{\partial n}\right)^2 v \, d\sigma$ is not definite on E_k.

(2) Assume that $\lambda_k > \lambda_{k-1}$ or $\lambda_k < \lambda_{k+1}$, and that for all $v \in \mathcal{P}_0(\partial\Omega)$, the quadratic form $q_v(u) = -\int_{\partial\Omega} \left(\frac{\partial u}{\partial n}\right)^2 v \, d\sigma$ is not definite on E_k. Then Ω is a critical domain for the kth eigenvalue of the Dirichlet Laplacian.

Proof: (1) Consider a function $v \in \mathcal{P}_0(\partial\Omega)$ and let $\Omega_\varepsilon = f_\varepsilon(\Omega)$ be an analytic perimeter preserving deformation of Ω such that $v = \langle \frac{d}{d\varepsilon} f_\varepsilon|_{\varepsilon=0}, n \rangle$ (such a deformation exists by Lemma 1.2.6). Let $(\Lambda_{i,\varepsilon})_{i \leq p}$ and $(u_{i,\varepsilon})_{i \leq p}$ be families of eigenvalues and eigenfunctions associated to λ_k like in Lemma 1.2.7. There exist two integers $i, j \leq p$ such that $\frac{d}{d\varepsilon}\lambda_{k,\varepsilon}|_{\varepsilon=0^-} = \frac{d}{d\varepsilon}\Lambda_{i,\varepsilon}|_{\varepsilon=0}$ and $\frac{d}{d\varepsilon}\lambda_{k,\varepsilon}|_{\varepsilon=0^+} = \frac{d}{d\varepsilon}\Lambda_{j,\varepsilon}|_{\varepsilon=0}$. The criticality of Ω implies that $\frac{d}{d\varepsilon}\Lambda_{i,\varepsilon}|_{\varepsilon=0} \times \frac{d}{d\varepsilon}\Lambda_{j,\varepsilon}|_{\varepsilon=0} \leq 0$ and from Lemma 1.2.8, it follows that q_v has both positive and negative eigenvalues, which means that q_v is not definite on E_k.

(2) Assume $\lambda_k > \lambda_{k-1}$ and let $\Omega_\varepsilon = f_\varepsilon(\Omega)$ be a perimeter-preserving deformation of Ω. Let $(\Lambda_{i,\varepsilon})_{i \leq p}$ and $(u_{i,\varepsilon})_{i \leq p}$ be families of eigenvalues and eigenfunctions associated to λ_k according to Lemma 1.2.7. For ε sufficiently small we have $\lambda_{k,\varepsilon} = \min_{i \leq p} \Lambda_{i,\varepsilon}$. Hence

$$\frac{d}{d\varepsilon}\lambda_{k,\varepsilon}\Big|_{\varepsilon=0^+} = \min_{i \leq p} \frac{d}{d\varepsilon}\Lambda_{i,\varepsilon}\Big|_{\varepsilon=0}$$

and

$$\frac{d}{d\varepsilon}\lambda_{k,\varepsilon}\Big|_{\varepsilon=0^-} = \max_{i \leq p} \frac{d}{d\varepsilon}\Lambda_{i,\varepsilon}\Big|_{\varepsilon=0}.$$

The non definiteness of q_v on E_k means that its smallest eigenvalue is non positive and its largest one is non negative. This implies that

$$\frac{d}{d\varepsilon}\lambda_{k,\varepsilon}\Big|_{\varepsilon=0^+} = \min_{i \leq p} \frac{d}{d\varepsilon}\Lambda_{i,\varepsilon}\Big|_{\varepsilon=0} \leq 0$$

and

$$\frac{d}{d\varepsilon}\lambda_{k,\varepsilon}\Big|_{\varepsilon=0^-} = \max_{i \leq p} \frac{d}{d\varepsilon}\Lambda_{i,\varepsilon}\Big|_{\varepsilon=0} \geq 0$$

which in turn implies the criticality of the domain Ω.

The case $\lambda_k < \lambda_{k+1}$ can be treated in a similar manner. $\qquad\square$

The next result provides a nice characterisation of the non-definitness of q_v. Note that unlike in [47], we have to add a hypothesis on $\mathcal{H}$. This hypothesis is natural when dealing with solutions of problem (1.1.2).(see [44], Section 4.)

Theorem 1.5.3. *Let k be a natural integer. If Ω is bounded and its curvature satisfies $\mathcal{H} \geq 0$ then the following two conditions are equivalent:*

(i) For all $v \in \mathcal{P}_0(\partial\Omega)$, the quadratic form q_v is not definite on E_k.

(ii) There exists a finite family of eigenfunctions $(u_i)_{i \leq m} \subset E_k$ satisfying

$$\sum_{i=1}^m \left(\frac{\partial u_i}{\partial n}\right)^2 = \mathcal{H} \text{ on } \partial\Omega.$$

Proof: To see that (ii) implies (i) it suffices to notice that, for any $v \in \mathcal{P}_0(\partial\Omega)$

$$\sum_{i \leq m} q_v(u_i) = -\sum_{i \leq m} \int_{\partial\Omega} \left(\frac{\partial u_i}{\partial n}\right)^2 v d\sigma = -\int_{\partial\Omega} \mathcal{H} v \, d\sigma = 0,$$

which means that q_v is not definite on E_k.

To prove the other implication we look at $K = \text{conv}\{\left(\frac{\partial u}{\partial n}\right)^2, \ u \in E_k\}$, and we want to prove that the function $\mathcal{H}$ belongs to K. Suppose that $\mathcal{H} \notin K$. Then, from the Hahn-Banach theorem (applied to the finite dimensional normed vector subspace of $C^1(\partial\Omega)$ spanned by K and $\mathcal{H}$), there exists a function $v \in C^1(\partial\Omega)$ such that $\int_{\partial\Omega} \mathcal{H} v \, d\sigma > 0$ and for all $u \in E_k$,

$$\int_{\partial\Omega} \left(\frac{\partial u}{\partial n}\right)^2 v \, d\sigma \leq 0.$$

Since v is not necessarily in $\mathcal{P}_0(\partial\Omega)$, we modify it by a constant term and define $v_0 = v - c$ where c is chosen such that $v_0 \in \mathcal{P}_0(\partial\Omega)$. The condition that c must satisfy is

$$0 = \int_{\partial\Omega} \mathcal{H}\, v_0\, d\sigma = \int_{\partial\Omega} \mathcal{H}\, v\, d\sigma - c \int_{\partial\Omega} \mathcal{H}\, d\sigma.$$

This last relation defines $c = \dfrac{\int_{\partial\Omega} \mathcal{H}\, v\, d\sigma}{\int_{\partial\Omega} \mathcal{H}\, d\sigma}$, since $\int_{\partial\Omega} \mathcal{H}\, d\sigma > 0$. The fact that $\int_{\partial\Omega} \mathcal{H} d\sigma > 0$ is a consequence of the fact that $\mathcal{H} \geq 0$ and Ω is bounded. With the above considerations, we see that $c > 0$.

For $u \in E_k$ we have

$$\begin{aligned}
q_{v_0}(u) &= -\int_{\partial\Omega} \left(\frac{\partial u}{\partial n}\right)^2 v_0\, d\sigma \\
&= -\int_{\partial\Omega} \left(\frac{\partial u}{\partial n}\right)^2 v\, d\sigma + c \int_{\partial\Omega} \left(\frac{\partial u}{\partial n}\right)^2 d\sigma \\
&\geq c \int_{\partial\Omega} \left(\frac{\partial u}{\partial n}\right)^2 d\sigma
\end{aligned}$$

and $\int_{\partial\Omega} \left(\frac{\partial u}{\partial n}\right)^2 d\sigma > 0$ for any non trivial Dirichlet eigenfunction u (due to Holmgren uniqueness theorem). In conclusion, we have found a function $v_0 \in \mathcal{P}_0(\partial\Omega)$ such that the quadratic form q_{v_0} is positive definite on E_k, which contradicts condition (i). $\qquad\square$

Corollary 1.5.4. *If Ω is a local minimizer for the problem* (1.1.2)

$$\min_{\mathrm{Per}(\Omega)=1} \lambda_k(\Omega)$$

with boundary of class C^3, then there exists a finite family of eigenfunctions $(u_i)_{i \leq m} \subset E_k$, such that

$$\sum_{i=1}^{m} \left(\frac{\partial u_i}{\partial n}\right)^2 = \mathcal{H}.$$

Proof: It is a direct result of the above theorems, noting that any solution Ω of the problem must verify $\mathcal{H} \geq 0$ [44]. $\qquad\square$

Remark 1.5.5. We note that Corollary 1.5.4 the number m of eigenfunctions that satisfy the optimality condition is not known. Numerical computations done in Section 1.6 suggest that m is equal to the multiplicity of λ_k.

Once this regularity result is established, we can apply the bootstrap procedure presented in [28], and conclude that Ω is smooth.

Corollary 1.5.6. *If Ω is a minimizer for the problem* (1.1.2)*, with boundary of class C^3, then Ω has boundary of class C^∞.*

Proof: If Ω is of class C^3, then Corollary 1.5.4 holds and we have the optimality relation

$$\sum_{i=1}^{m} \left(\frac{\partial u_i}{\partial n} \right)^2 = \mathcal{H}.$$

Since Ω is of class $C^{2,\alpha}$, it follows, using standard Shauder regularity estimates, that $\partial_n u_i^2$ is $C^{1,\alpha}$. The optimality relation, then implies that $\mathcal{H}$ is $C^{1,\alpha}$, and thus Ω is of class $C^{3,\alpha}$. Iterating this procedure we find that Ω is of class C^∞. □

In the article [28] the authors prove that the solution of (1.1.2) in the case $k = 2, d = 2$ has no segments and no arcs of circles in its boundary. The method used in the mentioned article works only in the case we know the corresponding eigenvalue is simple. Using the above corollary, we can partially extend this result to the general case. In the following, we call a *flat part* of $\mathbb{R}^d$, the nonempty intersection of a $d - 1$ dimensional hyperplane with a d-dimensional open ball.

Theorem 1.5.7. *If Ω is a local minimizer for the problem* 1.1.2

$$\min_{\mathrm{Per}(\Omega)=1} \lambda_k(\Omega)$$

then $\partial\Omega$ does not contain a flat part.

Proof: Suppose that Ω contains a flat part S in its boundary. Using the previous convention, $S = H \cap B$ where H is a $d - 1$ dimensional hyperplane and B is a d-dimensional ball. Then $\mathcal{H} = 0$ on that region S, and by Corollary 1.5.4, at least one eigenfunction u satisfies $\dfrac{\partial u}{\partial n} = 0$ on that S.

We then choose an extension $\Omega' = \Omega \cup B'$ of the domain Ω such that B' is a ball, $B' \subset B$, $B' \not\subset \Omega$ and B' is small enough such that $B' \cap \partial\Omega \subset S$. Define $u' = u$ on Ω and 0 on $\Omega' \setminus \Omega$. In this way, we create an eigenfunction u' on Ω' which is zero on an open set. This together with the analiticity of u' and the fact that u' is not identically zero brings us to a contradiction.

In conclusion, Ω cannot contain a flat part in its boundary. □

1.6 Numerical observation of the optimality conditions

By the above results, we know that if Ω is a minimizer for (1.1.2) then it exists a family of eigenfunctions $(u_i)_{i=1}^m \subset E_k$ such that

$$\sum_{i=1}^{m} \left(\frac{\partial u_i}{\partial n} \right)^2 = \mathcal{H}. \tag{1.6.1}$$

In order to evaluate the numerical quality of our solutions we would like to investigate how far our solutions satisfy this optimality condition. The question is whether we are able to find a

combination of eigenfunctions which realize this equality. Suppose that $\dim E_k = p$ and the p orthonormal eigenfunctions which span E_k are denoted $\mathfrak{u}_1, ..., \mathfrak{u}_p$. We may use indexes from 1 to p or from $k - p + 1$ to k. It is easy to see that (1.6.1) implies that

$$\mathcal{H} \in \text{span}\left(\left\{\left(\frac{\partial \mathfrak{u}_i}{\partial n}\right)^2, \ i = 1..p\right\} \bigcup \left\{\frac{\partial \mathfrak{u}_i}{\partial n}\frac{\partial \mathfrak{u}_j}{\partial n}, \ 1 \leq i < j \leq p\right\}\right).$$

This observation is a direct consequence of the fact that each eigenfunction u_i can be written as

$$u_i = \sum_{j=1}^{p} \alpha_j^i \mathfrak{u}_j.$$

Thus, in a first step, we can find the coefficients of $\mathcal{H}$ in the decomposition

$$\mathcal{H} = \sum_{i=1}^{p} \alpha_i \left(\frac{\partial \mathfrak{u}_i}{\partial n}\right)^2 + \sum_{1 \leq i < j \leq p} \beta_{i,j} \frac{\partial \mathfrak{u}_i}{\partial n}\frac{\partial \mathfrak{u}_j}{\partial n}$$

by solving an optimization problem. The normal derivatives $\frac{\partial u_i}{\partial n}$ and the curvature are known on a discretization $\{x_1, ..., x_l\}$ of the boundary $\partial\Omega$. To find the coefficients, we solve the quadratic, convex minimization problem

$$\min_{\substack{(\alpha_i)_{i=1}^{p}, \\ (\beta_{i,j})_{1 \leq i < j \leq n}}} \sum_{h=1}^{l}\left(\sum_{i=1}^{p} \alpha_i \left(\frac{\partial \mathfrak{u}_i}{\partial n}(x_h)\right)^2 + \sum_{1 \leq i < j \leq p} \beta_{i,j}\frac{\partial \mathfrak{u}_i}{\partial n}(x_h)\frac{\partial \mathfrak{u}_j}{\partial n}(x_h) - \mathcal{H}(x_h)\right)^2$$

Then, we transform this quadratic representation into a canonical representation by using the classical Gauss-Jacobi method. Of course, this representation is not unique. The claim of Corollary 1.5.4 is that this canonical representation will consist in a sum of squares: to test this, we checked if the matrix $(a_{i,j})$ defined by $a_{i,i} = \alpha_i$, $a_{i,j} = a_{j,i} = \beta_{i,j}/2$ is positive definite. The answer is affirmative for every optimizer, and a representation of the type (1.6.1) is presented for each $k = 1, ..., 15$ in Table 1.2. In all computations we check the pointwise optimality conditions presented in Table 1.2 up to an upper bound of order 10^{-4}.

We present below a few other numerical observations in connection with the optimality conditions.

- If $x \in \partial\Omega$ and $\mathcal{H}(x) = 0$, then all nodal lines corresponding to the eigenfunctions present in the optimality relation touch $\partial\Omega$ at x. This is observed numerically in Figure 1.3 for $k = 18$.

- Numerical observations suggest that the number of eigenfunctions m present in the optimality condition is equal to the multiplicity of the eigenvalue at the optimum. Furthermore, the relation seems to be a convex combination of the type

$$a_k(\partial_n \mathfrak{u}_k)^2 + a_{k-1}(\partial_n \mathfrak{u}_{k-1})^2 + ... + a_{k-m+1}(\partial_n \mathfrak{u}_{k-m+1})^2 = \mathcal{H},$$

where $a_k + a_{k-1} + ... + a_{k-m+1} = 1$.
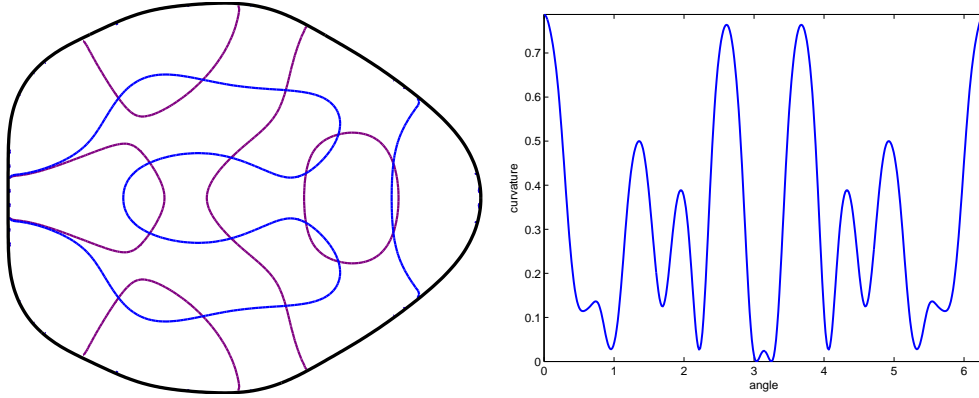
Figure 1.3: Optimal set Ω_{18} obtained for $k = 18$, together with the nodal lines of the eigenfunctions $\mathfrak{u}_{17}, \mathfrak{u}_{18}$ corresponding to $\lambda_{17}(\Omega_{18}) = \lambda_{18}(\Omega_{18})$. (left) Plot of the curvature of Ω_{18}; note that the nodal lines touch the boundary at the two points having zero curvature. (right)

- Motivated by [**?**], we studied numerically some convex combinations of eigenvalues under perimeter constraint. Suppose that Ω^* is solution of problem (1.1.2) and $\lambda_k(\Omega^*)$ is double, with observed numerical optimality relation

$$a(\partial_n \mathfrak{u}_k)^2 + (1-a)(\partial_n \mathfrak{u}_{k-1})^2 = \mathcal{H}.$$

  Then, we observed numerically that Ω^* is also a solution of the problem

$$\min_{\mathrm{Per}(\Omega)=1} \left(\alpha \lambda_k(\Omega) + (1-\alpha)\lambda_{k-1}(\Omega) \right),$$

  for every $\alpha \in [a, 1]$. This can be generalized to the cases where the eigenvalue has higher multiplicity.

Finally, we have observed that the optimality condition is a strong indicator of a local minimum. At first, when we verified if the optimality condition is satisfied on the results we obtained, we got large errors. We then decided to remake the initial computations and it turned out that in every situation where the optimality error was large, we were able to go further with the optimization and decrease even more the optimal value.

1.7 Further details and comparison with other known computations

We provide below some further details concerning the optimization of the first 50 eigenvalues of the Dirichlet Laplacian under perimeter constraint. We compare our results (column labelled "our λ_k") with the ones obtained by P. Antunes and P. Freitas in [10] (column labelled "λ_k AF"). In their computations the perimeter is fixed and it equals $2\sqrt{\pi}$, so in order to compare the results we rescaled our shapes so that they have the same perimeter. We present the optimality errors

k	mult.	Numerical optimality relation	L^2 error	L^∞ error
1	1	$(\partial_n \mathfrak{u}_1)^2 = \mathcal{H}$	0	0
2	1	$(\partial_n \mathfrak{u}_2)^2 = \mathcal{H}$	$3 \cdot 10^{-8}$	$4 \cdot 10^{-8}$
3	2	$(\frac{1}{\sqrt{2}}\partial_n \mathfrak{u}_2)^2 + (\frac{1}{\sqrt{2}}\partial_n \mathfrak{u}_3)^2 = \mathcal{H}$	$5 \cdot 10^{-4}$	$7 \cdot 10^{-4}$
4	2	$(0.16\partial_n \mathfrak{u}_3)^2 + (0.98\partial_n \mathfrak{u}_4)^2 = \mathcal{H}$	$3 \cdot 10^{-4}$	$6 \cdot 10^{-4}$
5	2	$(0.54\partial_n \mathfrak{u}_4)^2 + (0.84\partial_n \mathfrak{u}_5)^2 = \mathcal{H}$	$2 \cdot 10^{-4}$	$3 \cdot 10^{-4}$
6	1	$(\partial_n \mathfrak{u}_6)^2 = \mathcal{H}$	$3 \cdot 10^{-4}$	$5 \cdot 10^{-4}$
7	2	$(0.87\partial_n \mathfrak{u}_6)^2 + (0.48\partial_n \mathfrak{u}_7)^2 = \mathcal{H}$	$4 \cdot 10^{-4}$	$5 \cdot 10^{-4}$
8	2	$(0.39\partial_n \mathfrak{u}_7)^2 + (0.92\partial_n \mathfrak{u}_8)^2 = \mathcal{H}$	$3 \cdot 10^{-4}$	$3 \cdot 10^{-4}$
9	1	$(\partial_n \mathfrak{u}_9)^2 = \mathcal{H}$	$7 \cdot 10^{-5}$	10^{-4}
10	2	$(\frac{1}{\sqrt{2}}\partial_n \mathfrak{u}_9)^2 + (\frac{1}{\sqrt{2}}\partial_n \mathfrak{u}_{10})^2 = \mathcal{H}$	$2 \cdot 10^{-4}$	$2 \cdot 10^{-4}$
11	2	$(0.51\partial_n \mathfrak{u}_{10})^2 + (0.86\partial_n \mathfrak{u}_{11})^2 = \mathcal{H}$	$6 \cdot 10^{-4}$	$7 \cdot 10^{-4}$
12	3	$(0.31\partial_n \mathfrak{u}_{10})^2 + (0.51\partial_n \mathfrak{u}_{11})^2 +$ $(0.80\partial_n \mathfrak{u}_{12})^2 = \mathcal{H}$	$3 \cdot 10^{-5}$	$2 \cdot 10^{-5}$
13	1	$(\partial_n \mathfrak{u}_{13})^2 = \mathcal{H}$	$4 \cdot 10^{-4}$	$5 \cdot 10^{-4}$
14	2	$(0.82\partial_n \mathfrak{u}_{13})^2 + (0.57\partial_n u_{14})^2 = \mathcal{H}$	$2 \cdot 10^{-5}$	$2 \cdot 10^{-5}$
15	1	$(\partial_n \mathfrak{u}_{15})^2 = \mathcal{H}$	10^{-5}	10^{-5}

Table 1.2: Optimality conditions in two dimensions

as well as the multiplicities. The optimal eigenvalues are roughly the same, except some situations highlighted in the table where the optimal values found by our algorithm are significantly smaller (difference greater than 0.25). We note that in these highlighted cases even the optimal shapes are slightly different. We notice that optimal shapes corresponding to $k = 29, 43$ do not seem to have symmetry, while the optimal shapes proposed by Antunes and Freitas are all symmetric. On the other hand shapes corresponding to $k = 41, 49$ have a central symmetry and do not have a symmetry axis. Given these considerations it is not likely that a result concerning the symmetry of optimal shapes can be proved.

k	our λ_k	$\lambda_k +$ Per	Opt. error	λ_k AF	Difference	AF mult.	our mult.
1	18.168275	11.5507	0	18.17	-0.00173	1	1
2	42.064122	15.28065	4.9e-05	42.07	-0.00588	1	1
3	46.124753	15.757328	0.000796	46.13	-0.00525	2	2
4	72.826728	18.348539	0.000694	72.83	-0.00327	2	2
5	82.259531	19.108794	0.000252	82.27	-0.01047	2	2
6	95.605716	20.090889	0.000749	95.61	-0.00428	1	1
7	117.180624	21.500892	0.000377	117.19	-0.00938	2	2
8	125.981848	22.026249	0.000282	125.99	-0.00815	2	2
9	147.353967	23.207329	0.000859	147.36	-0.00603	1	1
10	153.977603	23.549972	9.4e-05	153.98	-0.00240	2	2
11	175.435026	24.596689	0.000727	177.01	-1.57497	2	2
12	178.583626	24.742966	2.6e-05	178.6	-0.01637	3	3

13	206.785187	25.982306	0.000565	206.79	-0.00481	1	1
14	217.721706	26.432513	2.3e-05	217.73	-0.00829	2	2
15	229.795526	26.912357	1e-05	229.8	-0.00447	1	1
16	238.618352	27.252467	0.000741	238.63	-0.01165	3	3
17	241.453665	27.359983	0.009599	241.45	0.003665	3	3
18	276.599134	28.627952	0.007984	276.62	-0.02087	3	2
19	289.904933	29.079688	0.008092	289.93	-0.02507	2	2
20	303.078565	29.513652	0.003324	303.57	-0.49143	3	3
21	306.435447	29.622216	3.2e-05	306.52	-0.08455	3	3
22	316.631478	29.947178	0.008933	316.67	-0.03852	1	2
23	324.632195	30.197414	0.008528	324.82	-0.18780	2	4
24	361.505011	31.299879	0.001318	361.52	-0.01499	2	2
25	368.455927	31.499487	0.014613	368.51	-0.05407	3	3
26	382.016789	31.881007	0.00478	382.02	-0.00321	3	3
27	383.067574	31.910211	0.007396	383.09	-0.02243	4	4
28	404.018996	32.481681	0.023895	404.04	-0.02100	1	3
29	418.269751	32.859181	0.008134	418.38	-0.11025	2	3
30	433.816974	33.261364	0.007602	433.86	-0.04303	2	3
31	456.106225	33.821527	0.004245	456.73	-0.62378	2	2
32	459.104802	33.895483	0.006554	459.12	-0.01520	3	3
33	467.407148	34.098583	0.003432	467.42	-0.01285	4	4
34	473.06016	34.2355	5.8e-05	473.08	-0.01984	3	3
35	502.991936	34.94285	0.009027	502.99	0.001936	3	3
36	517.814325	35.282763	0.010175	518.28	-0.46567	4	4
37	536.975953	35.712743	0.011331	539.99	-3.01405	3	3
38	548.576823	35.968061	0.003967	549.46	-0.88318	2	2
39	552.970701	36.063842	0.01613	553.04	-0.06930	2	3
40	557.337141	36.158524	0.00657	557.63	-0.29286	4	4
41	574.75261	36.531281	0.00672	574.88	-0.12739	3	3
42	578.401108	36.608414	0.000914	578.47	-0.06889	3	3
43	615.248826	37.369901	0.012761	615.7	-0.45117	4	3
44	625.603235	37.578336	0.011643	625.71	-0.10676	4	4
45	643.066958	37.924798	0.013028	643.2	-0.13304	3	3
46	650.617878	38.072659	0.000676	651.34	-0.72212	2	3
47	662.681925	38.30654	0.02032	662.86	-0.17808	3	3
48	672.35022	38.491935	0.006425	672.36	-0.00978	4	4
49	683.362305	38.700944	0.014663	683.77	-0.40769	3	3

| 50 | 688.796414 | 38.803256 | 8.7e-05 | 688.89 | -0.09359 | 3 | 3 |

Table 1.3: Detailed comparison of our results with the ones
of P. Antunes and P. Freitas in the two dimensional case

k	our λ_k	λ_k AF	Rel diff.
2	223.63	219.214786	0.02
3	252.48	244.120062	0.03
4	255.56	253.743653	0.007
5	343.75	330.200432	0.04
6	394.77	374.739770	0.05
7	412.2	400.128643	0.03
8	439.8	415.120168	0.06
9	446.58	417.441436	0.07
10	510	475.666586	0.07

Table 1.4: Detailed comparison of our results with the ones of P. Antunes and P. Freitas in the
three dimensional case
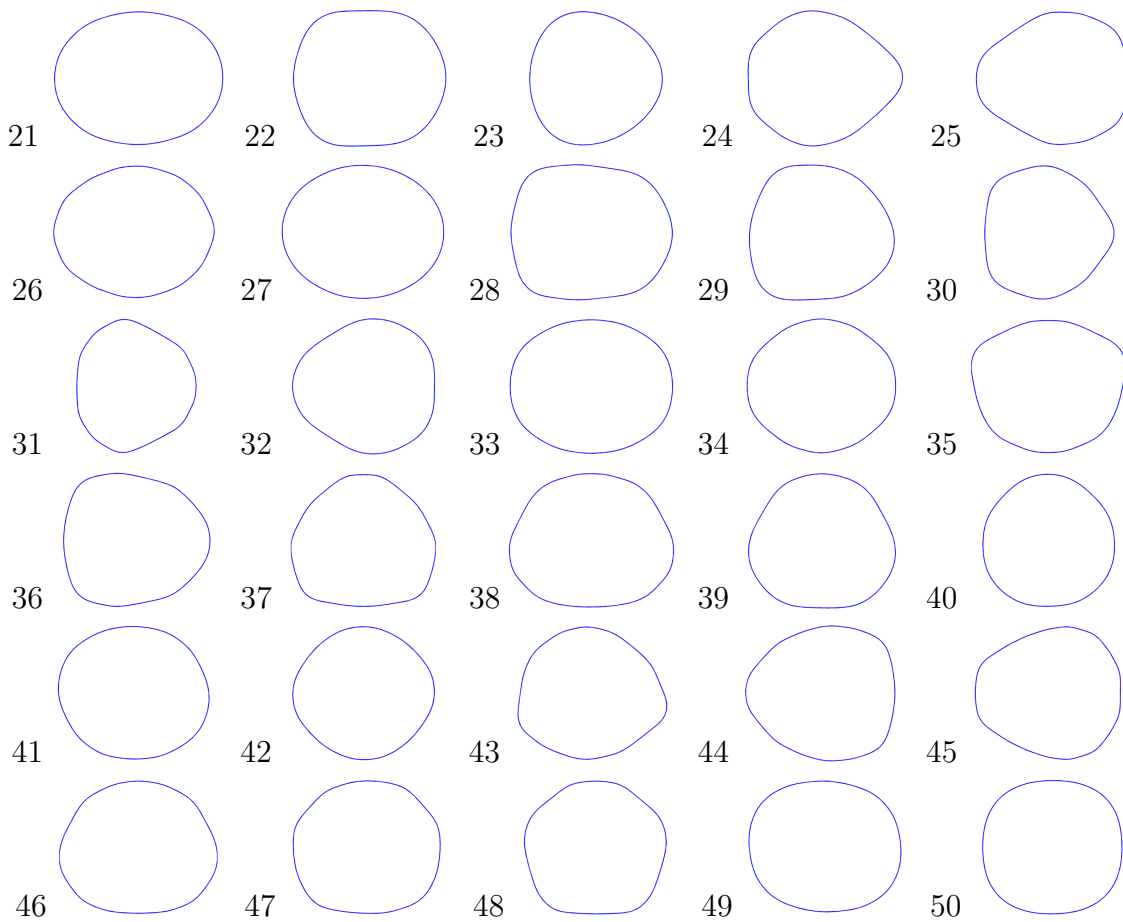
Figure 1.4: Shapes which minimize the k-th eigenvalue of the Dirichlet Laplacian under perimeter constraint with $k \in [21, 50]$

1.8 Related topics

1.8.1 Numerical computations - area constraint

The problem (1.1.1) has been studied numerically in two dimensions by [79] ($1 \leq k \leq 10$) and [9] ($1 \leq k \leq 15$). Using the software MpsPack and the framework presented in the study of the case of the perimeter constraint, we performed computations for $1 \leq k \leq 21$. The computational results are presented in Figure 1.5. In [9] it is conjectured that the multiplicity of the eigenvalue at the optimum increases with k, for $k \leq 15$. In our numerical computations we observe that the multiplicity varies, and it is not increasing, as conjectured. Of course, as we can see from the situation of the optimality errors shown below, it might be possible to further improve some of these shapes. It is interesting to note that for $k = 21$, the next triangular number after $k = 15$ we observed again an optimal shape which has a triangular symmetry.

As in the study of the perimeter case, we can wonder if there is an appropriate optimality condition, which is valid in the non-differentiable case where the multiplicity is higher than one. Note that in the case of the area constraint, the multiplicities are always higher than one. Such an optimality condition was proved by Ilias and El Soufi in [47], article which inspired us to prove the analogue relation in the perimeter constraint case. The corresponding optimality relation in the area constraint case is the following.

Theorem 1.8.1. *Suppose Ω^* is a local minimizer for the problem*

$$\min_{|\Omega|=1} \lambda_k(\Omega).$$

Then there exists a family of eigenfunctions $(u_i)_{i=1}^m$ in the eigenspace corresponding to λ_k such that

$$\sum_{i=1}^m (\partial_n u_i)^2 = 1.$$

In order to test the quality of our numerical results, we evaluated how well our shapes verify this optimality condition, using the same method used in the case of the perimeter constraint. The numerical results presented here are slightly better (in the sense of the optimal value of the functional) than the ones presented in [9]. Still, the optimality error is not small enough to be satisfied with our results. As in the perimeter case, we believe that a large optimality error means that we are not really at the optimum, and thus, even if these results are the best known, we believe that they can be slightly improved. An evaluation of the error and candidates for the optimality relations are presented in Table 1.5. We omit the expression of the optimality error for $k = 13$ and $k \in [16, 21]$ as the optimality error is quite large in some cases, and we believe that some of the results may be improved.

$\lambda_5 = 78.15$, mult = 2 $\lambda_6 = 88.47$, mult = 3 $\lambda_7 = 106.13$, mult = 3 $\lambda_8 = 118.86$, mult = 3

$\lambda_9 = 132.35$, mult = 3 $\lambda_{10} = 142.67$, mult = 4 $\lambda_{11} = 159.39$, mult = 4 $\lambda_{12} = 172.84$, mult = 4

$\lambda_{13} = 186.77$, mult = 4 $\lambda_{14} = 198.96$, mult = 4 $\lambda_{15} = 209.60$, mult = 5

$\lambda_{16} = 230.91$, mult = 4 $\lambda_{17} = 241.02$, mult = 3 $\lambda_{18} = 255.97$, mult = 4

$\lambda_{19} = 267.87$, mult = 5 $\lambda_{20} = 279.68$, mult = 5 $\lambda_{21} = 289.45$, mult = 4
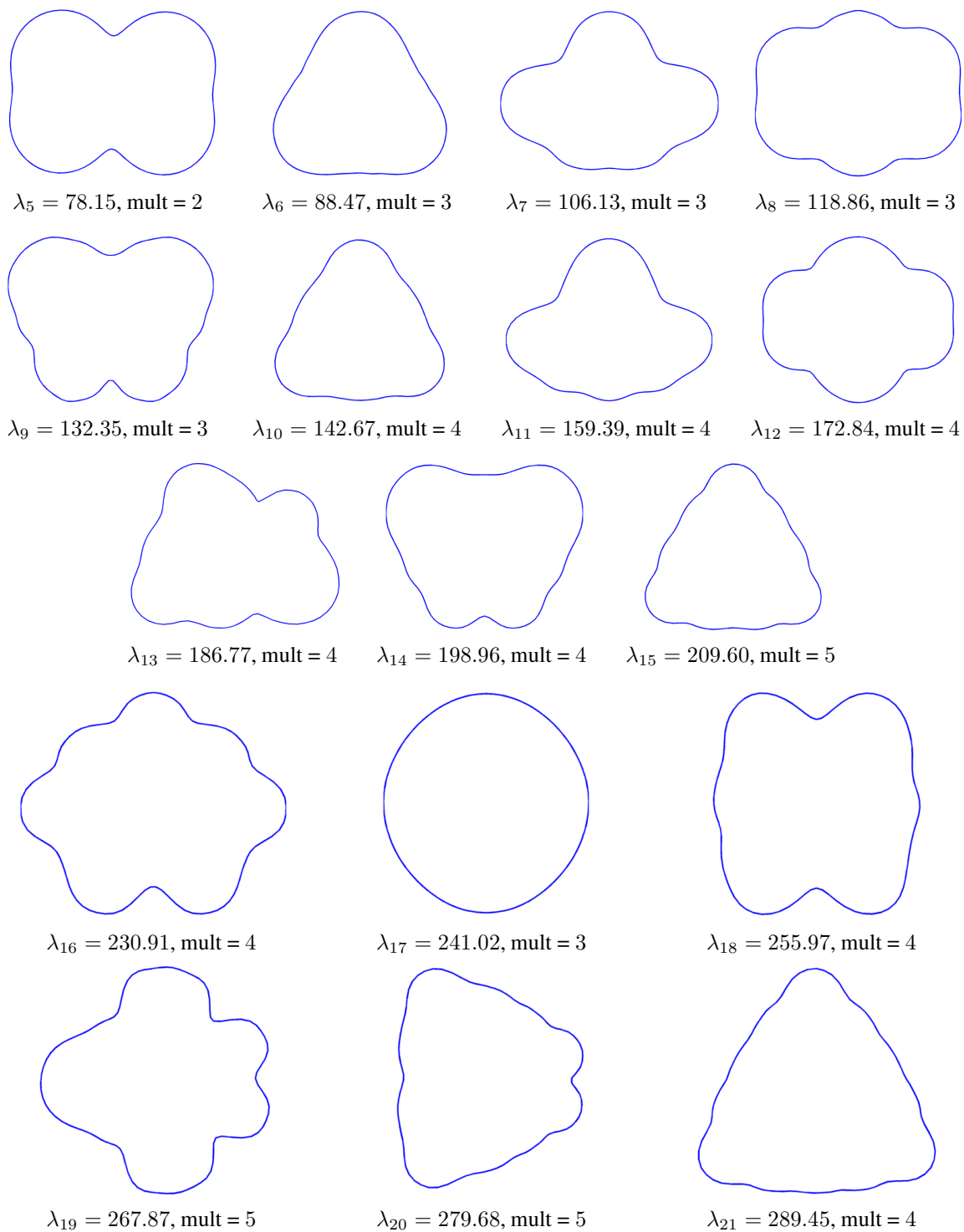
Figure 1.5: Numerical optimizers for problem 1.1.1 in 2D

k	mult.	Numerical optimality relation	L^2 error	L^∞ error
5	2	$(2.8\partial_n\mathfrak{u}_4)^2 + (1.7\partial_n\mathfrak{u}_5)^2 = 1$	$7\cdot10^{-3}$	$3\cdot10^{-2}$
6	3	$(0.56\partial_n\mathfrak{u}_4)^2 + (0.38\partial_n\mathfrak{u}_5)^2 + (0.38\partial_n\mathfrak{u}_6)^2 = 1$	10^{-3}	$4\cdot10^{-3}$
7	3	$(0.16\partial_n\mathfrak{u}_5 - 0.11\partial_n\mathfrak{u}_6)^2 + (0.19\partial_n\mathfrak{u}_6)^2 +$ $(0.2\partial_n\mathfrak{u}_7)^2 = 1$	0.05	0.15
8	3	$(0.31\partial_n\mathfrak{u}_6)^2 + (0.51\partial_n u_7)^2 + (0.3\partial_n\mathfrak{u}_8)^2 = 1$	0.03	0.07
9	3	$(0.18\partial_n\mathfrak{u}_7)^2 + (0.11\partial_n\mathfrak{u}_8)^2 + (0.18\partial_n\mathfrak{u}_9)^2 = 1$	0.04	0.11
10	4	$(0.26\partial_n\mathfrak{u}_7)^2 + (0.35\partial_n\mathfrak{u}_8)^2 + (0.35\partial_n\mathfrak{u}_9)^2 +$ $(0.21\partial_n\mathfrak{u}_{10})^2 = 1$	$8\cdot10^{-3}$	$2\cdot10^{-2}$
11	4	$(0.14\partial_n\mathfrak{u}_8)^2 + (0.14\partial_n\mathfrak{u}_9)^2 + (0.12\partial_n\mathfrak{u}_{10})^2 +$ $(0.13\partial_n\mathfrak{u}_{11})^2 = 1$	0.04	0.09
12	4	$(0.12\partial_n\mathfrak{u}_9)^2 + (0.24\partial_n\mathfrak{u}_{10})^2 + (0.31\partial_n\mathfrak{u}_{11})^2 +$ $(0.35\partial_n\mathfrak{u}_{12})^2 = 1$	0.01	0.02
13	4	-	0.07	0.4
14	4	$(0.1\partial_n\mathfrak{u}_{11})^2 + (0.09\partial_n\mathfrak{u}_{12})^2 + (0.11\partial_n\mathfrak{u}_{13})^2 +$ $(0.14\partial_n\mathfrak{u}_{14})^2 = 1$	0.06	0.15
15	5	$(0.26\partial_n\mathfrak{u}_{11})^2 + (0.26\partial_n\mathfrak{u}_{12})^2 + (0.22\partial_n\mathfrak{u}_{13})^2 +$ $(0.09\partial_n\mathfrak{u}_{14})^2 + (0.15\partial_n\mathfrak{u}_{15})^2 = 1$	0.01	0.05
16	4	-	0.06	0.15
17	4	-	0.007	0.02
18	4	-	0.02	0.06
19	5	-	0.02	0.23
20	5	-	0.07	0.23
21	4	-	0.04	0.11

Table 1.5: Optimality conditions in two dimensions - area constraint

1.8.2 Numerical study of Polya's conjecture

We may ask what happens if we try to optimize the Dirichlet-Laplace eigenvalues of polygonal shapes under different constraints. In the following, n denotes the number of sides of a polygon. It turns out that the problem is more difficult than it seems, even in the case of the first eigenvalue. Using Steiner symmetrization techniques one may prove the following facts:

- the equilateral triangle minimizes the first eigenvalue among triangles;

- the square minimizes the first eigenvalue among quadrilaterals.

The case $n \geq 5$ is an open problem, and there is a famous conjecture, due to Polya, which is a natural extrapolation of the cases $n = 3, 4$.

Conjecture 1.8.2. (Polya's conjecture) The regular polygon minimizes λ_1 among all polygons with n sides.

We do not have an answer to this conjecture, but we studied the problem numerically for $n \in [5, 15]$. Two ingredients are needed in order to perform this numerical study:

- A numerical method which allows us to compute the eigenvalues of a polygon.

51

- A formula of the derivative of the eigenvalue in terms of the vertices of the polygon.

We start by presenting the numerical method we used in the computation, which is based on fundamental solutions. Given a general shape P, whose boundary is well behaved, we wish to solve numerically the equation

$$\begin{cases} -\Delta u = \lambda u & \text{in } \Omega \\ u = 0 & \text{on } \partial\Omega \end{cases}$$

The idea behind the method of fundamental solutions is to consider only functions which already satisfy the equation $-\Delta u = \lambda u$ in Ω, and one way to do this is to consider

$$u = \alpha_1 \phi_1^\lambda + ... + \alpha_N \phi_N^\lambda,$$

where ϕ_i^λ, $i = 1...M$ are fundamental radial solutions of $-\Delta\phi = \lambda\phi$, with singularities outside Ω. We denote by (y_i) the singularities of the functions ϕ_i^λ which are points outside Ω. The coefficients $\alpha_1, ..., \alpha_N$ are found by imposing the boundary conditions on a discretization of $\partial\Omega$ denoted (x_i). This leads to a system of equations

$$\alpha_1 \phi_1^\lambda(x_i) + ... + \alpha_N \phi_N^\lambda(x_i) = 0, \ i = 1...N. \tag{1.8.1}$$

Of course, we are interested in the case where this system has a non-trivial solution, which means that the matrix $A_\lambda = (\phi_j(x_i)^\lambda)_{i,j=1}^N$ needs to be singular. Thus, in order to find the eigenvalues of a domain Ω which are situated in some interval I, it suffices to locate the points $\lambda \in I$ where $\det A_\lambda = 0$. Once such an eigenvalue is located, we can find a corresponding eigenfunction by solving the system (1.8.1). Note that in this form, when λ is an eigenvalue, the system does not have a unique solution. In order to address this issue, we add another equation corresponding to an interior point, where we impose that the combination $\sum \alpha_i \phi_i^\lambda$ does not vanish. Methods of this type have been considered in the literature by Alvez and Antunes [4].

In order to tackle the problem corresponding to polygons, we need to provide a family of radial functions which satisfies the eigenvalue equation and decide where to choose the points (x_i) and (y_i). We can find a family of fundamental solutions by looking at the equation corresponding to the laplacian written in polar coordinates. If $\phi = y(r)$ then $-\Delta\phi = \lambda\phi$ corresponds to

$$-y''(r) - \frac{1}{r}y'(r) = \lambda y,$$

which translates to

$$r^2 y''(r) + r y'(r) + r^2 \lambda y(r) = 0.$$

We make the change of variable $s = \sqrt{\lambda}r$. Then if $y(r) = z(s)$ we have $y'(r) = z'(s)\sqrt{\lambda}$ and $y''(r) = z''(s)\lambda$, which means that z satisfies the differential equation

$$s^2 z'' + s z' + s^2 z = 0.$$

Note that this corresponds to the Bessel function of the first kind, which satisfies the equation

$$s^2 z'' + s z' + (s^2 - \alpha^2)z = 0 \tag{1.8.2}$$

for $\alpha = 0$. Thus, we can choose our fundamental solutions to be of the form $\phi^\lambda(x) = z(\sqrt{\lambda}|x|)$ where z is a solution of (1.8.2) for $\alpha = 0$. In our numerical computations we choose as solutions the Hankel functions, which are a combination of an analytic and a singular solution of (1.8.2). In Matlab this corresponds to the function `besselh`.

We come now to the choice of points $(x_i), (y_i)$ which is important in the computations. As noted in [4], an arbitrary choice of these points may lead to inconclusive results. A somewhat uniform distribution and a good relation between the evaluation and source points is needed in order for the method to be successful. In the following, we only treat the case of polygons.

Given a polygon P, we want to distribute N points on its boundary in a uniform way. In order to do this, we compute the lengths of the sides of P, and we associate to each side of P a number of points proportional to its length. Then we distribute evenly the corresponding points on this side. The exterior source points (y_i) are chosen on the normals of the polygon, at a fixed distance. In my computations I used a distance of 0.3 for polygons of fixed area equal to 1. At the corners we choose the exterior source points on the bisector of the angle of the polygon, to better address the corner singularity present there. An example of points distribution is shown in Figure 1.6. Another example of point distribution is the Chebyshev distribution on every side[1]. The points are distributed on the segments according to the parameter $(\cos\left(\dfrac{2i-1}{2k}\pi\right) + 1)/2$, $i = 1...k$. I noted that this new distribution gains more precision for the same number of source points. This behaviour of the error with respect to the distribution of points can be seen in Table 1.8 for the particular case of a rectangle of side lengths 1.2×1. Note that for a rectangle of sides $L \times \ell$ the expression of the Dirichlet eigenvalues is given by $\lambda \in \{\pi^2\left(\dfrac{m^2}{L^2} + \dfrac{n^2}{\ell^2}\right) : m, n \geq 1\}$.

In the numerical computations we note that the determinant of A_λ is always close to zero. In order to better detect its zeros, we compute $\log(A_\lambda)$ for a discretization of the search interval, and we look for the singularities of this function using a golden search method. A plot of $\det(A_\lambda)$ on the interval $[1, 100]$ in the case of the equilateral triangle of side length 2 is presented in Figure 1.7. For this equilateral triangle, we can express the eigenvalues in analytic form: $\lambda \in \{\frac{4\pi^2}{9}(m^2 + mn + n^2), m, n \geq 1\}$. In Table 1.6 we present the first eigenvalues we obtained numerically, compared to their analytical correspondents.

Let's now turn to the numerical study of Polya's conjecture. We want to optimize numerically the first eigenvalue of a polygon with n sides. Note that in this particular case, the eigenvalue depends only on the $2n$ parameters corresponding to the coordinates of the vertices of the polygon. If we could write the expression of the derivative with respect to every parameter of the eigenvalue, then we could write a gradient descent algorithm in order to optimize this

---

[1] I thank Robert S. Jones for suggesting me this distribution
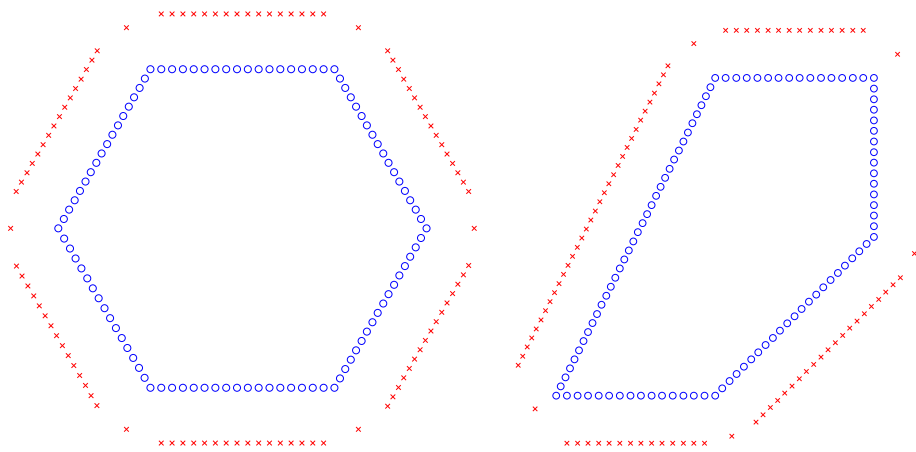
Figure 1.6: Configuration of source points (red) and evaluation points (blue) for a regular hexagon (left) and for a non-regular pentagon (right)
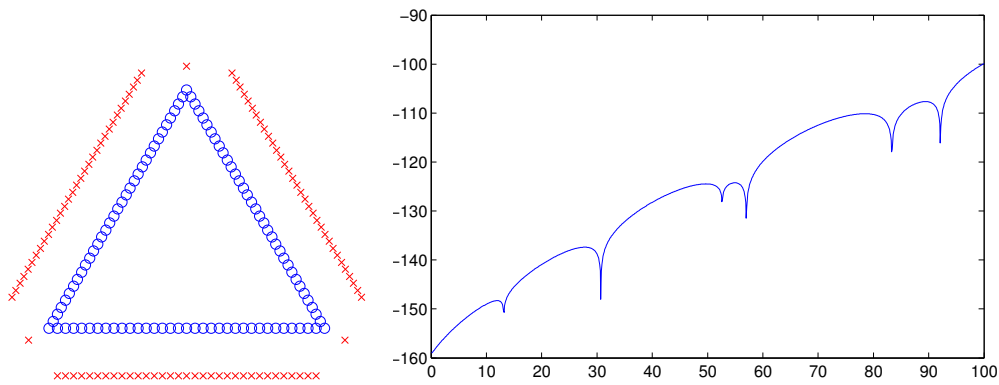

Figure 1.7: Configuration of source points and evaluation points for an equilateral triangle and the plot of $\lambda \mapsto \log|\det(A_\lambda)|$ for $\lambda \in [1, 100]$

Numerical values	Analytical value	Precision
13.1594725447	13.1594725347	7 digits
30.7054358009	30.7054359145	6 digits
52.6378888648	52.6378901391	4 digits
57.0243802270	57.0243809840	6 digits
83.3433209202	83.3433260536	5 digits
92.1163077702	92.1163077435	7 digits

Table 1.6: Comparison between numerical and analytical values for the equilateral triangle of side length 2

Regular	Chebyshev	Analytic
16.7234963700	16.7234963461	16.7234963462
37.2851722760	37.2851721817	37.2851721818
46.3323096064	46.3323095494	46.3323095495
66.8939856146	66.8939853848	66.8939853851
71.5546321129	71.5546319077	71.5546319078
95.6803315972	95.6803315556	95.6803315550

Table 1.7: Comparison between normal distribution, Chebyshev distribution and analytical values for the rectangle of sides 1 and 1.2. The different point distribution can be seen in Figure 1.8
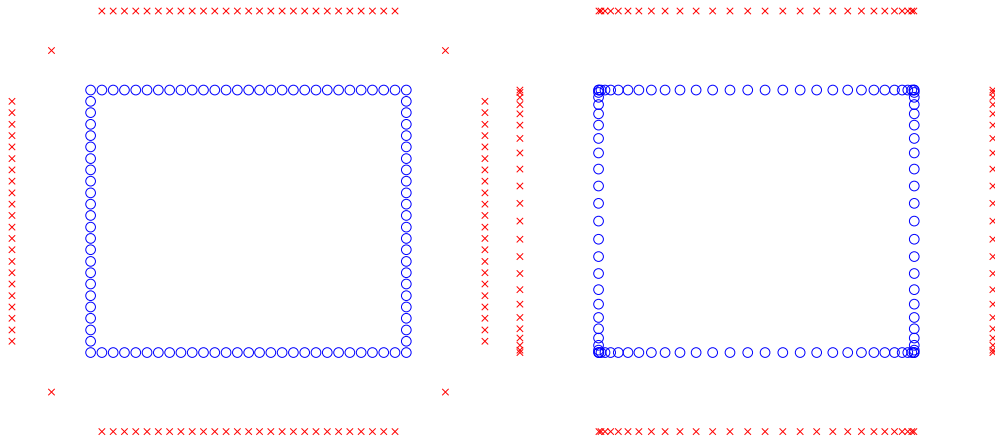

Figure 1.8: Normal point distribution (left) vs Chebyshev point distribution (right)

eigenvalue. In general, if a shape Ω is perturbed by a vector field V, the expression of the derivative of a simple eigenvalue is given by $\dfrac{d\lambda}{dV} = -\displaystyle\int_{\partial\Omega} \left(\dfrac{\partial u}{\partial n}\right)^2 V.n d\sigma$. We want to compute the derivative with respect to the parameters defining each vertex of the polygon. In order to do this, we consider particular vector fields V.

Let's fix the vertex A_i with neighbouring vertices A_{i-1}, A_{i+1} (notation modulo n). Denote the two coordinates of A_i by (x_{2i-1}, x_{2i}). If we want to find the derivative of λ_1 with respect to x_{2i-1} we make a perturbation of A_i with $(1, 0)$. This perturbation of one vertex induces a perturbation of the segments $A_{i-1}A_i, A_iA_{i+1}$ of P. In this particular case V has the following form on ∂P:

$$\begin{cases} \mathbb{I}_{i-1,i}(x)(1,0) & x \in [A_{i-1}A_i] \\ \mathbb{I}_{i+1,i}(x)(1,0) & x \in [A_iA_{i+1}] \\ 0 & \text{otherwise}, \end{cases}$$

where $\mathbb{I}_{j,l} : A_jA_l \to [0,1]$ is an affine function with $\mathbb{I}_{j,l}(A_j) = 0$, $\mathbb{I}_{j,l}(A_l) = 1$. Denoting $n_{j,j+1} = (n_{j,j+1}^2, n_{j,j+1}^2)$ the outer normal of the segment A_jA_{j+1} of ∂P, we have

$$\frac{d\lambda_1}{dx_{2i-1}} = -\int_{A_iA_{i-1}} \mathbb{I}_{i-1,i} \left(\frac{\partial u}{\partial n}\right)^2 n_{i-1,i}^1 d\sigma - \int_{A_iA_{i+1}} \mathbb{I}_{i+1,i} \left(\frac{\partial u}{\partial n}\right)^2 n_{i+1,i}^1 d\sigma.$$

In the same way we get

$$\frac{d\lambda_1}{dx_{2i}} = -\int_{A_iA_{i-1}} \mathbb{I}_{i-1,i} \left(\frac{\partial u}{\partial n}\right)^2 n_{i-1,i}^2 d\sigma - \int_{A_iA_{i+1}} \mathbb{I}_{i+1,i} \left(\frac{\partial u}{\partial n}\right)^2 n_{i+1,i}^2 d\sigma.$$

Once we have all these ingredients we can perform the numerical optimization using a standard gradient descent algorithm. The numerical results presented below all support Polya's conjecture for $n \in [5, 15]$. Results are presented in Figure 1.10. In order to evaluate how far these polygons are from being reguular, we compute in each case the standard deviation of the angles (denoted *sa*) and the standard deviation of the lengths of the sides (denoted *sl*).

The numerical results show that it is likely that Polya's conjecture is true also for $n \geq 5$. Despite the fact that we do not have a definite theoretical answer, it is possible to prove that the regular polygons are critical points of the first eigenvalue under area constraint.

Proposition 1.8.3. *For $n \geq 3$ the regular polygon with n sides is a critical point for the first eigenvalue of the Dirichlet Laplace operator among polygons with n sides under area constraint.*

Proof: In the following we denote with $\mathcal{P}_n$ the class of polygons with n sides. It is not difficult to prove that minimizing $\lambda_1(P)$ in $\mathcal{P}_n$ under area constraint is equivalent, up to an homothety, to solving the problem

$$\min_{P \in \mathcal{P}_n} \lambda_1(P) + |P|. \tag{1.8.3}$$

In the following we use this formulation in which we incorporate the constraint in the functional. We note that the first eigenfunction u_1 in the case P is a regular polygon is a H^2 function [59]. This allows us to see that in this case we can write the shape derivative of $\mathcal{G}(P) = \lambda_1(P) + |P|$, which is given by

$$\frac{d\mathcal{G}}{dV}(P) = -\int_{\partial P} \left(\frac{\partial u_1}{\partial n}\right)^2 V.n \, d\sigma + \int_{\partial P} V.n \, d\sigma$$

In the following we let P be the regular polygon which minimizes $\lambda_1(P) + |P|$. Since choosing a vector field V with $V.n = 1$ preserves the regularity of P, we can conclude by the shape derivative formula given above that

$$\int_{\partial P} \left(\frac{\partial u_1}{\partial n}\right)^2 d\sigma = \int_{\partial P} d\sigma = n\ell, \tag{1.8.4}$$

where ℓ is the side-length of the optimal regular polygon P for (1.8.3). We can give an explicit formula for the vector field V. Suppose that P is centered at the origin and has inradius equal to r. Then $V = |x|/r$ has the desired property that $V.n = 1$.

As discussed earlier, all relevant perturbations in the class of polygons can be described by the perturbations of the n vertices. Moreover, each perturbation of a vertex A_i can be expressed as a linear combination of perturbations of the type $A_i + \mu \overrightarrow{A_{i-1}A_i}$, as seen in Figure 1.9. Writing
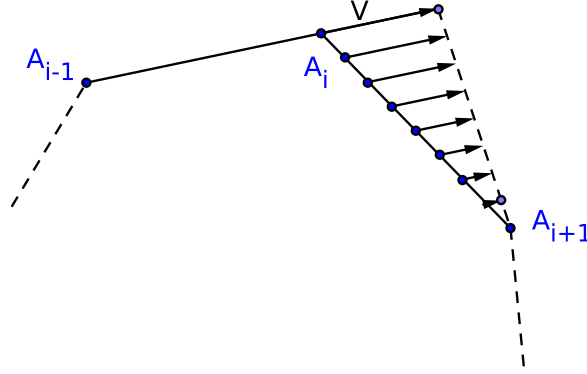
Figure 1.9: Particular vertex perturbation

the expression of the derivative of $\mathcal{G}$ with respect to this perturbation gives us

$$\frac{d\mathcal{G}}{dV}(P) = -\int_0^\ell (\partial_n u_1(p(t/\ell))^2 \frac{\ell - t}{\ell} V.ndt + \int_0^\ell \frac{\ell - t}{\ell} V.ndt,$$

where the parametrization of the side $A_i A_{i+1}$ was chosen $p(s) = (1 - s)A_i + sA_{i+1}$ and n is the normal vector to $A_i A_{i+1}$. Since $V.n$ is constant we conclude that

$$\frac{d\mathcal{G}}{dV}(P) = V.n(-\int_0^\ell (\partial_n u_1(p(t/\ell))^2 \frac{\ell - t}{\ell} dt + \ell/2)$$

Since the first eigenfunction has the same symmetries as the regular polygon we conclude that after a change of variables $t \mapsto \ell - t$ we have

$$\int_0^\ell (\partial_n u_1(p(t/\ell))^2 \frac{\ell - t}{\ell} = \int_0^\ell (\partial_n u_1(p(t/\ell))^2 \frac{t}{\ell} dt = \frac{\int_0^\ell (\partial_n u_1(p(t/\ell))^2 dt}{2} = \frac{\ell}{2},$$

where we used (1.8.4). As a consequence we deduce that $\frac{d\mathcal{G}}{dV}(P) = 0$ for every such particular perturbation V. Since every perturbation of the vertices of the polygon can be written as a linear combination of these simple vertex perturbation, we conclude, by the linearity of the shape derivative, that $\frac{d\mathcal{G}}{dV}(P) = 0$ for every admissible vertex perturbation V. Thus the regular polygon P is a critical point for $\mathcal{G}$.

$\square$

n=5, sl=7e-5, sa=1e-5   n=6, sl=1e-6, sa=1e-6   n=7, sl=3e-6, sa=3e-6   n=8, sl=2e-6, sa=2e-6

n=9, sl=4e-6, sa=3e-6   n=10, sl=3e-3, sa=3e-3   n=11, sl=2e-5, sa=3e-5   n=12, sl=3e-5, sa=3e-5

n=13, sl=2e-5, sa=2e-5   n=14, sl=1e-5,sa=1e-5   n=15, sl=2e-3, sa=2e-3
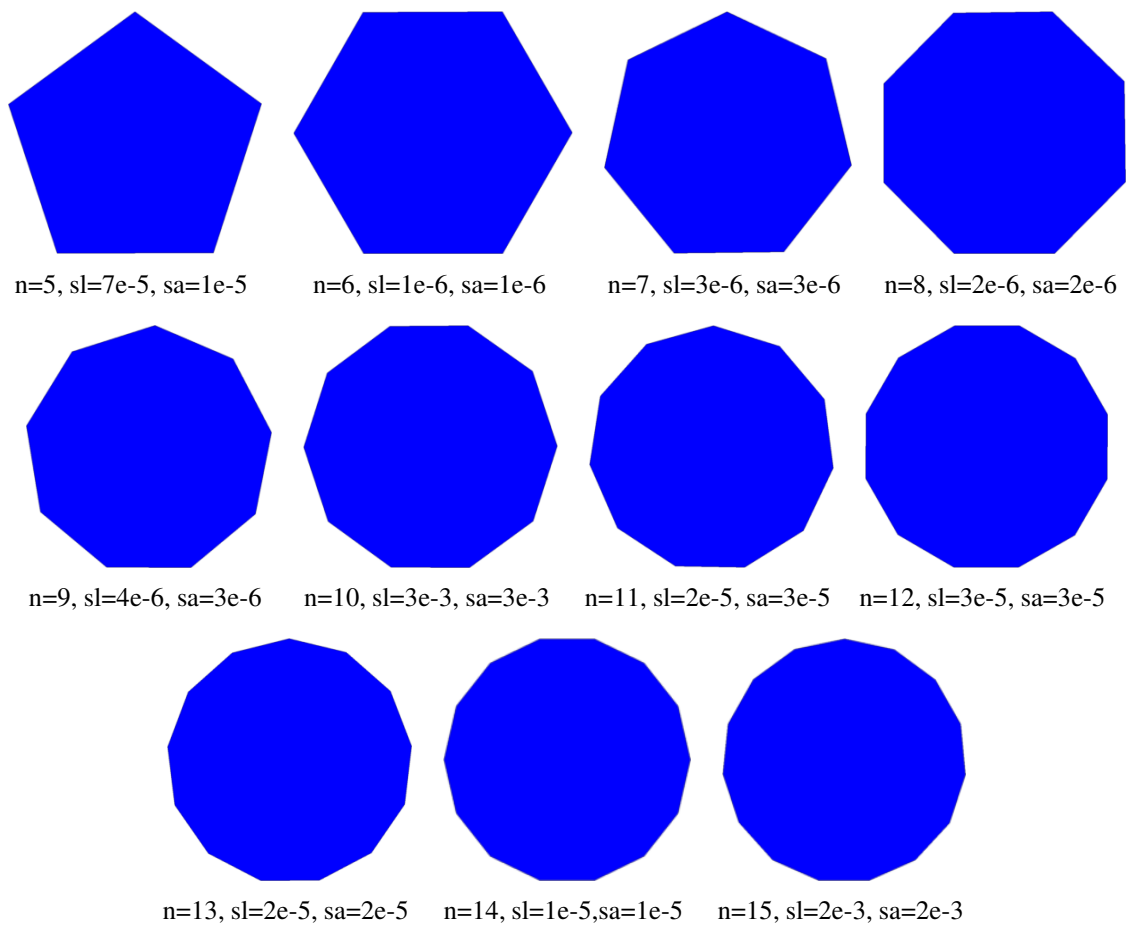
Figure 1.10: Numerical optimizers of λ_1 among polygons for $n \in [5, 15]$

Optimal partitions - anisotropic perimeters

Résumé

Dans ce chapitre on étudie le problème de partitionnement optimal d'un ensemble qui minimise la somme de certains périmètres anisotropes. Un périmètre anisotrope prend en compte les longueurs de façon différente selon la direction considérée. En conséquence, certaines directions sont favorisées. Le problème isopérimétrique est un résultat classique qui dit que si on veut minimiser le périmètre à volume constant, alors l'ensemble optimal est la boule. Si au lieu de minimiser le périmètre classique on minimise un périmètre anisotrope, l'optimiseur peut être différent de la boule. Considérons l'exemple suivant : pour un ensemble bidimensionnel Ω on considère le périmètre anisotrope $\mathrm{Per}_\varphi(\Omega) = \displaystyle\int_{\partial\Omega} \varphi(\vec{n})d\sigma$ avec $\varphi(x) = |x_1| + |x_2|$, $\vec{n}$ la normale sortante à $\partial\Omega$. Pour ce périmètre anisotrope deux directions sont favorisées : la direction horizontale et la direction verticale. Si on veut minimiser $\mathrm{Per}_\varphi(\Omega)$ à aire constante, l'optimiseur est un carré, qui est la forme de Wulff associée à la norme φ.

Comme on peut voir sur ce cas simple, changer le périmètre pour un périmètre anisotrope change complètement la solution du problème. Le cas des partitions en cellules de même aire qui minimisent la somme des périmètres anisotropes est encore plus difficile à traiter théoriquement. Ceci motive la conception d'un algorithme qui permet de calculer les partitions optimales pour des différents périmètres anisotropes.

Gérer les partitions d'un ensemble peut *a priori* être difficile si on considère des paramétrisations individuelles de chaque cellule. On contourne ces difficultés en utilisant une approche par relaxation. Chaque cellule ω_i est remplacée par une approximation φ_i de sa fonction caractéristique. Ici φ est une fonction définie sur le domaine à partitionner D et prend ses valeurs dans $[0, 1]$. La condition "$(\varphi_i)_{i=1}^n$ représente une partition" se traduit simplement en imposant que la somme de toutes fonctions φ_i, $i = 1, ..., n$ soit égale à 1.

Pour pouvoir calculer une approximation d'un périmètre anisotrope d'un ensemble ω_i appro-

ximé par une densité φ_i on a besoin de relaxer le périmètre anisotrope dans ce cadre. Il existe des variantes du théorème de Modica et Mortola pour le cas anisotrope. On donne la preuve d'un résultat de Γ-convergence pour la somme des périmètres anisotropes associés à une partition. On souligne le fait que la Γ-convergence n'est pas stable pour la somme. Le résultat n'est pas une simple conséquence du cas d'une seule phase. Une particularité de ce résultat de Γ-convergence est le fait que l'anisotropie peut dépendre non seulement de la direction, mais aussi de la position de la frontière.

Ce résultat de Γ-convergence nous permet d'implémenter un algorithme de calcul des partitions optimales anisotropes en dimension deux et trois. En utilisant cet algorithme on peut calculer numériquement les partitions optimales pour plusieurs périmètres anisotropes. On observe que dans les résultats, les frontières des ensembles qui forment la partition sont alignées avec les directions favorisées.

En fin de ce chapitre on présente quelques variations du même problème :

- étude numérique des configurations des bulles de savon ;

- partitions minimales pour le périmètre pour des domaines généraux avec une méthode basée sur des éléments finis;

2.1 Introduction

The notion of Γ-convergence was introduced in Definition 1.2.1 and its main properties were stated in Proposition 1.2.2. One classical Γ-convergence result is the Modica Mortola theorem. For the sake of completeness, we rewrite its statement below. For simplicity, we denote

$$X = \{u \in L^1(D) : \int_D u = c\},$$

where $c \in (0, |D|)$ is a fixed constant.

Theorem 2.1.1. *(Modica-Mortola) Let D be a bounded open set and let $W : \mathbb{R} \to [0, \infty)$ be a continuous function such that $W(z) = 0$ if and only if $z \in \{0, 1\}$. Denote $c = 2 \int_0^1 \sqrt{W(s)}ds$. We define $F_\varepsilon, F : L^1(D) \to [0, +\infty]$ by*

$$F_\varepsilon(u) = \begin{cases} \varepsilon \int_D |\nabla u|^2 + \frac{1}{\varepsilon} \int_D W(u) & u \in H^1(D) \cap X \\ +\infty & otherwise \end{cases}$$

and

$$F(u) = \begin{cases} c\,\mathrm{Per}(u^{-1}(1)) & u \in BV(D; \{0, 1\}) \cap X \\ +\infty & otherwise \end{cases}$$

then

$$F_\varepsilon \xrightarrow{\Gamma} F$$

in the $L^1(D)$ topology.
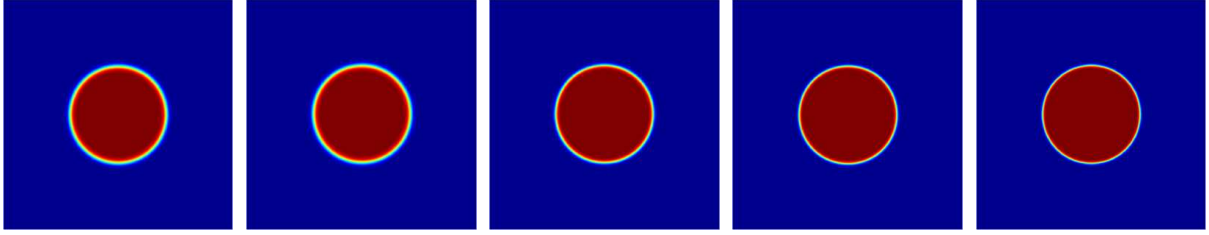
Figure 2.1: Minimizers of F_ε for $c = 1/7$ and $\varepsilon = 1/100, 1/150, 1/200, 1/250, 1/300$. The corresponding cost values are: $1.3089, 1.3216, 1.3276, 1.3311, 1.3398$

The numerical importance of this theorem was just recently observed. Indeed, when one wants to compute numerically the perimeter of a set Ω, the boundary $\partial\Omega$ must be well known. Using a parametric formulation might work if one only has to deal with one set. As soon as we consider multiple shapes which might touch, keeping track of each parametrized boundary is not a simple task. If we want to study a partitioning problem, using a parametric formulation rises difficulties in imposing the non-overlapping condition. This is a point where having a good relaxation for the perimeter, like the theorem mentioned above, becomes really useful.

In the following paragraphs, we take as a toy problem the isoperimetric problem. The third property stated in Proposition 1.2.2 justifies the following numerical approach. In order to approach the set which minimizes the perimeter at fixed volume, we find minimizers m_ε of F_ε for ε smaller and smaller. We expect that the minimizers m_ε approach the minimizer of F. We consider a straightforward finite differences discretization to compute F_ε on a fixed grid $N \times N$ in the unit square $[0,1]^2$. The procedure is as follows:

- Fix an initial ε_0 and a random initial condition, and then compute the numerical minimizer of F_{ε_0};

- Decrease ε and find the numerical minimizer of F_ε starting from the previous minimizer.

- Repeat until ε is small enough.

This simplistic approach has one drawback: the choice of ε_0 cannot be made independent of the grid step. The ε parameter governs the width of the interface between 0 and 1 for the minimizer of F_ε. If ε is less than $1/N$ then the gradient term in F_ε contains meaningless information, since the width of the interface is smaller than the width of the grid. To fix this issue, we start with $\varepsilon_0 \in [1/N, 4/N]$ and whenever we decrease ε we refine the grid and interpolate the initial condition on this new grid. We present the numerical results obtained using this procedure in the case $c = 1/7$. In this case, we know that in two dimensions, the solution of the isoperimetric problem is a disk, and the corresponding perimeter to a disk of area $1/7$ is $2\sqrt{\pi/7} = 1.3398$. Results can be seen in Figure 2.1. It is interesting to note that as ε becomes smaller and smaller, the minimal values of the functionals F_ε converge towards the minimal value of F, as expected.

We can consider the same problem in an anisotropic setting. If we consider a set $\Omega \subset \mathbb{R}^d$ with C^1 boundary, then its perimeter is equal to

$$\text{Per}(\Omega) = \int_{\partial\Omega} d\mathcal{H}^{n-1} = \int_{\partial\Omega} \|\vec{n}(x)\| d\mathcal{H}^{n-1}$$

where $\vec{n}(x)$ denotes the unit outer normal vector corresponding to $x \in \partial\Omega$. Thus, the perimeter treats all directions in the same way and no direction has an advantage over the others. Things change if we pick another norm φ on $\mathbb{R}^d$, different from the euclidean one. We can define the anisotropic perimeter associated to a norm φ by

$$\text{Per}_\varphi(\Omega) = \int_{\partial\Omega} \varphi(\vec{n}).$$

It is possible to prove a variant of the Modica-Mortola theorem in the anisotropic case. Proofs of this result can be found in [19],[20]. A local variant of this result, where the norm φ can also depend on the position of the point can be found in [6].

Theorem 2.1.2. *Let D be a bounded open set and let $W : \mathbb{R} \to [0, \infty)$ be a continuous function such that $W(z) = 0$ if and only if $z \in \{0, 1\}$. Consider φ a norm on $\mathbb{R}^d$. Denote $c = 2 \int_0^1 \sqrt{W(s)} ds$. We define $G_\varepsilon, G : L^1(D) \to [0, +\infty]$ by*

$$G_\varepsilon(u) = \begin{cases} \varepsilon \int_D \varphi(\nabla u)^2 + \frac{1}{\varepsilon} \int_D W(u) & u \in H^1(D) \cap X \\ +\infty & \textit{otherwise} \end{cases}$$

and

$$G(u) = \begin{cases} c \, \text{Per}_\varphi(u^{-1}(1)) & u \in BV(D; \{0, 1\}) \cap X \\ +\infty & \textit{otherwise} \end{cases}$$

then

$$G_\varepsilon \xrightarrow{\Gamma} G$$

in the $L^1(D)$ topology.

We repeat the same experiment as in the isotropic case. Pick $\varphi(x) = |x_1| + |x_2|$, a norm which favorizes the vertical and horizontal directions. Then the shape which minimizes $\text{Per}_\varphi(\Omega)$ with area constraint, the so-called Wulff shape associated to φ, is a square. When $c = 1/7$ the optimal value is $4/\sqrt{7} = 1.5118$. In Figure 2.2 we present the optimizers of G_ε for decreasing values of ε and we observe the same convergence behavior. We observe that the convergence speed is not as fast as in the case of the circle, but this may be due to the fact that in our case φ is not differentiable on the coordinate axes.

The next step is to consider partitioning problems. A famous result due to Hales [60] is the fact that, asymptotically, every partition of the plane into sets of unit areas has perimeter greater than the hexagonal honeycomb tiling. In $\mathbb{R}^3$ the problem of finding the optimal tilling with respect to the perimeter using shapes of equal volume is still open. Kelvin conjectured that
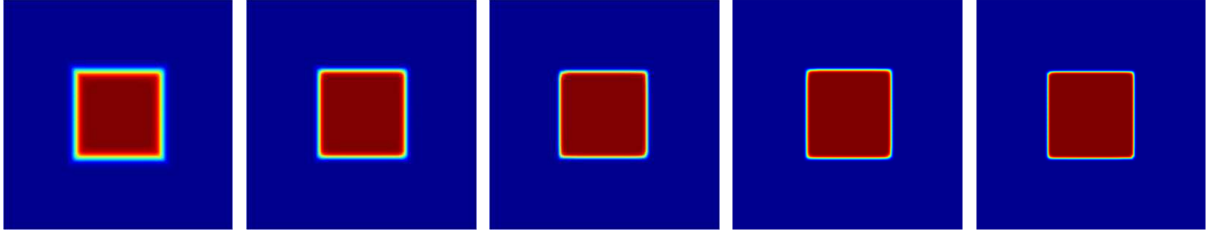
Figure 2.2: Minimizers of G_ε for $c = 1/7$ and $\varepsilon = 1/100, 1/150, 1/200, 1/250, 1/300$. The corresponding cost values are: $1.4851, 1.4914, 1.4979, 1.5031, 1.5049$

truncated octahedra may be optimal, but Weaire and Phelan [92] found a better tiling than the one of Kelvin. The study of the partitions which minimize the sum of anisotropic perimeters is even more challenging, since the optimal partition depends on the norm φ. This motivates the interest in providing efficient numerical algorithms which compute the optimal partitions.

One such method was developed by É. Oudet in [80] in the case of partitions minimizing the sum of perimeters of the cells in two and three dimensions. The author uses a generalization of the Modica-Mortola theorem to the case of partitions. The partition condition, in this functional case, is realized by imposing that the density functions $u_1, u_2, ..., u_n$, corresponding to the cells of the partition, satisfy the relation $u_1 + u_2 + ... + u_n = 1$. Note that this last condition is not too difficult to implement from a numerical point of view. With this framework, the author was able to recover the result of Hales in the periodic case in 2D. In three dimensions, the numerical optimizer was close to the Weaire-Phelan structure.

In this chapter we provide an extension of this numerical framework in the anisotropic case. First we provide a Γ-convergence result which generalizes Theorem 2.1.2 to the partition case. As always, we underline the fact that the Γ-convergence is not stable for the sum, so the result is not trivial. In fact, the (LI) property in the definition of the Γ-convergence comes at once from the one phase case, while the (LS) property requires a bit of work. In order to construct a recovery sequence, we use an approximation result proven by Baldo [11], which states that we can approximate well enough every admissible partition by a polygonal partition.

In the end, we present some numerical computations, for different anisotropy choices, and we observe the desired behavior: partition cells tend to have their boundaries aligned with the favorized directions. Although the theoretical framework is restricted to the case where φ is a norm, and thus, is convex, we observe numerically that non-convex anisotropies also produce the expected results and the rate of convergence is much higher in some cases. We may extend the finite difference method to non-rectangular domains by using only the nodes of the finite difference grid which lie inside the considered shape. We are able to improve some of the results of É. Oudet [80], notably when the number of the cells of the partition is high. Working with this finite differences approach allows us to study anisotropic partitions on non-rectangular domains. We also provide a different framework, based on finite elements, in order to study partitions of non-rectangular domains into equal area cells. Our results are comparable with

those obtained by Cox and Flikkema in [39]. This finite element approach has the advantage that it may be applied whenever we have a qualitative triangulation of the domain. This fact motivates the extension of this study to three dimensional surfaces in Chapter 5.

2.2 Main Results

We consider the following definition of the generalized perimeter, valid for every measurable set $D \subset \mathbb{R}^d$.

$$\mathrm{Per}(\Omega, D) = \sup\{\int_\Omega \mathrm{div}\, g dx : g \in C_0^\infty(D; \mathbb{R}^d), \|g\|_\infty \leq 1\}$$

This definition agrees with the classical one in the case Ω has a certain regularity (polyhedra, piecewise C^1, etc). Given a norm φ on $\mathbb{R}^d$ we can extend the above variational characterization to the anisotropic perimeter associated to φ by

$$\mathrm{Per}_\varphi(\Omega, D) = \sup\{\int_\Omega \mathrm{div}\, g dx : g \in C_0^\infty(D; \mathbb{R}^d), \varphi(g) \leq 1\}.$$

We make the assumption that φ is comparable with the Euclidean norm, i.e. there exist constants $c, C > 0$ such that $c|x| \leq \varphi(x) \leq C|x|$. Then if a set E has $\mathrm{Per}_\varphi(E, \Omega) < \infty$ then $\chi_E \in BV(\Omega)$, the space of functions of bounded variation on Ω.

Furthermore, we can choose norms which depend on the position of the considered point: $\varphi : D \times \mathbb{R}^N$ which are lower semicontinuous, positively 1-homogeneous and convex in the second variable. In addition, we assume the existence of $0 < m \leq M$ such that $m|\xi| \leq \varphi(x, \xi) \leq M|\xi|$ for every $(x, \xi) \in D \times \mathbb{R}^N$. Then a local anisotropic perimeter can be defined as follows

$$\mathrm{Per}_\varphi(\Omega, D) = \sup\{\int_\Omega \mathrm{div}\, g dx : g \in C_0^\infty(D; \mathbb{R}^d), \varphi(x, g(x)) \leq 1\}.$$

The purpose of the following paragraphs is to approximate by Γ-convergence the sum of the anisotropic perimeters of a partition of a bounded, open set D into n parts of equal volumes. We want to be able to have a result which is also valid for local anisotropies, where the norm φ, which determines the anisotropy may also depend on the point x. The Γ-convergence result is divided in two parts, corresponding to the two properties in its definition. The (LI) property can be deduced by studying the one phase case. The (LS) property needs some work in order to construct a suitable recovery sequence.

The double-well potential W is stated in a general form in the theorem, but we will assume that it has additional properties. In practice we use $W(s) = s^2(1-s)^2$, but we are only interested of the form of W in a neighborhood of $[0, 1]$. Therefore, we assume that W is bounded (by truncating it at a large level, if necessary). In order to simplify the construction of the recovery sequence, we assume that the graph of W is symmetric with respect to the line $x = 1/2$. The theorem stated below is a particular case of the one studied in [6]. We give a slightly different proof, and adapt it to the case of partitions.

Theorem 2.2.1. *Let D be an open, bounded domain in $\mathbb{R}^N$, and $f : D \times \mathbb{R}^N \to [0, \infty]$ be a lower semicontinuous function, positively 1-homogeneous and convex in the second variable, which satisfies $m|\xi| \le \varphi(x, \xi) \le M|\xi|$ for every $(x, \xi) \in D \times \mathbb{R}^N$, with $0 < m \le M$. We consider $W : \mathbb{R} \to [0, \infty)$ such that $W(0) = W(1) = 0$ and $W(x) > 0$ for $x \notin \{0, 1\}$. Define $F_\varepsilon, F : L^1(D) \to [0, \infty]$ as follows:*

$$F_\varepsilon(u) = \begin{cases} \varepsilon \displaystyle\int_D \varphi(x, \nabla u(x))^2 dx + \frac{1}{\varepsilon} \int_D W(u(x)) dx & \text{if } u \in H^1(D), \displaystyle\int_D u = c \\ +\infty & \text{otherwise} \end{cases}$$

$$F(u) = \begin{cases} c \displaystyle\int_{S(u)} \varphi(x, \nu_u) & \text{if } u \in BV(D, \{0, 1\}), \displaystyle\int_D u = c \\ +\infty & \text{otherwise} \end{cases}$$

where $c = 2 \int_0^1 W(s)^{1/2} ds$ and $S(u)$ is the jump set of u.

Then for every $u \in L^1(D)$ and every $(u_\varepsilon) \in L^1(D)$ such that $(u_\varepsilon) \to u$ in $L^1(D)$ we have

$$\liminf_\varepsilon F_\varepsilon(u_\varepsilon) \ge F(u).$$

Proof: This result follows naturally from the following remarks and from a variant of Reshetnyak's semicontinuity theorem.

Consider the function $\phi(t) = 2 \int_0^t W(s)^{1/2} ds$, which is Lipschitz continuous, in view of the fact that we assume that W is bounded above. In the following we show that $F(u) = \int_D \varphi(x, D(\phi \circ u))$, where we use the notation

$$\int_D \varphi(x, \mu) = \int_\Omega \varphi\left(x, \frac{d\mu}{d|\mu|}\right) d|\mu|,$$

for every Radon measure $\mu \in \mathcal{M}(D, \mathbb{R}^N)$. First note that if $u \in BV(D, \{0, 1\})$ then using the definition of the variation of a BV function we can see that $D(\phi \circ u) = \phi(1)Du$. Moreover, if we have a function $u \in BV(D)$ whose image contains only two real values, then the absolutely continuous part and the Cantor part of Du are zero, while the jump part is

$$D^j u(B) = \int_{B \cap S(u)} (u^+ - u^-) \nu_u d\mathcal{H}^{N-1}$$

where ν_u is the normal to the jump set $S(u)$ defined by $Du = \nu_u|Du|$. In this case, where $u \in \{0, 1\}$ a.e. we also have $Du = d\mathcal{H}^{N-1} \llcorner S(u)$. For details see [19]. Having these in mind and using the fact that φ is homogeneous of degree one in the second variable, we obtain

$$c \int_{S(u)} \varphi(x, \nu_u) d\mathcal{H}^{N-1} = c \int_\Omega \varphi\left(x, \frac{dDu}{d|Du|}\right) d\mathcal{H}^{N-1} \llcorner S(u)$$

$$= \phi(1) \int_\Omega \varphi\left(x, \frac{dDu}{d|Du|}\right) d|Du| = \int_\Omega \varphi\left(x, \frac{dD(\phi \circ u)}{d|D(\phi \circ u)|}\right) d|D(\phi \circ u)|$$

$$= \int_D \varphi(x, D(\phi \circ u)).$$

The following variant of Reshetnyak lower semicontinuity theorem can be found in [7, Theorem 2.38].

Theorem 2.2.2. *Let D be an open subset of $\mathbb{R}^N$ and μ, μ_n be $\mathbb{R}^n$-valued finite Radon measures in D. If $\mu_n \to \mu$ weakly* in D then*

$$\int_D f(x, \mu) \leq \liminf_{n \to \infty} \int_D f(x, \mu_n),$$

for every lower semicontinuous function $f : \Omega \times \mathbb{R}^n \to [0, \infty]$, positively 1-homogeneous and convex in the second variable.

First, let's note that the integral condition is preserved under $L^1(D)$ convergence, since

$$\left| \int_D u_\varepsilon - \int_D u \right| \leq \|u_\varepsilon - u\|_{L^1(D)}.$$

Since ϕ is Lipschitz continuous, $u_\varepsilon \to u$ in $L^1(D)$ implies that $\phi \circ u_\varepsilon \to \phi \circ u$ in $L^1(D)$. If we suppose that $\liminf_{\varepsilon \to 0} F_\varepsilon(u_\varepsilon) < +\infty$ (else there is nothing to prove) then, using the standard inequality $a + b \geq \sqrt{ab}$, we get that $F_\varepsilon(u_\varepsilon) \geq 2 \int_D \varphi(x, D(\phi \circ u_\varepsilon) \geq 2m \int_D D(\phi \circ u_\varepsilon)$. Therefore, we can assume that $\sup |D(\phi \circ u_\varepsilon)|(D) < +\infty$. According to [19, Definition 1.41, Remark 1.42] we can conclude that $D(\phi \circ u_\varepsilon) \rightharpoonup D(\phi \circ u)$ weakly* in $\mathcal{M}(D, \mathbb{R}^N)$ and Theorem 2.2.2 is applicable:

$$\liminf_{\varepsilon \to 0} F_\varepsilon(u_\varepsilon) \geq \liminf_{\varepsilon \to 0} 2 \int_D \varphi(x, \nabla u_\varepsilon) W(u_\varepsilon)^{1/2}$$
$$= \liminf_{\varepsilon \to 0} \int_D \varphi(x, \mathbf{D}(\phi \circ u_\varepsilon)) \geq \int_D \varphi(x, \mathbf{D}(\phi \circ u)) = F(u).$$

The construction of the recovery sequence is treated in the next theorem. It is inspired from [19]. $\qquad\square$

We are now able to state the Γ-convergence result concerning the partition case. We use the notation

$$X = \left\{ (u_i) \in L^1(D)^n : \int_D u_i = \frac{1}{n}, \ \sum_{i=1}^n u_i = 1. \right\}$$

We assume that the potential W satisfies the following properties:

- W satisfies the hypotheses of Theorem 2.2.1.

- $W(0.5 - t) = W(0.5 + t)$ for every $t \in \mathbb{R}$.

- W is bounded above.

We also assume that $\varphi : D \times \mathbb{R}^N \to [0, \infty)$ satisfies the hypotheses of Theorem 2.2.1 and that it is Lipschitz continuous in the first variable. We use the following bold notation to denote vectors of functions: $\mathbf{u} = (u_i) \in L^1(D)^n$.

In the following, we consider $X \subset L^1(D)^n$ to be the space containing the n-uples of function satisfying the partition condition and the area constraints:

$$X = \{\mathbf{u} \in L^1(D)^n : \int_D u_i = \frac{|D|}{n}, \ u_1 + ... + u_n = 1 \text{ in } D\}.$$

We note the fact that the proofs which follow do not change much if instead of the equal areas conditions we put only a fixed area condition on every one of the phases.

Theorem 2.2.3. *We consider the functionals $F_\varepsilon, F : (L^1(D))^n \to [0, \infty]$, defined by*

$$F_\varepsilon(\mathbf{u}) = \begin{cases} \sum_{i=1}^n \left(\varepsilon \int_D \varphi(x, \nabla u_i)^2 + \frac{1}{\varepsilon} \int_D W(u_i) \right) & \text{if } \mathbf{u} \in (H^1(D))^n \cap X \\ +\infty & \text{otherwise} \end{cases}$$

$$F(\mathbf{u}) = \begin{cases} \sum_{i=1}^n c \int_{S(u_i)} \varphi(x, \nu_{u_i}) & \text{if } \mathbf{u} \in (BV(D, \{0,1\}))^n \cap X \\ +\infty & \text{otherwise} \end{cases}$$

Then $F_\varepsilon \xrightarrow{\Gamma} F$ in the $(L^1(D))^n$ topology.

Proof: The (LI) part of this result follows at once from Theorem 2.2.1.

For the (LS) part we need to be able to construct a recovery sequence for every $\mathbf{u} \in L^1(D)$ such that $F(\mathbf{u}) < +\infty$. In order to do this, we reduce the problem to subset $\mathcal{D} \subset \{F < +\infty\}$ which is dense and has some good regularity properties. This is a classical procedure described in Proposition 1.2.3 and [19]. One such suitable dense class is provided by Baldo in [11] and consists of functions $\mathbf{u} \in BV(D, \{0,1\})^n \cap X$ which represent partitions of D into polygonal domains.

The result of Baldo says that for every $\mathbf{u} \in (BV(D, \{0,1\}))^n \cap X$ there exists a sequence $\mathbf{u}_n \in (BV(D, \{0,1\}))^n \cap X$ such that $\mathbf{u}_n \to \mathbf{u}$ in $(L^1(D))^n$, each component of $\mathbf{u}_n$ represents a set of finite perimeter, $\mathbf{Du}_n^i \rightharpoonup \mathbf{Du}^i$ weakly* in $\mathcal{M}(D, \mathbb{R}^N)$ and $|\mathbf{Du}_n^i|(D) \to |\mathbf{Du}^i|(D)$ (the corresponding perimeters converge). The Reshetnyak continuity theorem found in [7, Theorem 2.39] assures us that $F(\mathbf{u}_n) \to F(\mathbf{u})$. Thus, we can restrict our attention to functions $\mathbf{u}$ which represent partitions of D into polygonal domains of equal areas.

We consider the optimal profile problem

$$c = \min \left\{ \int_R (W(v) + |v'|^2) dt : v(-\infty) = 0, v(+\infty) = 1 \right\}$$

and the related problem

$$zc = \min \left\{ \int_R (W(v) + z^2 |v'|^2) dt : v(-\infty) = 0, v(+\infty) = 1 \right\} \tag{2.2.1}$$

Note that the solution of (2.2.1) satisfies the differential equation $v' = \sqrt{W(v)}/z$ and for symmetry reasons, we impose the initial condition $v(0) = 1/2$. Note that v is strictly increasing, and $v(t) \geq 1/2$ for $t \geq 0$. It is not difficult to see that $c = 2 \int_0^1 \sqrt{W(s)} ds$.
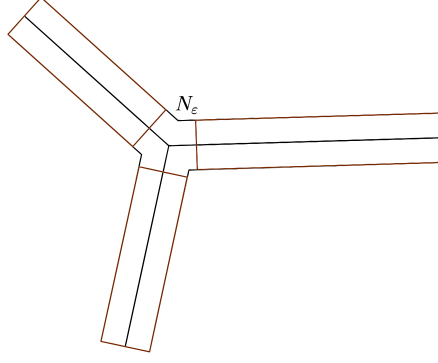
Figure 2.3: Example of a part of N_ε

Take v a solution to problem 2.2.1. We modify v such that it goes from 0 to 1 on a finite length interval in the following way (inspired from [20]):

$$v^\eta = \min\{\max\{0, (1 + 2\eta)v - \eta\}, 1\}.$$

We have

$$c^\eta = \int_\mathbb{R} (W(v^\eta) + |(v^\eta)'|^2) \to c \text{ as } \eta \to 0.$$

We denote $(\Omega_i)_{i=1}^n$ the polygonal partition determined by $\mathbf{u}$. We denote by N_ε the set of points which are close to triple (or multiple) points of the partition (Ω_i), such that

$$\{x \in D : d(x, \partial\Omega_i) < \varepsilon\} \setminus N_\varepsilon,$$

is a union of rectangles. An example is given in Figure 2.3.

In the following, we denote by $v_{\vec{n}}$ the optimal profile with $z = \varphi(\vec{n})$. We use the signed distance $d_E(x) = d(x, D \setminus E) - d(x, E)$ and define u_ε^i on $D \setminus N_\varepsilon$ by

$$u_\varepsilon^i(x) = \begin{cases} v_{\nabla d_{\Omega_i}(x)}^\eta \left(\frac{d_{\Omega_i}(x)}{\varepsilon}\right) & \text{if } |d_{\Omega_i}(x)| \leq T\varepsilon \\ 0 & \text{otherwise in } D \setminus \Omega_i \\ 1 & \text{otherwise in } \Omega_i \end{cases}$$

where T is great enough such that the support of $(v^\eta)'$ is contained in $[-T, T]$. Until here, u_ε is a Lipschitz continous function with values in $[0, 1]$ and a Lipschitz constant of order $1/\varepsilon$. We extend each u_ε^i to the whole D with the same Lipschitz constant (this is possible by Kirszbraun's theorem, see [51]).

In order that $\mathbf{u}_\varepsilon \in X$ we must treat the measure and the sum constraints. We deal with the sum constraint first. We have three types of points:

- $|d_{\Omega_i}(x)| > T\varepsilon$ for all i. Here the sum constraint is clear, since one component takes value 1 and the rest 0.

- There exist precisely 2 indexes i, j such that $|d_{\Omega_i}(x)|, |d_{\Omega_j}(x)| \leq T\varepsilon$. Here the symmetry of the optimal profile assures us that the $u_\varepsilon^i(x) + u_\varepsilon^j(x) = 1$, while the other components take the value 0.

- The points in N_ε.

We see that the only problems that can occur take place in N_ε. Here, we replace u_ε^i by $u_\varepsilon^i / (\sum_{j=1}^n u_\varepsilon^j)$. This operation is well defined, since each u_ε^i is greater than $1/2$ on Ω_i; thus their sum is always greater than $1/2$. Furthermore, doing this change still leaves the gradient of u_ε^i of the form $O(1/\varepsilon)$.

In the following we omit the substript from $v_{\nabla d_{\Omega_i}(x)}$, and we may do so without loss of generality, since the inequalities described below do not use this dependence until the last few inequalities. Because of the fact that u_ε^i varies only in the direction of the normal to Ω_i on $D \setminus N_\varepsilon$, we find that $\nabla u_\varepsilon^i(x)/|\nabla u_\varepsilon^i(x)|$ is a unit normal to Ω_i.

The integral constraints can be imposed in one of the following ways:

- by slightly moving the initial boundaries of (Ω_i) and then performing the algorithm described above.

- by performing the procedure described in [71]. We modify each phase in a ball of fixed, small enough size, which depends on ε in order to fix the volume constraints. In the end we note that these perturbations vanish in the limit.

We split the (LS) estimate in two parts, one on N_ε and one on $D \setminus N_\varepsilon$.

$$\int_{N_\varepsilon} \left(\varepsilon\varphi(x, \nabla u_\varepsilon^i)^2 + \frac{1}{\varepsilon}W(u_\varepsilon^i) \right)$$
$$\leq \frac{|N_\varepsilon| \max_{[0,1]} W}{\varepsilon} + \frac{|N_\varepsilon| \varepsilon \sup_{\mathbb{R}} |(v^\eta)'|^2 \sup_{\|\vec{n}\|=1} \varphi(x, \vec{n})^2}{\varepsilon} = O(\varepsilon),$$

since $|N_\varepsilon| = O(\varepsilon^2)$. This proves that the part corresponding to N_ε is negligible int the (LS) estimate.

We continue our estimate on $D \setminus N_\varepsilon$:

$$\int_{D\setminus N_\varepsilon} \left(\varepsilon\varphi(x, \nabla u_\varepsilon^i)^2 + \frac{1}{\varepsilon}W(u_\varepsilon^i) \right)$$
$$= \int_{D\setminus N_\varepsilon} \left(\varepsilon\varphi^2(x, \nabla u_\varepsilon/|\nabla u_\varepsilon|)|\nabla u_\varepsilon|^2 + \frac{1}{\varepsilon}W(v^\eta(d_{\Omega_i(x)}(x))/\varepsilon) \right)$$
$$= \int_{-T\varepsilon}^{T\varepsilon} \int_{\{d(x)=t\}\setminus N_\varepsilon} \left(\varepsilon\varphi^2(x, \nu_{\mathbf{u}^i})\frac{|(v^\eta)'(t/\varepsilon)|^2}{\varepsilon^2} + \frac{1}{\varepsilon}W(v^\eta(d_{\Omega_i(x)}(x))/\varepsilon) \right) d\mathcal{H}^{N-1}(x)dt$$
$$= \int_{S(\mathbf{u}_\varepsilon^i)\setminus N_\varepsilon} \int_{-T\varepsilon}^{T\varepsilon} \left(\frac{1}{\varepsilon}W(v^\eta(t/\varepsilon)) + \frac{1}{\varepsilon}\varphi^2(x, \nu_{\mathbf{u}_i}(x))|(v^\eta)'(t/\varepsilon)|^2 \right) dtd\mathcal{H}^{N-1}(x) + O(\varepsilon)$$
$$= \int_{S(\mathbf{u}_\varepsilon^i)\setminus N_\varepsilon} \int_{-T}^{T} \left(W(v^\eta(t)) + \varphi^2(x, \nu_{\mathbf{u}_i}(x))|(v^\eta)'(t)|^2 \right) dtd\mathcal{H}^{N-1}(x) + O(\varepsilon)$$

$$\leq c^\eta \int_{S(\mathbf{u}^i)} \varphi(x, \nu_{\mathbf{u}_i}) d\mathcal{H}^{N-1} + O(\varepsilon).$$

We have used the co-area formula. The fact that φ is Lipschitz continuous in the first variable allows us to write estimates of the form $\varphi(y, \xi) \leq \varphi(x, \xi) + L|x - y|$, and this is why we have an $O(\varepsilon)$ term after we change the order of integration. The (LS) property comes from summing the estimates obtained for every $(\mathbf{u}_\varepsilon^i)$.

2.3   Numerical Results

One of the main properties of the Γ-convergence is the fact that if $F_\varepsilon \xrightarrow{\Gamma} F$ then any limit point of a sequence (x_ε) of minimizers of F_ε is a minimizer for F. Based on this property, we assume that minimizing F_ε for ε small enough will get us close to a minimizer of F.

We want to approximate numerically partitions which minimize the sum of their anisotropic perimeters, with respect to some anisotropy φ. In order to do this, we search numerically for minimizers of

$$F_\varepsilon(\mathbf{u}) = \sum_{i=1}^n \left(\varepsilon \int_D \varphi(x, \nabla u_i)^2 + \frac{1}{\varepsilon} \int_D W(u_i) \right) \tag{2.3.1}$$

Using the fact that $\varphi(x, \xi) \geq c|\xi|$ for a constant $c > 0$, we deduce that if $\mathbf{u_n}$ is a minimizing sequence for F_ε then $(\nabla \mathbf{u}_n^i)$ is bounded in $L^2(D)$. Truncating $(\mathbf{u}_n)$ between 0 and 1 decreases $F_\varepsilon(\mathbf{u}_n)$, so $(\mathbf{u}_n)$ is also bounded in $L^2(D)^n$. Thus $(\mathbf{u}_n)$ is bounded in $H^1(D)^n$, which means that it has a subsequence which converges weakly H^1 to $\mathbf{u}$. The convexity of φ and the Fatou Lemma imply that

$$\liminf_{n \to \infty} F_\varepsilon(\mathbf{u}_n) \geq F(\mathbf{u}),$$

which means that (2.3.1) has a minimizer in $H^1(D)^n$. The lack of convexity of the potential W does not allow us to conclude that the minimizer is unique. In fact, domain symmetry and permutations of phases always lead to multiple optimizers.

We can devise an algorithm to approximate numerically such a minimizer. We discretize the unit square $D = [0, 1]^2$ using a finite differences grid, and use quadrature formulas to compute the integrals in the expression of F_ε. The choice of ε is important in order to have meaningful results. Morally, ε dictates the width of the interface between the sets $\{u_i = 0\}$ and $\{u_i = 1\}$, and it cannot be lower than the width of the discretization grid. Satisfactory results have been obtained for $\varepsilon \in [\frac{1}{N}, \frac{4}{N}]$. Note that if ε is large then the diffusion interface is bigger, and therefore the shapes can move more freely in order to find their optimal position. Forcing ε small in the beginning may lead to a local minimum. In order to diminish the size of the interface, we can iterate the optimization algorithm by decreasing ε.

We observe that the behavior of the algorithm depends heavily on the choice of φ. We have many options to choose the anisotropy φ:

- $\varphi(x) = |x_1| + |x_2|$ - horizontal and vertical directions;
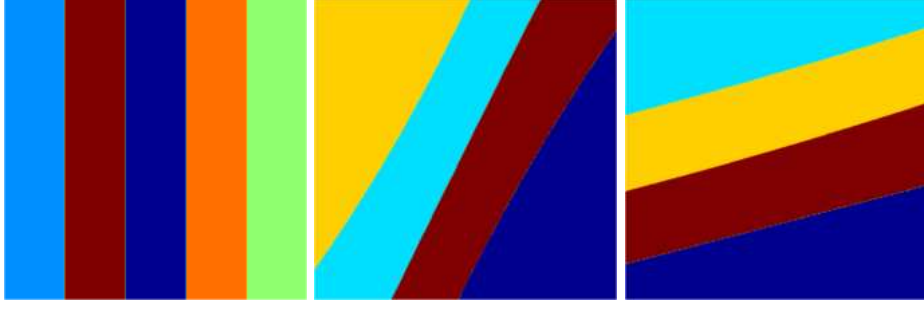
Figure 2.4: Examples of optimal partitions with one favorized direction

- $\varphi(x) = (|x_1|^p + |x_2|^p)^{1/p}$

- $\varphi(x) = |ax_1 + bx_2| + |cx_1 + dx_2|$ - variable directions corresponding to a, b.

- $\varphi(x) = (ax_1^2 + bx_2^2)^{1/2}$ with $a > b$: favorize one of the directions corresponding to coordinate axes.

We present below some numerical results we obtained using various norms and parameters.

The first example we study is the case where we have one favorized direction. Favorizing one direction parallel to the coordinate axis is not hard. It is enough to use a weighted norm like $\varphi(x) = \sqrt{x_1^2 + 100x_2^2}$ to favorize the vertical direction. Indeed, looking at the term $\int_D \varphi(\nabla u)$ we see that if the gradient ∇u has a second component which is large, then the quantity $\varphi(\nabla u)$ is large. Thus, in order to minimize our functional, the gradient of u should be close to zero in the second component. Thus u is close to a constant on each vertical line, and all boundaries will be vertical at the optimum. In order to favorize a general direction, one could use a rotation of the coordinate axis included in the norm. A few examples of optimal partitions with one favorized direction can be seen in Figure 2.4.

The next interesting situation is the case of two favorized directions. Since we work on rectangular domains, it is natural to consider vertical and horizontal favorized directions. This can be achieved using the ℓ^1 norm $\varphi(x) = |x_1| + |x_2|$. Another way of favorizing these two direction is presented below.

One natural way to favorize a direction corresponding to a coordinate axis is to use a norm of the form

$$\varphi(x) = \sqrt{ax_1^2 + bx_2^2},$$

with $a > b$. In order to favorize two directions we can think of using something of the form

$$\varphi(x) = \sqrt[4]{(100x_1^2 + x_2^2)(x_1^2 + 100x_2^2)}.$$

The problem with the above choice of φ is the lack of convexity, which goes out of the Γ-convergence framework of the theoretical result. Nevertheless, we observe that despite this non-convexity issue we obtain the same results as in the case of the ℓ^1 norm. Moreover, the convergence is accelerated in the case of the non-convex φ. We present in Figure 2.5 the partitions
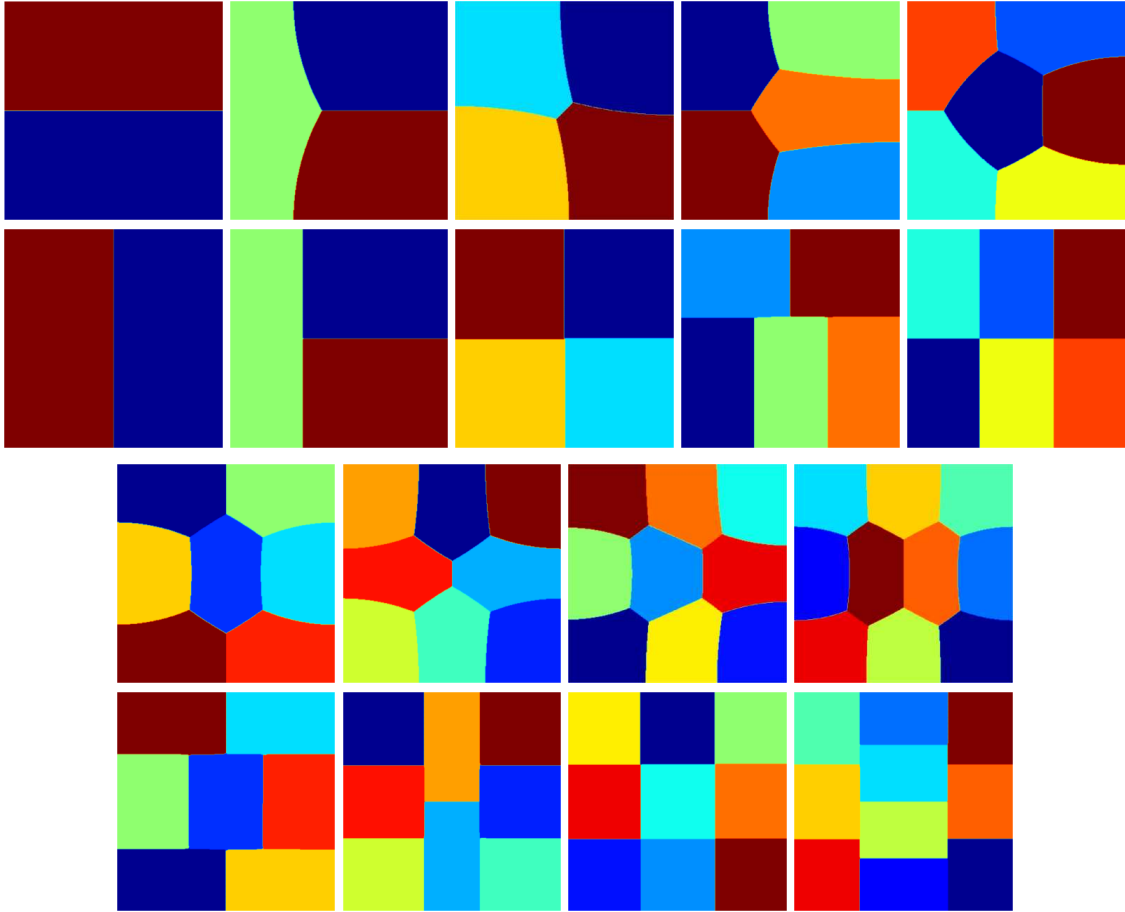
Figure 2.5: Optimal partitions obtained for $N \in [2, 10]$. The isotropic case (up) and the anisotropic case corresponding to $\varphi(x) = |x_1| + |x_2|$ (down)

of the unit square corresponding to the classic perimeter and the ones obtained favorizing horizontal and vertical directions. Since the results we obtained are all partitions of the square in rectangles of equal areas, we may ask if these rectangle configurations are optimal. The answer is yes, and the problem of partitioning a square into rectangles of equal areas which minimize their total perimeter has been completely answered in [68].

As in the case of one favorized direction, we can favorize any desired direction by introducing a suitable rotation in the formulation of the norm. For example, one can favorize the directions corresponding to the two axis bisectors by considering

$$\varphi(x) = |x_1 + x_2| + |x_1 - x_2|.$$

We can continue our study by considering three favorized directions. The choice of the norms is similar, but involving three directions instead of two. As before, we notice a faster convergence when considering non-convex variants of φ. This behavior could be attributed to the fact that in the non-convex case, the boundaries align immediately to the favorized directions, since along these directions the functional has much lower values. In Figure 2.7 you can see some plots of some of functions φ we considered, on the unit square. In these picture you can clearly see the favorized directions as the directions along which the lowest values can be found. In the
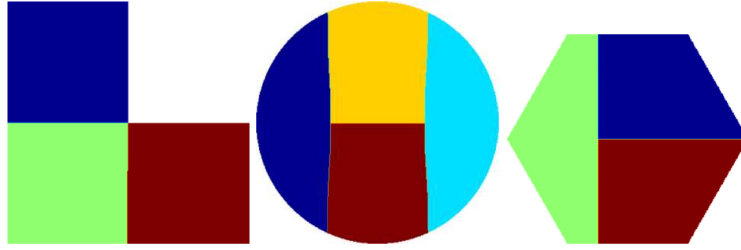
Figure 2.6: Examples of optimal partitions with two favorized directions on general non-rectangular domains
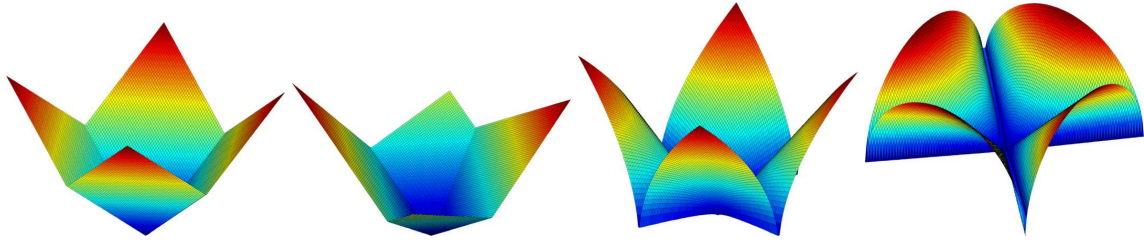
Figure 2.7: Plots of some of the norms we considered, on the unit square. In order left to right:
1. ℓ^1 norm, directions $0, \pi/2$.
2. ℓ^p norm, $p = 1.1$, directions $\pi/6, \pi/2$.
3. Square root of product of two norms, directions $0, \pi/2$.
4. Square root of product of two norms, directions $-\pi/4, \pi/4$.

non-convex cases, these directions are more emphasized. Some further computations involving cases where we have three favorized directions can be found in Figure 2.8.

We can use the finite difference framework in the case of non rectangular domain in the following way. We consider the general domain D as a subset of a rectangular region R. On this rectangular region a finite differences grid is considered. We apply the same algorithm with the difference that we ignore the grid points which are outside the domain D, by assigning them a fixed value zero for the density function and for the gradient of this function. The computation results are not always well behaved near the boundary of D, as expected. We present some of the results obtained on general domains in Figure 2.6. In order to fix the problems regarding the behaviour near ∂D we propose in the next section a different framework based on finite elements.

2.4   Related topics

2.4.1   General two dimensional domains

We want to generalize the numerical framework to non-rectangular domains. In order to do this we use a finite element framework. We consider a triangulation of the domain D and then we construct the mass matrix M and the rigidity matrix K. Since the computation of the quantities in the anisotropic setting is not straightforward to do on non-rectangular grids, we
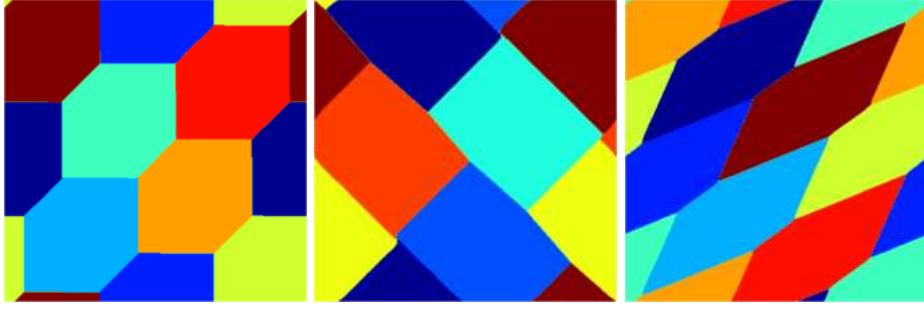
Figure 2.8: Optimal partitions for other anisotropies with two or three favorized directions, under periodicity conditions
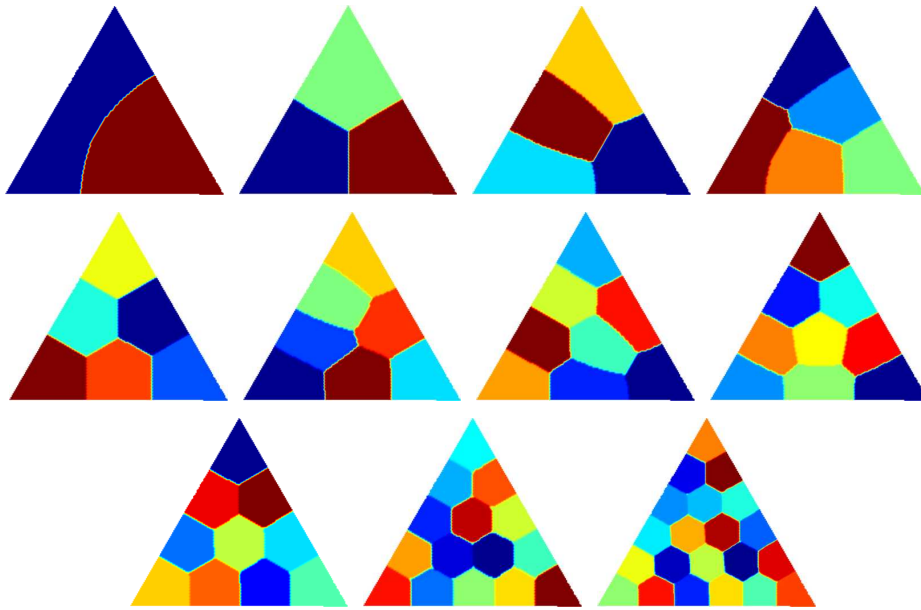

Figure 2.9: Various optimal perimeter partitions with equal area cells for an equilateral triangle

consider mainly the isotropic problem here, with the classic Modica-Mortola functionals. This is a particular case of our main theorem for $\varphi(x, \xi) = |\xi|$ for every $x \in D, \xi \in \mathbb{R}^n$.

The quantity $\int_D |\nabla u|^2$ can be computed using the form $u^T K u$ and the quantity $\int_D u^2 (1-u)^2$ can be computed using the form $v^T M v$ where $v = u \otimes (1-u)$ (pointwise multiplication). The meshes are constructed by hand, when possible, or using the software DistMesh [77]. We are able, in this way, to improve previous results due to Oudet [80], and we obtain a good correspondence with the ones provided by Cox and Flikkema in [39]. We present some numerical candidates in the case of the equilateral triangle (Figure 2.9), the circle (Figure 2.10), the regular pentagon and the regular hexagon (Figure 2.11).

2.4.2 Bubble clusters

It is possible to use the Γ-convergence results presented in this chapter in order to study optimal configurations of bubble clusters. The *bubble cluster problem* can be stated as follows: find the
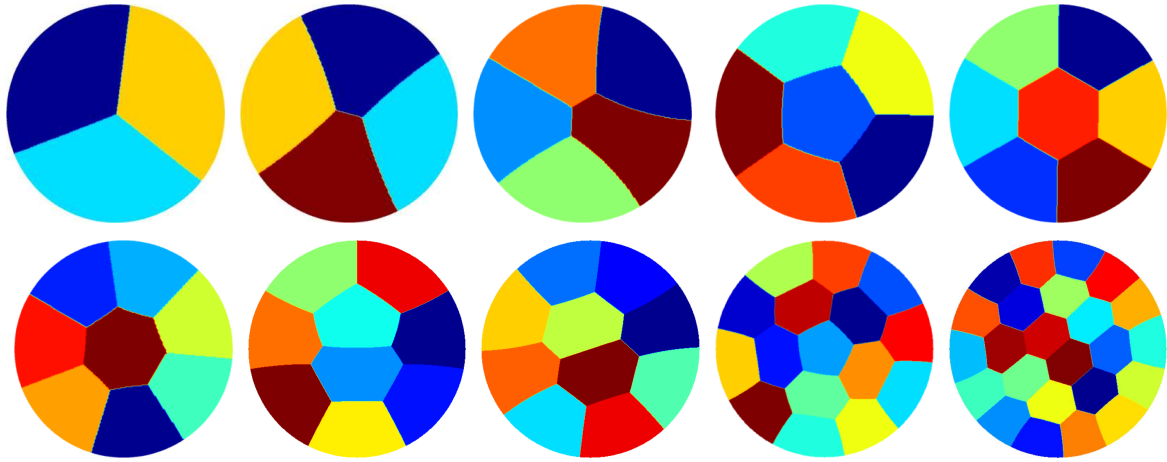
Figure 2.10: Optimal partitions on the circle for $N \in \{3, ..., 10, 16, 24\}$
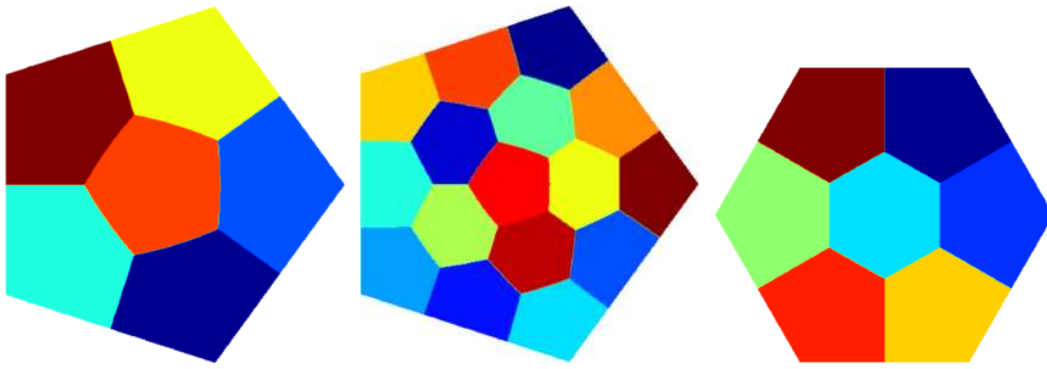

Figure 2.11: Various optimal perimeter partitions with equal area cells for the regular pentagon and the regular hexagon

optimal configuration of sets $\Omega_1, ..., \Omega_n \subset D \subset \mathbb{R}^d$, with prescribed volumes, such that the total $d-1$ dimensional of the boundaries $\mathcal{H}^{d-1}(\partial \Omega_1 \cup ... \cup \partial \Omega_n)$ is minimized. It is not hard to see that this is equivalent to minimize the following quantity:

$$\min \operatorname{Per}(\Omega_1) + ... + \operatorname{Per}(\Omega_n) + \operatorname{Per}(Ext),$$

where Ext denotes the empty space left by (Ω_i) in D. Qualitative properties of an optimal bubble configuration in the plane and on surfaces were given by F. Morgan in [74]. Numerical studies were performed by Cox and Flikkema in [39] using the numerical software Evolver [21]. By using the same Γ-convergence approach, but imposing different areas for the sets involved in the partition, we can obtain numerical results which agree with the known results concerning bubble clusters in dimension two. Some results in the case of two and three bubbles can be seen in Figures 2.12 and 2.13. We notice that all the interfaces between two phases or between a phase and the exterior are curves of constant curvature, fact which is proved in [74].
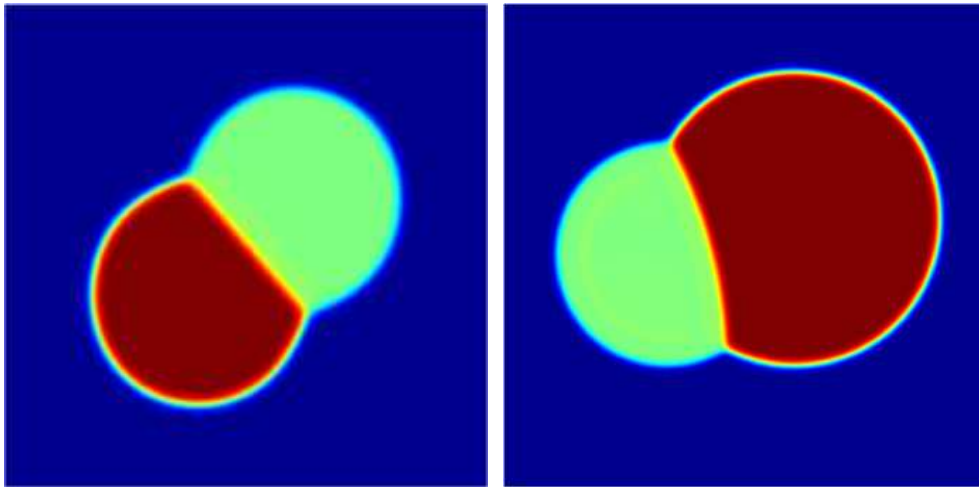
Figure 2.12: Double bubbles in 2D. Left: equal areas. Right: different areas
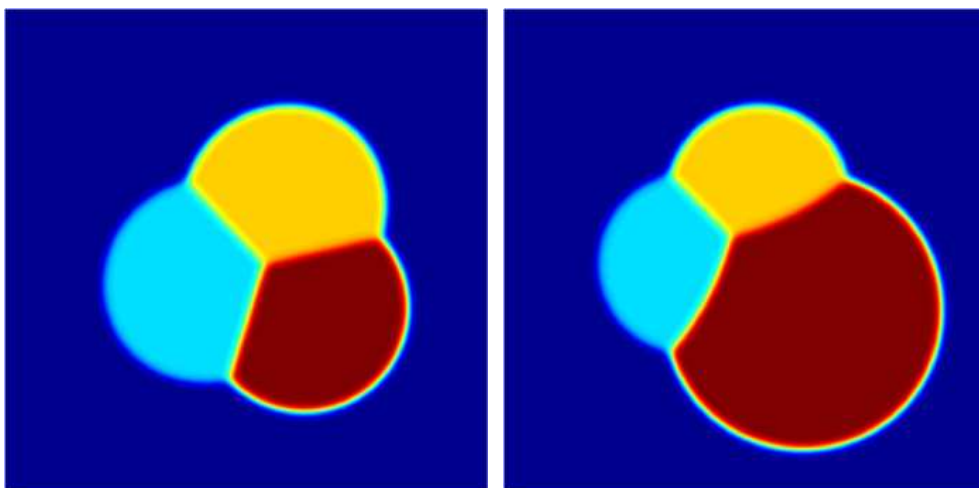
Figure 2.13: Triple bubbles in 2D. Left: equal areas. Right: different areas

Multiphase spectral problems

Résumé

Dans ce chapitre on s'intéresse à l'étude qualitative et numérique du problème multiphase

$$\min \sum_{i=1}^{h} (\lambda_1(\Omega_i) + \alpha|\Omega_i|),$$

où les ensembles Ω_i sont disjoints et contenus dans un domaine ouvert borné D. Il s'agit de continuer les travaux effectués dans [31] et de proposer une méthode numérique permettant de trouver les configurations optimales et d'observer numériquement les propriétés théoriques. Le contenu de ce chapitre est un article écrit en collaboration avec Bozhidar Velichkov, à paraître dans SIAM Journal on Numerical Analysis.

Il a été observé dans [31] que si $\alpha > 0$ alors la configuration optimale n'est pas une partition. De manière plus précise, il n'est pas possible d'avoir des points triples $x \in \partial\Omega_i \cap \partial\Omega_j \cap \partial\Omega_l$. On sait que pour $\alpha \to 0$ on approche le problème de partitionnement spectral étudié théoriquement par Caffarelli et Lin dans [35] et numériquement par Bourdin, Bucur et Oudet dans [18]. Comme il a été observé dans [18], pour h grand, on approche (numériquement) une partition hexagonale du domaine D. Pour α très grand, on peut montrer que la configuration optimale consiste en h disques disjoints contenus dans D. Il existe un paramètre optimal $\bar{\alpha}$ pour lequel ces disques disjoints ont un rayon maximal. Une telle configuration est appellée *circle packing*.

La première partie contient l'étude d'une nouvelle formule de monotonie pour deux phases qui nous permet de déduire des propriétés qualitatives près du bord du domaine D. En effet, les calculs numériques nous montrent que, en plus de l'absence des points triple dans D, on ne peut pas avoir des points triples de la forme $x \in \partial D \cap \partial\Omega_i \cap \partial\Omega_j$. Cette observation numérique peut être justifiée par le fait que dans les cas simples qu'on a considérés pour D (des rectangles, polygones) on peut ajouter à l'extérieur un disque tangent B. Ce disque est alors une sous-solution de forme (ou géométrique) du problème $\min \lambda_1(\Omega) + |\Omega|$, et donc on peut utiliser les

résultats de [31] pour conclure que $\partial B \cap \partial \Omega_i \cap \partial \Omega_j = \emptyset$. La formule de monotonie nous permet de prouver ce résultat dans le cas général où D est Lipschitz.

La deuxième partie du chapitre traite des aspects numériques du problème de minimisation. Dans un premier temps, on fait une étude théorique et numérique de l'erreur de la méthode de pénalisation utilisée pour calculer les valeurs propres en [18]. Si Ω est un sous-ensemble de D alors on peut définir pour $C > 0$ la valeur propre approchée $\lambda_k(\Omega, C)$ qui est solution de

$$-\Delta u + C(1 - \chi_\Omega)u = \lambda_k(\Omega, C)u.$$

Il est prouvé dans la référence précédemment citée que quand $C \to \infty$ la quantité $\lambda_k(\Omega, C)$ approche la vraie valeur propre $\lambda_k(\Omega)$ si Ω est régulier. Dans un premier temps on fait une approximation de l'erreur numérique commise en comparant le résultat obtenu en utilisant la méthode présentée ci-dessus avec les résultats obtenus avec le logiciel MpsPack [14] qui a une précision importante. La comparaison est faite en fonction de C et du pas de discrétisation du domaine D.

Dans la suite, on présente une estimation théorique de l'erreur, en fonction du paramètre C, et on déduit une borne explicite dans le cas où le domaine Ω est assez régulier. Ce résultat d'erreur utilise [25] et [29] qui donnent une borne supérieure de la différence des valeurs propres correspondant à deux mesures différentes, en utilisant des fonctions de torsion.

On présente une amélioration de l'algorithme de descente de gradient proposé dans [18], en ajoutant une procédure de recherche du pas optimal. On observe une stabilité améliorée de l'algorithme et une réduction du nombre d'itérations nécessaires pour la convergence. On propose de plus une approche éléments finis pour résoudre ce problème. Cette approche nous permet d'étudier les partitions spectrales et des problèmes multiphase sur des ensemble généraux, pas seulement rectangulaires.

Les calculs numériques effectués nous montrent quelques propriétés théoriques attendues comme l'absence de points triples à l'intérieur et sur le bord du domaine D, les ensembles d'une configuration optimale ne contient pas des coins, etc. Une autre propriété intéressante a été observée en étudiant le cas périodique.

- Pour $\alpha = 0$ on obtient la partition en hexagones réguliers comme observé avant dans [18].

- Pour $\alpha = \bar{\alpha}$ on observe une configuration du type circle packing.

- Pour $\alpha \in [0, \bar{\alpha}]$ on observe que les ensembles d'une configuration optimale sont congruents et qu'ils sont monotones pour l'inclusion par rapport au paramètre α.

Ce dernier aspect de monotonie nous permet de faire un rapprochement entre le problème de partitionnement spectral, qui est un problème ouvert et difficile, et le problème de circle packing, qui est résolu [87]. Ce fait justifie l'intérêt de considérer des problèmes multiphase, pour mieux comprendre le problème spectral.

Le cadre de ce problème peut être étendu aux problèmes multiphase concernant les valeurs propres de l'opérateur Laplace-Beltrami, avec conditions au bord de Dirichlet, des ensembles contenus dans des variétés. On présente aussi quelques calculs numériques concernant des problèmes multiphase sur des surfaces. On observe le même comportement monotone, qui relie le problème de partition au problème circle packing. Dans le cas de la sphère, tous les problèmes concernant les partitions spectrales optimales pour la somme sont ouverts pour $h \geq 3$. Une preuve théorique de la propriété de monotonie des formes pour le problème multiphase pourrait résoudre quelques questions ouvertes importantes (conjecture de Bishop, partitions régulières de la sphère, etc). Pour plus des détails concernant les partitions sur des variétés, le lecteur est invité à consulter le chapitre 5.

3.1 Introduction

In the following we consider a variational problem in which the variables are subsets of a given *ambient space* or *design region* D and the cost functional depends on the solution of a certain PDE on each of the domains. This type of problems are known as *shape optimization problems* and received a lot of attention from both the theoretical and the numerical community in the last years (we refer to the books [27], [66] and [65] for an introduction to the topic). A special type of shape optimization problems are the *multiphase shape optimization problems* in which the aim is to find the optimal configuration of h different disjoint sets $\Omega_1, \ldots, \Omega_h$ with respect to a certain cost functional $\mathcal{F}$

$$\min \left\{ \mathcal{F}\left(\Omega_1, \ldots, \Omega_h\right) \ : \ \Omega_i \subset D, \ \Omega_i \cap \Omega_j = \emptyset \right\}. \tag{3.1.1}$$

This type of problems may arise in some models studying the population dynamics of several highly competing species or in biology to simulate the behaviour of a cluster of cells. In some special cases it is not restrictive from mathematical point of view to assume that the sets Ω_i fill the entire region D. This is for example the case when the functional $\mathcal{F}$ is decreasing with respect to the set inclusion, i.e. if an empty space is left it will be immediately filled by some of the phases Ω_i decreasing the total optimization cost. Of course, it is always possible to write a multiphase problem as an optimal partition problem by adding the auxiliary phase $\Omega_{h+1} := D \setminus \left(\cup_{i=1}^{h} \Omega_i \right)$. On the other hand, we notice that in this way we violate the symmetry of the problem since this new phase does not appear in the functional. In some cases this does not change the nature of the problem. Consider for example an optimization cost given by the total length of the boundary $\partial\left(\cup_{i=1}^{h} \Omega_i \right)$, i.e.

$$\mathcal{F}(\Omega_1, \ldots, \Omega_h) = \sum_{i=1}^{h} |\partial\Omega_i| - \sum_{i \neq j} |\partial\Omega_i \cap \partial\Omega_j|.$$

In fact in this case we may introduce the new functional

$$\widetilde{\mathcal{F}}(\Omega_1, \ldots, \Omega_{h+1}) = \frac{1}{2} \sum_{i=1}^{h+1} |\partial \Omega_i|,$$

which is of the same type. In other cases the introduction of Ω_{h+1} may change the nature of the problem. Consider for example a functional depending on the principal eigenvalues on each set Ω_i and the Lebesgue measure $|\Omega_i|$

$$\mathcal{F}(\Omega_1, \ldots, \Omega_h) = \frac{1}{2} \sum_{i=1}^{h} \left(\lambda_1(\Omega_i) + |\Omega_i| \right).$$

Then, the corresponding optimal partition functional is given by

$$\widetilde{\mathcal{F}}(\Omega_1, \ldots, \Omega_{h+1}) = \frac{1}{2} \sum_{i=1}^{h} \lambda_1(\Omega_i) - |\Omega_{h+1}|,$$

and acts differently on the original sets Ω_i and the auxiliary set Ω_{h+1}.

We consider the multiphase shape optimization problem

$$\min \left\{ \sum_{i=1}^{h} \lambda_1(\Omega_i) + \int_{\Omega_i} W_i(x) \, dx \ : \ \Omega_i \text{ open}, \ \Omega_i \subset D, \ \Omega_i \cap \Omega_j = \emptyset \right\}, \qquad (3.1.2)$$

where

- the ambient space D is a bounded open set with Lipschitz boundary or more generally a compact manifold with or without boundary;

- $\lambda_1(\Omega_i)$ is the first Dirichlet eigenvalue of Ω_i;

- $W_i : D \to [0, +\infty]$ are given measurable functions.

Our aim is to provide a theoretical and numerical analysis of the problem and to study the qualitative behaviour of the solutions from both points of view. We notice that the optimal configurations consists of sets with rounded corners if the weight functions are sufficiently small. This phenomenon can be modelled in a direct way by adding a small curvature term, as $\varepsilon \int_{\partial \Omega} \kappa_i^2$, where κ_i is the curvature of $\partial \Omega_i$, but from the numerical point of view the volume term is much simpler to handle and gives the same qualitative behaviour.

In the next two examples we see the optimization problem from two different points of view.

Remark 3.1.1 (Two limit cases)**.** In the case $W_i \equiv \alpha$ on D, we obtain the following problem:

$$\min \left\{ \sum_{i=1}^{h} \lambda_1(\Omega_i) + \alpha |\Omega_i| \ : \ \Omega_i \text{ open}, \ \Omega_i \subset D, \ \Omega_i \cap \Omega_j = \emptyset \right\}. \qquad (3.1.3)$$

The variational problem (3.1.3) is widely studied in the literature in the case $\alpha = 0$ that corresponds to the classical optimal partition problem. We refer to the papers [38], [35], [62] and

[18] for a theoretical and numerical analysis in this case. The other limit case appears when the constant $\alpha > 0$ is large enough. Indeed, we recall that the solution of the problem

$$\min\left\{\lambda_1(\Omega) + \alpha|\Omega| : \Omega \text{ open}, \ \Omega \subset \mathbb{R}^2\right\}, \tag{3.1.4}$$

is a disk of radius $r_\alpha = \left(\dfrac{\lambda_1(B_1)}{\alpha\pi}\right)^{\frac{1}{4}}$. It is straightforward to check that if $\alpha > 0$ is such that there are h disjoint disks of radius r_α that fit in the box D, then the solution of (3.1.2) is given by the h-uple of these disks. Finding the smallest real number $\overline{\alpha} > 0$, for which the above happens, reduces to solving the optimal packing problem

$$\max\left\{r : \text{ there exist } h \text{ disjoint balls } B_r(x_1), \ldots, B_r(x_h) \text{ in } D\right\}. \tag{3.1.5}$$

In view of the previous remark the multiphase problem (3.1.3), in variation of the parameter α, can be seen as an interpolation between the optimal partition problem (corresponding to the case $\alpha = 0$) and the optimal packing problem (3.1.5). It is interesting to notice that in the asymptotic case when $D = \mathbb{R}^2$, the solution of the optimal packing problem consists of disks with centres situated in the vertices of a infinite hexagonal *honeycomb* partition of the plane. On the other hand, in the case $\alpha = 0$ Caffarelli and Lin conjectured that the optimal configuration is precisely the honeycomb partition.

Remark 3.1.2 (Competing species with diffusion). Suppose that Ω_i represents the habitat of a certain species and that the first eigenfunction u_i on Ω_i, solution of

$$-\Delta u_i = \lambda_1(\Omega_i)u_i \quad \text{in} \quad \Omega_i, \qquad u_i = 0 \quad \text{on} \quad \partial\Omega_i, \qquad \int_{\Omega_i} u_i^2 \, dx = 1,$$

is the population distribution. The condition $\Omega_i \cap \Omega_j = \emptyset$ corresponds to the limit assumption that the two species cannot coexists on the same territory. We suppose that $S_i \subset D$ is a closed set representing a distribution of resources and that $\varphi_i : [0, +\infty] \to [0, +\infty]$ is a given increasing function that corresponds to the cost of transportation of resources at a given distance. The population u_i will tend to choose an habitat close to S_i. This corresponds to the following multiphase problem

$$\min\left\{\sum_{i=1}^{h} \lambda_1(\Omega_i) + \int_{\Omega_i} \varphi_i\big(\text{dist}(x, S_i)\big) \, dx \ : \ \Omega_i \text{ open}, \ \Omega_i \subset D, \ \Omega_i \cap \Omega_j = \emptyset\right\}. \tag{3.1.6}$$

The first part of this chapter is dedicated to the analysis of the solutions of (3.1.2). We summarize the results in the following

Theorem 3.1.3. *Suppose that $D \subset \mathbb{R}^2$ is a bounded open set with Lipschitz boundary. Let $0 < a \leq A$ be two positive real numbers and $W_i : D \to [a, A]$, $i = 1, \ldots, h$ be given C^2 functions. Then there are disjoint open sets $\Omega_1, \ldots, \Omega_h \subset D$ solving the multiphase optimization problem (3.1.2). Moreover, any solution to (3.1.2) has the following properties:*

(i) *There are no triple points inside D, i.e. for every three distinct indices $i, j, k \in \{1, \ldots, h\}$ we have $\partial\Omega_i \cap \partial\Omega_j \cap \partial\Omega_k = \emptyset$.*

(ii) *There are no double points on the boundary of D, i.e. for every pair of distinct indices $i, j \in \{1, \ldots, h\}$ we have $\partial\Omega_i \cap \partial\Omega_j \cap \partial D = \emptyset$.*

(iii) *If the set D is of class C^2, then the first eigenfunctions $u_i \in H_0^1(\Omega_i)$ are Lipschitz continuous on $\overline{\Omega}_i$.*

(iv) *The set $\Omega = \bigcup_{i=1}^h \Omega_i$ has finite perimeter and the free reduced boundary $\partial^*\Omega$ is smooth in D. Equivalently the reduced boundary $\partial^*\Omega_{h+1}$ of the auxiliary phase $\Omega_{h+1} = D \setminus \Omega$ is smooth in D.*

Remark 3.1.4. We notice that the above result is still valid in dimension $d > 2$. We restrict our attention to dimension 2 since we can avoid some technicalities in the proofs of the Lipschitz continuity of the eigenfunctions and the decay monotonicity formula Lemma 3.3.10. In fact, a key step in the proof of the Lipschitz continuity of the eigenfunctions is to show their non-degeneracy on the boundary in terms of the gradients. This question can be handled easily in two dimensions, while for the case $d > 2$ we refer to [31, Theorem 5.9], where the case of the Dirichlet energy was considered.

For the computation of the optimal partition we use an approach that has as a starting point the algorithm used in [18]. We notice that the first eigenvalue of an open set $\Omega \subset D$ can be formally characterized as $\lambda_1(\Omega, +\infty)$, where

$$\lambda_1(\Omega, C) = \min_{u \in H_0^1(\Omega) \setminus \{0\}} \frac{\int_D |\nabla u|^2 + C \mathbb{1}_{D \setminus \Omega} u^2 \, dx}{\int_D u^2 \, dx}.$$

Replacing the characteristic function of Ω by a function $\varphi : D \to [0, 1]$ we can define

$$\lambda_1(\varphi, C) = \min_{u \in H_0^1(\Omega) \setminus \{0\}} \frac{\int_D |\nabla u|^2 + C(1 - \varphi) u^2 \, dx}{\int_D u^2 \, dx},$$

and then replace the optimal partition problem by

$$\min \left\{ \sum_{i=1}^h \lambda_1(\varphi_i, C) + \int_D \varphi_i(x) W_i(x) \, dx \; : \; \Omega_i \text{ open}, \; \varphi_i : D \to [0, 1], \; \sum_{i=1}^h \varphi_i \leq 1 \right\}. \quad (3.1.7)$$

In [18] it was proved that as $C \to +\infty$ and φ is the characteristic function of a regular set Ω, then the relaxed eigenvalue $\lambda_k(\varphi, C)$ converges to the actual eigenvalue $\lambda_k(\Omega)$. To the authors knowledge, there was no prior study of the rate of convergence in terms of C.

In Section 3.5 we observe the numerical error of a few simple shapes in terms of C and the discretization parameter, by comparing the values of the eigenvalues computed in the penalized setting, with the ones computed using MpsPack [14]. We observe that as C and the discretization parameter N increase, the errors decrease. In Section 3.6 we use the results of [29] in order

to obtain a theoretical upper bound for the relative error $|\lambda_k(\Omega) - \lambda_k(\Omega, C)|/\lambda_k(\Omega)$. Precisely we will prove the following.

Theorem 3.1.5. *Suppose $D \subset \mathbb{R}^N$ is a bounded open set and $\Omega \subset D$ a set with boundary of class C^2. Then there exists a constant $K > 0$ depending on Ω, D, N, for which we have*

$$\frac{|\lambda_k(\Omega) - \lambda_k(\mu_C)|}{\lambda_k(\Omega)} \leq KC^{-1/(N+4)}.$$

This bound on the error makes the convergence result proved in [18] more precise. In addition to this, we observe a good concordance between the theoretical bounds and the numerical errors observed in Section 3.5.

In Section 3.7 we present the main lines of the optimization procedure. One challenging issue was to manage the non overlapping condition $\sum_{i=1}^{h} \varphi_i \leq 1$. We introduce an extra phase φ_{h+1} which represents the void space. Thus we are left to manage an equality condition instead of an inequality. This allows us to adapt the framework presented in [18] to our problem. We use a standard gradient descent algorithm with a line search procedure in order to accelerate the convergence. We observe good stability properties of our proposed algorithm by performing a few optimizations starting from random densities and by observing that the resulting shape configuration and cost values are close. In addition to the finite difference framework on a rectangular grid we also propose an approach based on finite elements which can be generalized to general plane domains and even to surfaces in three dimensions.

In Section 3.8 we present some of the results obtained using the presented numerical frameworks, as well as some numerical observations which motivate the interest in the study of problem (3.1.3). First we mention that the numerical results satisfy the theoretical properties proved in [31] and in Theorem 3.1.3: the lack of triple points, the lack of triple points on the boundary and the lack of angles. Secondly we observe an interesting connection between the two interesting cases $\alpha = 0$ and the value of α which gives the circle packing in the periodic setting. It is well known that the hexagonal circle packing in the plane has the maximal density (result attributed to A. Thue with a first rigorous proof given by F. Toth). As mentioned above, in the case $\alpha = 0$ (the spectral partition) it is conjectured that the optimal asymptotic partition is the honeycomb partition. This conjecture was supported numerically by the results of [18]. As we already mentioned the problem 3.1.3 provides a connection between the established result of the circle packing configuration and the Caffarelli-Lin conjecture that the regular honeycomb tiling is the solution of the spectral optimal partition problem. In our computations we observe that starting from the parameter $\overline{\alpha}$ which realizes the circle packing in the periodic setting and decreasing α, the shapes forming the optimal partition grow in a monotone fashion. If this observed monotonicity property could be proved theoretically then a proof that the honeycomb partition is optimal for $\alpha = 0$ will follow. Note that this also applies in the case of the sphere,

where it is expected that for $h \in \{3, 4, 6, 12\}$ the optimal spectral partitions are realized by regular tilling of the sphere.

The chapter is organized as follows. In Section 3.2 we recall the known results and we introduce the basic notions that we use in the proof of the above results. Section 3.3 is dedicated to the proof of Theorem 3.1.3. In Section 3.5 we present the eigenvalue computation method and we make a few numerical tests by comparing our results to other methods or to analytical results. Section 3.6 is dedicated to the proof of Theorem 3.1.5. In Section 3.7 we present the optimization algorithm used for calculating the numerical minimizers of (3.1.2). The numerical results and other observations are discussed in Section 3.8.

3.2 Preliminaries and main tools

3.2.1 Eigenvalues and eigenfunctions

Let $\Omega \subset \mathbb{R}^2$ be an open set. We denote with $H_0^1(\Omega)$ the Sobolev space obtained as the closure in $H^1(\mathbb{R}^2)$ of $C_c^\infty(\Omega)$, i.e. the smooth functions with compact support in Ω, with respect to the Sobolev norm

$$\|u\|_{H^1} := \left(\|\nabla u\|_{L^2}^2 + \|u\|_{L^2}^2\right)^{1/2} = \left(\int_{\mathbb{R}^2} |\nabla u|^2 + u^2 \, dx\right)^{1/2}.$$

We note that $H_0^1(\Omega)$ can be characterized as

$$H_0^1(\Omega) = \left\{u \in H^1(\mathbb{R}^2) : \text{ cap}\left(\{u \neq 0\} \setminus \Omega\right) = 0\right\}, \tag{3.2.1}$$

where the capacity $\text{cap}(E)$ of a measurable set $E \subset \mathbb{R}^2$ is defined as

$$\text{cap}(E) = \min\left\{\|u\|_{H^1}^2 : \ u \geq 1 \text{ in a neighbourhood of } E\right\}^1.$$

We notice that the sets of zero capacity have also zero Lebesgue measure, while the converse might be false. We may use the notion of capacity to choose more regular representatives of the functions of the Sobolev space $H^1(\mathbb{R}^d)$. In fact, every function $u \in H^1(\mathbb{R}^d)$ has a representative which is quasi-continuous, i.e. continuous outside a set of zero capacity. Moreover, two quasi-continuous representatives of the same Sobolev function coincide outside a set of zero capacity. Thus we may consider $H^1(\mathbb{R}^2)$ as a space consisting of quasi-continuous functions equipped with the usual H^1 norm.

The k-th eigenvalue of the Dirichlet Laplacian can be defined through the min-max variational formulation

$$\lambda_k(\Omega) := \min_{S_k \subset H_0^1(\Omega)} \max_{u \in S_k \setminus \{0\}} \frac{\int_\Omega |\nabla u|^2 \, dx}{\int_\Omega u^2 \, dx}, \tag{3.2.2}$$

---

[1] for more details see, for example, [51] or [66]

where the minimum is over all k dimensional subspaces S_k of $H_0^1(\Omega)$. There are functions u_n, $n \geq 1$ in $H_0^1(\Omega)$, orthonormal in $L^2(\Omega)$, that solve the equation

$$-\Delta u_k = \lambda_k(\Omega) u_k, \qquad u_k \in H_0^1(\Omega),$$

in a weak sense in $H_0^1(\Omega)$. In particular, if $k = 1$, then the first eigenfunction u_1 of Ω is the solution of the minimization problem

$$\lambda_1(\Omega) := \min_{u \in H_0^1(\Omega) \setminus \{0\}} \frac{\int_\Omega |\nabla u|^2 \, dx}{\int_\Omega u^2 \, dx}. \tag{3.2.3}$$

In the sequel we will often see λ_1 as a functional on the family of open sets. We notice that this functional can be extended to the larger class of quasi-open sets, i.e. the sets $\Omega \subset \mathbb{R}^2$ such that for every $\varepsilon > 0$ there exists an open set ω_ε of capacity $\mathrm{cap}(\omega_\varepsilon) \leq \varepsilon$ such that $\Omega \cap \omega_\varepsilon$ is an open set. We define $H_0^1(\Omega)$ as the set of Sobolev functions $u \in H^1(\mathbb{R}^2)$ such that $u = 0$ *quasi-everywhere* (i.e. outside a set of zero capacity) on Ω^c. The first eigenvalue and the first eigenfunctions are still characterized as the minimum and the minimizer of (3.2.3).

We notice that since $|u_1|$ is also a solution of (3.2.3), from now on we will always assume that u_1 is non-negative and normalized in L^2. Moreover, we have the following properties of u_1 on a generic open[2] set Ω of finite measure:

- u_1 is bounded and we have the estimate[3]

$$\|u_1\|_{L^\infty} \leq \frac{1}{\pi} \lambda_1(\Omega) |\Omega|^{1/2}. \tag{3.2.4}$$

- $u_1 \in H^1(\mathbb{R}^2)$, extended as zero outside Ω, satisfies the following inequality in sense of distributions:

$$\Delta u_1 + \lambda_1(\Omega) u_1 \geq 0 \qquad \text{in} \qquad \left[C_c^\infty(\mathbb{R}^2) \right]'. \tag{3.2.5}$$

- Every point $x_0 \in \mathbb{R}^2$ is a Lebesgue point for u_1. Pointwise defined as

$$u_1(x_0) := \lim_{r \to 0} \fint_{B_r(x_0)} u(x) \, dx,$$

u_1 is upper semi-continuous on $\mathbb{R}^2$.

- u_1 is almost subharmonic in the sense that for every $x_0 \in \mathbb{R}^2$, we have

$$u_1(x_0) \leq \|u_1\|_{L^\infty} \lambda_1(\Omega) r^2 + \fint_{B_r(x_0)} u_1(x) \, dx, \qquad \forall r > 0. \tag{3.2.6}$$

---

[2]The same properties hold for the first eigenfunction on quasi-open set of finite measure.

[3]We note that the infinity norm of u_1 can also be estimated in terms of $\lambda_1(\Omega)$ only as $\|u_1\|_{L^\infty} \leq C\lambda_1(\Omega)^{d/4}$. This estimate is more general and can be found in [43, Example 8.1.3].

3.2.2 Sets of finite perimeter and reduced boundary

In the proof of Theorem 3.1.3 *(iv)* we will need the notion of a reduced boundary. Let $\Omega \subset \mathbb{R}^d$ be a set of finite Lebesgue measure. If the distributional gradient of its characteristic function $\nabla \mathbb{1}_\Omega$ is a Radon measure such that its total variation $|\nabla \mathbb{1}_\Omega|(\mathbb{R}^d)$ is finite, then we say that Ω is of finite perimeter. The perimeter $P(\Omega)$ is the total variation of the gradient and for regular sets coincides with the usual notion of perimeter as surface integral. The reduced boundary $\partial^* \Omega$ of a set Ω of finite perimeter is defined as the set of points where one can define the normal vector to Ω in the following sense: $x_0 \in \partial^* \Omega$, if the limit $\lim\limits_{r \to 0} \dfrac{\nabla \mathbb{1}_\Omega(B_r(x_0))}{|\nabla \mathbb{1}_\Omega|(B_r(x_0))}$ exists and has Euclidean norm equal to one. We notice that if a point x_0 belongs to the reduced boundary, then the density of Ω in x_0 is precisely $1/2$, i.e. $\lim\limits_{r \to 0} \dfrac{|\Omega \cap B_r(x_0)|}{|B_r(x_0)|} = \dfrac{1}{2}$. For more details on the sets of finite perimeter we refer to the books [58] and [70].

3.2.3 The existence theory of Buttazzo and Dal Maso

The multiphase shape optimization problems of the form (3.1.1) admit solutions for a very general cost functionals $\mathcal{F}(\Omega_1, \dots, \Omega_h)$. The main existence result in this direction is well known and is due to the classical Buttazzo-Dal Maso result from [53]. The price to pay for such a general result is that one has to relax the problem to a wider class of domains, which contains the open ones. Indeed, one notes that the capacitary definition of a Sobolev space (3.2.1) can be easily extended to generic measurable sets. In particular, it is well known (we refer, for example, to the books [66] and [27]) that it is sufficient to restrict the analysis to the class of *quasi-open* sets, i.e. the level sets of Sobolev functions. Since the definition of the first eigenvalue (3.2.3) is of purely variational character, one may also extend it to the quasi-open sets and then apply the theorem of Buttazzo and Dal Maso [53] to obtain existence for (3.1.1) in the family of quasi-open sets under the minimal assumptions of monotonicity and semi-continuity of the function F. Thus, the study of the problem of existence of a solution of (3.1.1) reduces to the analysis of the regularity of the optimal quasi-open sets. The precise statement of the Buttazzo-Dal Maso Theorem that we are going to adopt is the following.

Theorem 3.2.1. *Suppose that D is a bounded open sets, $k_1, \dots, k_h$ are natural numbers, $F : \mathbb{R}^h \to \mathbb{R}$ is a continuous function increasing in each variable and let $W_i : D \to [0, +\infty]$ be given measurable functions. Then there is a solution to the problem*

$$\min \left\{ F(\lambda_{k_1}(\Omega_1), \dots, \lambda_{k_h}(\Omega_h)) + \sum_{i=1}^{h} \int_{\Omega_i} W_i(x)\, dx \ : \ \Omega_i \subset D \text{ quasi-open}, \Omega_i \cap \Omega_j = \emptyset \right\}.$$

3.2.4 Regularity of the optimal sets for the first eigenvalue

The regularity of the optimal sets for the Dirichlet eigenvalues is a difficult question and even in the case of a single phase it is open for higher eigenvalues. For the principal eigenvalue of

the Dirichlet Laplacian we have the following result by Lamboley and Briançon which relies on an adaptation of the classical Alt-Caffarelli regularity theory to the case of eigenfunctions. We state the result here with a smooth weight function as in the original paper [2].

Theorem 3.2.2. *Suppose that $D \subset \mathbb{R}^2$ is a bounded open set, $W : D \to [a, A]$ is a smooth function and Ω is a solution of the shape optimization problem*

$$\min \left\{ \lambda_1(\Omega) + \int_\Omega W(x) \, dx \; : \; \Omega \subset D \text{ quasi-open} \right\}. \qquad (3.2.7)$$

Then Ω is open set of finite perimeter and the boundary $D \cap \partial\Omega$ is locally a graph of a smooth function.

3.2.5 Shape subsolutions and their properties

We say that the quasi-open set $\Omega \subset \mathbb{R}^2$ is a shape subsolution for the functional $\lambda_1 + \alpha| \cdot |$ if for every quasi-open set $\omega \subset \Omega$ we have

$$\lambda_1(\Omega) + \alpha|\Omega| \leq \lambda_1(\omega) + \alpha|\omega|.$$

The notion of a shape subsolution was introduced by Bucur in [26] in order to study the existence of an optimal set for the kth eigenvalue and then was more extensively studied in [31]. We recall the main results from [26] and [31] in the following

Theorem 3.2.3. *Suppose that Ω is a shape subsolution for the functional $\lambda_1 + \alpha| \cdot |$. Then*

(a) Ω is bounded and its diameter $\text{diam}(\Omega)$ is estimated by a constant depending on α, $\lambda_1(\Omega)$ and $|\Omega|$;

(b) Ω is of finite perimeter and we have the estimate

$$P(\Omega) \leq \alpha^{-1/2} \lambda_1(\Omega) |\Omega|^{1/2}; \qquad (3.2.8)$$

(c) there is a lower bound on the eigenvalue $\lambda_1(\Omega)$ given by

$$\lambda_1(\Omega) \geq \left(4\pi\alpha \right)^{1/2}; \qquad (3.2.9)$$

(d) If Ω' is also a shape subsolution for the same functional such that $\Omega \cap \Omega' = \emptyset$, then there are disjoint open sets D and D' such that $\Omega \subset D$ and $\Omega' \subset D'$.

3.2.6 Monotonicity formulas for eigenfunctions

The monotonicity formula of Alt-Caffarelli-Friedman is an essential tool in the study of the behaviour of the eigenfunctions in the points of the common boundary of the optimal sets. Since the eigenfunctions are not subharmonic, but satisfy (3.2.5), we will need another version of the

monotonicity formula from [3]. We state here the following monotonicity theorem for eigenfunctions from [38], which is a version of the Alt-Caffarelli-Friedman monotonicity formula. We use this result to prove that the eigenfunctions of the optimal sets are Lipschitz continuous everywhere in D.

Theorem 3.2.4 (Two-phase monotonicity formula). *Consider the unit ball $B_1 \subset \mathbb{R}^2$. Let $u^+, u^- \in H^1(B_1) \cap L^\infty(B_1)$ be two non-negative functions with disjoint supports and let $\lambda_+, \lambda_- \geq 0$ be two real numbers such that*

$$\Delta u^+ + \lambda_+ u^+ \geq 0 \qquad and \qquad \Delta u^- + \lambda_- u^- \geq 0.$$

Then there are constants $1/2 \geq r_0 > 0$ and $C > 0$, depending on d, λ_+ and λ_-, such that for every $r \in (0, r_0)$ we have

$$\left(\frac{1}{r^2}\int_{B_r}|\nabla u^+|^2\,dx\right)\left(\frac{1}{r^2}\int_{B_r}|\nabla u^-|^2\,dx\right) \leq C\left(1 + \|u^+ + u^-\|^2_{L^\infty(B_{2r_0})}\right)^2. \qquad (3.2.10)$$

We note that the estimate (3.2.10) follows by the more general result by Caffarelli, Jerison and Kënig (see [34] and also the note [90], where the continuity assumption was dropped). In order to obtain (3.3.21) we use the idea of Conti, Terracini and Verzini (see [38]) that follows the spirit of the original Alt-Caffarelli-Friedman monotonicity formula. It works exclusively for eigenfunctions (linear or nonlinear), but can be easily refined to obtain finer qualitative results as (3.3.21).

The three-phase version of Theorem 3.2.4 is the main tool that allows to exclude the presence of triple boundary points in the optimal configuration. The following three-phase monotonicity formula was proved for eigenfunctions in [38], while the general three-phase version of the Caffarelli-Jerison-Kënig result can be found in [31] (see also [90] for the detailed proof). This formula is used in the proof of the fact that in the optimal configuration there are not triple points. In the following, B_1 denotes the unit ball in $\mathbb{R}^2$.

Theorem 3.2.5 (Three-phase monotonicity formula). *Let $u_1, u_2, u_3 \in H^1(B_1) \cap L^\infty(B_1)$ be three non-negative functions with disjoint supports and let $\lambda_1, \lambda_2, \lambda_3 \geq 0$ be real numbers such that*

$$\Delta u_i + \lambda_i u_i \geq 0, \qquad \forall i = 1, 2, 3.$$

Then there are constants $0 < r_0 \leq 1/2$, $C > 0$ and $\varepsilon > 0$, depending on d, λ_1, λ_2 and λ_3, such that for every $r \in (0, r_0)$ we have

$$\prod_{i=1}^{3}\left(\frac{1}{r^2}\int_{B_r}|\nabla u_i|^2\,dx\right) \leq Cr^\varepsilon\left(1 + \|u_1 + u_2 + u_3\|^2_{L^\infty(B_{2r_0})}\right)^3. \qquad (3.2.11)$$

The three phase monotonicity formula is not just a consequence of the two phase formula. In fact if we apply the Alt-Caffarelli-Friedman formula to each pair of the tree sets Ω_i, Ω_j and Ω_k, then in (3.2.11) there will be no decay term r^ε. Roughly speaking the presence of the third

phase forces the other two to occupy less space which in turn gives some decay with $\varepsilon > 0$. The same phenomenon appears when there are only two phases that cannot occupy a certain sufficiently big region. This is the idea that we develop in Lemma 3.3.10 which we will use to deduce the lack of double points on the boundary of the design region D and also the regularity of the reduced boundary of the auxiliary phase Ω_{h+1}.

3.3 Proof of Theorem 3.1.3

3.3.1 Existence of optimal open sets

An existence of an optimal configuration in the class of quasi-open sets follows by the Buttazzo-Dal Maso Theorem. Let $\Omega_1, \ldots, \Omega_h$ be the optimal quasi-open sets. Then for every quasi-open set $\omega_i \subset \Omega_i$ we have that the configuration is not optimal which gives that

$$\lambda_1(\omega_i) - \lambda_1(\Omega_i) \geq \int_{\Omega_i} W_i \, dx - \int_{\omega_i} W_i \, dx \geq a|\Omega_i| - a|\omega_i|.$$

Thus Ω_i is a shape subsolution for the functional $\lambda_1 + a|\cdot|$ and so we can apply the result from [31] Theorem 3.2.3 (d). Thus each of the sets Ω_i is contained in an open set D_i and solves

$$\min \left\{ \lambda_1(\Omega) + \int_\Omega W_i(x) \, dx \; : \; \Omega \subset D_i \text{ quasi-open} \right\}.$$

By Theorem 3.2.2 the sets Ω_i are open.

3.3.2 Lipschitz continuity of the eigenfunctions

In this section we prove that the first eigenfunctions on the optimal sets for (3.1.2) are Lipschitz continuous. To fix the notation, in the rest of this section we will denote with $(\Omega_1, \ldots, \Omega_h)$ a generic solution of (3.1.2) and with $u_i \in H_0^1(\Omega_i)$ the first eigenfunction on Ω_i, i.e. u_i are non-negative function such that $\int_{\mathbb{R}^2} u_i^2 \, dx = 1$ satisfying (3.2.4), (3.2.5) and the equation

$$-\Delta u_i = \lambda_1(\Omega_i) u_i, \qquad u_i \in H_0^1(\Omega),$$

weakly in $H_0^1(\Omega_i)$.

Non-degeneracy of the eigenfunctions. We first note that for every $\omega_i \subset \Omega_i$, the optimality of $(\Omega_1, \ldots, \Omega_i, \ldots, \Omega_h)$ tested against the h-uple of open sets $(\Omega_1, \ldots, \omega_i, \ldots, \Omega_h)$ gives the inequality

$$\lambda_1(\Omega_i) + \alpha|\Omega_i| \leq \lambda_1(\omega_i) + \alpha|\omega_i|,$$

i.e. Ω_i is a *subsolution* for the functional $\lambda_1 + \alpha|\cdot|$. Thus using the argument from the Alt-Caffarelli non-degeneracy lemma (see [2, Lemma 3.4] and also [31, Section 3]), we have the following result.

Lemma 3.3.1. *Suppose that $(\Omega_1, \ldots, \Omega_h)$ is optimal for* (3.1.2). *Then there are constants C_{nd} and $r_0 > 0$ such that for all the first eigenfunctions u_i, every $0 < r \leq r_0$ and every $x_0 \in \mathbb{R}^2$ we have the following implication*

$$\left(B_{r/2}(x_0) \cap \Omega_i \neq \emptyset \right) \Rightarrow \left(\frac{1}{r} \fint_{B_r(x_0)} u_i \, dx \geq C_{nd} \right). \tag{3.3.1}$$

Remark 3.3.2. Together with the estimate (3.2.6), Lemma 3.3.1 gives that there is $r_0 > 0$ such that

$$\|u_i\|_{L^\infty(B_{r/2}(x_0))} \leq 5 \fint_{B_r(x_0)} u_i \, dx, \qquad \forall r \leq r_0 \text{ such that } B_{r/2}(x_0) \cap \Omega_i \neq \emptyset. \tag{3.3.2}$$

On the common boundary of two optimal sets the non-degeneracy (3.3.1) of $\fint_{B_r(x_0)} u_i \, dx$ gives a bound from below for the gradient $\fint_{B_r(x_0)} |\nabla u_i|^2 \, dx$. This fact follows by the elementary lemma proved below.

Lemma 3.3.3. *Let $R > 0$, $B_R(x_0) \subset \mathbb{R}^2$ and $U \in H^1(B_R(x_0))$ be a Sobolev function such that for almost every $r \in (0, R)$ the set $\{U = 0\} \cap \partial B_r(x_0)$ is non-empty. Then we have*

$$\frac{1}{R} \fint_{B_R(x_0)} U \, d\mathcal{H}^1 \leq 2 \left(\fint_{B_R(x_0)} |\nabla U|^2 \, dx \right)^{1/2}. \tag{3.3.3}$$

Proof. Without loss of generality we suppose that $x_0 = 0$. We first note that for almost every $r \in (0, R)$ the restriction $U|_{\partial B_r}$ is Sobolev. If, moreover, $\{U = 0\} \cap \partial B_r \neq \emptyset$, then we have

$$\int_{\partial B_r} U^2 \, d\mathcal{H}^1 \leq 4r^2 \int_{\partial B_r} |\nabla U|^2 \, d\mathcal{H}^1.$$

Applying the Cauchy-Schwartz inequality and integrating for $r \in (0, R)$, we get

$$\left(\frac{1}{R} \fint_{B_R} U \, dx \right)^2 \leq \frac{1}{R^2} \fint_{B_R} U^2 \, dx \leq 4 \fint_{B_R} |\nabla U|^2 \, dx.$$

$\square$

Corollary 3.3.4. *Suppose that $(\Omega_1, \ldots, \Omega_h)$ is optimal for* (3.1.2). *Then there is a constant $r_0 > 0$ such that for every $x_0 \in \partial \Omega_i \cap \partial \Omega_j$, for some $i \neq j$ we have*

$$\fint_{B_r(x_0)} |\nabla u_i|^2 \, dx \geq 4C_{nd}^2, \forall r \in (0, r_0), \tag{3.3.4}$$

where $C_{nd} > 0$ is the non-degeneracy constant from Lemma 3.3.1.

Proof. Since $x_0 \in \partial \Omega_i \cap \partial \Omega_j$, we have that for every $r > 0$ $\Omega_i \cap B_r(x_0) \neq \emptyset$ and $\Omega_j \cap B_r(x_0) \neq \emptyset$. In view of Lemma 3.3.1, it is sufficient to check that $\Omega_i \cap \partial B_r(x_0) \neq \emptyset$ and $\Omega_j \cap \partial B_r(x_0) \neq 0$, for almost every $r \in (0, r_0)$. Indeed, suppose that this is not the case and that $\Omega_i \cap \partial B_r(x_0) = \emptyset$. Since Ω_i is connected, we have that $\Omega_i \subset B_r(x_0)$, which gives $\lambda_1(\Omega_i) \geq \lambda_1(B_{r_0})$, which is impossible if we choose r_0 small enough. $\square$

Growth estimate of the eigenfunctions on the boundary. We now prove the two key estimates of the growth of u_i close to the boundary $\partial\Omega_i$. We consider two kinds of estimates, one holds around the points, where two phases Ω_i and Ω_j are close to each other, and is reported in Lemma 3.3.5. The other estimate concerns the one-phase points, i.e. the points on one boundary, say $\partial\Omega_i$, which are far away from all other sets Ω_j.

Lemma 3.3.5. *Suppose that* $(\Omega_1, \ldots, \Omega_h)$ *is optimal for* (3.1.2). *Then there are constants* C_2 *and* $r_0 > 0$ *such that if* $x_0 \in \partial\Omega_i$ *is such that* $\Omega_j \cap B_r(x_0) \neq \emptyset$, *for some* $j \neq i$ *and* $r \leq r_0$, *then*

$$\|u_i\|_{L^\infty(B_r(x_0))} \leq C_2 r. \tag{3.3.5}$$

Proof. Without loss of generality we suppose that $0 = x_0 \in \partial\Omega_i$. Let now $0 < r \leq r_0$ be such that $\Omega_j \cap B_r \neq \emptyset$. Choosing r_0 small enough we may apply Lemma 3.3.1 obtaining that

$$\fint_{B_{3r}} u_j \, dx \geq 3C_{nd}\, r.$$

Again by choosing r_0 small enough we may suppose that for every $r \in (0, r_0)$ we have $\partial B_{3r} \cap \Omega_i \neq 0$. Indeed, if this is not the case for some r, then the set Ω_i is entirely contained in B_{3r} and so $\lambda_1(\Omega_i) \geq \lambda_1(B_{3r}) \geq \lambda_1(B_{3r_0})$, contradicting the optimality of Ω_i. Thus, we may apply the estimate (3.3.3) for u_j obtaining

$$C_{nd}^2 \leq \left(\frac{1}{3r}\fint_{B_{3r}} u_j \, dx\right)^2 \leq 4\fint_{B_{3r}} |\nabla u_j|^2 \, dx.$$

By the two-phase monotonicity formula applied for u_i and u_j, we get that there is a constant $C > 0$ such that

$$\frac{4C}{C_{nd}^2} \geq \fint_{B_{3r}} |\nabla u_i|^2 \, dx.$$

Since $B_r \cap \Omega_j \neq \emptyset$, by choosing r_0 small enough an reasoning as above we may suppose that for every $\tilde{r} \in (r, 3r)$ $\partial B_{\tilde{r}} \cap \Omega_j \neq 0$. Thus, reasoning as in Lemma 3.3.3, we get that

$$4(3r)^2 \int_{B_{3r}\setminus B_{2r}} |\nabla u_i|^2 \, dx \geq \int_{B_{3r}\setminus B_{2r}} u_i^2 \, dx \geq \frac{1}{5\pi r^2}\left(\int_{B_{3r}\setminus B_{2r}} u_i \, dx\right)^2.$$

By the mean value formula, there is $R \in (2r, 3r)$ such that

$$\int_{\partial B_R} u_i \, dx \leq \frac{1}{r}\int_{2r}^{3r}\left(\int_{\partial B_s} u_i \, d\mathcal{H}^1\right) ds \leq 27r\left(\int_{B_{3r}} |\nabla u_i|^2 \, dx\right)^{1/2} \tag{3.3.6}$$

We now note that by (3.2.5) the function $v(x) = u_i(x) - \lambda_1(\Omega_i)\|u_i\|_{L^\infty}(R^2 - |x|^2)$ is subharmonic. Then, for every $x \in B_r$, we use the Poisson formula

$$u_i(x) - \lambda_1(\Omega_i)\|u_i\|_{L^\infty}(3r)^2 \leq \frac{R^2 - |x|^2}{2\pi R}\int_{\partial B_R} \frac{u_i(y)}{|y-x|^2} \, d\mathcal{H}^1(y) \leq 9\fint_{\partial B_R} u_i \, d\mathcal{H}^1. \tag{3.3.7}$$

Using the non-degeneracy of u_i (Lemma 3.3.1) and combining the estimates from (3.3.6) and (3.3.7) we get

$$\|u_i\|_{L^\infty(B_r)} \leq 3^6 r\left(\fint_{B_{3r}} |\nabla u_i|^2 \, dx\right)^{1/2} \leq \frac{2\sqrt{C}3^6}{C_{nd}}r. \tag{3.3.8}$$

$\square$

The following Lemma is similar to [2, Lemma 3.2] and [23, Lemma 3.1]. We sketch the proof below for the sake of completeness.

Lemma 3.3.6. *Suppose that $(\Omega_1, \ldots, \Omega_h)$ is optimal for (3.1.2). Then there are constants $C_1 > 0$ and $r_0 > 0$ such that if $x_0 \in \partial\Omega_i$ and $0 < r \le r_0$ are such that $\Omega_j \cap B_{2r}(x_0) = \emptyset$, for every $j \neq i$, then*

$$\|u_i\|_{L^\infty(B_r(x_0))} \le C_1 r. \tag{3.3.9}$$

Proof. Without loss of generality we may suppose that $x_0 = 0$. Since $\Omega_j \cap B_{2r} = \emptyset$, for every $j \neq i$, we may use the h-uple $(\Omega_1, \ldots, \Omega_i \cap B_{2r}, \ldots, \Omega_h)$ to test the optimality of $(\Omega_1, \ldots, \Omega_i, \ldots, \Omega_h)$. Thus we have

$$\int_{\mathbb{R}^2} |\nabla u_i|^2 \, dx + \alpha|\Omega_i| = \lambda_1(\Omega_i) + \alpha|\Omega_i| \le \lambda_1(\Omega_i \cup B_{2r}) + \alpha|\Omega_i \cup B_r|$$

$$\le \frac{\int_{\mathbb{R}^2} |\nabla \widetilde{u}_i|^2 \, dx}{\int_{\mathbb{R}^2} \widetilde{u}_i^2 \, dx} + \alpha|\Omega_i \cup B_{2r}| \le \int_{\mathbb{R}^2} |\nabla \widetilde{u}_i|^2 \, dx + \alpha|\Omega_i \cup B_{2r}|, \tag{3.3.10}$$

where we used the test function $\widetilde{u}_i \in H_0^1(\Omega_i \cap B_{2r})$ defined as $\widetilde{u}_i = v_i \mathbb{1}_{B_{2r}} + u_i \mathbb{1}_{B_{2r}^c}$ and $v_i \in H^1(B_{2r})$ is the solution of the obstacle problem

$$\min\left\{ \int_{B_{2r}} |\nabla v|^2 \, dx : v \in H^1(B_{2r}), \ v - u_i \in H_0^1(B_{2r}), \ v \ge u_i \right\}. \tag{3.3.11}$$

By (3.3.10) an the fact that v_i is harmonic on the set $\{v_i > u_i\}$, we get

$$\int_{B_{2r}} |\nabla(u_i - v_i)|^2 \, dx = \int_{B_{2r}} \left(|\nabla u_i|^2 - |\nabla v_i|^2 \right) dx \le \alpha|B_{2r} \setminus \Omega_i|. \tag{3.3.12}$$

Now, reasoning as in [2, Lemma 3.2] (see also [89, Lemma 4.3.20] and [31]), there is a constant $C > 0$ such that

$$\left|\{u_i = 0\} \cap B_{2r}\right| \left(\frac{1}{2r} \fint_{\partial B_{2r}} u_i \, d\mathcal{H}^1 \right)^2 \le C \int_{B_{2r}} |\nabla(u_i - v_i)|^2 \, dx. \tag{3.3.13}$$

Now we note that by the optimality of Ω_i, we have $\Omega_i = \{u_i > 0\}$ and $|B_{2r} \cap \{u_i = 0\}| > 0$ (if $|B_{2r} \cap \{u_i = 0\}| = 0$, then by the optimality $v_i = u_i$ in B_{2r}; thus u_i is superharmonic in B_{2r} and so $u_i > 0$ in B_{2r}, which contradicts the assumption $0 \in \partial\Omega_i$). Now (3.3.12) and (3.3.13) give

$$\frac{1}{2r} \fint_{\partial B_{2r}} u_i \, d\mathcal{H}^1 \le \sqrt{C/\alpha}. \tag{3.3.14}$$

Since the function $\left\{ x \mapsto \left(u_i(x) - \lambda_1(\Omega_i)\|u_i\|_{L^\infty}(4r^2 - |x|^2) \right) \right\}$ is subharmonic, we can use the Poisson formula for every $x \in B_r$

$$u_i(x) - 4\lambda_1(\Omega_i)\|u_i\|_{L^\infty} r^2 \le \frac{(2r)^2 - |x|^2}{4\pi r} \int_{\partial B_{2r}} \frac{u_i(y)}{|y - x|^2} \, d\mathcal{H}^1(y) \le 4 \fint_{\partial B_{2r}} u_i \, d\mathcal{H}^1. \tag{3.3.15}$$

By the non-degeneracy of u_i (Lemma 3.3.1) and (3.3.15), we have that for r_0 small enough

$$\frac{\|u_i\|_{L^\infty(B_r)}}{r} \leq \frac{5}{2r} \fint_{\partial B_{2r}} u_i \, d\mathcal{H}^1 \leq 5\sqrt{C/\alpha},$$

which gives the claim. $\qquad\square$

We combine the estimates from Lemma 3.3.6 and Lemma 3.3.5, obtaining the following

Proposition 3.3.7. *Suppose that $(\Omega_1, \ldots, \Omega_h)$ is optimal for* (3.1.2). *Then there are constants $r_0 > 0$ and $C_{12} > 0$ such that for every $i \in \{1, \ldots, h\}$ we have*

$$\|u_i\|_{L^\infty(B_r(x_0))} \leq C_{12} \, r, \qquad \forall r \in (0, r_0). \tag{3.3.16}$$

Conclusion of the proof of the Lipschitz continuity of the eigenfunctions. We now use the estimate from Proposition 3.3.7 to deduce the Lipschitz continuity of u_i. The argument is standard and we recall it briefly for the sake of completeness. It is based on the following classical lemma.

Lemma 3.3.8. *Suppose that $B_r \subset \mathbb{R}^2$, $f \in L^\infty(B_r)$ and $u \in H^1(B_r)$ satisfies the equation*

$$-\Delta u = f \quad \text{weakly in} \quad [H_0^1(B_r)]'.$$

Then there is a dimensional constant $C > 0$ such that the following estimate holds

$$\|\nabla u_i\|_{L^\infty(B_{r/2})} \leq C \left(\|f\|_{L^\infty(B_r)} + \frac{\|u\|_{L^\infty(B_r)}}{r} \right). \tag{3.3.17}$$

We prove the following result which implies Theorem 3.1.3 *(iii)* since if the bounded open set $D \subset' \mathbb{R}^2$ has boundary of class C^2, then the function w_D defined below is Lipschitz continuous on $\overline{D}$.

Theorem 3.3.9. *Let $D \subset \mathbb{R}^2$ be a bounded open set. Let $(\Omega_1, \ldots, \Omega_h)$ be optimal for* (3.1.2). *Then the corresponding first eigenfunctions $u_1, \ldots, u_h$ are locally Lipschitz continuous in D. If, moreover, D is such that the weak solution w_D of the problem*

$$-\Delta w_D = 1, \qquad w_D \in H_0^1(D),$$

is Lipschitz continuous on $\mathbb{R}^2$, then the first eigenfunctions $u_1, \ldots, u_h$ are globally Lipschitz continuous on $\mathbb{R}^2$.

Proof. Let $r_0 > 0$ be the constant from Proposition 3.3.7 and fix $r_1 \leq r_0/2$. Let $x_0 \in \Omega_i$ be such that $\mathrm{dist}(x_0, \partial D) \geq r_1$. If $r := \mathrm{dist}(x_0, \partial \Omega_i) \geq r_1$, then by (3.3.17), we have

$$|\nabla u_i(x_0)| \leq C \left(\lambda_1(\Omega_i) + r_1^{-1} \right) \|u_i\|_{L^\infty}. \tag{3.3.18}$$

If $r := \text{dist}(x_0, \partial\Omega_i) < r_1$, then we set $y_0 \in \partial\Omega_i$ to be such that $|x_0 - y_0| = \text{dist}(x_0, \partial\Omega_i)$. Using Proposition 3.3.7 and again (3.3.17), we have

$$
\begin{aligned}
|\nabla u_i(x_0)| \ &\leq\ C\left(\lambda_1(\Omega_i)\|u_i\|_{L^\infty} + \frac{\|u_i\|_{L^\infty(B_r(x_0))}}{r}\right) \\[2ex]
&\leq\ C\left(\lambda_1(\Omega_i)\|u_i\|_{L^\infty} + \frac{\|u_i\|_{L^\infty(B_{2r}(y_0))}}{r}\right) \leq C\left(\lambda_1(\Omega_i)\|u_i\|_{L^\infty} + 2C_{12}\right),
\end{aligned}
$$
(3.3.19)

which gives the local Lipschitz continuity of u_i.

If the function w_D is Lipschitz continuous on $\mathbb{R}^d$, we consider for every point $x_0 \in \Omega_i$ two possibilities for $r := \text{dist}(x_0, \partial\Omega_i)$: if $3r \geq \text{dist}(x_0, \partial D)$, then the maximum principle $u_i \leq \lambda_1(\Omega_i)\|u_i\|_{L^\infty} w_D$ and the gradient estimate (3.3.17) gives

$$
\begin{aligned}
|\nabla u_i(x_0)| \ &\leq\ C\left(\lambda_1(\Omega_i)\|u_i\|_{L^\infty} + \frac{\|u_i\|_{L^\infty(B_r(x_0))}}{r}\right) \\[2ex]
&\leq\ C\lambda_1(\Omega_i)\|u_i\|_{L^\infty}\left(1 + \frac{\|\nabla w_D\|_{L^\infty}}{r}\big(\text{dist}(x_0, \partial D) + r\big)\right) \\[2ex]
&\leq\ C\lambda_1(\Omega_i)\|u_i\|_{L^\infty}\left(1 + 4\|\nabla w_D\|_{L^\infty}\right).
\end{aligned}
$$
(3.3.20)

If $3r \leq \text{dist}(x_0, \partial D)$ and $r \leq r_0/2$, then the gradient estimate (3.3.17) gives again (3.3.19). If $r \geq r_0/2$, then we have (3.3.18) with $r_1 = r_0/2$ and this concludes the proof. $\qquad\square$

3.3.3 A monotonicity formula with decay

In order to prove the lack of double points on the boundary of D and the regularity of the auxiliary phase Ω_{h+1} we will need special type of a two phase monotonicity formula in which the supports of the eigenfunctions cannot invade certain prescribed zone. In this case the product of the two gradients $\left(\dfrac{1}{r^2}\displaystyle\int_{B_r}|\nabla u^+|^2\,dx\right)\left(\dfrac{1}{r^2}\displaystyle\int_{B_r}|\nabla u^-|^2\,dx\right)$ decays as $r \to 0$. The result is in the spirit of the three phase formula but the proof follows the idea of the proof of the two phase formula that was carried out in [38].

Lemma 3.3.10. *Consider the unit ball $B_1 \subset \mathbb{R}^2$. Let $u^+, u^- \in H^1(B_1) \cap L^\infty(B_1)$ be two non-negative functions with disjoint supports, i.e. such that $\int_{B_1} u^+ u^-\,dx = 0$, and let $\lambda_+, \lambda_- \geq 0$ be two real numbers such that*

$$
\Delta u^+ + \lambda_+ u^+ \geq 0 \qquad \text{and} \qquad \Delta u^- + \lambda_- u^- \geq 0.
$$

If, moreover, the set $\Omega := B_1 \cap \{u^+ = 0\} \cap \{u^- = 0\}$ has positive density in 0 in sense that

$$
\liminf_{r \to 0} \frac{|\Omega \cap B_r|}{|B_r|} = c > 0,
$$

then there is some $\varepsilon > 0$, depending on d, λ_+, λ_- and c such that

$$\left(\frac{1}{r^2} \int_{B_r} |\nabla u^+|^2 \, dx \right) \left(\frac{1}{r^2} \int_{B_r} |\nabla u^-|^2 \, dx \right) = o(r^\varepsilon). \tag{3.3.21}$$

The proof of Lemma 3.3.10 is based on Lemma 3.3.12, which involves the auxiliary functions U_1 and U_2 constructed below. Let $\lambda := \max\{\lambda_+, \lambda_-\}$ and let $r_0 > 0$ be small enough such that there is a positive radially symmetric function $\varphi \in H^1(B_{r_0})$ satisfying

$$-\Delta\varphi = \lambda\varphi \ \text{ in } \ B_{r_0}, \qquad 0 < a \leq \varphi \leq b, \tag{3.3.22}$$

for some constants $0 < a \leq b$ depending on d, λ and r_0. We now introduce the notation

$$U_1 := \frac{u^+}{\varphi} \qquad \text{and} \qquad U_2 := \frac{u^-}{\varphi}. \tag{3.3.23}$$

Remark 3.3.11. A direct computation of the gradient of U_i on B_{r_0} gives

$$\nabla U_1 = \ \varphi^{-1}\nabla u^+ - \varphi^{-2}u^+\nabla\varphi$$

We define the function $\Phi : [0, r_0] \to \mathbb{R}^+$ as

$$\Phi(r) := \left(\frac{1}{r^2} \int_{B_r} \varphi^2 |\nabla U_1|^2 \, dx \right) \left(\frac{1}{r^2} \int_{B_r} \varphi^2 |\nabla U_2|^2 \, dx \right). \tag{3.3.24}$$

Lemma 3.3.12. *Consider the unit ball $B_1 \subset \mathbb{R}^2$. Let $u^+, u^- \in H^1(B_1) \cap L^\infty(B_1)$ be as in Lemma 3.3.10 and let $\Phi : [0, r_0] \to \mathbb{R}^+$ be given by (3.3.24). Then*

(a) Φ is increasing on the interval $(0, r_0)$;

(b) If, moreover, the set $\Omega := B_1 \cap \{u^+ = 0\} \cap \{u^- = 0\}$ has positive density in 0, then there are constants $C > 0$ and $\varepsilon > 0$ such that

$$\frac{1}{r^\varepsilon}\Phi(r) \leq \frac{C}{r_0^\varepsilon}\Phi(r_0).$$

Proof. We first estimate the derivative of Φ, using the notations $\nabla_n u$ and $\nabla_\tau u$ respectively for

the normal and the tangential part of the gradient ∇u on the boundary of ∂B_r.

$$\frac{\Phi'(r)}{\Phi(r)} = -\frac{4}{r} + \sum_{i=1,2} \frac{\int_{\partial B_r} \varphi^2 |\nabla U_i|^2 \, d\mathcal{H}^1}{\int_{B_r} \varphi^2 |\nabla \widetilde{U}_i|^2 \, dx}$$

$$\geq -\frac{4}{r} + \sum_{i=1,2} \frac{\int_{\partial B_r} \varphi^2 \left(|\nabla_\tau U_i|^2 + |\nabla_n U_i|^2 \right) d\mathcal{H}^1}{\int_{\partial B_r} \varphi^2 U_i |\nabla_n U_i| \, d\mathcal{H}^1} \tag{3.3.25}$$

$$\geq -\frac{4}{r} + \sum_{i=1,2} \frac{2 \left(\int_{\partial B_r} \varphi^2 |\nabla_n U_i|^2 \, d\mathcal{H}^1 \right)^{1/2} \left(\int_{\partial B_r} \varphi^2 |\nabla_\tau U_i|^2 \, d\mathcal{H}^1 \right)^{1/2}}{\left(\int_{\partial B_r} \varphi^2 U_i^2 \, d\mathcal{H}^1 \right)^{1/2} \left(\int_{\partial B_r} \varphi^2 |\nabla_n U_i|^2 \, d\mathcal{H}^1 \right)^{1/2}} \tag{3.3.26}$$

$$= -\frac{4}{r} + 2 \sum_{i=1,2} \left(\frac{\int_{\partial B_r} |\nabla_\tau U_i|^2 \, d\mathcal{H}^1}{\int_{\partial B_r} U_i^2 \, d\mathcal{H}^1} \right)^{1/2} \tag{3.3.27}$$

$$\geq -\frac{4}{r} + 2 \sum_{i=1,2} \sqrt{\lambda_1(\partial B_r \cap \{U_i > 0\})}$$

$$\geq -\frac{4}{r} + \sum_{i=1,2} \frac{2\pi}{\mathcal{H}^1(\partial B_r \cap \{U_i > 0\})}, \tag{3.3.28}$$

where (3.3.25) follows by integration by parts and the inequality $-\operatorname{div}(\varphi^2 \nabla U_i) \leq 0$ obtained using Remark 3.3.11; (3.3.26) is obtained by applying the mean quadratic-mean geometric inequality in the nominator and the Cauchy-Schwartz inequality in the denominator; (3.3.27) is due to the fact that φ is constant on ∂B_r; (3.3.28) follows by a standard symmetrization argument. Setting

$$\theta(r) := \frac{\mathcal{H}^1(\Omega \cap \partial B_r)}{\mathcal{H}^1(\partial B_r)},$$

and applying the mean arithmetic-mean harmonic inequality to (3.3.28), we get

$$\frac{\Phi'(r)}{\Phi(r)} \geq \frac{4}{r}\left(-1 + \frac{1}{1 - \theta(r)} \right) \geq \frac{4\theta(r)}{r}, \tag{3.3.29}$$

which gives (a). In order to prove (b), we note that for $r_0 > 0$ small enough we have the density estimate

$$|\Omega \cap B_r| \geq c|B_r|, \qquad \forall 0 < r \leq r_0.$$

Using the fact that $\frac{\partial}{\partial r}|\Omega \cap B_r| = \mathcal{H}^1(\Omega \cap \partial B_r) = 2\pi r \theta(r)$ we get

$$\int_0^r 2\pi s(\theta(s) - c) \, ds \geq 0, \qquad \forall r \in (0, r_0). \tag{3.3.30}$$

As a consequence we have that

$$\int_{rc/2}^r 2\pi s \left(\theta(s) - \frac{c}{2} \right) ds \geq 0, \qquad \forall r \in (0, r_0). \tag{3.3.31}$$

Indeed, if this is not the case, then

$$0 \leq \int_0^r 2\pi s(\theta(s) - c) \, ds \leq \int_0^{cr/2} 2\pi s(1 - c) \, ds - \int_{cr/2}^r 2\pi s \frac{c}{2} \, ds \leq -\pi r^2 c(1 - c)^2,$$

96

which is in contradiction with (3.3.30). By (3.3.31), we get that there is a constant $c_0 > 0$ such that

$$\int_{rc/2}^{r} \theta(s)\, ds \geq c_0 r, \qquad \forall r < r_0. \tag{3.3.32}$$

By (3.3.29) we have

$$\begin{aligned}
\log\left(r^{-\varepsilon}\Phi(r)\right) - \log\left(\left(rc/2\right)^{-\varepsilon}\Phi(rc/2)\right) &= \int_{rc/2}^{r}\left(-\frac{\varepsilon}{s} + \frac{\Phi'(s)}{\Phi(s)}\right)\, ds \\
&\geq \int_{rc/2}^{r}\frac{4}{s}\left(-\frac{\varepsilon}{4} + \theta(s)\right)\, ds \geq \varepsilon\log(c/2) + 4c_0,
\end{aligned}$$

which is positive for $\varepsilon > 0$ small enough. Thus, we obtain that the sequence

$$a_n := r_n^{-\varepsilon}\Phi(r_n), \qquad \text{where} \quad r_n = (c/2)^n r_0,$$

is decreasing and so, by rescaling we obtain (b). $\qquad\square$

Proof of Lemma 3.3.10. We first note that as a consequence of Remark 3.3.11, we have the estimates:

$$\begin{aligned}
\int_{B_r}\frac{|\nabla u^{\pm}|^2}{|x|^{d-2}}\, dx &\leq 2\int_{B_r}\varphi^2\frac{|\nabla U_{12}|^2}{|x|^{d-2}}\, dx + 2\|\varphi^{-1}\nabla\varphi\|_{L^{\infty}(B_{r_0})}^2\int_{B_r}\frac{u^2}{|x|^{d-2}}\, dx, \\[2mm]
\int_{B_r}\varphi^2\frac{|\nabla U_{12}|^2}{|x|^{d-2}}\, dx &\leq 2\int_{B_r}\frac{|\nabla u^{\pm}|^2}{|x|^{d-2}}\, dx + 2\|\varphi^{-1}\nabla\varphi\|_{L^{\infty}(B_{r_0})}^2\int_{B_r}\frac{u^2}{|x|^{d-2}}\, dx.
\end{aligned} \tag{3.3.33}$$

Taking in consideration the inequality

$$\int_{B_{r_0}}\frac{|\nabla u^{\pm}|^2}{|x|^{d-2}}\, dx \leq C\left(1 + \int_{B_{2r_0}}|u^{\pm}|^2\, dx\right), \tag{3.3.34}$$

proved in [34], we obtain the claim by Lemma 3.3.12 and simple arithmetic. $\qquad\square$

3.3.4 Multiphase points and regularity of the free boundary

This subsection is dedicated to the proof of (i), (ii) and (iv) of Theorem 3.1.3.

Lack of triple points. The lack of triple points was proved in [31] in the more general case of partitions concerning general functionals depending on the spectrum of the Dirichlet Laplacian. The original proof uses the notion of an energy subsolution. In the present case the lack of triple points follows directly. In fact if there are three phases Ω_i, Ω_j, Ω_k such that the intersection of their boundaries contains a point x_0, then by the non-degeneracy of the gradient (Corollary 3.3.4) we have that the product $\prod_{i=1}^{3}\left(\frac{1}{r^2}\int_{B_r}|\nabla u_i|^2\, dx\right)$ remains bounded from below by a strictly positive constant, which is in contradiction with the three-phase monotonicity formula (Theorem 3.2.5).

Lack of two-phase points on the boundary of the box. Our first numerical simulations showed the lack of double points (i.e. points on the boundary of two distinct sets) on the

boundary of the box D. We first notice that there is a quick argument that proves the above claim in the case when the boundary ∂D is smooth. Indeed, if this is the case and if $x_0 \in \partial D$, then there is a ball $B \subset D^c$ such that $x_0 \in \partial B$. Since the gradient of the first eigenfunction u on B satisfies the non-degeneracy inequality (3.3.4), we can use the three-phase monotonicity formula to conclude the proof.

If the boundary ∂D is only Lipschitz we need to use Lemma 3.3.10. Suppose, by absurd, that there is a point $x_0 \in \partial \Omega_i \cap \partial \Omega_j \cap \partial D$. If u_i and u_j are the first eigenfunctions on Ω_i and Ω_j, by Corollary 3.3.4 we have

$$\fint_{B_r(x_0)} |\nabla u_i|^2 \, dx \geq C_{nd} \qquad \text{and} \qquad \fint_{B_r(x_0)} |\nabla u_j|^2 \, dx \geq C_{nd}, \qquad (3.3.35)$$

for small enough $r > 0$ and some non-degeneracy constant $C_{nd} > 0$. Since ∂D is Lipschitz, we have the density estimate $\liminf_{r \to 0} \dfrac{|D^c \cap B_r(x_0)|}{|B_r|} > 0$ and so, we can apply Lemma 3.3.10, obtaining a contradiction.

Regularity of the auxiliary set $\Omega_{h+1} = D \setminus \left(\bigcup_{i=1}^{h} \Omega_i \right)$. We first notice that since each of the sets $\Omega_1, \ldots, \Omega_h$ is a shape subsolution for $\lambda_1 + a| \cdot |$, we have that each of these sets has finite perimeter by Theorem 3.2.3. As a consequence Ω_{h+1} also has finite perimeter. Suppose that $x_0 \in D \cap \partial^* \Omega_{h+1}$.

Suppose that x_0 is on the boundary of at most one phase, i.e. that there is ball $B_r(x_0)$ and an index $i \in \{1, \ldots, h\}$ such that $B_r(x_0) = \left(B_r(x_0) \cap \Omega_i \right) \cup \left(B_r(x_0) \cap \Omega_{h+1} \right)$. Then the set Ω_i is a solution of

$$\min \left\{ \lambda_1(\Omega) + \int_\Omega W_i(x) \, dx \ : \ \Omega \subset D_i \cap B_r(x_0), \ \Omega \text{ open} \right\},$$

where the set D_i is given by Theorem 3.2.3. By the regularity result of Briançon and Lamboley Theorem 3.2.2 we have that $\partial^* \Omega_{h+1} = \partial \Omega_{h+1}$ in $B_r(x_0)$ and is locally a graph of a smooth function.

Thus in order to conclude it is sufficient to prove that x_0 belonging to the boundary of just one of the phases is the only possible case. Indeed, suppose that there is $j \neq i$ such that for every ball $B_r(x_0)$ the sets $B_r(x_0) \cap \Omega_i$ and $B_r(x_0) \cap \Omega_j$ are both non-empty. By the non-degeneracy of the gradients of the eigenfunctions u_i and u_j we have that $\int_{B_r(x_0)} |\nabla u_i|^2 \, dx \geq C_{nd} r^2$ and $\int_{B_r(x_0)} |\nabla u_j|^2 \, dx \geq C_{nd} r^2$. On the other hand, since x_0 is in the reduced boundary of Ω_{h+1} we have that

$$\lim_{r \to 0} \frac{|B_r(x_0) \cap \Omega_{h+1}|}{|B_r(x_0)|} = \frac{1}{2}.$$

Thus by the decay monotonicity formula Lemma 3.3.10 we get

$$\lim_{r \to 0} \left(\frac{1}{r^2} \int_{B_r(x_0)} |\nabla u_i|^2 \, dx \right) \left(\frac{1}{r^2} \int_{B_r(x_0)} |\nabla u_j|^2 \, dx \right) = 0,$$

which is a contradiction. Thus every point of the reduced boundary belongs to at most one phase and $\partial^* \Omega_{h+1}$ is smooth.

98

3.4   Further remarks and open questions

This section is dedicated to some further developments around Theorem 3.1.3. In particular, using the decay monotonicity formula from Lemma 3.3.10 and the same argument as in Theorem 3.1.3 *(iv)* we prove that the optimal set for the second eigenfunction has smooth reduced boundary. We also discuss the extension of Theorem 3.1.3 to smooth surfaces and the analogous result in this case.

3.4.1   On the regularity of the optimal set for the second eigenvalue

Consider the shape optimization problem

$$\min\Big\{\lambda_2(\Omega) + \alpha|\Omega| \ : \ \Omega \text{ open}, \ \Omega \subset D\Big\}, \tag{3.4.1}$$

where $D \subset \mathbb{R}^2$ is a bounded open set and $\alpha > 0$. By the Buttazzo-Dal Maso Theorem this problem admits a solution in the class of quasi-open sets. The question of regularity of the solutions is quite involved and no progress was made for almost two decades until in [26] it was proved that every solution has finite perimeter and in [31] it was proved that there is an open solution characterized through a multiphase problem. In the Theorem below we answer the question of the regularity of the reduced boundary $\partial^*\Omega$ of the solutions of (3.4.1).

Theorem 3.4.1. *Let Ω be a solution of* (3.4.1). *Then the reduced boundary $D \cap \partial^*\Omega$ is smooth.*

Proof. We first notice that it was proved in [31] that for every solution Ω of the problem (3.4.1) there are disjoint open sets $\omega_1, \omega_2 \subset \Omega$ of the same measure as Ω, i.e. $|\Omega \setminus (\omega_1 \cup \omega_2)| = \emptyset$ such that the set $\omega_1 \cup \omega_2$ is still a solution of (3.4.1) and such that the couple (ω_1, ω_2) is a solution to the multiphase problem

$$\min\Big\{ \max\{\lambda_1(\omega_1), \lambda_1(\omega_2)\} + \alpha|\omega_1| + \alpha|\omega_2| \ : \ \omega_1, \omega_2 \text{ open}, \ \omega_{1,2} \subset D, \ \omega_1 \cap \omega_2 = \emptyset\Big\}. \tag{3.4.2}$$

We notice that necessarily ω_1 and ω_2 are both connected and $\lambda_1(\omega_1) = \lambda_1(\omega_2)$, otherwise it would be possible to construct a better competitor for (3.4.2). Thus, by confronting the couple ω_1, ω_2 with a couple $\widetilde{\omega}_1, \omega_2$ where $\widetilde{\omega}_1 \subset \omega_1$ we get that ω_1 is a shape subsolution for the functional $\lambda_1 + \alpha|\cdot|$ and analogously ω_2 is a shape subsolution for the same functional. In particular, all the conclusions of Theorem 3.2.3 are valid. Let now $x_0 \in \partial^*\Omega$. Using the non-degeneracy of the gradient of the first eigenfunctions $u_1 \in H_0^1(\omega_1)$ and $u_2 \in H_0^1(\omega_2)$ in x_0 and the decay monotonicity formula Lemma 3.3.10, and reasoning as in the proof of Theorem 3.1.3 *(iv)* we get that there is a ball $B_r(x_0)$ that does not intersect one of the sets ω_1 and ω_2. Without loss of generality $B_r(x_0) \cap \omega_2 = \emptyset$. Now by the regularity result of Briançon and Lamboley [23] and the fact that $\partial^*\omega_1 = \partial^*\Omega$ in $B_r(x_0)$ we get that $\partial^*\Omega$ is regular in a neighbourhood of x_0. □

Remark 3.4.2. We notice that an estimate on the Hausdorff dimension of the set $\partial\Omega \setminus \partial^*\Omega$ is not available at the moment.

3.4.2 Multiphase shape optimization problems on smooth manifolds

We notice that all the arguments that we use are local and Theorem 3.1.3 can easily be extended to the case where the box (D, g) is a riemannian manifold with or without boundary. In fact the existence of an optimal partition follows by the analogous of the Buttazzo - Dal Maso Theorem proved in [31]. The Laplace-Beltrami operator Δ_g in local coordinates satisfies $\varepsilon\Delta \leq \Delta_g \leq \varepsilon^{-1}\Delta$ as an operator, where $\varepsilon > 0$ depends on D and g, and analogously the gradient satisfies $\varepsilon|\nabla u| \leq |\nabla_g u| \leq \varepsilon^{-1}|\nabla u|$, for any function $u \in H^1(D)$ expressed in local coordinates. Thus, the two and three-phase monotonicity formulas are still valid as well as the non-degeneracy of the gradient, the lack of triple points inside D and the lack of double points on the boundary of D. We present the results that are still valid in the following Theorem.

Theorem 3.4.3. *Suppose that D is a compact riemannian surface. Let $0 < a \leq A$ be two positive real numbers and $W_i : D \to [a, A]$, $i = 1, \ldots, h$ be given C^2 functions. Then there are disjoint open sets $\Omega_1, \ldots, \Omega_h \subset D$ solving the multiphase optimization problem (3.1.2) in D. Moreover, any solution to (3.1.2) satisfies the conditions (i), (ii) and (iii) of Theorem 3.1.3.*

3.5 Numerical eigenvalue computation on a fixed grid

There are multiple ways of computing numerically the low Dirichlet-Laplace eigenvalues of a shape Ω, most of them requiring a good description of the boundary (for example finite elements, or fundamental solutions). In our case it is necessary to compute the first eigenvalue of a number of shapes, for which it is difficult to keep track of their boundaries. Thus, having a method which allows us to work on a fixed domain D containing the shape, greatly simplifies the treatment of the problem. Methods of this kind were used in [18],[36] in the study of spectral minimal partitions. In our study we use the method presented in [18]. We did not found any other works in the literature which study the numerical error associated to this method. In this section we present the discretization algorithm, as well as the errors obtained for a few simple shapes.

This eigenvalue computation method is inspired from penalized problems of the form

$$-\Delta u + \mu u = \lambda_k(\mu)u, \qquad u \in H^1(D) \cap L^2(D, \mu), \tag{3.5.1}$$

where D is a bounded open set in $\mathbb{R}^2$, and μ is a measure such that $\mu(A) = 0$ whenever A has capacity zero. The case where λ_k corresponds to a Dirichlet Laplace eigenvalue of a set $\Omega \subset D$ is included in the formulation (3.5.1). Indeed, if ∞_{Ω^c} is defined as follows:

$$\infty_{\Omega^c}(A) = \begin{cases} 0 & \text{if } \mathrm{cap}(A \cap \Omega) = 0 \\ \infty & \text{otherwise} \end{cases},$$

then $\lambda_k(\infty_{\Omega^c}) = \lambda_k(\Omega)$. We have denoted $\mathrm{cap}(A)$ the capacity of the set A. For further details about the penalized formulation (3.5.1), we refer to [27, Chapter 6].

N	$C = 10^3$	$C = 10^4$	$C = 10^5$	$C = 10^6$	$C = 10^7$	$C = 10^8$	$C = 10^9$
100	$5.2 \cdot 10^{-2}$	$1.8 \cdot 10^{-2}$	$1.2 \cdot 10^{-2}$	$1.1 \cdot 10^{-2}$	$1.1 \cdot 10^{-2}$	$1.1 \cdot 10^{-2}$	$1.1 \cdot 10^{-2}$
200	$5.1 \cdot 10^{-2}$	$1.1 \cdot 10^{-2}$	$1.5 \cdot 10^{-3}$	$5.5 \cdot 10^{-4}$	$7 \cdot 10^{-4}$	$7.2 \cdot 10^{-4}$	$7.2 \cdot 10^{-4}$
300	$5.6 \cdot 10^{-2}$	$1.6 \cdot 10^{-2}$	$4.7 \cdot 10^{-3}$	$2.8 \cdot 10^{-3}$	$2.6 \cdot 10^{-3}$	$2.6 \cdot 10^{-3}$	$2.6 \cdot 10^{-3}$
400	$5.7 \cdot 10^{-2}$	$1.6 \cdot 10^{-2}$	$3.9 \cdot 10^{-3}$	$1.6 \cdot 10^{-3}$	$1.3 \cdot 10^{-3}$	$1.3 \cdot 10^{-3}$	$1.3 \cdot 10^{-3}$
500	$5.7 \cdot 10^{-2}$	$1.6 \cdot 10^{-2}$	$3.8 \cdot 10^{-3}$	$1.1 \cdot 10^{-3}$	$7.9 \cdot 10^{-4}$	$7.6 \cdot 10^{-4}$	$7.5 \cdot 10^{-4}$

Table 3.1: Relative errors for the unit disk

N	$C = 10^3$	$C = 10^4$	$C = 10^5$	$C = 10^6$	$C = 10^7$	$C = 10^8$	$C = 10^9$
100	$5.1 \cdot 10^{-2}$	$1.9 \cdot 10^{-2}$	$1.3 \cdot 10^{-2}$	$1.3 \cdot 10^{-2}$	$1.3 \cdot 10^{-2}$	$1.3 \cdot 10^{-2}$	$1.3 \cdot 10^{-2}$
200	$4.4 \cdot 10^{-2}$	$5.7 \cdot 10^{-3}$	$3.7 \cdot 10^{-3}$	$4.8 \cdot 10^{-3}$	$5 \cdot 10^{-3}$	$5 \cdot 10^{-3}$	$5 \cdot 10^{-3}$
300	$6.2 \cdot 10^{-2}$	$2.2 \cdot 10^{-2}$	$1.2 \cdot 10^{-2}$	10^{-2}	10^{-2}	10^{-2}	10^{-2}
400	$5.7 \cdot 10^{-2}$	$1.6 \cdot 10^{-2}$	$5 \cdot 10^{-3}$	$2.9 \cdot 10^{-3}$	$2.7 \cdot 10^{-3}$	$2.7 \cdot 10^{-3}$	$2.7 \cdot 10^{-3}$
500	$5.4 \cdot 10^{-2}$	$1.3 \cdot 10^{-2}$	$8.3 \cdot 10^{-4}$	$1.7 \cdot 10^{-3}$	$2 \cdot 10^{-3}$	$2 \cdot 10^{-3}$	$2 \cdot 10^{-3}$

Table 3.2: Relative errors for the square of side length 2

This formulation suggests the following numerical method: we choose $\mu = (1 - \mathbb{1}_\Omega)Cdx$, where $\mathbb{1}_\Omega$ is the characteristic function of Ω, and C is large. In [18] it is proved that as $C \to \infty$ we have $\lambda_k(C(1 - \mathbb{1}_\Omega)dx) \to \lambda_k(\Omega)$. In the following we propose to study the behaviour of this eigenvalue computation method with respect to the discretization parameter N and with respect to the choice of C. We compare these values with the ones provided by the MpsPack software [14], which is quite precise.

We consider the domain $D = [-1.5, 1.5]^2$ and on it we take a $N \times N$ uniform grid. We discretize a function $u : D \to \mathbb{R}$ by considering its values on this regular grid. For sets $\Omega \subset D$ we consider the approximation of problem (3.5.1) defined as

$$-\Delta u + C(1 - \mathbb{1}_\Omega)u = \lambda_k(C\mathbb{1}_{\Omega^c}dx)u. \tag{3.5.2}$$

This leads us to the discretized matrix problem

$$(A + C\text{diag}(1 - \mathbb{1}_\Omega))u = \lambda u,$$

where A is the finite difference discretization of the laplacian operator.

We present below the relative error, compared to MpsPack, in function of the measure parameter C and the discretization parameter N. In tables 3.1,3.2,3.3 and 3.4 we present the maximal relative error $|\lambda_k^{\text{approx}} - \lambda_k|/\lambda_k$ (with $1 \leq k \leq 10$) for the unit disk, for the square of side length 2 and for the shapes presented in Figure 3.1. Here λ_k stands for the analytical value (when available) or the value computed with MpsPack.

In our experiments we observed that for a fixed discretization parameter N, the relative error stabilizes itself when C is large enough. This numerical effect seems to be due to the fact that Ω is approximated using a rectangular grid, so at a given N, for large C we only compute the eigenvalue of this discrete approximation of Ω.

N	$C = 10^3$	$C = 10^4$	$C = 10^5$	$C = 10^6$	$C = 10^7$	$C = 10^8$	$C = 10^9$
100	$6 \cdot 10^{-2}$	$1.8 \cdot 10^{-2}$	$1 \cdot 10^{-2}$	$9.5 \cdot 10^{-3}$	$9.4 \cdot 10^{-3}$	$9.4 \cdot 10^{-3}$	$9.4 \cdot 10^{-3}$
200	$6.5 \cdot 10^{-2}$	$1.8 \cdot 10^{-2}$	$6.1 \cdot 10^{-3}$	$4.4 \cdot 10^{-3}$	$4.2 \cdot 10^{-3}$	$4.2 \cdot 10^{-3}$	$4.2 \cdot 10^{-3}$
300	$6.7 \cdot 10^{-2}$	$1.9 \cdot 10^{-2}$	$4.9 \cdot 10^{-3}$	$2.5 \cdot 10^{-3}$	$2.2 \cdot 10^{-3}$	$2.2 \cdot 10^{-3}$	$2.2 \cdot 10^{-3}$
400	$6.8 \cdot 10^{-2}$	$1.9 \cdot 10^{-2}$	$4.7 \cdot 10^{-3}$	$1.8 \cdot 10^{-3}$	$1.4 \cdot 10^{-3}$	$1.4 \cdot 10^{-3}$	$1.4 \cdot 10^{-3}$
500	$6.9 \cdot 10^{-2}$	$2 \cdot 10^{-2}$	$5.3 \cdot 10^{-3}$	$1.9 \cdot 10^{-3}$	$1.4 \cdot 10^{-3}$	$1.4 \cdot 10^{-3}$	$1.4 \cdot 10^{-3}$

Table 3.3: Relative errors for the shape presented in Figure 3.1 (left)

N	$C = 10^3$	$C = 10^4$	$C = 10^5$	$C = 10^6$	$C = 10^7$	$C = 10^8$	$C = 10^9$
100	$6.9 \cdot 10^{-2}$	$2.2 \cdot 10^{-2}$	$1.4 \cdot 10^{-2}$	$1.3 \cdot 10^{-2}$	$1.3 \cdot 10^{-2}$	$1.3 \cdot 10^{-2}$	$1.3 \cdot 10^{-2}$
200	$7.2 \cdot 10^{-2}$	$2 \cdot 10^{-2}$	$6.8 \cdot 10^{-3}$	$4.8 \cdot 10^{-3}$	$4.6 \cdot 10^{-3}$	$4.6 \cdot 10^{-3}$	$4.6 \cdot 10^{-3}$
300	$7.4 \cdot 10^{-2}$	$2.1 \cdot 10^{-2}$	$5.9 \cdot 10^{-3}$	$3.3 \cdot 10^{-3}$	$3 \cdot 10^{-3}$	$2.9 \cdot 10^{-3}$	$2.9 \cdot 10^{-3}$
400	$7.6 \cdot 10^{-2}$	$2.2 \cdot 10^{-2}$	$6.1 \cdot 10^{-3}$	$2.8 \cdot 10^{-3}$	$2.4 \cdot 10^{-3}$	$2.4 \cdot 10^{-3}$	$2.4 \cdot 10^{-3}$
500	$7.6 \cdot 10^{-2}$	$2.3 \cdot 10^{-2}$	$5.6 \cdot 10^{-3}$	$1.8 \cdot 10^{-3}$	$1.3 \cdot 10^{-3}$	$1.3 \cdot 10^{-3}$	$1.3 \cdot 10^{-3}$

Table 3.4: Relative errors for the shape presented in Figure 3.1 (right)
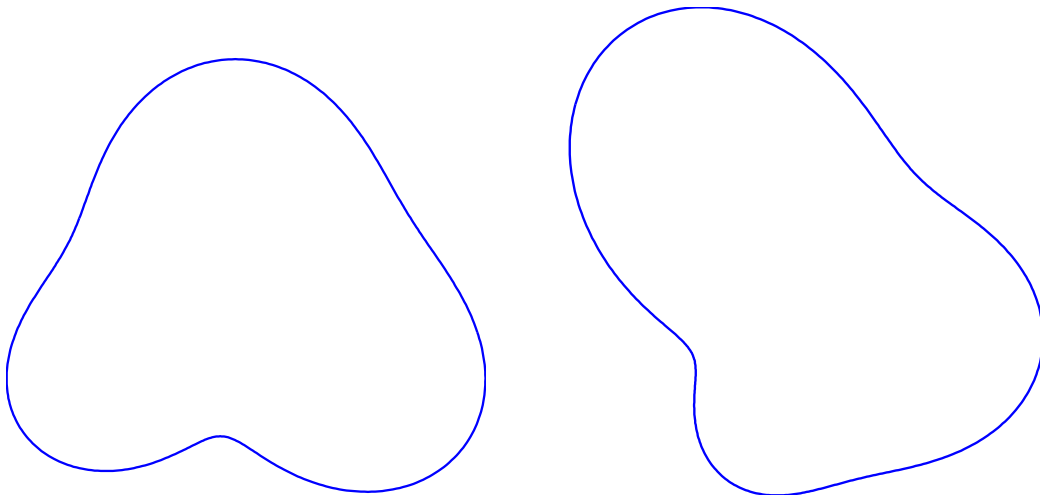
Figure 3.1: Shapes for which we test the method in Table 3.3 (left) and Table 3.4 (right)

3.6 Proof of Theorem 3.1.5

In this section, we give a theoretical estimate of the relative error obtained when working with the penalized method. We study the difference between the eigenvalue $\lambda_k(C\mathbb{1}_{\Omega^c}dx)$, given by (3.5.2), and $\lambda_k(\Omega)$. We fix $\Omega \subset D$ to be an open set with boundary of class C^2. In the following, we denote $\mu_C = C\mathbb{1}_{\Omega^c}dx$.

We consider the functions w, w_C defined as follows

$$-\Delta w = 1 \text{ in } \Omega, \ w \in H_0^1(\Omega),$$

$$-\Delta w_C + C\mathbb{1}_{\Omega^c}w_C = 1 \text{ in } D, w_C \in H_0^1(D).$$

Note that the standard maximum principle implies that $w_C \geq w$ on D. Using the terminology

defined in [29] we note that $\mu_C dx \prec \infty_{\Omega^c}$ so cf. [29, Lemma 4.3] and [26, Lemma 4.1] the following estimate holds

$$\|\mathcal{R}_{\mu_C} - \mathcal{R}_{\infty_{\Omega^c}}\|_{\mathcal{L}(L^2)} \leq C_{N,\Omega}\|w_C - w\|_{L^1}.$$

In general, we denote R_μ the resolvent operator associated to the problem

$$-\Delta u + u\mu = f, \ u \in H_0^1(D) \cap L^2(D, \mu).$$

Using [27, Corollary 6.1.8] we obtain the estimate

$$\left|\frac{1}{\lambda_k(\mu_C)} - \frac{1}{\lambda_k(\Omega)}\right| \leq \|\mathcal{R}_{\mu_C} - \mathcal{R}_{\infty_{\Omega^c}}\|_{\mathcal{L}(L^2)} \leq C_{N,\Omega}\|w_C - w\|_{L^1}.$$

Thus, we have

$$\frac{|\lambda_k(\Omega) - \lambda_k(\mu_C)|}{\lambda_k(\Omega)} \leq \lambda_k(\mu_C)C_{N,\Omega}\int_D w_C - w.$$

The monotonicity property stated in [27, Proposition 6.1.5] shows that $\lambda_k(\mu_C) \leq \lambda_k(\Omega)$. In order to finish the proof, it suffices to give an upper bound for $\int_D w_C - w$.

We clearly have

$$\int_D |\nabla w_C|^2 + C\int_{\Omega^c} w_C^2 = \int_D w_C.$$

When $C \to \infty$ we have $w_c \rightharpoonup w$ in $H_0^1(D)$, and as a consequence $\lim_{C\to\infty} C\int_{\Omega^c} w_C^2 = 0$. This proves that for C large enough there exists a constant M such that

$$\left(\int_{\Omega^c} w_C\right)^2 \leq |\Omega^c|\int_{\Omega^c} w_C^2 \leq \frac{M}{C}.$$

Thus

$$\int_{\Omega^c} w_C - w \leq \frac{M}{C^{1/2}}.$$

For the estimate of $\int_\Omega w_C - w$ we use the fact that $w_C - w$ is harmonic in Ω, so

$$\int_\Omega w_C - w \leq \sup_{\partial\Omega} w_C |\Omega|.$$

It remains to estimate $\sup_{\partial\Omega} w_C$.

Assume that $B_{x_0,r_0} \subset \Omega^c$. Then

$$-\Delta w_C \leq 1 \text{ in } D,$$

so $w_C + \dfrac{|x - x_0|^2}{2N}$ is subharmonic in D. This implies

$$w_C(x_0) \leq \frac{1}{\omega_N r_0^N}\int_{B_{x_0,r_0}}(w_c + \frac{|x - x_0|^2}{2N}) \leq \frac{r_0^2}{2N} + \frac{1}{\omega_N^{1/2} r_0^{N/2}}\left(\int_{B_{x_0,r_0}} w_C^2\right)^{1/2},$$

103

where we used the fact that $|x - x_0| \leq r$ and we applied the Cauchy Schwarz inequality. Thus, for C large enough we have

$$w_C(x_0) \leq \frac{r_0^2}{2N} + \frac{M}{\omega_N^{1/2} r_0^{N/2} C^{1/2}}.$$

Next, we choose r_0 of the form $C^{-\alpha}$, which gives us

$$w_C(x_0) \leq \frac{1}{2NC^{2\alpha}} + \frac{M}{\omega_N^{1/2} C^{(1-N\alpha)/2}}.$$

We choose $\alpha = 1/(N + 4)$, which gives the same exponent for C in the two terms of the above sum. Thus

$$w_C(x_0) \leq \left(\frac{1}{2N} + \frac{M}{\omega_N^{1/2}} \right) C^{-2/(N+4)}.$$

Clearly, as $C \to \infty$, x_0 can be chosen closer and closer to $\partial\Omega$. The fact that Ω is of class C^2 implies that Ω satisfies an exterior ball condition B_ρ. If $d(x_0, \partial\Omega) < \rho$ then we can apply the previous estimate.

To go from x_0 to the boundary $\partial\Omega$ we note that the Minkowski sum $\Omega + B_{C^{-\alpha}}$ satisfies an interior and exterior ball condition, if C is large enough. For simplicity, we denote $\Omega' = \Omega + B_{C^{-\alpha}}$ in the sequel. Thus Ω' is of class $C^{1,\alpha}$ and $\nabla w_{\Omega'}$ is well defined on $\partial\Omega'$. Furthermore, consider $B_{\rho'}$ an exterior ball tangent to Ω' and another concentric ball B_R such that B_R contains Ω'. The annulus A determined by $B_{\rho'}, B_R$ contains Ω', and thus $w_{\Omega'} \leq w_A$ in Ω' and $|\nabla w_{\Omega'}| \leq |\nabla w_A|$ on $\partial\Omega'$. It is well known that w_A is Lipschitz, with a Lipschitz constant depending on ρ' and the diameter of Ω'. Thus, on $\partial\Omega'$ we have that $|\nabla w_{\Omega'}|$ is bounded, and since $|\nabla w_{\Omega'}|$ is maximal on the boundary, it follows that $w_{\Omega'}$ is Lipschitz.

The function $w_C - w_{\Omega'}$ is subharmonic on $\partial\Omega'$. As a consequence, we have

$$w_{\Omega+B_{C^{-\alpha}}} \geq \left(w_C - \left(\frac{1}{2N} + \frac{M}{\omega_N^{1/2}} \right) C^{-2/(N+4)} \right)^+,$$

which together with the Lipschitz continuity of $w_{\Omega+B_{C^{-\alpha}}}$ gives us that

$$w_C|_{\partial\Omega} \leq \left(\frac{1}{2N} + \frac{M}{\omega_N^{1/2}} \right) C^{-2/(N+4)} + M_2 C^{-\alpha},$$

where M_2 is the constant in the Lipschitz continuity result.

Thus

$$w_C|_{\partial\Omega} \leq \left(\frac{1}{2N} + \frac{M}{\omega_N^{1/2}} \right) C^{-2/(N+4)} + M_2 \ell^{1/2} C^{-1/(N+4)}.$$

Consequently, there exists a constant M_3, depending on ε, N, D, such that

$$\int_D w_c - w \leq M_3 C^{-1/(N+4)}.$$

In conclusion, for C large enough, there exists a constant K such that

$$\frac{|\lambda_k(\Omega) - \lambda_k(\mu_C)|}{\lambda_k(\Omega)} \leq KC^{-1/(N+4)}.$$

$\square$

Remark 3.6.1. Using techniques similar to [66, Lemma 3.4.11] we are able to prove that there is an upper bound of the form $KC^{-\delta}$ (with $K, \delta > 0$) for the relative error even in the more general case when Ω satisfies a ε-cone condition (equivalently, a uniform Lipschitz condition). The drawback is that we do not have an explicit formula for δ, like in the case presented above.

We remark that in the case $N = 2$, studied numerically in the previous section, the relative error is bounded theoretically by a term of order $C^{-1/6}$. If we look at the numerical errors, we see that from $C = 10^3$ to $C = 10^9$ the errors roughly decrease by one order of magnitude. This is in good correspondence with the theoretical result which predicts a decrease of the relative error by approximately one order of magnitude when C is multiplied by 10^6. This correspondence shows that this theoretical error bound is close to being sharp in two dimensions.

3.7   Numerical setting and optimization algorithm

In order to compute numerically the shape and the position of the optimal sets, we use the procedure described in Section 3.5. This technique has been introduced in [18] for the study of the case $\alpha = 0$. We recall that the problem we study has the form

$$\min\Big\{ \sum_{i=1}^{h} \lambda_k(\Omega_i) + \alpha|\Omega_i| \,:\, \Omega_i \subset D \text{ quasi-open}, \ \Omega_i \cap \Omega_j = \emptyset \Big\}. \tag{3.7.1}$$

where with $\lambda_k(\Omega)$ we denote the k-th eigenvalue of the Dirichlet Laplacian on $\Omega \subset D$.

For a given measurable function $\varphi : \Omega \in [0,1]$ and constant $C > 0$, we consider the spectrum of the operator $-\Delta + C(1 - \varphi)$ on D, consisting on the eigenvalues with variational characterization

$$\lambda_k(\varphi, C) := \min_{S_k \subset H_0^1(\Omega)} \max_{u \in S_k} \frac{\int_\Omega |\nabla u|^2 + C(1 - \varphi)u^2 \, dx}{\int_\Omega u^2 \, dx},$$

where the minimum is over all k-dimensional subspaces S_k of $H_0^1(D)$. The corresponding k-th eigenfunction satisfies the equation

$$-\Delta u_k + C(1 - \varphi)u_k = \lambda_k(\varphi, C)u_k, \qquad u_k \in H_0^1(D), \quad \int_D u_k^2 \, dx = 1. \tag{3.7.2}$$

By the general existence theorem of Buttazzo and Dal Maso [53], there is a solution $(\varphi_1^C, \ldots, \varphi_h^C)$ of the problem

$$\min\Big\{ \sum_{i=1}^{h} \Big(\lambda_k(\varphi_i, C) + \alpha \int_D \varphi_i \, dx\Big) \,:\, \varphi_i : D \to [0,1] \text{ measurable}, \ \sum_{i=1}^{h} \varphi_i \leq 1 \Big\}. \tag{3.7.3}$$

Moreover, by the approximation result [18, Theorem 2.4], or the result given by Theorem 3.1.5, we have that, for every $i = 1 \ldots h$,

$$\lim_{C \to +\infty} \lambda_1(\varphi_i^C, C) = \lambda_1(\Omega_i) \qquad \text{and} \qquad \lim_{C \to +\infty} \varphi_i^C = \mathbb{1}_{\Omega_i},$$

where the second limit is strong in $L^1(D)$ and the h-uple $(\Omega_1, \ldots, \Omega_h)$ is optimal for (3.7.1).

We were not able to prove that for $k \geq 2$ the functions φ_i^C converge to characteristic functions as $C \to \infty$. In [18] a concavity argument was used to prove the result, and this argument does not extend to the case $k \geq 2$. In the description of the algorithm we keep k general, but the numerical results presented are for $k = 1$. Although we don't have a theoretical justification of the convergence in the case $k = 2$, the algorithm behaves well and produces the expected results. For $k \geq 3$ we did not manage to obtain conclusive results.

Note that for $\alpha > 0$ solutions of problem 3.7.1 do not consist of partitions of D. Therefore the functions φ_l satisfy the non-overlapping constraint $\sum_{i=1}^h \varphi_i \leq 1$. This inequality constraint is not easy to treat numerically, so we choose to add an additional phase, representing the empty space. Define $\varphi_{h+1} := 1 - \sum_{i=1}^h \varphi_i$, the empty phase associated to the multiphase problem. Thus (3.7.3) is equivalent to

$$\min \left\{ \sum_{i=1}^h \lambda_k(\varphi_i, C) - \alpha \int_D \varphi_{h+1} \, dx \; : \; \varphi_i : D \to [0, 1] \text{ measurable}, \; \sum_{i=1}^{h+1} \varphi_i = 1 \right\}, \quad (3.7.4)$$

which is more suitable for numerical implementation. In this way (3.7.1) is reformulated as an optimal partitioning problem

$$\min \left\{ \sum_{i=1}^h \lambda_k(\Omega_i) - \alpha |\Omega_{h+1}| \; : \; \Omega_i \subset \mathbb{R}^d \text{ quasi-open}, \; \Omega_i \cap \Omega_j = \emptyset, \text{ for } i, j = 1, \ldots, h+1 \right\}.$$

In this setting the numerical cost computation of the above problem involves the discrete approximation of the measure of Ω_{h+1} given by

$$|\Omega_{h+1}| \simeq \frac{1}{N^2} \sum_{i,j=1}^{N^2} \varphi_{i,j}^{h+1}.$$

In order to use an optimization algorithm we approximate the derivative of the eigenvalues $\lambda_k(\varphi_l, C)$ as a function of the values of the phases φ_l on the grid points. The precise expression of this derivative was given in [18] and has the form

$$\partial_{i,j} \lambda_k(\varphi_l, C) = -C(U_{i,j}^l)^2, \quad (3.7.5)$$

where U^l is the l-th normalized eigenvector solution of the corresponding discrete equation. The discrete derivative of the volume is given by

$$\partial_{i,j} |\Omega_{h+1}| = 1/N^2.$$

106

In order to perform the optimization under the constraint $\sum_{l=1}^{h+1} \varphi_l = 1$ we use the projection operator on the simplex

$$\mathbb{S}^h = \left\{ X = (X_1, .., X_{h+1}) \in [0,1]^{h+1} : \sum_{l=1}^{h+1} X_l = 1 \right\},$$

defined by

$$\left(\Pi_{\mathbb{S}^h} \varphi^l \right)_{i,j} = \frac{|\varphi_{i,j}^l|}{\sum_{l=1}^{h+1} |\varphi_{i,j}^l|}.$$

More details about the justification of the choice of this non orthogonal projection operator can be found in [18]. We did not manage to improve this projection procedure. We observed that both aspects: the condition that the sum is equal to 1 and that the functions φ^l take values in $[0,1]$, are essential in the optimization process, and this projection operator preserves them both.

The optimization procedure proposed in [18] was based on a steepest descent algorithm with an adaptive step length. We improve the descent algorithm by introducing a linesearch procedure in order to determine the step length. A description of the procedure can be found in Algorithm 2. The number of iterations is significantly reduced, but each iteration needs multiple function evaluations.

Algorithm 2 Linesearch algorithm

Require: γ_0, $\omega > 1$, x, d (descent direction)
  1: $\gamma = \gamma_0$
  2: Evaluate the cost c corresponding to x
  3: $c_0 = c$ (variable which keeps previous cost)
  4: **repeat**
  5:     $x_t = x + \gamma d$
  6:     $x_p = \Pi_{\mathbb{S}^h}(x_t)$ (projection on the constraint)
  7:     Evaluate the cost c_p corresponding to x_p
  8:     **if** $c_p < c_0$ **then**
  9:         $\gamma \leftarrow \omega \gamma$
10:     **else**
11:         **break**
12:     **end if**
13:     $c_0 = c_p$
14: **until**
       return γ

In order to test the stability of our modified algorithm, we took a rectangular box which can be paved with regular hexagons, with one edge oriented horizontally, in a periodic setting. One possibility is to choose the edges of the rectangle having a ratio of $\sqrt{3}$, in the case of 6 cells, or $2/\sqrt{3}$ in the case of 12 cells. In each case we performed the optimization starting from random densities with sum 1. We observe that the resulting partitions are equivalent, and the corresponding costs are close. Results can be seen in Figure 3.3 (the case of 6 cells) and Figure 3.4 (the case of 12 cells). The cost evolution, in the case of 6 cells, is plotted in Figure 3.2.

Algorithm 3 General form of the optimization algorithm
___
Require: k, α, h, ε, γ_0, p_{max}
  1: $p = 1$
  2: Choose random initial densities (φ^l) and project them on the constraint
  3: **repeat**
  4:      Compute $c = F(\varphi^l)$ (the cost functional)
  5:      Choose descent direction $d = -\nabla F(\varphi^l)$
  6:      Find step length γ using the linesearch algorithm
  7:      Update $\varphi^l \leftarrow \varphi^l - \gamma d$
  8:      $\varphi^l \leftarrow \Pi_{\mathbb{S}^h}(\varphi^l)$ (project on the constraint)
  9:      $p \leftarrow p + 1$
 10: **until** $p = p_{max}$ or $\gamma \|\nabla F(\varphi^l)\|_{\ell^\infty} < \varepsilon$
___
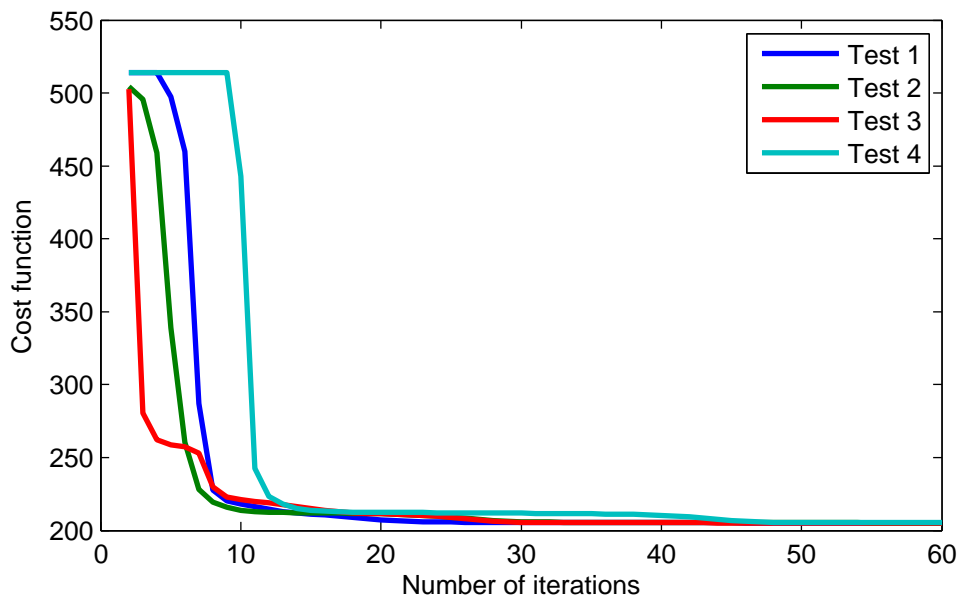
Figure 3.2: Cost evolution in the four cases presented in Figure 3.3
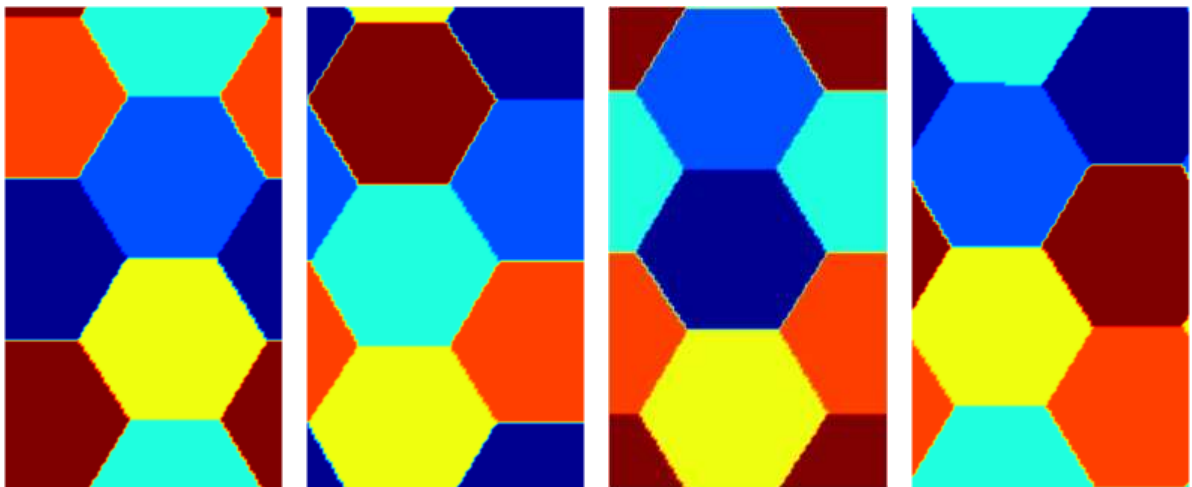
Figure 3.3: Optimal results - 6 cells on a periodic domain, starting each time from random densities. Optimal numerical value (left to right): $205.21, 205.23, 205.22, 205.22$
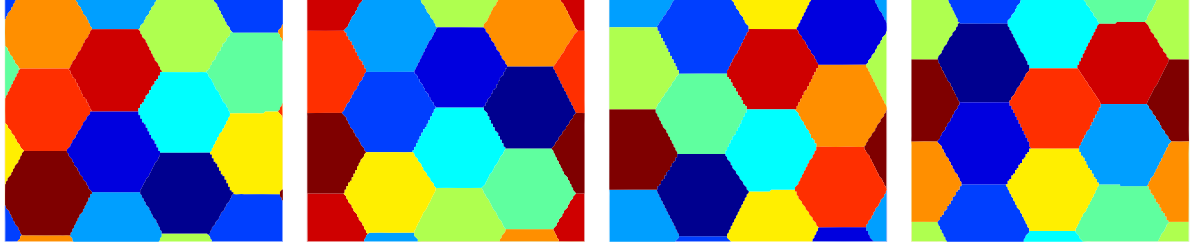
Figure 3.4: Optimal results - 12 cells on a periodic domain, starting each time from random densities. Optimal numerical value (left to right): $1512.85, 1512.83, 1513.12, 1513.26$

In order to be able to study the minimizers of problem 3.7.1 in the case where D is not rectangular, we use a finite elements approach. We find a triangulation of D using the software Distmesh [77], or by specifying a regular triangulation directly (when possible). We compute the associated rigidity and mass matrices K and M, respectively. Then, if φ is a vector containing the values of the discretization of Ω, we are left to solve the problem

$$\int_D \nabla u \nabla v + \int_D C(1 - \varphi)uv = \lambda \int_D uv,$$

which has the discrete form

$$v^T K u + C v^T \text{diag}(1 - \varphi)Mu = \lambda v^T Mu.$$

Since this is true for each v, we are left with the generalized eigenvalue problem

$$(K + C\text{diag}(1 - \varphi)M)u = \lambda Mu.$$

In this way, we are able to find numerical minimizers for problem 3.7.1 even when D is not rectangular (see Figures 3.7,3.10). The drawback is that finding generalized eigenvalues is more time consuming than finding eigenvalues. When working on a rectangular domain, using finite differences, we can easily handle discretizations of 500×500 (250000 points) on a single machine[4]. For the finite elements case we use triangulations with roughly 10000 points. The advantage of this finite elements approach is that once we have a good triangulation of the domain, the problem can be easily treated, and this inspired the framework we use in Chapter 5 for the study of optimal partitions on manifolds. If we want more precision, in terms of discretization points, we can use the finite differences formulation and use the same penalization method to determine the domain D inside the square.

3.8   Discussion of the numerical results

In this section we present some numerical simulations that confirm the theoretical results stated in Theorem 3.1.3 and the article [31]. Furthermore, the numerical simulations in the periodic

[4]Processor: i7 quad-core 2.2Gh, 6GB of RAM
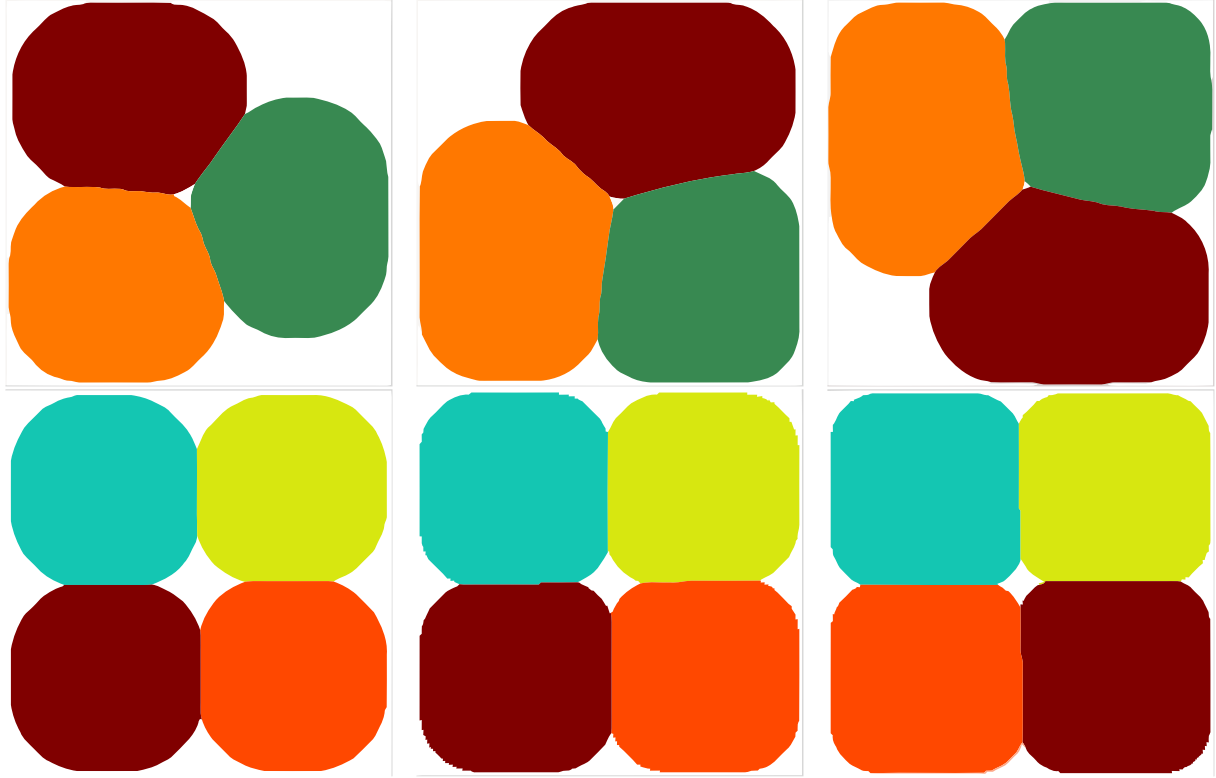
Figure 3.5: $k = 1$, 200×200 non-periodic grid, 3 phases ($\alpha = 170, 100, 80$) and 4 phases ($\alpha = 250, 150, 100$)

case, indicate that as α decreases, the cells of the multiphase configuration are monotonically increasing. This was also observed in the case of non-periodic conditions, when the domain has a certain symmetry, which allows a well behaved circle packing. Note that, when the size of the box is well chosen, there exists an optimal parameter α, such that the optimal configuration consists of the hexagonal circle packing configuration. If the observed shape monotonicity property is true, then the actual spectral partitioning problem ($\alpha = 0$) can be solved, and the optimal partition is formed of regular hexagons. We note that this result concerning the case $\alpha = 0$ is still an open problem, while results of [18] confirm numerically this conjecture (see Figures 3.6, 3.7, as well as Figure 3.5).

In all the cases the lack of triple junction points, proved in [31], is clearly observed, provided that the parameter $\alpha > 0$ is large enough. The lack of double points on the boundary of the square proved in Theorem 3.1.3 can also be noticed in Figures 3.5, 3.10. Another phenomenon that can be observed is that the sets Ω_i near the corners of D do not fill the corner. This is a fact that can be easily proved by adding a ball B (i.e. subsolution for the functional $\lambda_1 + \alpha | \cdot |$) outside D, for which the corner of the square lies on the sphere ∂B. Now the claim can be deduced by the monotonicity Theorem 3.2.4 (B), as in Theorem 3.1.3.

Some fine qualitative properties of the optimal configurations $(\Omega_1, \ldots, \Omega_h, \Omega_{h+1})$, which are still open questions, were observed during the numerical simulations.

- The set of one-phase points $\partial\Omega_j \cap \partial\Omega_{h+1}$ on the boundary of the jth optimal cell Ω_j is
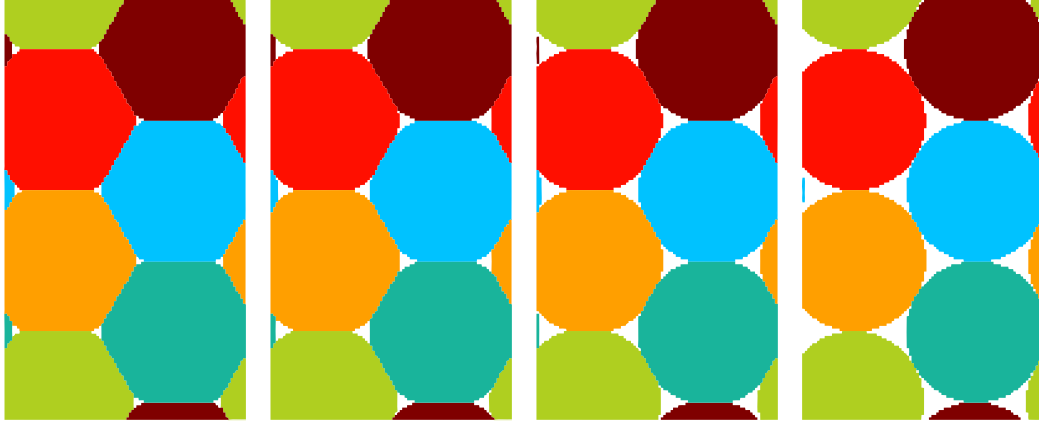
Figure 3.6: $k = 1$, illustration of the monotonicity property. Values of α: $150, 200, 250, 300$ (left to right)
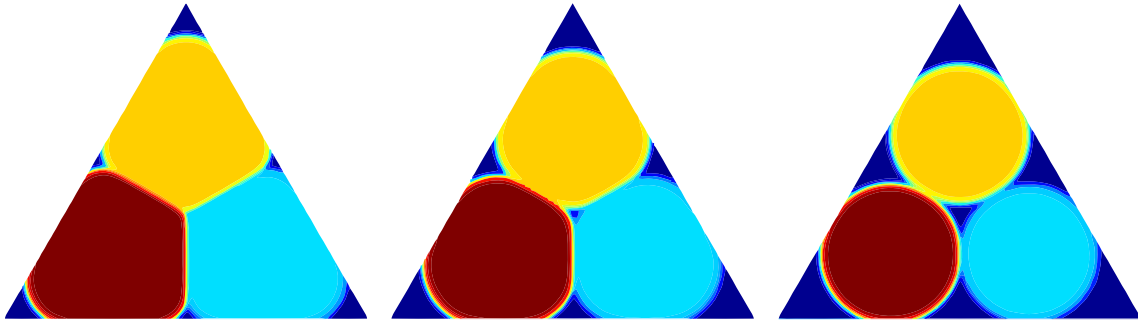

Figure 3.7: $k = 1$, illustration of the monotonicity property in the case of an equilateral triangle. Values of α: $10, 25, 50$ (left to right)

locally a graph of a *convex function*.

- For each pair of distinct indices $i, j \in \{1, \ldots, h\}$, there are exactly two boundary two-phase points on the common boundary $\partial\Omega_i \cap \partial\Omega_j$, i.e.

$$\mathcal{H}^0\big(\partial\Omega_i \cap \partial\Omega_j \cap \partial\Omega_{h+1}\big) = 2.$$

- If $x_0 \in \partial\Omega_i \cap \partial\Omega_j \cap \partial\Omega_{h+1}$ is a boundary two-phase point, then the set $\Omega_i \cap \Omega_j$ has a cusp in x_0. More precisely, for $r > 0$ small enough, the free boundaries $\partial\Omega_i \cap \partial\Omega_{h+1} \cap B_r(x_0)$ and $\partial\Omega_j \cap \partial\Omega_{h+1} \cap B_r(x_0)$ are graphs of convex functions meeting tangentially in the origin x_0.

Finally, we considered the periodic version of the problem (3.1.2) on the square $[0, 1] \times [0, 1]$ and in other rectangular domains, in attempt to simulate a "partition" of the whole space $\mathbb{R}^2$ (see Figure 3.8, Figure 3.6). For small enough constants $\alpha > 0$ we obtain a configuration with touching hexagons with rounded corners, in support of the numerical results in [18].

Most of the tests we made were in the case $k = 1$, but the algorithm works for $k = 2$ as well. The main issue in the case of higher eigenvalues concerns the differentiability of
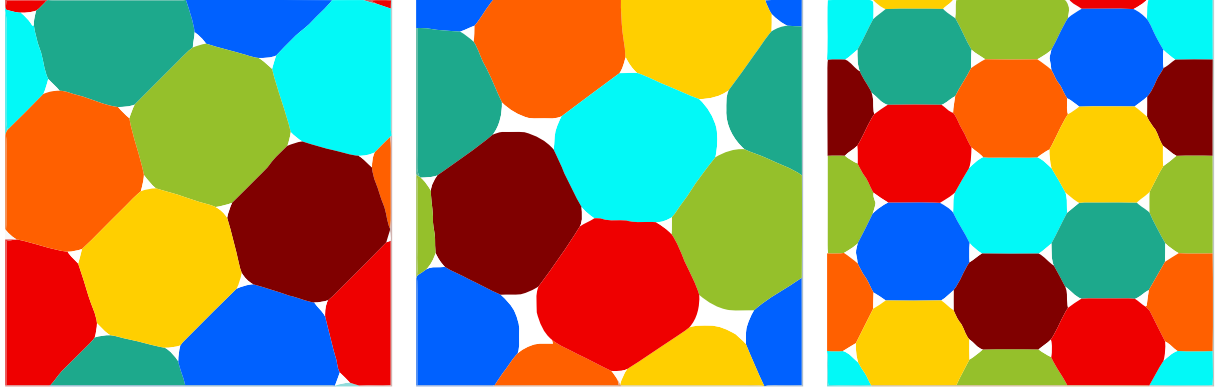
Figure 3.8: $k = 1$, 200×200 periodic grid, 8 phases, $\alpha = 500, 580$ and $k = 2$, 8 phases, $\alpha = 270$
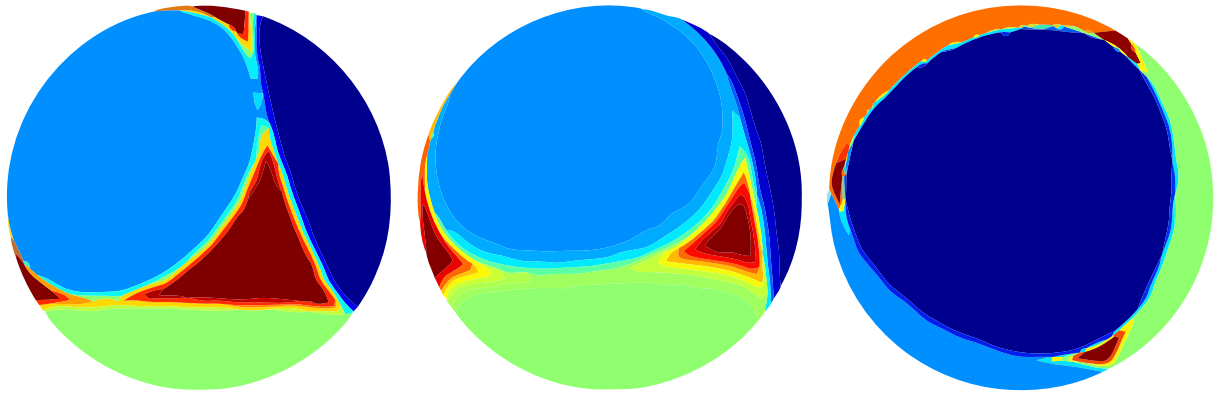
Figure 3.9: Optimal configurations on the sphere in the case of four phases, for decreasing values of α

the eigenvalues with respect to perturbations, which is well known to be closely related to their multiplicity. Secondly, we were not able to prove that for $k \geq 2$ the relaxed formulation converges to the actual problem when $C \to +\infty$. Nevertheless, we were able to obtain some interesting numerical results also in the case $k = 2$ and one example can be seen in Figure 3.8.

As stated in Theorem 3.4.3 the theoretical results also extend to the case of the Laplace-Beltrami fundamental eigenvalues on surfaces. Using the same finite elements procedure as in the case of non-rectangular domains, we were able to compute numerically some optimal configurations on the sphere, observing the same behaviour as in the plane: the lack of triple points and monotonicity with respect to α. (see Figure 3.9) We notice that in the cases $h \in \{3, 4, 6, 12\}$ the optimal configurations converge to the corresponding regular tiling of the sphere (Y partition, regular tetrahedron, cube, dodecahedron) as $\alpha \to 0$.
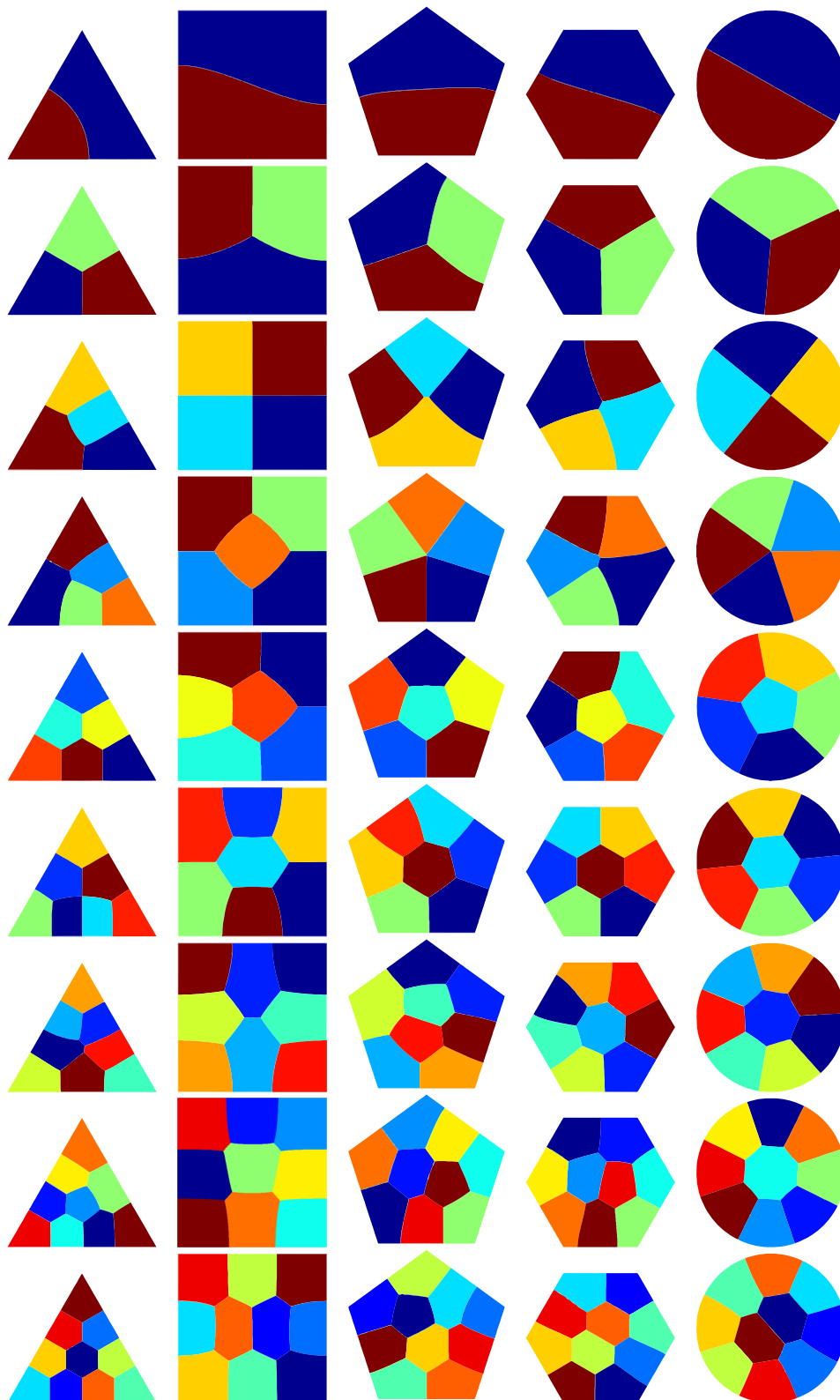
Figure 3.10: Optimal partitions ($\alpha = 0$) for some generic domains D

Boundary eigenvalue problems

Résumé

Ce chapitre traite de quelques aspects théoriques et numériques pour des problèmes aux valeurs propres définis sur le bord d'un domaine. La différence entre ces problèmes et les problèmes aux valeurs propres étudiés en chapitres 1 et 3 est le fait que l'équation de valeur propre est imposée comme une condition au bord et à l'intérieur du domaine les fonctions propres sont harmoniques. Un première modèle concernant ces types de problèmes est le problème de Steklov: pour un ouvert Ω à frontière Lipschitz on a

$$\begin{cases} \Delta u = 0 & \text{dans } \Omega \\ \frac{\partial u}{\partial n} = \sigma u & \text{sur } \partial\Omega. \end{cases}$$

Les valeurs σ pour lesquelles le probleme ci-dessus admet une solution non triviale forment une suite croissante divergente

$$0 = \sigma_0 \leq \sigma_1 \leq \sigma_2 \leq \cdots \to \infty.$$

Comme dans les chapitres précédents, on regarde ce problème dans le cas où Ω est un ouvert variable, et on se demande quels sont les ensembles qui optimisent ce type de valeurs propres sous différentes contraintes. En regardant l'équation définissant ce problème, on peut voir que toute fonction constante est une fonction propre correspondant à la valeur propre 0. En conséquence, on commence la numérotation des valeurs propres par 0 et on pose $\sigma_0(\Omega) = 0$. Des nombreux travaux traitent ces problèmes d'optimisation des valeurs propres Steklov. On présente ci-dessous les résultats les plus connus :

- le disque maximise $\sigma_1(\Omega)$ parmi les ensembles d'aire fixée (Brock [24]) et parmi les ensembles simplement connexes de périmètre fixé (Weinstock [93]);

- parmi les ensembles simplement connexes en dimension deux, de périmètre fixé ou d'aire fixée, les problèmes suivants sont résolus par le disque :

$$\max \sigma_1(\Omega)\sigma_2(\Omega), \ \min \left(\frac{1}{\sigma_1(\Omega)} + ... + \frac{1}{\sigma_n(\Omega)} \right),$$

$\forall n \in \mathbb{N}$ (Hersch-Payne-Schiffer [67]).

Hersch-Payne-Shiffer ont prouvé que parmi les ensembles simplement connexes, la deuxième valeur propre Steklov, $\sigma_2(\Omega)$, est bornée supérieurement par la deuxième valeur propre Steklov de deux disques de même périmètre que Ω. Girouard et Polterovich [55] ont prouvé que cette borne est optimale dans le cas des ensembles simplement connexes. Dans le cas où on a une contrainte de périmètre, si on enlève la condition de simple connexité, le disque n'est plus optimal pour σ_1. Si on fait un petit trou dans le centre du disque et si on redimensionne l'ensemble pour avoir le même périmètre, alors la première valeur propre augmente. Ceci montre que le cas non-simplement connexe nécessite une attention spéciale quand on considère une contrainte de périmètre.

La première partie de ce chapitre traite la question de stabilité et semicontinuité supérieure des valeurs propres Steklov pour certains types de convergence des ensembles. Le contenu de cette première partie est un article, à paraître dans Applied Mathematics and Optimization. La motivation de ce résultat est de pouvoir traiter des questions d'existence pour un problème d'optimisation concernant les valeurs propres Steklov. Tous les résultats d'existence trouvés dans la littérature concernant le problème de Steklov sont prouvés en identifiant une borne explicite et en trouvant un ensemble qui réalise cette valeur (par exemple le disque). Le résultat central de la première partie du chapitre est le suivant :

Théorème. *Si Ω_n est un suite d'ensembles vérifiant une condition de cône uniforme et $\Omega_n \to \Omega$ pour la topologie de Hausdorff et dans la topologie L^1, alors*

$$\limsup_{n \to \infty} \sigma_k(\Omega_n) \leq \sigma_k(\Omega).$$

Si de plus $\mathrm{Per}(\Omega_n) \to \mathrm{Per}(\Omega)$*, alors*

$$\sigma_k(\Omega_n) \to \sigma_k(\Omega).$$

Ce théorème permet d'énoncer et de prouver des résultats d'existence des solutions concernant les problèmes Steklov sous contrainte de convexité ou sous contrainte de ε-cône.

La deuxième partie de ce chapitre traite de la conception et de la mise en œuvre d'une méthode de calcul des valeurs propres Steklov pour des ensembles qui peuvent être paramétrés par une fonction radiale. Notre approche fait partie de la classe des méthodes basées sur des solutions fondamentales. L'idée est de considérer des combinaisons linéaires des fonctions qui vérifient de manière analytique l'équation à l'intérieur du domaine (dans ce cas, des fonctions harmoniques) et d'imposer les conditions au bord sur un nombre fini de points. Des méthodes similaires ont été proposées par P. Antunes et P. Alvez en [4],[5] dans le cas des valeurs propres du Laplacien avec conditions Dirichlet, Neumann ou Robin.

La méthode permet de traiter une classe large de domaines et sa précision est assez importante. On compare la méthode des solutions fondamentales avec des méthodes de maillage

grâce au logiciel FreeFem++ [61]. On observe qu'en raffinant les maillages, les valeurs propres obtenues avec les maillages convergent vers les valeurs propres obtenues avec solutions fondamentales. Un avantage important de la méthode développée est sa rapidité par rapport aux méthodes basées sur des maillages. Le temps d'exécution est cent fois plus rapide pour notre méthode, et la précision est meilleure. Pour évaluer cette précision, on a prouvé un résultat similaire à celui présenté dans [73], dans le cadre du problème de Steklov :

Théorème. *Soit Ω borné, régulier, et u_ε qui satisfait*

$$\begin{cases} -\Delta u_\varepsilon = 0 & in\ \Omega \\ \dfrac{\partial u_\varepsilon}{\partial n} = \sigma_\varepsilon u_\varepsilon + f_\varepsilon & on\ \partial\Omega. \end{cases}$$

avec $\|u_\varepsilon\|_{L^2(\partial\Omega)} = 1$ et $\|f_\varepsilon\|_{L^2(\partial\Omega)} = \delta < 1$. Alors il existe $k \in \mathbb{N}^*$ tel que

$$\frac{|\sigma_\varepsilon - \sigma_k|}{\sigma_k} \leq \delta.$$

Ce théorème montre que dans le cas du cercle, la précision de notre méthode est 10^{-12} et en général la précision est de 10^{-6}.

Avec cette méthode numérique et la formule de dérivée de forme pour les valeurs propres Steklov trouvée dans [42] on peut étudier numériquement une classe assez large des problèmes d'optimisation. En pratique, on observe que si le minimiseur est en dehors de la classe des ensembles représentables en paramétrisation radiale, l'algorithme ne converge pas, et il s'arrête en essayant de déconnecter la forme pour atteindre une autre classe des domaines. On conjecture le fait que si on considère des contraintes d'aire, l'ensemble qui maximise $\sigma_k(\Omega)$ existe et il est connexe. Les formes obtenues numériquement sont présentées à la fin de ce chapitre.

La méthode numérique peut être generalisée à d'autres classes des problèmes. En particulier, au cours de cet chapitre on étudie numériquement des questions liées aux problèmes suivants :

- Problème de Wentzell

$$\begin{cases} \Delta u = 0 & dans\ \Omega \\ -\beta\Delta_\tau u + \frac{\partial u}{\partial n} = \sigma u & sur\ \partial\Omega, \end{cases}$$

   où Δ_τ est l'opérateur Laplace-Beltrami associé à $\partial\Omega$.

- Problème de Steklov modifié

$$\begin{cases} -\Delta u + u = 0 & dans\ \Omega \\ \frac{\partial u}{\partial n} = \sigma u & sur\ \partial\Omega. \end{cases}$$

   en lien avec des inégalités de trace.

La dernière contribution de ce chapitre est une extension de la méthode radiale qui doit pouvoir traiter tous les domaines simplement connexes. Au lieu de considérer des courbes paramétrées par une fonction radiale, on peut considérer des courbes paramétriques $(x(t), y(t))$

pour $t \in [0, 2\pi]$ avec x, y des fonctions périodiques. On fait la même chose que dans le cas des fonctions radiales : on développe x, y en séries de Fourier et on retient un nombre fini de coefficients. On peut calculer la dérivée de la valeur propre par rapport à tous ses coefficients et on peut étudier de la même manière des problèmes d'optimisation. Cette méthode est nouvelle et, à ma connaissance, n'a pas été étudié dans la littérature auparavant.

4.1 Introduction

For an open, bounded, simply connected set Ω with Lipschitz boundary, we can consider the Steklov eigenvalue problem:
$$\begin{cases} \Delta u = 0 & \text{in } \Omega \\ \frac{\partial u}{\partial n} = \sigma u & \text{on } \partial\Omega. \end{cases}$$
The Steklov spectrum of Ω consists of a sequence of the form
$$0 = \sigma_0(\Omega) \leq \sigma_1(\Omega) \leq \sigma_2(\Omega)... \to +\infty.$$

Various optimization problems for functionals of the Steklov spectrum under certain constraints on the geometric properties of Ω have been studied.

Weinstock [93] observed that $\sigma_1(\Omega)$ is bounded above by $2\pi / \operatorname{Per}(\Omega)$ in the class of simply connected sets. This means that the disk maximizes the first Steklov eigenvalue in the class of two dimensional simply connected sets, under a perimeter constraint. It is straightforward to see that this implies that the disk maximizes $\sigma_1(\Omega)$ under volume constraint (see Remark 4.2.4). Girouard and Polterovich proved in [56] that the estimate

$$\sigma_k(\Omega) \operatorname{Per}(\Omega) \leq 2k\pi$$

provided by Hersch, Payne and Schiffer is sharp in the class of simply connected domains, but is not attained in that class. We refer to [56],[65, Section 7.3] for further details.

In general, the known results concerning the optimization of functionals of the Steklov spectrum are proved by finding an optimizer explicitly. Once an optimizer Ω^* is identified, it is proved that the value of the functional on Ω^* is the best possible. In the cases where the optimal shape is not known explicitly, we would like to be able to provide at least an existence result.

First, let's note that in the case of the Steklov eigenvalues, it is only relevant to study optimization problems in which the Steklov eigenvalues are maximized. Indeed, Colbois, El Soufi and Girouard proved in [37] that the Steklov eigenvalues satisfy the bound

$$\sigma_k(\Omega) \leq c_d k^{\frac{2}{d}} \frac{|\Omega|^{\frac{d-2}{d}}}{\operatorname{Per}(\Omega)}. \tag{4.1.1}$$

Thus, keeping constant volume and increasing the perimeter, we can make the Steklov eigenvalues as small as we want.

118

A natural way to study optimization problems is to use the classical methods of the calculus of variations. In order to study the problem

$$\max_{\Omega \in \mathcal{A}} \sigma_k(\Omega),$$

where $\mathcal{A}$ is an admissibility class (containing, eventually, some constraints), we need a result concerning the upper semicontinuity of σ_k with respect to some type of convergence.

We mainly deal with the convergence related to the Hausdorff distance, but in a stronger sense which is described in the following. Note that maximizing $\sigma_k(\Omega)$ under perimeter or volume constraint, together with the bound (4.1.1), means that a maximizing sequence (Ω_n) will have a bound on the perimeters $(\mathrm{Per}(\Omega_n))$. It is well known that a perimeter bound, together with a bounding box constraint implies L^1 compactness of characteristic functions. These considerations allow us to work directly with maximizing sequences converging in the Hausdorff distance and in L^1.

The main results of the first part of this chapter concern inequalities of the type

$$\limsup_{n \to \infty} \sigma_k(\Omega_n) \leq \sigma_k(\Omega), \tag{4.1.2}$$

under certain regularity assumptions on (Ω_n) and Ω. We work in the framework of sets which satisfy an ε-cone condition, which is equivalent to a uniform Lipschitz property. In particular, this allows us to extend functions in $H^1(\Omega)$ to $H^1(D)$, when $\Omega \subset D$. Another advantage is that we can work with graphs of Lipschitz functions instead of dealing with general sets. We believe that our results could be extended to a more general class of sets described in [88].

We found that in order to prove inequalities of the type (4.1.2) it is essential to have a result on the lower semi-continuity of traces of Sobolev functions on moving boundaries presented in Proposition 4.3.2. The main result is Theorem 4.3.5 and it states that if the sequence of sets (Ω_n) satisfy a ε-cone condition and converge to Ω in the Hausdorff topology then (4.1.2) holds. Moreover, if the perimeters of Ω_n converge to the perimeter of Ω then we have equality in (4.1.2). We give a direct proof that the Steklov spectrum of a convex set is close to zero if the diameter is large. This result is a direct consequence of the bound (4.1.1), but it avoids the use of the technical argument presented in [37]. In the end, we are able to provide existence results in the class of sets satisfying a uniform ε-cone condition, as well as in the class of convex sets. In Figure 4.8 we present some convex sets obtained numerically for which we have observed the highest, area normalized, k-th Steklov eigenvalue for $k \in [2, 10]$. These shapes were obtained using shape gradients and performing a projection on the convex hull.

As stated above, the semi-continuity result, and the existence results are proved in the class of sets which satisfy a uniform ε-cone condition. It is not clear if these results still hold if this hypothesis is removed and we work in the class of general Lipschitz domains. In the case of the area constraint, Brock proved in [24] that the disk maximizes the first non-trivial Steklov eigenvalue, without any assumptions on the topology of the domain. Ongoing research suggests that in the case of the volume constraint, an existence result can be obtained for a

relaxed formulation of the Steklov eigenvalues. Furthermore, numerical results presented in the end of this chapter show that is likely that in the case of the area constraint we may have an existence result even without additional topological assumptions.

As you can see in Figure 4.5, the perimeter constraint gives a different behaviour. If we remove the simple connectedness condition, then the disk is no longer the maximizer of σ_1; making a suitably sized hole in the center of the disk increases the scale invariant Steklov eigenvalue. This behaviour has been announced in [57].

The second part of this chapter presents a new numerical method for computing the Steklov spectrum on two dimensional domains. The method is inspired by the work of Alvez and Antunes [4] and it uses fundamental solutions. The idea is to work with functions which are already harmonic in an analytic way, and search for those which satisfy the good boundary eigenvalue condition. In order to do this, we choose a set of points $(x_i), i = 1, ..., N$ on $\partial\Omega$ and a set of associated exterior points $(y_i), \ i = 1, ..., N$. We consider radial harmonic functions ϕ_i with centers y_i and we search solutions of the form

$$u = \alpha_1 \phi_1 + ... + \alpha_N \phi_N.$$

The coefficients $\alpha_1, ..., \alpha_N$ are the only unknowns here, and they satisfy a generalized eigenvalue equation. The corresponding eigenvalues are good approximations of the Steklov spectrum of the domain Ω.

We perform many tests in order to test our method. The first such test is to compare the eigenvalues obtained using our method with the ones given by an algorithm which uses meshes for the eigenvalue computation. A straightforward implementation can be done in FreeFem++. We notice that as the meshes are refined, the corresponding eigenvalues converge to the ones obtained using fundamental solutions. We applied techniques similar to the ones used in the result of Moler and Payne [73] and we obtained a theoretical error estimate for our algorithm, which has the following form

Theorem. 4.6.3 *Consider Ω to be a bounded, regular open set and let u_ε be a solution of*

$$\begin{cases} -\Delta u_\varepsilon = 0 & in \ \Omega \\ \dfrac{\partial u_\varepsilon}{\partial n} = \sigma_\varepsilon u_\varepsilon + f_\varepsilon & on \ \partial\Omega. \end{cases}$$

with $\|u_\varepsilon\|_{L^2(\partial\Omega)} = 1$ and $\|f_\varepsilon\|_{L^2(\partial\Omega)} = \delta < 1$. Then it exists $k \in \mathbb{N}^*$ such that $\dfrac{|\sigma_\varepsilon - \sigma_k|}{\sigma_k} < \delta$.
Using this result, we approximate numerically the error $\partial_n u - \sigma u$ on $\partial\Omega$ by looking at a family of points which is 100 times more dense on $\partial\Omega$. The numerical computations and the above result suggest that the errors made are of order 10^{-6}. The method and the error result can be extended to a larger class of problems in relation to the Wentzell spectrum, which will be described in the second part of this chapter.

Once we have a method which is fast and precise, we can perform numerical optimization algorithms. We can use the same parametrization of the radial functions with Fourier coefficients that was presented in Chapter 1. With the aid of the shape derivatives formulas presented

in [42], we are able to compute the gradient of the Steklov/Wentzell eigenvalues with respect to every Fourier coefficient. This numerical algorithm allows us to study a variety of problems regarding the Steklov spectrum. The speed of the algorithm computing the spectrum allows us to perform a thousand iterations in the descent algorithm in just a few seconds.

We would like to remove the rather strict limitation that is to work in the class of star-shaped domains. We devised a method which consists of parametrizing each of the coordinates in a general parametrization $t \mapsto (x(t), y(t))$ using Fourier coefficients. In this way, we can work directly in the class of simply connected domains while still keeping only a finite number of parameters. We used this parametric method to study the problem of maximizing the k-th Steklov eigenvalue in the class of sets with fixed area. Using this method we did not obtain any significant improvements over the results obtained in the radial case. Nevertheless, working with a general parametrization allowed us to explore a wider class of domains. After obtaining these results we are more confident that the optimal shapes are indeed star-shaped, and that working with a radial parametrization is not an assumption which is too strict.

4.2 Preliminaries

We recall below some theoretical tools needed to prove our results.

4.2.1 Convergence of sets

In the study of optimization problems where the variable is the shape of a domain it is often necessary to define a topology on a family of shapes. The choice of such a topology is not obvious, and different situations require different topologies. In our study, we use the Hausdorff compelentary convergence on open sets and the L^1 convergence of a of characteristic functions. We recall that the Hausdorff distance between two compact sets K_1, K_2 is given by

$$d_H(K_1, K_2) = \max\{\sup_{x \in K_1} \inf_{y \in K_2} d(x, y), \sup_{y \in K_2} \inf_{x \in K_1} d(x, y)\}.$$

If we consider a bounded open set D and the open sets $\Omega_1, \Omega_2 \subset D$ then we define the Hausdorff complementary distance as

$$d_{H^c}(\Omega_1, \Omega_2) = d_H(D \setminus \Omega_1, D \setminus \Omega_2).$$

These two types of convergence are not equivalent in general. Still, it is possible to prove that if we have a bounding box, then any sequence of open sets (Ω_n) has a subsequence converging in the Hausdorff topology to Ω. Furthermore, if the sequence of perimeters of (Ω_n) is bounded, then (Ω_n) has a subsequence which converges in both topologies presented above. We will consider this combined convergence, which provides, in addition to the properties of the Hausdorff convergence, continuity for the volume and lower semi-continuity for the perimeter.

4.2.2 Uniform cone condition

We recall the following definition from [66, Chapter 2].

Definition 4.2.1. *Let y be a point in $\mathbb{R}^d$, ξ a unit vector and $\varepsilon > 0$. We define the cone $C(y, \xi, \varepsilon)$ of vertex y, direction ξ and dimension ε by*

$$C(y, \xi, \varepsilon) = \{x \in \mathbb{R}^d : \langle z - y, \xi \rangle \geq \cos \varepsilon |z - y| \text{ and } 0 < |z - y| < \varepsilon\}.$$

We say that an open set Ω has the ε-cone condition if for every $x \in \partial\Omega$ there exists a unit vector ξ_x such that for every $y \in \overline{\Omega} \cap B(x, \varepsilon)$ we have $C(y, \xi_x, \varepsilon) \subset \Omega$.

In the proof of our results we use the fact that sets which have the ε-cone condition can be represented locally as the graph of a Lipschitz function. Theorem 2.4.7 from [66] assures us that the ε-cone condition is equivalent to the following uniform Lipschitz condition.

Definition 4.2.2. *We say that a subset Ω of $\mathbb{R}^d$ has a uniform Lipschitz boundary if there are some uniform constants L, a, r such that for any point $x_0 \in \partial\Omega$ there exists an orthonormal system of coordinates S with origin at x_0, a cylinder $K = B_{d-1}(x_0, r) \times (-a, a)$, and a function $\varphi : B_{d-1}(x_0, r) \to [-a, a]$ which is Lipschitz, with constant L and $\varphi(0) = 0$ such that*

$$\partial\Omega \cap K = \{(y, \varphi(y)) : y \in K\},$$

$$\Omega \cap K = \{(y, x_N) \in K : x_N > \varphi(y)\}.$$

One advantage of working with sets satisfying an ε-cone condition is the fact that the two types of sets convergence defined before are connected. The Hausdorff complementary convergence of a sequence of sets implies the convergence of characteristic functions in $L^1(D)$ to the same limit. We refer to [66, Theorem 2.4.10] for a proof. Furthermore, if Ω satisfies a ε-cone condition, then the constants L, a, r in the above theorem depend only on ε.

The following proposition mentions an interesting property of the sets which satisfy an ε-cone condition. Using the fact that the boundary of such a set has a local representation as the graph of a Lipschitz function, we can find a bound on the perimeter.

Proposition 4.2.3. *Suppose D is a bounded, open set in $\mathbb{R}^d$ and suppose that $\Omega \subset D$ satisfies a ε-cone condition. Then $\mathrm{Per}(\Omega)$ is uniformly bounded by a constant which depends only on ε and D.*

Proof: The above remarks, allow us to say that for every $x_0 \in \partial\Omega$ there exist a cylinder K of the form $B_{d-1}(x_0, r) \times (-a, a)$ centred at x_0 such that $\partial\Omega \cap K$ is the graph of a Lipschitz function with Lipschitz constant L. Furthermore, L, a, r depend only on ε. Note that the perimeter of Ω restricted to K, denoted $\mathrm{Per}_K(\Omega)$, can be expressed as

$$\mathrm{Per}_K(\Omega) = \int_{B_{d-1}(x_0, r)} \sqrt{1 + |\nabla\varphi(x)|^2} dx \leq |B_{d-1}(x_0, r)| \sqrt{1 + L^2}.$$

Therefore, in every such cylinder K, the relative perimeter of Ω is bounded by a constant which depends only on ε.

We claim that the boundary of Ω can be covered with M such cylinders K, where M depends on D. To see this, we propose the following construction. Choose $x_1 \in \partial\Omega$ and let K_1 be the associated cylinder, like in Definition 4.2.2. At step n, choose $x_n \notin K_1 \cup ... \cup K_{n-1}$ and denote K_n its corresponding cylinder. This operation must end at some point, since pairwise distances between x_i and x_j, with $i \neq j$ are bounded below by a constant $c = \min\{a, r\}$ depending on ε.

To see that there exist a maximal number of points inside D satisfying this property, it is enough to cover D with cubes with a diameter $c' < c$. Obviously, since D is bounded, it is possible to cover D with a finite number M of such cubes. Each cube can contain at most one of the points x_i, since it's diameter is smaller than c. Therefore, the above construction ends in at $n \leq M$ steps.

As a consequence

$$\operatorname{Per}(\Omega) \leq \sum_{i=1}^{n} \operatorname{Per}_{K_i}(\Omega) \leq M|B_{d-1}(x_0, r)|\sqrt{1 + L^2}.$$

Thus, the perimeter of Ω is uniformly bounded by a constant depending on ε and D. $\qquad\square$

4.2.3 The Steklov spectrum

Let Ω be a simply-connected bounded planar domain with Lipschitz boundary. The *Steklov* eigenvalue problem is

$$\begin{cases} -\Delta u = 0 & \text{in } \Omega, \\ \frac{\partial u}{\partial n} = \sigma u \text{ on } \partial\Omega, \end{cases}$$

where $\frac{\partial}{\partial n}$ is the outward normal derivative. The spectrum of the Steklov problem is discrete and its eigenvalues

$$0 = \sigma_0 < \sigma_1(\Omega) \leq \sigma_2(\Omega) \leq \sigma_3(\Omega) \leq ... \to +\infty$$

satisfy the following variational characterization

$$\sigma_n(\Omega) = \min_{S_n} \max_{u \in S_n \setminus \{0\}} \frac{\int_\Omega |\nabla u|^2 dx}{\int_{\partial\Omega} u^2 d\sigma}, \ n = 1, 2, ...$$

The infimum is taken over all n-dimensional subspaces S_n of $H^1(\Omega)$ that are orthogonal to constants on $\partial\Omega$, i.e. $\int_{\partial\Omega} u d\sigma = 0$.

The Steklov eigenvalues behave well under domain scaling. Indeed, if we denote $t\Omega$ an image of Ω by a homothety of ratio $t > 0$ then we have

$$\sigma_k(t\Omega) = \frac{1}{t}\sigma_k(\Omega). \tag{4.2.1}$$

Remark 4.2.4. In view of property (4.2.1), the quantities $\sigma_k(\Omega)\operatorname{Per}(\Omega)$ and $\sigma_k(\Omega)|\Omega|^{1/2}$ are scale invariant. Thus maximizing $\sigma_k(\Omega)$ under perimeter constraint is equivalent to the problem

$$\max \sigma_k(\Omega)(\operatorname{Per}(\Omega))^{\frac{1}{d-1}},$$

and maximizing $\sigma_k(\Omega)$ under volume constraint is equivalent to the problem

$$\max \sigma_k(\Omega)|\Omega|^{1/d}.$$

Combining the above formulations with the classical isoperimetric inequality, we can conclude that if the ball maximizes σ_k, or another well behaving function of the Steklov spectrum, under a perimeter constraint, then the ball also maximizes the same function under volume constraint.

4.3 Stability of Steklov Spectrum under Hausdorff Convergence

We recall the following result, which can be found in a similar form in in [50, Theorem 2.3.1]. The weak L^2 convergence coupled with the convergence of a certain integral sequence implies strong L^2 convergence.

Lemma 4.3.1. *Let Ω be a measurable subset of $\mathbb{R}^n$ and suppose $F : \mathbb{R}^n \to \mathbb{R}$ is a strongly convex function of class C^1, i.e. it exists $\mu > 0$ such that*

$$F(y) \geq F(x) + \nabla F(x) \cdot (y - x) + \mu|y - x|^2,$$

for every $x, y \in \mathbb{R}^n$. Furthermore, we assume that F has the property that if $u \in L^2(\Omega; \mathbb{R}^n)$ then $\nabla F(u)$ is also in $L^2(\Omega; \mathbb{R}^n)$. Let (u_k) be a sequence in $L^2(\Omega, \mathbb{R}^n)$ such that $u_k \rightharpoonup u$ in $L^2(\Omega, \mathbb{R}^n)$. Suppose the following inequality holds:

$$\limsup_{k \to \infty} \int_\Omega F(u_k)dx \leq \int_\Omega F(u)dx$$

Then

$$u_k \to u \text{ in } L^2(\Omega; \mathbb{R}^n).$$

Proof: For every x we have

$$F(u_k(x)) \geq F(u(x)) + \nabla F(u(x)) \cdot (u_k(x) - u(x)) + \mu|u_k(x) - u(x)|^2.$$

Integrating on Ω we have

$$\int_\Omega F(u_k(x))dx \geq \int_\Omega F(u(x))dx + \int_\Omega \nabla F(u(x)) \cdot (u_k(x) - u(x))dx + \mu|u_k - u|^2_{L^2(\Omega;\mathbb{R}^n)}. \quad (4.3.1)$$

124

Note that since $\nabla F(u)$ is in $L^2(\Omega; \mathbb{R}^n)$ and $u_k \rightharpoonup u$ weakly in $L^2(\Omega; \mathbb{R}^n)$ we have

$$\lim_{n \to \infty} \int_\Omega \nabla F(u(x)) \cdot (u_k(x) - u(x)) dx = 0,$$

Taking $n \to \infty$ in (4.3.1) and using the hypothesis we obtain

$$0 \geq \mu \limsup_{n \to \infty} \|u_k - u\|_{L^2(\Omega; \mathbb{R}^n)},$$

which implies that $u_k \to u$ strongly in $L^2(\Omega; \mathbb{R}^n)$. $\qquad\square$

We apply this Lemma in the case where $F = \sqrt{1 + \|x\|^2}$. This function is not strongly convex on all $\mathbb{R}^n$, but it is strongly convex on every bounded open set. Furthermore, $\nabla F = \frac{x}{\sqrt{1+|x|^2}}$ so F satisfies all the hypotheses of Lemma 4.3.1.

The following general proposition is a central result of the first part of this chapter, that will allow us to prove a result of shape continuity for the Steklov spectrum. It allows us pass to the limit when considering traces of a weakly H^1 convergent sequence on moving boundaries that converge in the Hausdorff distance. A similar result has been proved in [30] for the more restrictive class of convex domains.

Proposition 4.3.2. *(Convergence of traces) Let D be an open, bounded subset of $\mathbb{R}^d$. Suppose $(\Omega_n), \Omega \subset D$ are open, connected sets which satisfy a uniform ε-cone property and $\Omega_n \xrightarrow{H^c} \Omega$.*

(A) For every $(u_n) \subset H^1(D)$ which converges weakly to u in $H^1(D)$ we have

$$\liminf_{n \to \infty} \int_{\partial \Omega_n} |u_n|^p \geq \int_{\partial \Omega} |u|^p$$

(B) Consider $p \in [1, 2]$. Then $\mathrm{Per}(\Omega_n) \to \mathrm{Per}(\Omega)$ if and only if for every $(u_n) \subset H^1(D)$ which converges weakly to u in $H^1(D)$ we have

$$\int_{\partial \Omega_n} |u_n|^p \to \int_{\partial \Omega} |u|^p.$$

Proof: We start with part (B). Note that if the integral convergence holds for any $(u_n), u$ such that $u_n \rightharpoonup u$, then taking $u_n, u \equiv 1$ we obtain exactly $\mathrm{Per}(\Omega_n) \to \mathrm{Per}(\Omega)$.

To prove the converse implication, suppose $\mathrm{Per}(\Omega_n) \to \mathrm{Per}(\Omega)$. First, let's note that is enough to prove convergence result for a subsequence of (u_n). Indeed, from the trace theorem, we know there exists a constant C which depends uniformly on L (see, for example, [51]), such that

$$\|u_n\|_{L^2(\partial \Omega_n)} \leq C \|u_n\|_{H^1(\Omega)}.$$

The fact that u_n converges weakly in $H^1(D)$ implies that (u_n) is bounded in $H^1(D)$ and, by the above inequality, (u_n) is bounded in $L^2(\partial \Omega)$. Furthermore, if $p < 2$, the fact that Ω_n have finite perimeter, $(\mathrm{Per}(\Omega_n))$ is bounded and $2/p > 1$ allows us to conclude, via the Hölder inequality, that $(\int_{\partial \Omega_n} |u_n|^p)$ is also bounded. If we prove the convergence for a subsequence, then any other

convergent subsequence will have the same limit, so the whole sequence will converge. This means that in the course of the proof we may pass to a subsequence of (u_n, Ω_n) whenever it is necessary.

Consider the open sets $U_{x_0} = B(x_0, r) \times (-a, a)$ given for each x_0 by Definition 4.2.2. These open sets cover $\partial\Omega$ which is compact. Thus we can extract a finite cover $\{U_1, ..., U_N\}$. We can assume, that for n great enough, each $\partial\Omega_n$ is representable as the graph of a Lipschitz function in the same coordinate system as $\partial\Omega$. We refer to [66, Chapter 2] for more details.

Consider a partition of unity $\phi_1, ..., \phi_N$ subordinated to the cover $\{U_1, ..., U_N\}$. It remains to prove that

$$\int_{\partial\Omega_n \cap U_i} |u_n|^p \phi_i d\sigma \to \int_{\partial\Omega \cap U_i} |u|^p \phi_i d\sigma.$$

Since $u_n \rightharpoonup u$ in $H^1(D)$ implies $u_n \phi \rightharpoonup u\phi$ in $H^1(D)$, we can drop the ϕ_i in the above limit and look only at integrals of u_n and u.

Denote by $g_n, g : B = B(x_0, r) \to \mathbb{R}$ the functions whose graphs represent the boundaries of $\partial\Omega_n, \partial\Omega$, respectively, in an orthogonal coordinate system in a neighbourhood if x_0. Note that B has dimension $d-1$ so when we speak of almost every $x \in B$ we will mean up to a set of $\mathcal{H}^{d-1}$ measure zero. The fact that $\Omega_n \xrightarrow{H^c} \Omega$ implies $\|g_n - g\|_\infty \to 0$. Since g, g_n are Lipschitz continuous functions, they are differentiable almost everywhere and $|\nabla g|, |\nabla g_n| \leq L$, where L is their common Lipschitz constant. Denote by v the function u after the change of variables in the new orthogonal coordinate system. It remains to prove that

$$\int_B |v_n(x, g_n(x))|^p \sqrt{1 + |\nabla g_n(x)|^2} dx \to \int_B |v(x, g(x))|^p \sqrt{1 + |\nabla g(x)|^2} dx.$$

The condition $\mathrm{Per}(\Omega_n) \to \mathrm{Per}(\Omega)$, the fact that $\mathcal{H}^{d-1}(\Omega_n \cap U_i) = 0$ and the lower semi-continuity of the perimeter under L^1 convergence imply that

$$\lim_{n\to\infty} \mathrm{Per}(\Omega_n \cap U_i) \geq \mathrm{Per}(\Omega \cap U_i),$$

and

$$\lim_{n\to\infty} \mathrm{Per}(\Omega_n \setminus U_i) \geq \mathrm{Per}(\Omega \setminus U_i).$$

This, in turn implies that we have equality, namely

$$\lim_{n\to\infty} \mathrm{Per}(\Omega_n \cap U_i) = \mathrm{Per}(\Omega \cap U_i).$$

Translated into the considered coordinate system this becomes

$$\lim_{n\to\infty} \int_B \sqrt{1 + |\nabla g_n(x)|^2} dx = \int_B \sqrt{1 + |\nabla g(x)|^2} dx.$$

Furthermore, considering measurable sets of the form $V = B' \times [-a, a]$ and the fact that $\mathrm{Per}(\Omega_n \cap V) \to \mathrm{Per}(\Omega \cap V)$, we deduce that

$$\lim_{n\to\infty} \int_{B'} \sqrt{1 + |\nabla g_n(x)|^2} dx = \int_{B'} \sqrt{1 + |\nabla g(x)|^2} dx, \tag{4.3.2}$$

for every measurable set $B' \subset B$.

Since v_n is a $H^1(D)$ function, for almost every $x \in B$ we have

$$v_n(x, g_n(x)) = v_n(x, g(x)) + \int_{g(x)}^{g_n(x)} \frac{\partial v_n}{\partial y}(x, y)dy.$$

To simplify the computations, we denote $J_n(x) = \sqrt{1 + |\nabla g_n(x)|^2}$, $J(x) = \sqrt{1 + |\nabla g|^2}$. We obviously have $J_n(x), J(x) \in [1, \sqrt{1 + L^2}]$. We use the inequality

$$||a + h|^p - |a|^p| \leq p(|h||a|^{p-1} + |h|^p),$$

which is trivial for $p = 1$ and is a direct consequence of the mean value theorem applied to the function $t \mapsto |t|^p$ when $p > 1$.

Thus we have

$$\left| \int_B |v_n(x, g_n(x))|^p J_n(x)dx - \int_B |v_n(x, g(x))|^p J_n(x)dx \right|$$

$$\leq \int_B ||v_n(x, g_n(x))|^p - |v_n(x, g(x))|^p| J_n(x)dx$$

$$\leq p \int_B \left| \int_{g(x)}^{g_n(x)} \frac{\partial v_n}{\partial y}(x, y)dy \right|^p J_n(x)dx \tag{A_n}$$

$$+ p \int_B |v_n(x, g(x))|^{p-1} \left| \int_{g(x)}^{g_n(x)} \frac{\partial v_n}{\partial y}(x, y)dy \right| J_n(x)dx \tag{B_n}$$

Study of (A_n). Since we only know bounds on the L^2 norm of the gradient of v_n, we apply Cauchy-Schwarz inequality and then Hölder's inequality to get

$$A_n \leq p \int_B |g_n(x) - g(x)|^{\frac{p}{2}} \left| \left[\int_{g(x)}^{g_n(x)} \frac{\partial v_n^2}{\partial y}(x, y)dy \right]^{\frac{1}{2}} \right|^p J_n(x)dx$$

$$\leq p \|g_n - g\|_\infty^{\frac{p}{2}} \sqrt{1 + L^2} \int_B \left[\int_{g(x)}^{g_n(x)} \frac{\partial v_n^2}{\partial y}(x, y)dy \right]^{\frac{p}{2}} dx$$

$$\leq p \|g_n - g\|_\infty^{\frac{p}{2}} \sqrt{1 + L^2} \left(\int_B \int_{g(x)}^{g_n(x)} \frac{\partial v_n^2}{\partial y}(x, y)dy \right)^{\frac{p}{2}} |B|^{1/q}$$

$$\leq C' \|g_n - g\|_\infty^{\frac{p}{2}} \|\nabla u_n\|_{H^1(D)}^p,$$

where C' is a constant which depends on B, p, L and q is chosen such that $\frac{p}{2} + \frac{1}{q} = 1$. As a consequence of the fact that $\|g_n - g\|_\infty \to 0$ we have $(A_n) \to 0$.

Study of (B_n). We apply Hölder's inequality for p and its conjugate $\frac{p}{p-1}$

$$B_n \leq p \int_B |v_n(x, g(x))|^{p-1} \left| \int_{g(x)}^{g_n(x)} \frac{\partial v_n}{\partial y}(x, y)dy \right| J_n(x)dx$$

$$\leq p \sqrt{1 + L^2} \left(\int_B |v_n(x, g(x))|^p dx \right)^{\frac{p-1}{p}} \left(\int_B \left| \int_{g(x)}^{g_n(x)} \frac{\partial v_n}{dy}(x, y)dy \right|^p \right)^{\frac{1}{p}} dx$$

Using arguments similar as in the study of (A_n) we can see that the last integral is bounded by a term of the form $C\|g_n - g\|_\infty^{\frac{1}{2}}$. To conclude that $(B_n) \to 0$ it remains to justify that the first integral is bounded. For this, we apply again Hölder's inequality for $\frac{2}{p} \geq 1$ and its conjugate q to get

$$\int_B |v_n(x, g(x))|^p dx \leq \left(\int_B v_n^2(x, g(x)) dx \right)^{\frac{p}{2}} |B|^{\frac{1}{q}}.$$

Using the trace theorem on $\partial\Omega$ we have

$$\int_B v_n^2(x, g(x)) dx \leq \int_B (v_n^2(x, g(x)) J(x) dx \leq \int_{\partial\Omega} u_n^2 \leq C\|u_n\|_{H^1(D)}^2.$$

This finishes the proof of the fact that $(B_n) \to 0$.

To conclude the proof of (B), it is enough to prove that

$$\lim_{n\to\infty} \int_B |v_n(x, g(x))|^p J_n(x) dx = \int_B |v(x, g(x))|^p J(x) dx$$

First, let's note that the fact that $u_n \to u$ in $L^2(\partial\Omega)$ implies $v_n(x, g(x)) \to v(x, g(x))$ for almost every $x \in B$.

Since g_n, g have Lipschitz constants bounded by L, and B is a bounded set, we deduce that $|\nabla g_n(x)|$ is bounded in $L^2(B)$, so it has a subsequence ∇g_{n_k} that converges weakly in $L^2(B)$ to a function h.

Thus, up to a subsequence, we have $\nabla g_n \rightharpoonup h$ in $L^2(B; \mathbb{R}^n)$ and

$$\lim_{n\to\infty} \int_\Omega F(\nabla g_n) \geq \int_\Omega F(h),$$

where $F(x) = \sqrt{1 + |x|^2}$ is a strictly convex function, if we consider it defined on $\{x \in \mathbb{R}^n : \|x\| \leq L\}$. Thus we can apply Lemma 4.3.1 and find that $\nabla g_n \to h$ strongly in $L^2(B; \mathbb{R}^n)$. Passing to a subsequence and relabelling, we can assume that $\nabla g_n \to h$ almost everywhere in B. Since $(g_n) \to g$ in $L^2(B)$ and $\nabla g_n \rightharpoonup h$ we must have $g \in H^1(B)$ and $h = \nabla g$.

We define the measures $\mu_n = J_n(x) dx$, $\mu = J(x) dx$. We note that property (4.3.2) implies that μ_n converges set-wise to μ. We use the terminology defined in [83, Chapter 11, Section 4]. This allows us to use versions of the integral convergence theorems provided in the above reference. We recall these results in Remark 4.3.3.

Using the bounds on J_n, J we have

$$|v_n(x, g(x))|^p \leq \sqrt{1 + L^2} |v_n(x, g(x))|^p \frac{J(x)}{J_n(x)}.$$

Since $u_n \to u$ in $L^2(\partial\Omega)$ and $\mathrm{Per}(\Omega)$ is finite, we have

$$|v_n(x, g(x))|^p J(x) \to |v(x, g(x))|^p J(x)$$

in $L^1(B)$, for every $p \in [1, 2]$. This means that

$$\lim_{n\to\infty} \int_B |v_n(x, g(x))|^p \frac{J(x)}{J_n(x)} d\mu_n \to \int_B |v(x, g(x))|^p d\mu.$$

Furthermore, since $J_n \to J$ almost everywhere, it follows that, up to a subsequence,

$$|v_n(x, g(x))|^p \frac{J(x)}{J_n(x)} \to |v(x, g(x))|^p$$

almost everywhere.

Applying a generalized integral convergence theorem, stated in Remark 4.3.3 (ii), we deduce that

$$\lim_{n\to\infty} \int_B |v_n(x, g(x))|^p d\mu_n = \int_B |v(x, g(x))|^p d\mu.$$

This finishes the proof of part (B).

For part (A) the proof is the same, except the last part where instead of applying the integral convergence theorem we apply the variant of Fatou's Lemma presented in Remark 4.3.3 (i). Note that general, the measures μ_n do not necessarily converge set-wise to μ. We have the weaker hypothesis $\liminf\limits_{n\to\infty} \mu_n(B') \geq \mu(B')$, which combined with the estimate $\mu_n(B') \leq \sqrt{1 + L^2}\mu(B')$ is enough to reach the same conclusions. $\qquad\square$

Remark 4.3.3. Let Ω be a measurable set. Suppose $f_n(x) \to f(x)$ for almost every $x \in \Omega$. Consider the measures μ_n, μ defined on Ω which satisfy for every measurable set $A \subset \Omega$ the equality

$$\lim_{n\to\infty} \mu_n(A) = \mu(A).$$

Following the terminology found in [83, Chapter 11, Section 4] we say that μ_n converges *setwise* to μ.

(i) If $(f_n), f$ are non negative functions we have

$$\int_\Omega f d\mu \leq \liminf_{n\to\infty} \int_\Omega f_n d\mu_n$$

(ii) If there exist functions g_n such that g_n are integrable with respect to μ_n, $|f_n| \leq g_n$, $g_n \to g$ almost everywhere, and

$$\lim_{n\to\infty} \int_\Omega g_n d\mu_n = \int_\Omega g d\mu < \infty$$

then

$$\lim_{n\to\infty} \int_\Omega f_n d\mu_n = \int_\Omega f d\mu.$$

For the part (i), the hypothesis $\mu_n(A) \to \mu(A)$ for every measurable set A can be relaxed to

$$\liminf_{n\to\infty} \mu_n(A) \geq \mu(A), \ \mu_n(A) \leq C\mu(A),$$

where $C > 0$ is a constant.

Remark 4.3.4. It will be necessary to apply Proposition 4.3.2 part (B) in the case $p = 1$ without the absolute values. Under the same hypothesis we want to prove that

$$\lim_{n\to\infty} \int_{\partial\Omega_n} u_n = \int_{\partial\Omega} u.$$

To achieve this it is enough to note that if $u_n \rightharpoonup u$ in $H^1(D)$ then $u_n^+ \rightharpoonup u^+$ and $u_n^- \rightharpoonup u^-$ in $H^1(D)$. We have denoted by u^+, u^- the positive, respective the negative part of u. We refer to [66, Corollary 3,1,12] for a proof of this result. We apply Proposition 4.3.2 for $u_n^+ \rightharpoonup u^+$ and $u_n^- \rightharpoonup u^-$ to find that

$$\lim_{n\to\infty} \int_{\partial\Omega_n} u_n^+ = \int_{\partial\Omega} u^+$$

and

$$\lim_{n\to\infty} \int_{\partial\Omega_n} u_n^- = \int_{\partial\Omega} u^-.$$

Subtracting these two equalities we get the desired result.

The above proposition helps us to prove the following shape continuity result for the Steklov spectrum. A general approach has been described in [25] in the case where the operators are defined on a common space. Another similar result is presented in [30] for the first biharmonic Steklov eigenvalue in the particular case of convex open sets.

Theorem 4.3.5. *(Shape Stability for the Steklov spectrum) Let D be a bounded open subset of $\mathbb{R}^d$. Suppose $(\Omega_n), \Omega \subset D$ are open sets which satisfy a uniform ε-cone condition and $\Omega_n \xrightarrow{H^c} \Omega$.*

(A) The following inequality holds:

$$\limsup_{n\to\infty} \sigma_k(\Omega_n) \leq \sigma_k(\Omega).$$

(B) If $\mathrm{Per}(\Omega_n) \to \mathrm{Per}(\Omega)$ then for every $k \geq 1$ we have

$$\lim_{n\to\infty} \sigma_k(\Omega_n) = \sigma_k(\Omega).$$

Proof: We start with part (B). We divide the proof in two parts:

$$\limsup_{n\to\infty} \sigma_k(\Omega_n) \leq \sigma_k(\Omega) \tag{4.3.3}$$

and

$$\liminf_{n\to\infty} \sigma_k(\Omega_n) \geq \sigma_k(\Omega) \tag{4.3.4}$$

For an open set Ω we denote by $V(\Omega)$ the space of functions on $H^1(\Omega)$ which are orthogonal to constants in $L^2(\partial\Omega)$. Note that if Ω has finite perimeter then $V(\Omega)$ is closed under weak convergence in $H^1(\Omega)$ (Straightforward application of Proposition 4.3.2 together with Remark 4.3.4).

1. Proof of (4.3.3). Let $\varepsilon > 0$ and consider a k-dimensional subspace S_k of V such that

$$\sigma_k(\Omega) + \varepsilon \geq \max_{u\in S_k\backslash\{0\}} \frac{\int_\Omega |\nabla u|^2}{\int_{\partial\Omega} u^2}.$$

Let $\{u_1, .., u_k\}$ an orthonormal basis for S_k. Since $S_k \subset H^1(\Omega)$ and Ω has Lipschitz boundary, each u_i can be extended to $\tilde{u}_i \in H^1(D)$.

For $n \geq 1$ we modify each $\tilde{u}_i$ in order to make them admissible as test functions on Ω_n. To do this, we modify them with a constant term in order to have zero averages on $\partial \Omega_n$. This is possible since Ω_n has finite perimeter and we can simply define $u_i^n = \tilde{u}_i - c_i^n$, where c_i^n is a constant defined by $0 = \int_{\partial \Omega_n} (\tilde{u}_i - c_i^n) d\sigma = \int_{\partial \Omega_n} \tilde{u}_i d\sigma - c_i^n \operatorname{Per}(\Omega_n)$. Therefore $c_i^n = \frac{1}{\operatorname{Per}(\Omega_n)} \int_{\partial \Omega_n} \tilde{u}_i d\sigma$. Since $\operatorname{Per}(\Omega_n) \to \operatorname{Per}(\Omega) > 0$ and $\int_{\partial \Omega_n} \tilde{u}_i d\sigma \to \int_{\partial \Omega} u_i d\sigma = 0$, we find that $\lim_{n \to \infty} c_i^n = 0$ for $i = 1, ..., k$. This implies that $u_i^n \to \tilde{u}_i$ in $H^1(D)$.

For n great enough, the functions u_i^n span a k-dimensional subspace $S_k^n \subset H^1(D)$ which is admissible as a test subspace for $\sigma_k(\Omega_n)$. This implies that

$$\sigma_k(\Omega_n) \leq \max_{u \in S_k^n \setminus \{0\}} \frac{\int_{\Omega_n} |\nabla u|^2}{\int_{\partial \Omega_n} u^2} = \frac{\int_{\Omega_n} |\nabla v_n|^2}{\int_{\partial \Omega_n} v_n^2},$$

where we have denoted v_n a choice of the maximizers of the Rayleigh quotient on S_k^n. The maximizer v_n exists since S_k^n is finite dimensional.

Consider now $u_0 \in S_k$ arbitrary. Then there exist coefficients $a_1, ..., a_k$ such that

$$u_0 = a_1 u_1 + ... + a_k u_k.$$

Consider also the functions $u_0^n \in S_k^n$ defined by

$$u_0^n = a_1 u_1^n + ... + a_k u_k^n.$$

It easily follows that $u_0^n \to \tilde{u}_0$ in $H^1(D)$, since they differ only by a constant term which converges to 0 as $n \to \infty$. The maximality property of (v_n) implies

$$\frac{\int_{\Omega_n} |\nabla u_0^n|^2}{\int_{\partial \Omega_n} (u_0^n)^2} \leq \frac{\int_{\Omega_n} |\nabla v_n|^2}{\int_{\partial \Omega_n} v_n^2}. \tag{4.3.5}$$

We want to prove that $\limsup_{n \to \infty} \sigma_k(\Omega_n) \leq \sigma_k(\Omega)$. Without loss of generality, we can assume that $\lim_{n \to \infty} \sigma_k(\Omega_n)$ exists. If not, we take a subsequence which realizes the $\limsup$. We can find a decomposition $v_n = b_1^n u_1^n + ... + b_k^n u_k^n$. Since the Rayleigh quotient is scale invariant, we can choose the coefficients such that $|b_i^n| \leq 1$. Using a diagonal argument we can choose a subsequence of v_n such that $b_i^n \to b_i$ for $i = 1, ..., m$. Up to relabelling the sequence, we can assume that $v_n \to v$ in $H^1(D)$ where v is given by

$$v = b_1 \tilde{u}_1 + ... + b_k \tilde{u}_k.$$

Taking $n \to +\infty$ in inequality (4.3.5) and using Proposition 4.3.2 we obtain that

$$\frac{\int_{\Omega} |\nabla u_0|^2}{\int_{\partial \Omega} u_0^2} \leq \frac{\int_{\Omega} |\nabla v|^2}{\int_{\partial \Omega} v^2}.$$

Since u_0 was chosen arbitrary, we have that

$$\max_{u_0 \in S_k \setminus \{0\}} \frac{\int_{\Omega} |\nabla u_0|^2}{\int_{\partial \Omega} u_0^2} \leq \frac{\int_{\Omega} |\nabla v|^2}{\int_{\partial \Omega} v^2}.$$

The restriction of v to Ω is also in S_k, so the above inequality is, in fact, an equality.

We have just proved that

$$\limsup_{n\to\infty} \sigma_k(\Omega_n) \leq \lim_{n\to\infty} \frac{\int_{\Omega_n} |\nabla u_n|^2}{\int_{\partial\Omega_n} u_n^2} = \frac{\int_{\Omega} |\nabla v|^2}{\int_{\partial\Omega} v^2} = \max_{u\in S_k\setminus\{0\}} \frac{\int_{\Omega} |\nabla u|^2}{\int_{\partial\Omega} u^2} \leq \sigma_k(\Omega) + \varepsilon.$$

Taking $\varepsilon \to 0$ we obtain the $\limsup$ inequality.

2. Proof of (4.3.4)**.** Consider $\varepsilon > 0$ and subspaces S_k^n of $H^1(D)$ such that

$$\sigma_k(\Omega_n) + \varepsilon \geq \max_{u\in S_k^n\setminus\{0\}} \frac{\int_{\Omega_n} |\nabla u|^2}{\int_{\partial\Omega_n} u^2}. \tag{4.3.6}$$

We want to prove that $\liminf_{n\to\infty} \sigma_k(\Omega_n) \geq \sigma_k(\Omega)$. We can assume that the limit exists by taking a subsequence which realizes it. Consider for each S_k^n an orthonormal basis $\{u_1^n, ..., u_k^n\}$. Up to choosing a diagonal subsequence, we can assume that each (u_i^n) converges weakly in $H^1(D)$ to some u_i, $i = 1, ..., k$. Using Proposition 4.3.2 and Remark 4.3.4 it follows that $\int_{\partial\Omega} u_i = 0$, so $S_k = \text{Span}\{u_1, ..., u_k\}$ is admissible as a test space for $\sigma_k(\Omega)$.

Take $u = a_1 u_1 + ... + a_k u_k \in S_k \setminus \{0\}$. Then $v_n = a_1 u_1^n + ... + a_k u_k^n \in S_m^n \setminus \{0\}$ satisfies $v_n \rightharpoonup u$ in $H^1(D)$. The inequality (4.3.6) implies that

$$\sigma_k(\Omega_n) + \varepsilon \geq \frac{\int_{\Omega_n} |\nabla v_n|^2}{\int_{\partial\Omega_n} v_n^2}.$$

The weak convergence of (v_n) to u and Proposition 4.3.2 imply that

$$\liminf_{n\to\infty} \int_{\Omega_n} |\nabla v_n|^2 \geq \int_{\Omega} |\nabla u|^2 \text{ and } \lim_{n\to\infty} \int_{\partial\Omega_n} v_n^2 = \int_{\partial\Omega} u^2.$$

As a consequence, we have

$$\liminf_{n\to\infty} \sigma_k(\Omega_n) + \varepsilon \geq \frac{\int_{\Omega_n} |\nabla u|^2}{\int_{\partial\Omega_n} u^2}.$$

Since u was chosen arbitrary, we can take the maximum for $u \in S_k \setminus \{0\}$ in the right hand side of the above inequality and we get

$$\liminf_{n\to\infty} \sigma_k(\Omega_n) + \varepsilon \geq \max_{u\in S_k\setminus\{0\}} \frac{\int_{\Omega_n} |\nabla u|^2}{\int_{\partial\Omega_n} u^2} \geq \sigma_k(\Omega).$$

Taking $\varepsilon \to 0$ se obtain

$$\liminf_{n\to\infty} \sigma_k(\Omega_n) \geq \sigma_k(\Omega).$$

Combining the two parts of the proof we conclude that under the hypotheses we considered we have

$$\lim_{n\to\infty} \sigma_k(\Omega_n) = \sigma_k(\Omega).$$

In order to prove part (A) we argue by contradiction. Suppose that $\limsup\limits_{n\to\infty} \sigma_k(\Omega_n) > \sigma_k(\Omega)$. The variational formulation implies the existence of some $\varepsilon > 0$ and a k dimensional subspace S_k of $V(\Omega)$ such that up to a subsequence we have

$$\lim_{n\to\infty} \sigma_k(\Omega_n) > \sigma_k(\Omega) + \varepsilon > \max_{u\in S_k} \frac{\int_\Omega |\nabla u|^2}{\int_{\partial\Omega} u^2}.$$

Therefore, for n great enough we have

$$\sigma_k(\Omega_n) > \sigma_k(\Omega) + \varepsilon > \max_{u\in S_k} \frac{\int_\Omega |\nabla u|^2}{\int_{\partial\Omega} u^2}.$$

Consider a basis $\{u_1, ..., u_k\}$ of S_k. Like in the proof of part (B), we construct the functions u_i^n which are perturbations by constants of H^1 extensions of u_i to the whole D such that $\int_{\partial\Omega_n} u_i^n = 0$. In this way we construct the k-dimensional subspaces $S_k^n = \{u_1^n, ...u_k^n\}$ which are admissible as test spaces for $\sigma_k(\Omega_n)$. Thus we have

$$\max_{u\in S_k^n} \frac{\int_{\Omega_n} |\nabla u|^2}{\int_{\partial\Omega_n} u^2} \geq \sigma_k(\Omega_n) > \sigma_k(\Omega) + \varepsilon > \max_{u\in S_k} \frac{\int_\Omega |\nabla u|^2}{\int_{\partial\Omega} u^2}.$$

Denote v_n a choice of maximizers of the Rayleigh quotient on S_k^n. We have the representation $v_n = b_1^n u_1^n + ... + b_k^n u_k^n = b_1^n \tilde{u}_1 + ... + b_k^n \tilde{u}_k - (b_1^n c_1^n + ... + b_k^n c_k^n)$. Like in the first part we have $c_i^n = \frac{1}{\text{Per}(\Omega_n)} \int_{\partial\Omega_n} \tilde{u}_i d\sigma$, and we can choose the coefficients (b_i^n) such that $|b_i^n| \leq 1$. Note that in this setting we do not necessarily have $c_i^n \to 0$ as $n \to \infty$, but there is a uniform bound for (c_i^n). We can choose a subsequence and relabel it such that $v_n \to b_1\tilde{u}_1 + ... + b_k\tilde{u}_k - C = u_0 - C$ in $H^1(D)$.

Using Proposition 4.3.2 part (B), we have

$$\liminf_{n\to\infty} \int_{\partial\Omega_n} v_n^2 \geq \int_{\partial\Omega} (u_0 - C)^2 = \int_{\partial\Omega} u_0^2 - 2C \int_{\partial\Omega} u_0 + C^2 \text{Per}(\Omega) \geq \int_{\partial\Omega} u_0^2,$$

since $\int_{\partial\Omega} u_0 = 0$. Furthermore, the fact that $v_n \to u_0 - C$ in $H^1(D)$ and $\chi_{\Omega_n} \to \chi_\Omega$ in $L^1(D)$ imply that

$$\lim_{n\to\infty} \int_{\Omega_n} |\nabla v_n|^2 = \int_\Omega |\nabla u_0|^2.$$

Taking $n \to \infty$ in the following inequality

$$\frac{\int_{\Omega_n} |\nabla v_n|^2}{\int_{\partial\Omega_n} v_n^2} \geq \sigma_k(\Omega_n) > \sigma_k(\Omega) + \varepsilon$$

we obtain

$$\max_{u\in S_k} \frac{\int_\Omega |\nabla u|^2}{\int_{\partial\Omega} u^2} < \sigma_k(\Omega) + \varepsilon \leq \limsup_{n\to\infty} \frac{\int_{\Omega_n} |\nabla v_n|^2}{\int_{\partial\Omega_n} v_n^2} \leq \frac{\int_\Omega |\nabla u_0|^2}{\int_{\partial\Omega} u_0^2}.$$

This is a contradiction, since $u_0 \in S_k$. $\qquad\square$

The hypothesis that $\text{Per}(\Omega_n) \to \text{Per}(\Omega)$ was crucial in the proof of part (B) of the above theorem, and cannot be discarded. To justify this fact, we propose the following counterexample.

Example 4.3.6. Denote by S the unit square and by S_n the unit square where we have added a saw-tooth shape with 2^n sides on the upper side of S. For example, we can take S_1 to be S with a right isosceles triangle glued to S. S_2 can be obtained by cutting a square of length $\sqrt{2}/4$ from the top of the "tooth" of S_1. S_3 can be obtained from S_2 by cutting squares of side $\sqrt{2}/8$ from the top of each tooth of S_2. This procedure constructs inductively the sets S_n. Note that the sets S_n satisfy a uniform cone condition.

Furthermore, all the shapes S_n have the same perimeter, equal to $3 + \sqrt{2}$, thus $\mathrm{Per}(S_n) \to 3 + \sqrt{2} > 4 = \mathrm{Per}(S)$. We will show that the Steklov spectrum of S_n does not converge to the Steklov spectrum of S.

Proof: In the proof we will denote by T the edge of the square S to which the saw-tooth is glued, and B the other three edges of the square S. We denote by g_n the function whose graph represents the sawtooth in an orthogonal system of coordinates where the horizontal axis is directed by T. Note that in this case $|g_n'(x)| = 1$ for almost every $x \in T$. Denote by T_n the graph of g_n on T.

Let $u \in H^1(S)$ be an eigenfunction of S, corresponding to $\sigma_1(S)$. Since S is a Lipschitz domain, u can be extended to $H^1(\mathbb{R}^2)$, and then take the restrictions of u to S_n as test functions in the definition of $\sigma_1(S_n)$.

To do this, we need to make these restrictions admissible by modifying them with a constant in order to have the orthogonality to a constant function on S_n. We define $u_n = u - c_n$ such that

$$0 = \int_{\partial S_n} u_n = \int_{\partial S_n} u - c_n \, \mathrm{Per}(S_n).$$

This implies $c_n = \frac{1}{\mathrm{Per}(S_n)} \int_{\partial S_n} u.$

With the above notations we have

$$\int_{T_n} u = \int_T u(x, g_n(x)) \sqrt{1 + |g_n'(x)|^2} dx$$

$$= \sqrt{2} \int_T u(x, 0) dx + \sqrt{2} \int_T \int_0^{g_n(x)} \frac{\partial u}{\partial y}(x, y) dy dx.$$

Using techniques similar to the ones involved in the proof of Proposition 4.3.2, we find that

$$\int_{T_n} u \to \sqrt{2} \int_T u \text{ as } n \to \infty.$$

In the same way, we can prove that

$$\int_{T_n} u^2 \to \sqrt{2} \int_T u^2 \text{ as } n \to \infty.$$

We evaluate

$$\int_{\partial S_n} (u - c_n)^2 = \int_{\partial S_n} u^2 - c_n^2 \, \mathrm{Per}(S_n)$$

$$= \int_B u^2 + \int_{T_n} u^2 - \frac{\left(\int_B u + \int_{T_n} u \right)^2}{3 + \sqrt{2}}$$

and we see that for $n \to \infty$ we have

$$\lim_{n\to\infty} \int_{\partial S_n} u_n^2 = \int_B u^2 + \sqrt{2} \int_T u^2 - \frac{(\sqrt{2}-1)^2}{3+\sqrt{2}} \left(\int_T u\right)^2.$$

$$= \int_{\partial S} u^2 + (\sqrt{2}-1) \int_T u^2 - \frac{(\sqrt{2}-1)^2}{3+\sqrt{2}} \left(\int_T u\right)^2$$

$$> \int_{\partial S} u^2,$$

by the Cauchy-Schwarz inequality. The equality could take place only if u is constant zero on T, but if this happens for every side of the square, then u is zero on the whole S, which is a contradiction.

Thus

$$\sigma_1(S) = \frac{\int_S |\nabla u|^2}{\int_{\partial S} u^2} > \lim_{n\to\infty} \frac{\int_{S_n} |\nabla u_n|^2}{\int_{\partial S_n} u_n^2} \geq \liminf_{n\to\infty} \sigma_1(S_n).$$

Therefore the sequence of first Steklov eigenvalues of S_n does not converge to the first Steklov eigenvalue of S. $\qquad\square$

There exist examples in the literature which illustrate the fact that the ε-cone condition is also essential. Girouard and Polterovich consider in [55] one such examples. It consists of taking Ω_ε being two disks of radius 1 connected by a thin tube of length ε and width ε^3. In the limit, these connected disks converge to Ω which is formed of two tangent disks. Obviously, such sets do not satisfy a uniform cone condition. We have $\mathrm{Per}(\Omega_\varepsilon) \to \mathrm{Per}(\Omega)$, but the Steklov eigenvalues of Ω_ε converge to zero.

4.4 Existence results for the optimization of functionals of the Steklov spectrum

In this sections we present some consequences of the facts proved in the previous sections. We are able to establish some existence results for the problem of maximizing the Steklov eigenvalue of Ω under different constraints.

Theorem 4.4.1. *Suppose D is a bounded, open set in $\mathbb{R}^d$. Denote by $\mathcal{O}_\varepsilon$ the class of open subsets of D which satisfy an ε-cone property and have unit volume. Then the problem*

$$\max_{\Omega \in \mathcal{O}_\varepsilon} \sigma_k(\Omega)$$

has a solution.

Proof: Take (Ω_n) a maximizing sequence. The Hausdorff convergence is compact, $\mathcal{O}_\varepsilon$ is closed under this convergence and therefore there exists an open set $\Omega \in \mathcal{O}_\varepsilon$ such that up to taking a subsequence and relabeling, we have $\Omega_n \xrightarrow{H^c} \Omega$. Proposition 4.2.3 or the estimate (4.1.1) implies that there exists an upper bound for $\mathrm{Per}(\Omega_n)$. The compactness properties of

the perimeter (see for example [70, Theorem 12.26]) imply that there exists a subsequence denoted again (Ω_n) such that (Ω_n) converges to Ω in the sense of characteristic functions and furthermore, $\lim_{n \to \infty} \text{Per}(\Omega_n) \geq \text{Per}(\Omega)$ and applying Theorem 4.3.5 (A) we deduce that

$$\limsup_{n \to \infty} \sigma_k(\Omega_n) \leq \sigma_k(\Omega).$$

The fact that (Ω_n) is a maximizing sequence coupled with the above inequality proves that Ω is the set which maximizes $\sigma_k(\Omega)$ in the class $\mathcal{O}_\varepsilon$. $\square$

Note that convex sets Ω satisfy a ε-cone condition, with ε depending on the radius of a ball contained in Ω, as well as of the box D containing Ω. We would like to give a general existence result for the maximization of $\sigma_k(\Omega)$ in the family of the convex sets. In order to apply the results of the previous section, we would need a bounding box for Ω. The result given below proves that a maximizing sequence for $\sigma_k(\Omega)$ is always confined in a bounded open set D.

Proposition 4.4.2. *Suppose that (Ω_n) is a sequence of open, convex sets with unit volume, which satisfy the property that $diam(\Omega_n) \to \infty$. Then $\sigma_k(\Omega_n) \to 0$.*

Proof: This result is a consequence of the bound (4.4.1) proved in [37], which states that if we denote by $I(\Omega) = \text{Per}(\Omega)/|\Omega|^{\frac{d-1}{d}}$ then

$$\sigma_k(\Omega) \leq c_d k^{\frac{2}{d}} \frac{|\Omega|^{\frac{d-2}{d}}}{\text{Per}(\Omega)}. \tag{4.4.1}$$

Indeed, we could consider a diameter of length M and make a Steiner symmetrization in the direction of the diameter. There exists a section ω orthogonal to the diameter which maximizes $\mathcal{H}^{n-1}(\omega)$. The fact that Ω has unit volume implies $\mathcal{H}^{n-1}(\omega) \geq 1/M$. Consider the cone C generated by ω and the considered diameter. This cone is contained in Ω, and by convexity, the perimeter of Ω is bounded from below by the perimeter of the cone C. Using techniques similar to those in our proof presented below, we can see that the $\text{Per}(C) \geq cM^{\frac{1}{d-1}}$, where c is a dimensional constant. This, together with (4.4.1) implies that $\sigma_k(\Omega) \to 0$ as $M \to \infty$.

In the case of convex sets it is possible to give a direct proof, which we present below. This proof avoids the technical measure theory result used in [37] to prove (4.4.1).

Let Ω be an open, convex set of $\mathbb{R}^d$, having unit volume. Denote by M its diameter, and denote $X_0 X_k$ one of its diameters. In order to make the proof easier to read, we divide it into several parts.

Part 1. Bound from below of the volume of a region. We call a *cap* of Ω the part of Ω contained in a halfspace determined by a hyperplane α orthogonal to the diameter $X_0 X_k$. We call *region* of Ω a subset of Ω contained between two hyperplanes α, β which are orthogonal to $X_0 X_k$.

Let's start by giving a lower bound for the volume of a cap. Denote $Y = \alpha \cap X_0 X_k$ and the length $X_0 Y$ by L. Denote Ω^- and Ω^+ the caps of Ω determined by α, which contain X_0 and X_k, respectively. Denote C^- the cone with vertex X_0 and base $\Omega \cap \alpha$. Denote also with C^+ the

cone which is the dilated of C^- with center X_0 and a factor M/L. The convexity of Ω implies

$$C^- \subset \Omega^- \text{ and } C^+ \setminus C^- \supset \Omega^+.$$

Therefore we have

$$\frac{|\Omega^-|}{|\Omega^+|} \geq \frac{|C^-|}{|C^+| - |C^-|} = \frac{L^d}{M^d - L^d},$$

which, in turn, implies $|\Omega^-| \geq L^d/M^d|\Omega|$.

If instead of a cap, we consider a region, we can apply two times the above bound and find a similar lower bound. Denote Ω^- the part of Ω contained in the halfspace determined by γ which contains X_0, Ω^+ the part of Ω contained in the halfspace determined by β whcih contains X_k and Ω_0 the region determined by α and β. Denote also $A = \alpha \cap X_0 X_k$, $B = \beta \cap X_0 X_k$.

Using the bound on a cap, we have

$$|\Omega_0| \geq \frac{AB^d}{AX_k^d}|\Omega_0 \cup \Omega^+|,$$

and

$$|\Omega^+ \cup \Omega_0| \geq \frac{AX_k^d}{X_0 X_k^d}|\Omega|.$$

Combining the two bounds, we arrive at

$$|\Omega_0| \geq \frac{L^d}{M^d}|\Omega|,$$

where we have denoted the length of AB by L.

Part 2. Bound from below of the perimeter of a region. Suppose we have a region Ω_0 of width L, like in the previous section. In the following, we will denote by c_d a constant which depends only on the dimension of the space. We perform a Steiner-symmetrization of this region with respect to the direction AB, which we denote Ω_0^*. For an introduction to Steiner symmetrization see [66, Chapter 6] or [27, Chapter 6]. It is known that performing a Steiner symmetrization preserves the volume, preserves the convexity and decreases the perimeter. Thus, as a first consequence, $\mathrm{Per}(\Omega_0^*) \leq \mathrm{Per}(\Omega_0)$. Another property of the Steiner symmetrized set Ω_0^* is that all slices with a hyperplane orthogonal to AB are $d-1$-dimensional balls. Among these balls, there is one, denoted ω, having radius r_0, which has the maximal $\mathcal{H}^{d-1}$ measure. Denote $a = d(A, \omega), b = d(B, \omega)$. Obviously, we have $a + b = L$. Since

$$|\Omega_0^*| \geq \frac{L^d}{M^d},$$

we deduce that $\mathcal{H}^{d-1}(\omega) \geq \frac{L^{d-1}}{M^d}$, which gives us a lower bound $r \geq c_d \frac{L}{M^{\frac{d}{d-1}}}$.

We denote $\omega_1 = \alpha \cap \Omega, \omega_2 = \beta \cap \Omega$. The fact that Ω_0 is convex, and its $d-1$-dimensional slices orthogonal to AB are disks, means that the truncated cones determined by $T_1 = (\omega, \omega_1)$ and $T_2 = (\omega, \omega_2)$ are contained in Ω.

We know from [27, Lema 2.2.2] that since $T_1 \cup T_1 \subset \Omega_0^*$ and $T_1 \cup T_2, \Omega_0^*$ are convex, we have $\mathrm{Per}(T_1 \cup T_1) \leq \mathrm{Per}(\Omega_0^*)$. If we denote by R the region of $\mathbb{R}^d$ situated between the

hyperplanes α, β, then $\mathrm{Per}(T_1 \cup T_2, R) \leq \mathrm{Per}(\Omega_0^*, R)$. This inequality is true because the part of the perimeters of Ω_0^* and $T_1 \cup T_2$ which is contained in ∂R is the same for both sets.

All we need in order to conclude, is to bound from below the lateral area of a truncated cone. If we denote by r_1, r the two radii of ω_1, ω, then we have two cases. If $r_1 = r$ then T_1 is a cylinder and the lateral area of T_1 is equal to $a\mathcal{H}^{d-2}(\omega) = c_d a r^{d-2}$. If $r_1 < r$ then the lateral area is given by

$$\int_{\omega \setminus \mathrm{proj}_\omega \omega_1} \sqrt{1 + \frac{a^2}{(r - r_1)^2}} \geq c_d a \frac{r^{d-1} - r_1^{d-1}}{r - r_1} \geq c_d a r^{d-2}.$$

Thus the lateral area of $T_1 \cup T_2$ is bounded below by

$$\mathrm{Per}(T_1 \cup T_2, R) \geq c_d L r^{d-2}.$$

Combining all the above estimates, we arrive at

$$\mathrm{Per}(\Omega_0) \geq c_d \frac{L^{d-1}}{M^{\frac{d(d-2)}{d-1}}}.$$

Thus for a region Ω_0 of Ω with width $L = \alpha M$ we have

$$\mathrm{Per}(\Omega_0) \geq c_d \alpha^{d-1} M^{\frac{1}{d-1}}.$$

Part 3. Upper bound on the Steklov spectrum

For $k \geq 1$ divide the diameter $X_0 X_k$ into k equal parts using points X_i, and use orthogonal hyperplanes α_i through X_i to divide Ω into k subsets of width M/k (in the direction of $X_0 X_k$). We define k functions $(u_i) \subset H^1(\Omega)$ such that u_i is supported in region i. We choose them to depend only on the distance from the bounding hyperplanes. One choice is the following:

- u_i starts from 0 on α_{i-1} and increases with gradient 1 until it reaches 1.

- u_i is constant for a while.

- u_i descends with gradient 1 until it reaches -1.

- u_i is constant for a while.

- u_i increases with gradient 1 until it reaches 0.

A schematic picture can be found in Figure 4.1. Furthermore, we can translate the part where u_i grows from -1 to 1 so that $\int_{\partial\Omega} u_i = 0$. With this construction we have the following bound on the Rayleigh quotient corresponding to u_i:

$$\frac{\int_\Omega |\nabla u_i|^2}{\int_{\partial\Omega} u_i^2} \leq \frac{1}{\mathcal{H}^{d-1}(\partial\Omega \cap \{u_i = \pm 1\})}$$
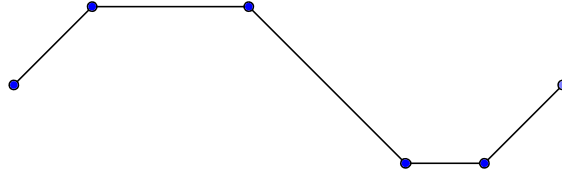
Figure 4.1: Form of the function u_i in the direction of the diameter

Using the bounds obtained in the previous section, we have

$$\mathcal{H}^{d-1}(\partial\Omega \cap \{u_i = 1\}) \geq c_d \alpha_1^{d-1}(M/k)^{\frac{1}{d-1}}$$
$$\mathcal{H}^{d-1}(\partial\Omega \cap \{u_i = -1\}) \geq c_d \alpha_2^{d-1}(M/k)^{\frac{1}{d-1}}$$

where $\alpha_1 + \alpha_2 \geq 1 - \frac{4k}{M}$. Thus

$$\mathcal{H}^{d-1}(\partial\Omega \cap \{u_i = 1\}) + \mathcal{H}^{d-1}(\partial\Omega \cap \{u_i = -1\}) \geq c_d(\alpha_1 + \alpha_2)^{d-1}(M/k)^{\frac{1}{d-1}}.$$

These bounds allow us to conclude that as $M \to \infty$ we have

$$\frac{\int_\Omega |\nabla u_i|^2}{\int_{\partial\Omega} u_i^2} \leq c_d \frac{k^{\frac{1}{d-1}}}{(1 - 4k/M)^{d-1} M^{\frac{1}{d-1}}} \overset{M\to\infty}{\longrightarrow} 0.$$

As a consequence, we have the bound

$$\sigma_k(\Omega) \leq \max \frac{\int_\Omega |\nabla \sum a_i u_i|^2}{\int_{\partial\Omega}(\sum a_i u_i)^2} \leq \max \frac{\int_\Omega |\nabla u_i|^2}{\int_{\partial\Omega} u_i^2},$$

where we have used the fact that the functions u_i have disjoint support in Ω. This means that

$$\sigma_k(\Omega) \to 0 \text{ as } M \to \infty.$$

$\square$

Using the previous result, we can deduce the existence of a maximizer for the k-th Steklov eigenvalue in the class of convex sets.

Corollary 4.4.3. *The problem*

$$\max_{|\Omega|=1} \sigma_k(\Omega)$$

has a solution in the class of convex sets.

Proof: Take (Ω_n) a sequence of sets with measure 1 such that $\sigma_k(\Omega_n) \to \sup_{|\Omega|=1} \sigma_k(\Omega)$. If (Ω_n) contains a subsequence such that $\text{diam}(\Omega_n) \to \infty$, then by Theorem 4.4.2, $\sigma_k(\Omega_n)$ would have a subsequence converging to zero. This is impossible, since (Ω_n) is a maximizing sequence. Thus the diameters of (Ω_n) are bounded from above, and therefore we can assume that all the sets Ω_n are contained in a bounded open set D.

The by the compactness of Hausdorff convergence, there exists a subsequence denoted (Ω_n) such that $\Omega_n \xrightarrow{H^c} \Omega$. The properties of the Hausdorff convergence imply that Ω is also convex and contains a compact ball B (see [66, Chapter 2]). Proposition 2.2.15 in [66] proves that for n large enough, we must have $B \subset \Omega_n$. Proposition 2.4.4 in [66] allows us to say that for n large enough, the sets Ω_n and the set Ω satisfy a uniform cone condition. Thus, we can apply Theorem 4.3.5 to conclude that

$$\limsup_{n\to\infty} \sigma_k(\Omega_n) \leq \sigma_k(\Omega).$$

The Hausdorff convergence implies the convergence of characteristic functions in $L^1(D)$, which, in turn implies that $|\Omega| = \lim_{n\to\infty} |\Omega_n| = 1$. Thus Ω maximizes $\sigma_k(\Omega)$ among convex sets of the same measure. $\qquad\square$

Remark 4.4.4. The treatment of the perimeter constraint, in the case of convex sets, is also straightforward, since we can apply Theorem 4.3.2 directly, for a maximizing sequence.

Corollary 4.4.5. *In the following, we consider $\mathcal{A}$ to be the class of ε-cone sets contained in a bounded open set D, or the class of convex sets.*

(A) If $F : \mathbb{R}^k \to \mathbb{R}$ is upper semi-continuous and increasing in every variable, then the problem

$$\max_{\Omega \in \mathcal{A}} F(\sigma_1(\Omega), ..., \sigma_k(\Omega)).$$

has a solution.

(A) If $G : \mathbb{R}^k \to \mathbb{R}$ is lower semi-continuous and increasing in every variable, then the problem

$$\min_{\Omega \in \mathcal{A}} G(1/\sigma_1(\Omega), ..., 1/\sigma_k(\Omega)).$$

has a solution.

We may ask if this existence result can be improved by dropping or weakening the hypothesis on the regularity of the domain. We discuss below the perspectives by treating separately the perimeter and area constraints.

- **Perimeter constraint.** Recent works announced by I. Polterovich and his PhD student ... suggest that if we drop the ε-cone condition, we do not have existence. Their argument is based on the fact that making small holes in certain well chosen spots in the domain increases the first rescaled Steklov eigenvalue. Thus, having no constraint on the number of holes or on the simple connectedness of the domains does not seem allow us to have an existence result.

- **Area constraint.** The case of the area constraint is different, and this can be seen from the study of the first Steklov eigenvalue. Brock's optimality result in the case of the area

constraint does not assume any regularity of the domain. On the other hand, Weinstock's result depends crucially on the fact that only simply connected domains are admitted. Numerical results shown in further sections suggest that in the case of the area constraint, optimal domains exist in general and are simply connected.

4.5   A numerical method for computing the Steklov/Wentzell spectrum

Steklov eigenvalues can be computed using mesh-based methods. The difficulty is the fact that we need to work with boundary meshes for the treatment of the boundary condition equation. This can be done rather quick in FreeFem++ [61], and an example code is given in Section 4.11. The mesh-based method has the disadvantage that high precision computations needs a fine mesh. On the other hand, as meshes become more and more refined, computations become slower. We present below a numerical method which is fast and precise for computing the Steklov spectrum in cases where the boundary behaves nice enough. This method can be applied to a more general class of problems. The Steklov eigenvalue problem can be seen as a particular case of the following type of problems called Wentzell eigenvalue problems.

$$\begin{cases} -\Delta u = 0 & \text{dans } \Omega, \\ -\beta \Delta_\tau u + \partial u_n = \sigma u & \text{sur } \partial\Omega. \end{cases}$$

It is easy to see that the Steklov case corresponds to $\beta = 0$. We consider the case of star-shaped domains, which have the advantage that their boundary can be parametrized by a radial function. In the end of this chapter we present a different approach which can treat general simply connected domains.

The method of fundamental solutions, introduced in [69], is a part of the class of so called mesh-free numerical methods. The goal is to approximate the solution of a problem of the type

$$\begin{cases} Au = 0 \text{ in } \Omega \\ Bu = 0 \text{ on } \partial\Omega \end{cases}, \tag{4.5.1}$$

where A, B are suitable linear differential operators. In contrast to methods using meshes, the method of fundamental solutions considers a sufficiently rich class of functions which satisfy $Au = 0$ analytically in Ω. Thus a linear combination satisfies directly $Au = 0$ in Ω, and the coefficients in the linear combination are be chosen such that $Bu = 0$ is close to zero on $\partial\Omega$. As we will see in the following, the condition $Bu = 0$ can only be imposed in a finite number of points, so the condition $Bu = 0$ will be satisfied only in an approximate manner on $\partial\Omega$. To justify our numerical approach, an error bound is provided in Section 4.6, which basically says that if Bu is small enough, then u is close to the real solution. This type of method was successfully used in [4] in the study of the eigenvalues of the Dirichlet Laplacian in two and three dimensions.

In our case, the operator A is the Dirichlet Laplacian and the operator B is given by $-\beta \Delta_\tau + \dfrac{\partial}{\partial n} - \sigma u$, where Δ_τ is the Laplace-Beltrami operator associated to $\partial\Omega$. Our set of fundamental solutions will consist of harmonic, radial functions, with centers outside Ω. In this way, any linear combination of such functions will still solve $\Delta u = 0$. The only thing we need to do is to find the right coefficients so that the condition $-\beta\Delta_\tau u + \dfrac{\partial u}{\partial n} = \sigma u$ is satisfied on $\partial\Omega$. In order to compute the Laplace-Beltrami on $\partial\Omega$ we use the expression

$$\Delta u = \Delta_\tau u + \mathcal{H}\frac{\partial u}{\partial n} + \frac{\partial^2 u}{\partial n^2},$$

which is valid on $\partial\Omega$. We have used the notation $\dfrac{\partial^2 u}{\partial n^2}$ to denote $(D^2 u.n).n$. As usual, $\mathcal{H}$ denotes the curvature of $\partial\Omega$. For more details we refer to [66, Chapter 5].

In $\mathbb{R}^2 \setminus \{0\}$ a radial solution of the Laplace equation is given by $\phi(x) = \ln|x|$. Note that this solution has a singularity at $x = 0$. For every $y \in \mathbb{R}^2$ the function $\psi_y(x) = \phi(x - y)$ is harmonic in $\mathbb{R}^2 \setminus \{y\}$ and radial with center y. Given $\Omega \subset \mathbb{R}^2$ we choose $y_1, ..., y_N \in \mathbb{R}^2 \setminus \Omega$ and $x_1, ..., x_N \in \partial\Omega$. The function $x \mapsto \alpha_1 \psi_{y_1}(x) + ... + \alpha_N \psi_{y_N}(x)$ is harmonic in Ω for every choice of the coefficients $(\alpha_i)_{i=1}^N$. We impose the boundary relation

$$\left(-\beta\Delta_\tau + \frac{\partial}{\partial n}\right)(\alpha_1\psi_{y_1}(x_i) + ... + \alpha_N\psi_{y_N}(x_i)) = \lambda(\alpha_1\psi_{y_1}(x_i) + ... + \alpha_N\psi_{y_N}(x_i)),\ i = 1...N$$

(4.5.2)

This amounts to solving a generalized eigenvalue problem for square matrices.

In this statement, it is straightforward to find the first eigenvalues corresponding to the generalized eigenvalue problem determined (4.5.2), using, for example the `eigs` solver in Matlab. One of the main difficulties is the choice of the points $(x_i)_{i=1}^N, (y_i)_{i=1}^N$. As noted in [4], an arbitrary choice for $(x_i), (y_i)$ may give fail to give us a valid approximate solution for the desired eigenvalue problem. We have noticed the same behavior, and for this, we discuss below the choice of the points $(x_i), (y_i)$.

We use two choices for the points (x_i). The first one consists in taking a uniform division (θ_i) of $[0, 2\pi]$ into N intervals and then choose $x_i = \rho(\theta_i)(\cos\theta_i, \sin\theta_i)$, where ρ is the radial function which parametrizes $\partial\Omega$. A second choice is choosing x_i at equal arclength distances on the boundary $\partial\Omega$. Having chosen (x_i), we can compute the corresponding outer normals $(\vec{n}_i)$ and we define $y_i = x_i + 0.1 \cdot \vec{n}_i$ (for figures with diameter roughly equal to 2). It seems that the choice of the factor 0.1 is essential in our setting. Even slight perturbations of this factor give results which are far from the actual Steklov eigenvalues of Ω. This is due to the fact that for larger or smaller values of this parameter, the matrices involved in the computation are ill conditioned.

4.6 Error estimates

In the case of the Dirichlet Laplacian, the result proved by Moler and Payne in [73], states that if a function u satisfies $-\Delta u = \lambda u$ in Ω and u is sufficiently small on $\partial\Omega$ then λ is close to an

Test figure.   Positions of $(x_i), (y_i)$
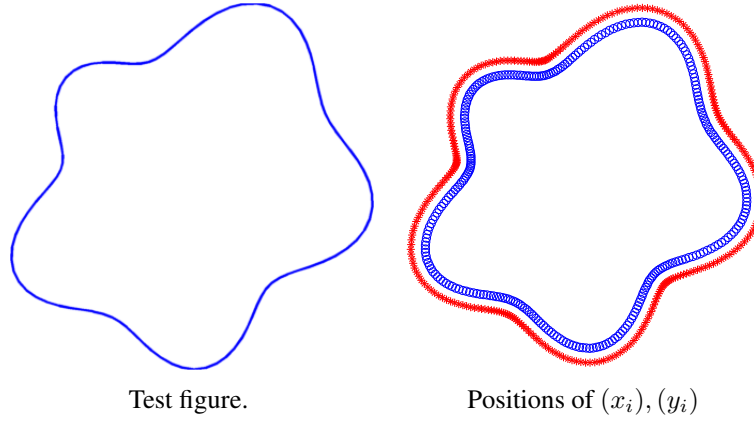
Figure 4.2: Figure given by Fourier coefficients: $[1, 0.1, 0, 0, 0, 0.1, 0, 0.1, 0, 0, -0.1]$

eigenvalue of the Dirichlet-Laplace operator associated to Ω. In order to validate our numerical computations, we provide a similar result below, in the case of the Steklov eigenvalue problem. In the following paragraphs we assume that Ω has Lipschitz boundary and that it has finite perimeter. In the following we denote $V(\Omega) = \{u \in L^2(\partial\Omega) : \int_{\partial\Omega} u = 0\}$.

As in [42] we introduce the Hilbert space $H(\Omega) = \{u \in H^1(\Omega) : \mathrm{Tr}(u) \in H^1(\partial\Omega), \int_{\partial\Omega} u = 0\}$ where Tr is the trace operator. In the case $\beta = 0$ it suffices to take $H(\Omega) = \{u \in H^1(\Omega) : \int_{\partial\Omega} u = 0\}$. Consider for $f \in V(\Omega)$ the minimization problem

$$\min_{u \in H(\Omega)} \frac{1}{2}\left(\int_\Omega |\nabla u|^2 + \beta \int_{\partial\Omega} |\nabla_\tau u|^2\right) - \int_{\partial\Omega} uf$$

which has a unique solution. This solution satisfies the weak formulation

$$\int_\Omega \nabla u \cdot \nabla \varphi + \beta \int_{\partial\Omega} \nabla_\tau u \nabla_\tau \varphi = \int_{\partial\Omega} f\varphi, \ \forall \varphi \in C^1(\Omega), \tag{4.6.1}$$

of the partial differential equation

$$\begin{cases} -\Delta u = 0 & \text{in } \Omega \\ -\beta \Delta_\tau u + \frac{\partial u}{\partial n} = f & \text{on } \partial\Omega. \end{cases}, \tag{4.6.2}$$

where Δ_τ is the Laplace-Beltrami operator and ∇_τ is the tangential gradient associated to $\partial\Omega$. Thus, we can define the resolvent operator $R_\beta : V(\Omega) \to H(\Omega)$ associated to this problem. The trace operator $T : H(\Omega) \to V(\Omega)$ being continuous it follows that the operator $T \circ R_\beta : V(\Omega) \to V(\Omega)$ is compact and injective. We can define its inverse $A_\beta : D(A_\beta) \subset V(\Omega) \to V(\Omega)$. Since $T \circ R_\beta$ is a compact operator, the spectrum of the operator A_β consists of an increasing sequence of eigenvalues $\lambda_{k,\beta}(\Omega)$ which diverges. The corresponding eigenfunctions form a Hilbert basis for $V(\Omega)$. By considering the constant function 1 associated to the zero eigenvalue of this operator, we can say that the set of corresponding eigenfunctions forms a Hilbert basis of $L^2(\partial\Omega)$. The following result proves that the operator $T \circ R_\beta$ is bounded and gives an idea of how to find its norm. By abuse of notation we denote the trace of a function $w \in H^1(\Omega)$ by w.

Proposition 4.6.1. *Let Ω be a bounded, open domain with Lipschitz boundary. Suppose $f \in V(\Omega)$ and $w = R_\beta f \in H^1(\Omega)$. Then there exists a constant C, depending only on Ω, such that*

$$\|w\|_{L^2(\partial\Omega)} \leq C\|f\|_{L^2(\partial\Omega)}.$$

Proof: The trace inequality (Chapter 4.3 [51]) for Ω implies the existence of a constant C_1 (depending only on Ω) such that $\|u\|_{L^2(\partial\Omega)} \leq C_1\|u\|_{H^1(\Omega)}$ for every $u \in H^1(\Omega)$. The Poincare-Wirtinger inequality implies the existence of a constant C_2 which depends only on Ω such that $\|\tilde{w}\|_{L^2(\Omega)} \leq C_2\|\nabla w\|_{L^2(\Omega)}$, where $\tilde{w} = w - \frac{1}{|\Omega|}\|w\|_{L^2(\Omega)}$. The weak formulation of the equation $A_\beta w = f$ and the Cauchy-Schwarz inequality imply that

$$\int_\Omega |\nabla\tilde{w}|^2 + \beta \int_{\partial\Omega} |\nabla_\tau\tilde{w}|^2 = \int_{\partial\Omega} f\tilde{w} \leq \|f\|_{L^2(\partial\Omega)}\|\tilde{w}\|_{L^2(\partial\Omega)}.$$

Using the remarks above, we obtain

$$\|\tilde{w}\|_{L^2(\partial\Omega)}^2 \leq C_1^2(\|\tilde{w}\|_{L^2(\Omega)}^2 + \|\nabla\tilde{w}\|_{L^2(\Omega)}^2) \leq C_1^2(1 + C_2^2)\|\nabla\tilde{w}\|_{L^2(\Omega)}^2.$$

Thus

$$\|\tilde{w}\|_{L^2(\partial\Omega)}^2 \leq C_1^2(1 + C_2^2)\|f\|_{L^2(\partial\Omega)}\|\tilde{w}\|_{L^2(\partial\Omega)},$$

which implies

$$\|\tilde{w}\|_{L^2(\partial\Omega)} \leq C_1^2(1 + C_2^2)\|f\|_{L^2(\partial\Omega)}.$$

On the other hand, since w has average 0 on $\partial\Omega$, we know that the $L^2(\partial\Omega)$ norm of $w + c$ is minimal when $c = 0$ (here c is a constant). Therefore

$$\|w\|_{L^2(\partial\Omega)} \leq \|\tilde{w}\|_{L^2(\partial\Omega)} \leq C_1^2(1 + C_2^2)\|f\|_{L^2(\partial\Omega)}.$$

$\square$

Using ideas similar to the ones used by Moler and Payne in [73], we are able to prove the following error estimate. For simplicity of notation we omit the reference to β from R_β.

Theorem 4.6.2. *Consider Ω a bounded, open, regular domain, and suppose that u_ε satisfies the following approximate eigenvalue problem:*

$$\begin{cases} -\Delta u_\varepsilon = 0 & \text{in } \Omega \\ -\beta\Delta_\tau u_\varepsilon + \dfrac{\partial u_\varepsilon}{\partial n} = \lambda_\varepsilon u_\varepsilon + f_\varepsilon & \text{on } \partial\Omega. \end{cases} \tag{4.6.3}$$

Denote $w_\varepsilon = Rf_\varepsilon$. Let $\delta = \dfrac{\|w_\varepsilon\|_{L^2(\partial\Omega)}}{\|u_\varepsilon\|_{L^2(\partial\Omega)}}$ and suppose that $\delta < 1$. Then there exists an Wentzell eigenvalue λ_k satisfying

$$\frac{\lambda_\varepsilon}{1+\delta} \leq \lambda_k \leq \frac{\lambda_\varepsilon}{1-\delta}.$$

Proof: We know that there exists a Hilbert basis of $L^2(\partial\Omega)$ formed of Wentzell eigenfunctions (u_n) corresponding to the Wentzell eigenvalues λ_n of Ω. We denote the standard scalar product in $L^2(\partial\Omega)$ by $(u,v) = \int_{\partial\Omega} uv$. Let $a_n = (u_\varepsilon, u_n)$, $b_n = (w_\varepsilon, u_n)$. The resolvent operator R is symmetric and therefore $(u_\varepsilon, Ru_n) = (Ru_\varepsilon, u_n)$. This implies that $R(\lambda_\varepsilon u_\varepsilon + f_\varepsilon) = u_\varepsilon$ and $Ru_n = \dfrac{1}{\lambda_n}u_n$. Thus

$$
\begin{aligned}
a_n = (u_\varepsilon, u_n) &= (R(\lambda_\varepsilon u_\varepsilon + f_\varepsilon), u_n) \\
&= (\lambda_\varepsilon u_\varepsilon + f_\varepsilon, Ru_n) \\
&= \frac{1}{\lambda_n}(\lambda_\varepsilon u_\varepsilon + f_\varepsilon, u_n) \\
&= \frac{1}{\lambda_n}(\lambda_\varepsilon a_n + \lambda_n b_n).
\end{aligned}
$$

Thus, for every n we have $\dfrac{\lambda_n - \lambda_\varepsilon}{\lambda_n} = \dfrac{b_n}{a_n}$. Since (λ_n) is increasing and divergent, there exists an index k such that

$$
\frac{|\lambda_k - \lambda_\varepsilon|}{|\lambda_k|} = \min_n \frac{|\lambda_n - \lambda_\varepsilon|}{|\lambda_n|}.
$$

For this index k we have

$$
\frac{|\lambda_k - \lambda_\varepsilon|}{|\lambda_k|}|a_n| \le |b_n|,
$$

for all n and

$$
\frac{|\lambda_k - \lambda_\varepsilon|^2}{|\lambda_k|^2}\sum_{n=1}^{\infty} a_n^2 \le \sum_{n=1}^{\infty} b_n^2.
$$

This is exactly

$$
\frac{|\lambda_k - \lambda_\varepsilon|}{|\lambda_k|} \le \delta,
$$

which finishes the proof. $\qquad\square$

The only hypothesis in the above theorem which needs to be verified in order to apply it in our case is that we can solve the partial differential equation $A_\beta w_\varepsilon = f_\varepsilon$ in the case where f_ε is a combination of our fundamental solutions. It is a standard application of Lax-Milgram's theorem ([22] Chapter 5) to see that the necessary and sufficient condition is that $\int_{\partial\Omega} f = 0$. Note that this condition can always be satisfied by adding a constant function to the family of fundamental solutions.

4.7   Testing the numerical method

Let's note that the first Wentzell eigenvalue of Ω is $\lambda_{0,\beta}(\Omega) = 0$, corresponding to a constant eigenfunction. We will denote $\lambda_{k,\beta}(\Omega)$ the k-th Wentzell eigenvalue after $\lambda_{0,\beta}(\Omega)$. There are few shapes for which the Wentzell spectrum (or the Steklov spectrum in the case $\beta = 0$) is known analytically. One such shape is the unit disk D_1, which has the eigenvalues

$$
\lambda_{k,\beta}(D_1) = \left\lfloor \frac{k+1}{2} \right\rfloor + \beta \left\lfloor \frac{k+1}{2} \right\rfloor^2.
$$
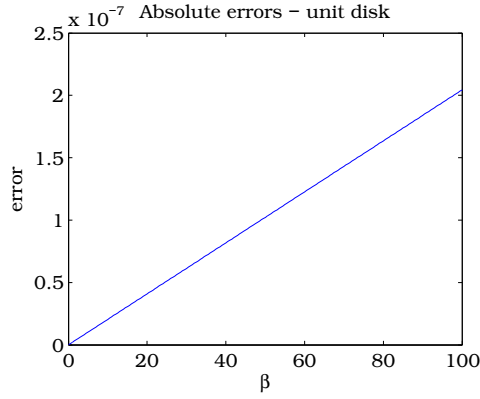
Figure 4.3: Absolute errors for $\beta \in [0, 100]$ - the case of the disk

As an initial test for our algorithm, we computed the Wentzell spectrum of the disk. With $N = 300$ points on ∂D_1 and 300 corresponding fundamental solutions. For $\beta = 0$ we have 10 digits of precision for the first 10 lowest eigenvalues. In Figure 4.3 we plot the absolute error for the first 10 Wentzell eigenvalues $\beta \in [0, 100]$. We note that for $\beta = 100$ we still have 6 digits of precision.

In order to test our algorithm for shapes for which no analytical expression is known for the Wentzell eigenvalues, we used FreeFem++ [61], which uses meshing in order to solve the problem. The tests we performed show that as the number of triangles increase, the values found with FreeFem++ approach the values found with our algorithm. The downside of the mesh-based method is the execution time, which is significantly more important. An example of implementation is presented in Section 4.11. In Tables 4.1, 4.2, 4.3 we compare the Wentzell eigenvalues computed with our method (MFS) and the ones obtained with FreeFem++. As a test case we take the shape found in Figure 4.2, for various values of β. Note that as the number of triangles increases, the values computed with the FreeFem++ method approach the values found with our algorithm. We underline the fact that our algorithm runs in approximately 0.1 seconds[1], whereas the FreeFem++ algorithm, with over 450000 triangles takes about a minute on the same machine.

Another way of testing our algorithm is to do numerical optimization procedures for shape optimization problems with known optimizers. There are many such results for the case $k = 0$ (the Steklov eigenvalue problem). We start from a random shape and look if the algorithm converges to the expected shape. We mention that all computations are made in the class of simply connected sets. We were able to test our algorithm in the following cases:

- $\max \sigma_1(\Omega)$ is achieved when Ω is a disk, in the case of perimeter and area constraints ([93],[24]);

- $\max \sigma_1(\Omega)\sigma_2(\Omega)$ is achieved when Ω is a disk, in the case of perimeter and area constraints ([67]);

[1]Machine configuration: 2.2 Ghz quad-core i7 processor, 6 Gb RAM memory

146

	our algorithm	FreeFem++ (refined meshes)			
k	MFS	19146 ▲	53236 ▲	211290▲	474634▲
1	0.712751	0.712989	0.712837	0.712773	0.712761
2	0.940247	0.940538	0.940352	0.940274	0.940259
3	1.381278	1.38211	1.38158	1.38135	1.38131
4	1.443204	1.44411	1.44353	1.44329	1.44324
5	3.146037	3.14712	3.14643	3.14614	3.14608
6	3.443637	3.44496	3.44411	3.44376	3.44369
7	3.757833	3.761	3.75897	3.75812	3.75796
8	3.922821	3.9263	3.92407	3.92313	3.92296
9	4.274362	4.28034	4.27651	4.2749	4.2746
10	4.693206	4.70035	4.69578	4.69385	4.6935

Table 4.1: Comparison with FreeFem++, $\beta = 0$ (Steklov) for the shape given in Figure 4.2

	our algorithm	FreeFem++ (refined meshes)			
k	MFS	19146 ▲	53236 ▲	211290▲	474634▲
1	2.375744	2.37628	2.37594	2.37579	2.37577
2	2.644741	2.6453	2.64494	2.64479	2.64476
3	8.042223	8.04527	8.04332	8.0425	8.04234
4	8.257585	8.26043	8.25861	8.25784	8.2577
5	16.909967	16.9197	16.9135	16.9108	16.9104
6	17.383930	17.3932	17.3873	17.3848	17.3843
7	28.883924	28.9094	28.8931	28.8862	28.8849
8	29.113307	29.1374	29.122	29.1155	29.1143
9	43.718607	43.77	43.7371	43.7232	43.7207
10	44.142742	44.1996	44.1632	44.1479	44.145

Table 4.2: Comparison with FreeFem++, $\beta = 2$ for the shape given in Figure 4.2

	our algorithm	FreeFem++ (refined meshes)			
k	MFS	19146 ▲	53236 ▲	211290▲	474634▲
1	4.750048	4.75121	4.75047	4.75015	4.75009
2	5.02106	5.02224	5.02148	5.02117	5.02111
3	17.557103	17.5638	17.5595	17.5577	17.5574
4	17.774667	17.781	17.777	17.7752	17.7749
5	38.179237	38.2016	38.1873	38.1812	38.1801
6	38.65575	38.6771	38.6634	38.6577	38.6566
7	66.764114	66.8228	66.7852	66.7694	66.7665
8	66.995238	67.0507	67.0152	67.0002	66.9975
9	102.91875	103.038	102.962	102.929	102.924
10	103.34252	103.474	103.39	103.354	103.348

Table 4.3: Comparison with FreeFem++, $\beta = 5$ for the shape given in Figure 4.2

- $\min \sum_{k=1}^{n} \dfrac{1}{\sigma_k(\Omega)}$ is achieved when Ω is a disk, in the case of perimeter and area constraints [67]);

- $\max \sigma_k(\Omega)$ under a rotational symmetry of order q is achieved by a disk in the case of the perimeter constraint ([13]).

We may ask whether this method of fundamental solutions can be adapted to compute the Laplace-Beltrami spectrum of a two dimensional closed simple curve. We can consider solving the equation

$$\Delta_\tau(\alpha_1 \psi_{y_1}(x_i) + ... + \alpha_N \psi_{y_N}(x_i)) = \lambda(\alpha_1 \psi_{y_1}(x_i) + ... + \alpha_N \psi_{y_N}(x_i)), \ i = 1...N \quad (4.7.1)$$

which also leads to a generalized eigenvalue problem. The Laplace-Beltrami spectrum of a one dimensional curve depends only on its length and is given by $\lambda_k = \left\lfloor \dfrac{k+1}{2} \right\rfloor^2 \left(\dfrac{2\pi}{L}\right)^2$. The method of fundamental solutions computes these values with a relative error of order 10^{-7} (with the same parameters: 300 boundary points and exterior points at distance 0.1 of the boundary).

We may use Theorem 4.6.2 in order to have a more precise evaluation of the error on a general domain. The result cited above states that the relative error made in the numerical computations are of the order of $\|f_\varepsilon\|_{L^2(\partial\Omega)}$, where f_ε is the error term in (4.6.3). We may estimate numerically f_ε as follows: given a shape Ω, we compute its Steklov/Wentzell eigenvalues with the algorithm presented in previous sections. We know that the eigenvalue equation is satisfied to machine precision on the discretization points chosen on $\partial\Omega$. In order have a more precise evaluation of what happens between these points, we make a refinement containing 100 times more points on $\partial\Omega$, which gives 100 supplementary points between every two discretization points. We evaluate the error made in the eigenvalue equation (that is f_ε) in each of these points. The maximal point wise error will give us information on the general error. Below you can see plots of f_ε for the first 10 eigenvalues in three different cases. By looking at the maximal errors, we can observe that $\|f_\varepsilon\|_{L^2(\partial(\Omega))}$ is of order 10^{-6} or smaller. As expected, different domains give different behaviours, and the precision can be much higher.

4.8 Numerical optimization of functionals depending on the Wentzel spectrum

Using the algorithm presented in the previous sections, we can study numerically shape optimization problems regarding the Wentzell spectrum, in the particular setting where the domains are star-shaped.

We consider our domain parametrized by its radial function $\rho : [0, 2\pi) \to \mathbb{R}_+$. We approximate ρ by the truncation of its Fourier series to $2n+1$ coefficients:

$$\rho(\theta) \approx a_0 + \sum_{i=1}^{n} a_i \cos(i\theta) + \sum_{i=1}^{n} b_i \sin(i\theta).$$
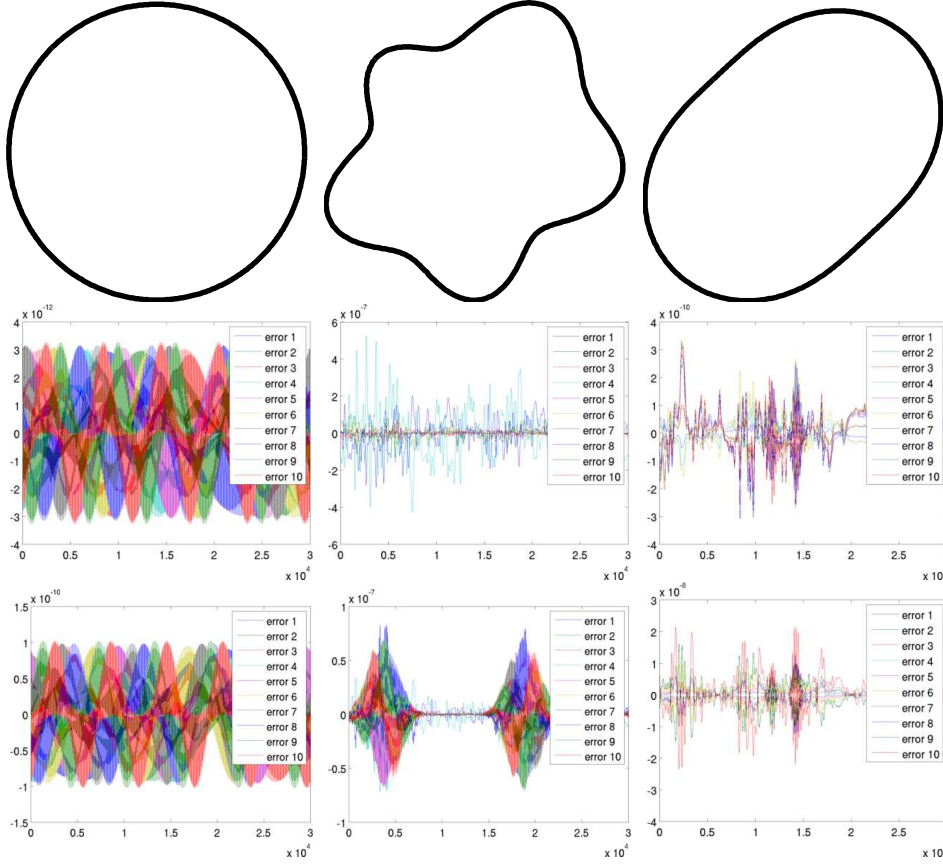
Figure 4.4: Graph of the error term in the computation of the Steklov and Wentzell eigenvalues (various values of β).

In this way, we express an approximation of $\sigma_k(\Omega)$ using a finite number of parameters. Using the shape derivative formula provided in [42, Section E] we can deduce that

$$\frac{\partial \sigma_k}{\partial a_i} = \int_0^{2\pi} \left(|\nabla_\tau u_k|^2 - |\partial_n u_k|^2 - \lambda \mathcal{H} |u_k|^2 + \beta (\mathcal{H} I - 2D^2 b) \nabla_\tau u_k . \nabla_\tau u_k \right) \rho(\theta) \cos(i\theta) d\theta$$

and

$$\frac{\partial \sigma_k}{\partial b_i} = \int_0^{2\pi} \left(|\nabla_\tau u_k|^2 - |\partial_n u_k|^2 - \lambda \mathcal{H} |u_k|^2 + \beta (\mathcal{H} I - 2D^2 b) \nabla_\tau u_k . \nabla_\tau u_k \right) \rho(\theta) \sin(i\theta) d\theta$$

We use the notation $\mathcal{H}$ for the mean curvature of $\partial\Omega$. We denote by $D^2 b$ the hessian of the signed distance function, or equivalently, the differential of the normal vector. We have denoted u_k the eigenfunction corresponding to $\sigma_k(\Omega)$ normalized in $L^2(\partial\Omega)$.

Since we can approximate $\sigma_k(\Omega)$ by a function $\sigma_k(a_0, a_1, ..., a_n, b_1, ..., b_n)$ for which we know the gradient with respect to every component, we can use a gradient descent approach for solving different optimization problems related to the Steklov eigenvalues. This approach was used in [78] and [9] for optimizing functionals of the eigenvalues of the Dirichlet Laplacian.

In the recent article of Dambrine, Lamboley and Kateb [42], the authors prove that the ball is a local minimizer for the first non-zero Wentzel eigenvalue if $\beta \geq 0$, under volume constraint. Using the fact that $\lambda_{1,\beta}(B_R)$ is decreasing with respect to R (we denote B_R the ball of radius

R), we can deduce that if the ball is a maximizer for the perimeter constraint, then it is also a maximizer for the volume constraint. It is a well known fact, due to Weinstock [93] and Brock [24], that when $\beta = 0$, the ball is the optimizer for both volume and perimeter constraints. Using our algorithm, we searched for the shape which optimizes $\lambda_{1,\beta}(\Omega)$ in two dimensions. For both perimeter and volume constraints, we obtained that the disk is the numerical maximizer of $\lambda_{1,\beta}$ among two dimensional simply connected shapes. We performed tests for $\beta \in [0, 100]$, but we believe it to be true for every $\beta > 0$ since for large values of β, $\lambda_{1,\beta}(\Omega)/\beta$ converges to the first Laplace-Beltrami eigenvalue of $\partial\Omega$. We also performed tests in the case of the area constraint for $k = 2, 3, 4, 5$ and we present the results in Table 4.4.

We present some interesting conjectures, verified numerically using our algorithm. Many of them are related to results known to be true in the Steklov case ($\beta = 0$), namely, the Hersch-Payhe-Schiffer results [67]. All these results are for domains which are simply connected with a radial parametrization.

- $\max \lambda_{1,\beta}(\Omega)$ is acheived by the disk;

- $\min \sum_{k=1}^{n} \dfrac{1}{\lambda_{k,\beta}(\Omega)}$ is achieved by the disk;

- We say that $A \subset \{0, 1, 2, 3, ...\}$ has the property (P) if $1 \in A$ and $2k \in A \Rightarrow 2k - 1 \in A$. If A has the property (P) then $\sum_{k \in A} \dfrac{1}{\lambda_{k,\beta}(\Omega)}$ is minimized by the disk in the case of a volume and perimeter constraint. For example $\dfrac{1}{\lambda_{1,\beta}(\Omega)} + \dfrac{1}{\lambda_{3,\beta(\Omega)}} + \dfrac{1}{\lambda_{4,\beta}(\Omega)}$ is minimized by the disk in the case of the volume constraint and the perimeter constraint. This was verified for various sets A with property (P) with $A \subset \{0, 1, ..., 15\}$.

As underlined before, in the Steklov case with perimeter constraint, the simple connectedness is essential. Making a small hole in the center of the disk and rescaling in order to have the same perimeter increases the first eigenvalue. This behaviour can be seen in Figure 4.5 in some computations made with FreeFem++.

As proved by Brock [24], if we impose an area constraint then the simple connectedness condition is not necessary. The disk maximizes the first Steklov eigenvalue. We may ask if this is the case for Wentzell eigenvalues. The answer is negative, as can be seen in Figure 4.6 for $\beta = 0.1$. Making a small hole and rescaling to have the same area increases the first Wentzell eigenvalue of a disk.

In the case of the volume constraint, for Lipschitz domains, it is possible to prove that suppressing holes increases the normalized Steklov eigenvalue. It is enough to observe that filling *holes* modifies all the quantities in the variational characterization in the right way.

	λ_1	λ_2	λ_3	λ_4	λ_5
$\beta = 0$ Steklov	$\lambda_1 = 1$	$\lambda_2 = 1.64$	$\lambda_3 = 2.33$	$\lambda_4 = 2.97$	$\lambda_5 = 3.66$
$\beta = 0.1$	$\lambda_1 = 1.1$	$\lambda_2 = 1.80$	$\lambda_3 = 2.65$	$\lambda_4 = 3.42$	$\lambda_5 = 4.3$
$\beta = 0.5$	$\lambda_1 = 1.5$	$\lambda_2 = 2.39$	$\lambda_3 = 4$	$\lambda_4 = 4.53$	$\lambda_5 = 7.5$
$\beta = 100$ (large)	$\lambda_1 = 101$	$\lambda_2 = 101$	$\lambda_3 = 402$	$\lambda_4 = 402$	$\lambda_5 = 903$
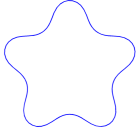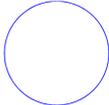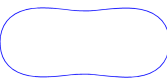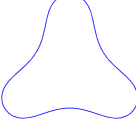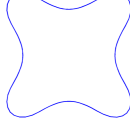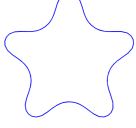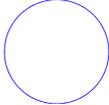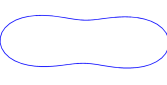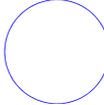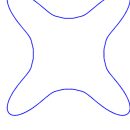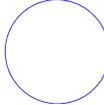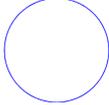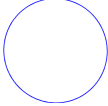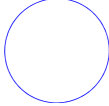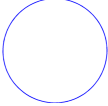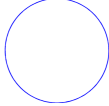
Table 4.4: Numerical maximizers for the first five Wentzell eigenvalues for different values of β. The areas of the domains are equal to π

1.02885   1.03776
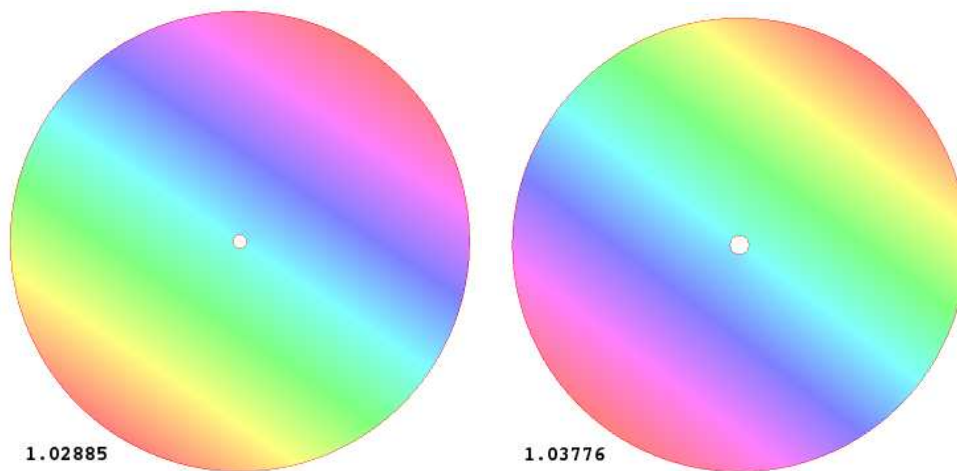
Figure 4.5: Behaviour of the Steklov eigenvalue when making holes. The images represent a unit disk with holes of radii 0.03 and 0.04, rescaled to have total perimeter 2π. Note that the corresponding first eigenvalues are higher than 1 which is the first eigenvalue of a disk of perimeter 2π.
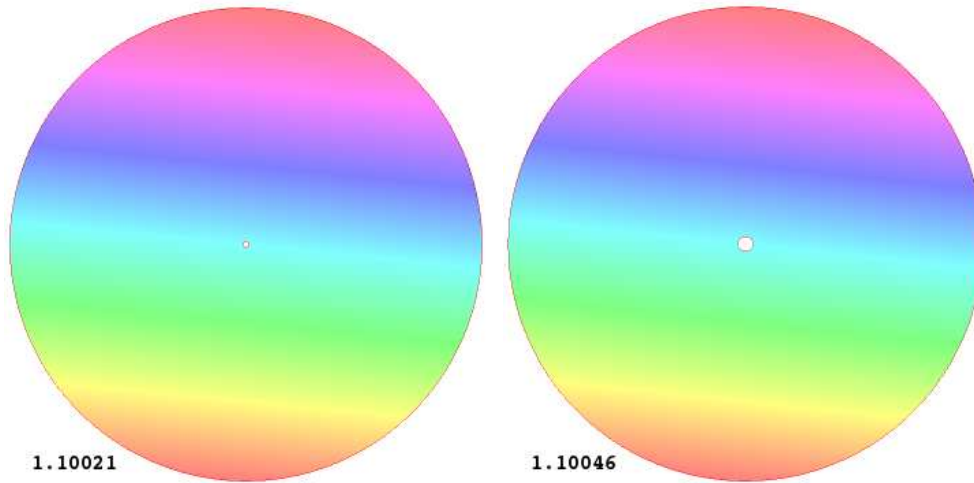
Figure 4.6: Behaviour of the Wentzell eigenvalue when making holes. The images represent two disks with holes in their centers rescaled to area π. The first eigenvalues are higher that 1.1 which is the Wentzell eigenvalue of a disk for $\beta = 0.1$.

- $\partial\Omega$ is Lipschitz, and thus every function in $H^1(\Omega \setminus B)$ can be extended to $H^1(\Omega)$. Thus, the admissible set of test functions is the same for $\Omega \setminus B$ and Ω.

- The numerator increases passing from $\Omega \setminus B$ to Ω.

- The denominator decreases passing from $\Omega \setminus B$ to Ω.

- The volume increases by filling holes.

Thus, it is not restrictive to assume that the optimal domain for the Steklov eigenvalues, in the case of the volume constraint, does not have any holes.

To illustrate the flexibility of our numerical framework, we present in Table 4.5 the results for various shape optimization problems depending on the Steklov spectrum in the case of the area constraint. Some of the functionals studied numerically, like for example the sum of the first Steklov eigenvalues, are of interest in the literature (see for example [54])

4.9 Treatment of general parametric simply connected domains

As mentioned before, restricting the class of study to star-shaped domains is not satisfactory. Indeed, proving that the optimal set for a shape optimization problem belongs to this class is hard or impossible, unless other stronger properties, like convexity, are present (see Chapter 1 for the optimization of λ_k with the perimeter constraint). The purpose of this section is to propose a new method for the study of general parametric simply connected domains.

$$\max \sigma_1 + \sigma_2 = 3.75 \qquad \max \sigma_1 + \sigma_2 + \sigma_3 = 4\sqrt{\pi} \qquad \max \sigma_1 + ... + \sigma_4 = 6\sqrt{\pi}$$

$$\max \sigma_1 + ... + \sigma_5 = 9\sqrt{\pi} \qquad \max \sigma_1 + \sigma_4 = 6.49 \qquad \max \sigma_1 + \sigma_6 = 8.93$$

$$\max \sigma_4 + \sigma_6 = 10.8 \qquad \max \sigma_5 + \sigma_6 = 12.99 \qquad \max \sigma_4 + \sigma_7 = 11.86$$

$$\min \frac{1}{\sigma_1} + \frac{1}{\sigma_4} = 0.82 \qquad \min \frac{1}{\sigma_3} + \frac{1}{\sigma_5} = 0.46 \qquad \min \frac{1}{\sigma_5} + \frac{1}{\sigma_{11}} = 0.26$$

$$\min \frac{1}{\sigma_4} + \frac{1}{\sigma_6} + \frac{1}{\sigma_{10}} = 0.49 \qquad \max \sigma_2 \cdot \sigma_3 = 8.69 \qquad \max \sigma_3 \cdot \sigma_4 = 17.18$$
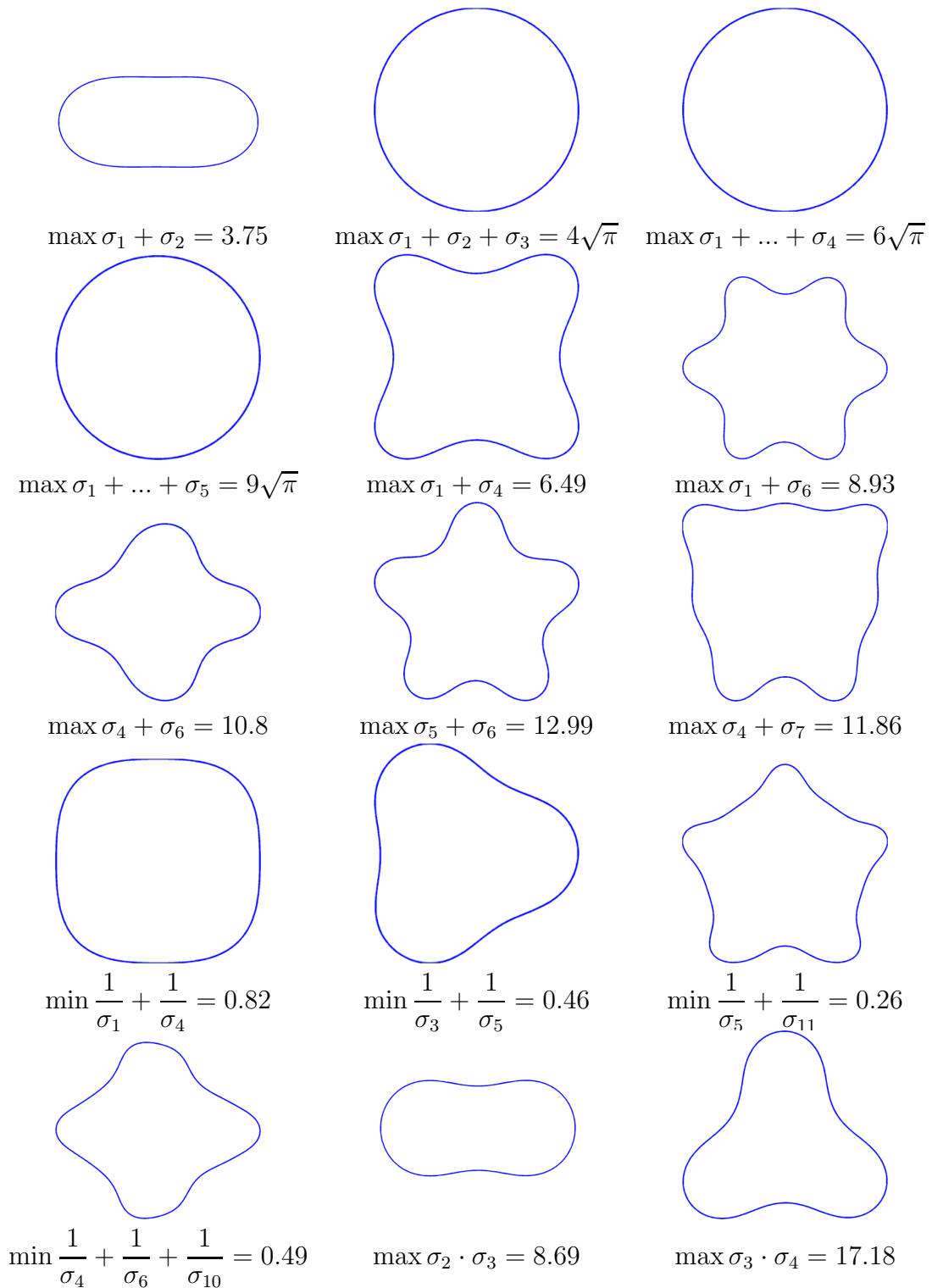
Table 4.5: Various numerical optimizations of functionals depending on the Steklov spectrum

The idea is to consider a general parametrization $\gamma : t \mapsto (\mathbf{x}(t), \mathbf{y}(t))$ for $t \in [0, 2 * pi]$. The coordinate functions $\mathbf{x}, \mathbf{y}$ are supposed to be periodic of period 2π. Thus, these functions have the following Fourier series expansions

$$\mathbf{x}(t) = a_0 + \sum_{j=1}^{\infty} a_j \cos(j\theta) + \sum_{j=1}^{\infty} b_j \sin(j\theta)$$

$$\mathbf{y}(t) = c_0 + \sum_{j=1}^{\infty} c_j \cos(j\theta) + \sum_{j=1}^{\infty} d_j \sin(j\theta).$$

Supposing that the shape Ω bounded by the curve γ is regular enough, the coefficients (a_j), (b_j), (c_j), (d_j) deccay very rapidly to 0. Thus, we expect that truncating these Fourier series to their first coefficients up to a certain treshold, we don't lose much information on the shape Ω.

As in the radial case, the general shape derivative formula provided in [42, Section E] allows us to find the derivatives of the Steklov eigenvalues with respect to the coefficients $(a_j), (b_j), (c_j), (d_j)$:

$$\frac{d\sigma_k}{da_j} = \int_0^{2\pi} (|\nabla_\tau u_k|^2 - (\partial_n u_k)^2 - \sigma_k \mathcal{H} u_k^2) \mathbf{y}'(\theta) \cos(j\theta) d\theta$$

$$\frac{d\sigma_k}{db_j} = \int_0^{2\pi} (|\nabla_\tau u_k|^2 - (\partial_n u_k)^2 - \sigma_k \mathcal{H} u_k^2) \mathbf{y}'(\theta) \sin(j\theta) d\theta$$

$$\frac{d\sigma_k}{dc_j} = -\int_0^{2\pi} (|\nabla_\tau u_k|^2 - (\partial_n u_k)^2 - \sigma_k \mathcal{H} u_k^2) \mathbf{x}'(\theta) \cos(j\theta) d\theta$$

$$\frac{d\sigma_k}{dd_j} = -\int_0^{2\pi} (|\nabla_\tau u_k|^2 - (\partial_n u_k)^2 - \sigma_k \mathcal{H} u_k^2) \mathbf{x}'(\theta) \sin(j\theta) d\theta,$$

where u_k is $L^2(\partial\Omega)$ unit normalized eigenfunction associated to σ_k. All quantities containing the eigenfunction u_k in the above integrals are always evaluated in $(\mathbf{x}(\theta), \mathbf{y}(\theta))$.

Having all these formulas we can perform numerical optimizations just as in previous sections. We underline the fact that the actual computation of the Steklov eigenvalue is the same as before, using fundamental solutions. In the course of optimization we must pay more attention to the size of the descent step, since large steps may produce artificial self intersections. Thus, a basic gradient descent algorithm with small descent step is used in the optimisation process.

In Figure 4.7 we present the numerical candidates for the maximizers of $\sigma_k(\Omega)$ under area constraint for $k \in [2, 10]$. All the computations performed using the general parametrization give the same shapes as in the radial parametric case. This gives us confidence in the fact that the optimizers do indeed belong to the class of star-shaped domains. We notice some interesting properties of these maximizers:

- The numerical shape which maximizes σ_k seems to have a dihedral symmetry of order k.

- As in other eigenvalue optimization problems, we are interested in the multiplicity of the optimal eigenvalues. It turns out that for all $k \in [2, 10]$ the shape which maximizes σ_k is
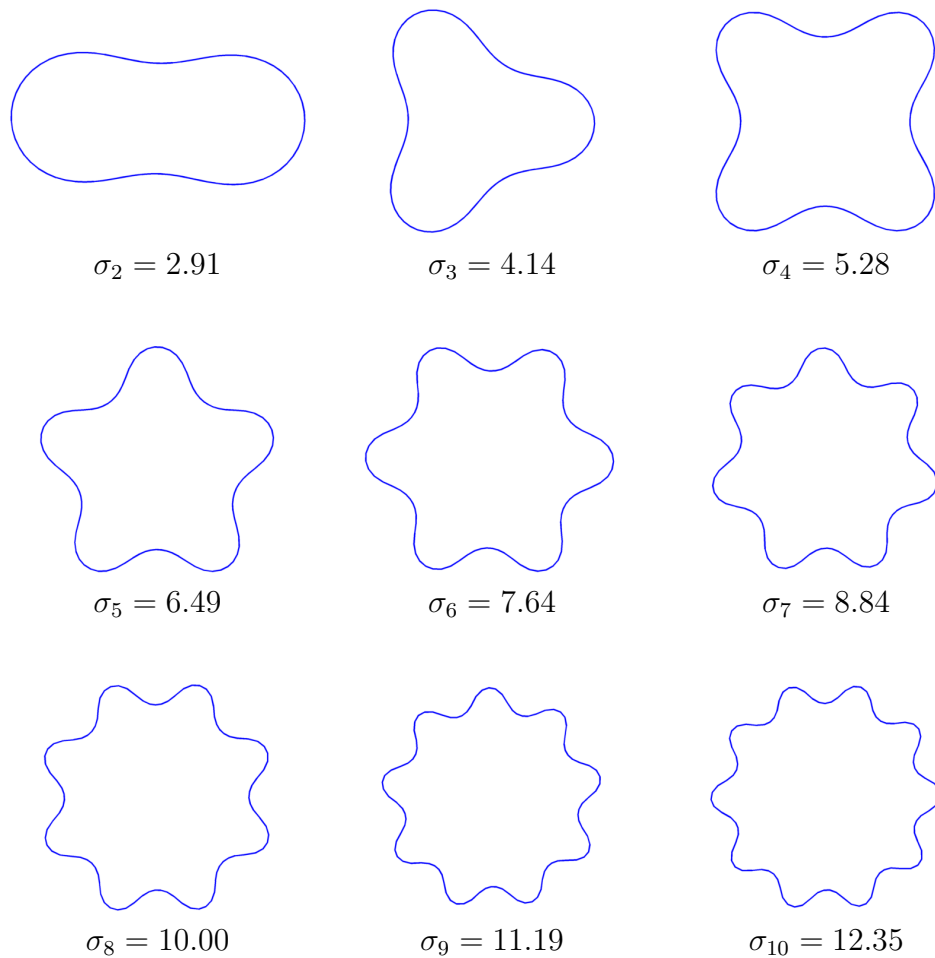
Figure 4.7: Shapes which maximize the k-th Steklov eigenvalue under area constraint, $k = 2, 3, ..., 10$.

such that the eigenvalue σ_k is multiple. Moreover, the multiplicity clusters begins at σ_k, i.e $\sigma_k > \sigma_{k-1}$. This is exactly opposite as the behavior observed in the minimization of the Dirichlet eigenvalues λ_k, where the multiplicity cluster ends at λ_k. We believe that this behaviour is due to the fact that here we study a maximizing problem, as opposed to the case mentioned above, where we have a minimizing problem.

In previous sections we proved that the problem of maximizing the k-th Steklov eigenvalue under fixed area constraint has a solution in the class of convex domains. We use the numerical method developed in previous sections to find some candidates for these convex optimal shapes. Performing optimizations in the class of convex sets is not straightforward. In our computations we chose to use a gradient descent algorithm together with an operator which, at each iteration, projects the shape onto its convex hull. These numerical results can be seen in Figure 4.8.

| $\sigma_1 = 1$ | $\sigma_2 = 2.88$ | $\sigma_3 = 3.91$ | $\sigma_4 = 4.64$ | $\sigma_5 = 5.66$ |

| $\sigma_6 = 6.29$ | $\sigma_7 = 7.43$ | $\sigma_8 = 8.03$ | $\sigma_9 = 9.21$ | $\sigma_{10} = 9.79$ |
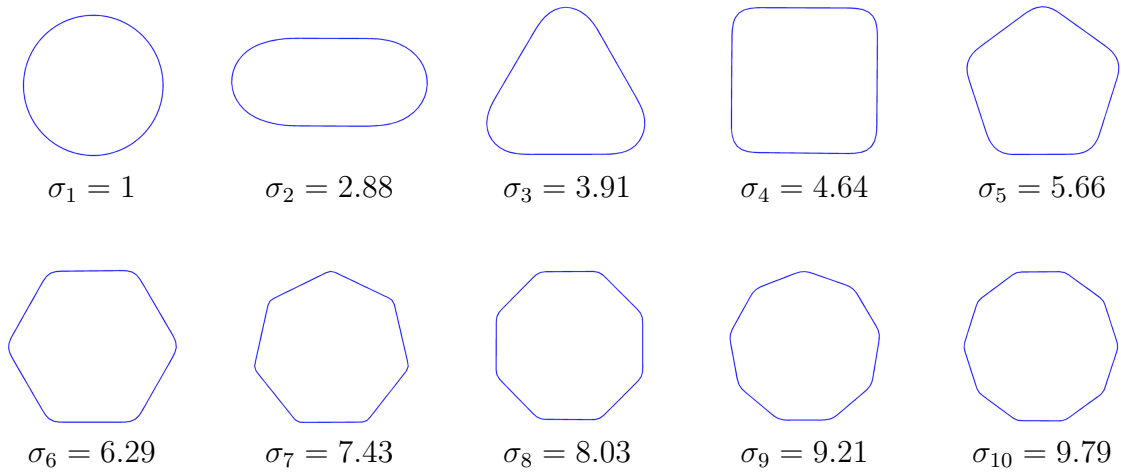
Figure 4.8: Convex shapes with unit area which give highest k-th Steklov eigenvalue in our numerical observations

4.10   A modified Steklov problem

In this section, we study numerically the domain which optimizes the following quantity related to the best constant in the trace inequality:

$$\sigma(\Omega) = \min \frac{\int_\Omega |\nabla u|^2 + \int_\Omega u^2}{\int_{\partial\Omega} u^2}. \qquad (4.10.1)$$

It is not hard to see that $\sigma(\Omega)$ is the first eigenvalue associated to the following eigenvalue problem:

$$\begin{cases} -\Delta u + u = 0 & \text{in } \Omega \\ \frac{\partial u}{\partial n} = \sigma u & \text{on } \partial\Omega, \end{cases} \qquad (4.10.2)$$

which is a modified Steklov problem. It is conjectured that the disk maximizes $\sigma(\Omega)$ among the simply connected planar domains with the same area. In the following paragraphs, we give an idea for computing $\sigma(\Omega)$ numerically, using the method of fundamental solutions, and we confirm numerically the stated conjecture.

The only point which is a bit different from the Steklov case previously studied is the family of fundamental solutions involved. Indeed, we need to work with radial functions which satisfy $-\Delta\phi + \phi = 0$. Suppose that $\phi(x) = f(r)$ where $r = |x|$. We obtain that f satisfies the following differential equation

$$r^2 f''(r) + r f'(r) - r^2 f(r) = 0,$$

which is the modified bessel equation of order 0. Once we have the form of the fundamental solution, we perform the same procedure described in the previous sections in order to compute the eigenvalues of a shape Ω. The operator $-\Delta + I$ is self-adjoint, thus the shape derivative formula is the same as in the Steklov case. Performing the numerical optimization we observe that the disk maximizes σ in the plane in both cases of the area constraint and the perimeter

156

constraint. We make the same remark that here we work in the class of simply connected domains.

4.11 The FreeFem++ code for solving the Wentzell eigenvalue problem

```
int i;
real t,beta = 2;
// Domain definition using a radial function
border C(t=0,2* pi){x=cos(t)*(1+0.1*cos(t)+0.1*cos(5*t)+
                            0.1*sin(2*t)-0.1*sin(5*t));
                y=sin(t)*(1+0.1*cos(t)+0.1*cos(5*t)+
                            0.1*sin(2*t)-0.1*sin(5*t));}
mesh Th = buildmesh (C(500));
fespace Vh(Th,P1); // Build P1 finite element space
Vh uh,vh;
// Define the problem via weak formulation
varf va(uh, vh) = int2d(Th)( dx(uh)*dx(vh)+dy(uh)*dy(vh))+
                int1d(Th,1)(beta*(dx(uh)*dx(vh)-
    dx(uh)*N.x*(N.x*dx(vh)+N.y*dy(vh))-
    dx(vh)*N.x*(N.x*dx(uh)+N.y*dy(uh))+
    N.x*(dx(vh)*N.x+dy(vh)*N.y)*N.x*(dx(uh)*N.x+dy(uh)*N.y)+
    dy(uh)*dy(vh)-
    dy(uh)*N.y*(dx(vh)*N.x+dy(vh)*N.y)-
    dy(vh)*N.y*(dx(uh)*N.x+dy(uh)*N.y)+
    (N.y)^2*(dx(vh)*N.x+dy(vh)*N.y)*(dx(uh)*N.x+dy(uh)*N.y)));
varf vb(uh, vh) = int1d(Th,1)(uh * vh);
// Solve the generalized eigenvalue problem
matrix A = va(Vh, Vh ,solver = sparsesolver);
matrix B = vb(Vh, Vh);
real cpu=clock(); // get the clock
int eigCount = 10; // Get first Eigenvalues
real[int] ev(eigCount); // Holds Eigenfunctions
Vh[int] eV(eigCount); // Holds Eigenfunctions
// Solve Ax=l*Bx
int numEigs = EigenValue(A,B,sym=true,sigma=0,
                            value=ev,vector=eV);
for(int i=0;i<eigCount;i++) // Plot the spectrum
```

```
 plot(eV[i],fill=true,value=true,cmm= ev[i]);
cout << " CPU time = " << clock()-cpu << endl;
for(i = 0;i<eigCount;i++)
 cout << ev[i] << endl;
```

Optimal partitions on manifolds

Résumé

Dans ce chapitre on propose une méthode pour étudier les partitions optimales sur des surfaces. L'idée générale est d'étendre les méthodes utilisées en dimensions deux, au cas des surfaces. On voudrait utiliser des fonctions densités pour représenter les formes, et traiter la condition de partition en imposant que la somme des fonctions représentatives est égale à 1 partout. Les deux ingrédients essentiels sont alors de

- trouver une bonne discrétisation de la surface en utilisant un algorithme de triangulation,

- trouver une formulation relaxée adaptée pour la fonctionnelle à optimiser.

On arrive à construire des méthodes qui nous permettent d'étudier deux problèmes de partitionnement optimal sur des surfaces :

1. Minimiser la somme des périmètres d'une partition de la surface en aires égales.

2. Minimiser la somme des premières valeurs propres Laplace-Beltrami correspondant aux ensembles d'une partition d'une surface.

Pour ces deux problèmes l'étape initiale est la même : construire une triangulation qualitative de la surface et représenter les fonctions densités comme des fonctions linéaires sur chaque triangle du maillage (éléments finis P_1).

Le premier problème consiste à étudier les partitions qui minimisent le périmètre sous contrainte d'aire. Ce problème a été étudié par Cox et Flikkema en [39] en utilisant le solveur Evolver [21]. Ils font le calcul direct du périmètre de chaque cellule, et ils ont besoin de trouver la topologie optimale dans chaque situation. L'approche utilisant les densités proposée ici a l'avantage que la topologie ne doit pas être imposée au cours de l'algorithme. Pour implémenter cette méthode on a besoin d'un résultat de relaxation du type Modica-Mortola pour le périmètre sur des surfaces. Un tel résultat est présenté en [12] et il consiste juste à remplacer le gradient par le gradient tangentiel dans la formulation relaxée.

Un autre avantage de cette méthode est qu'elle peut être utilisée pour n'importe quelle surface, à condition de pouvoir fournir un maillage de bonne qualité. On présente des exemples des partitions obtenues pour la sphère, le tore et d'autres surfaces. Il n'est pas possible de comparer directement nos résultats avec ceux de Cox et Flikkema, car la valeur donnée par notre fonctionnelle est une valeur approchée du périmètre. Pour pouvoir faire cette comparaison on profite de la structure spéciale de ces partitions sur la sphère (cf. [74]). Vu que les frontières des cellules sont des arcs de cercles on extrait la structure topologique et on fait une nouvelle optimisation en calculant exactement les périmètres et les aires a l'aide du théorème de Gauss-Bonnet. La conclusion est que notre methode nous permet d'obtenir tous les résultats de Cox et Flikkema et les valeurs optimales obtenues sont les mêmes.

Le deuxième problème considéré consiste à trouver les partitions d'une surface en ensembles qui minimisent la somme de leurs premières valeurs propres. Cette étude est motivée par les questions ouvertes, de nature théorique, qui sont liées à ce problème. Même pour les partitions dans un nombre petit de cellules il n'existe pas de résultats théoriques concernant la structure ou les composantes d'une partition optimale. Une première étude numérique a été faite par Elliott et Ranner dans [48] en utilisant une formulation énergétique du problème et des méthodes d'éléments finis sur des surfaces.

Notre méthode est inspirée des méthodes utilisées dans [18] et dans le chapitre 3. Pour chaque densité représentant un ensemble de partitions on résout un problème pénalisé qui nous permet de trouver une approximation numérique de la valeur propre en travaillant sur un domaine fixe. Cette première étape nous permet de trouver une bonne approximation de la partition optimale. On peut observer que les partitions optimales sont formées par des ensembles qui sont des polygones géodésiques, aspect qui motive une deuxième étape d'optimisation.

La deuxième étape, de raffinement, est faite en faisant une extraction de la topologie optimale et en calculant précisément les valeurs propres en faisant un maillage de chaque cellule. Pour calculer les valeurs propres d'un tel ensemble on utilise deux méthodes :

- des éléments finis ;

- des solutions fondamentales.

Ayant un candidat pour la partition optimale, ayant une structure de polygones géodésiques, on peut optimiser la position des sommets de cette partition pour obtenir une description plus fine de la partition. On observe que si la topologie obtenue n'est pas optimale, l'algorithme de raffinement détecte cet aspect et il s'arrête en essayant de changer la topologie.

On présente les candidats pour les partitions optimales sur la sphère pour $n \in [3, 24] \cup \{32\}$. On observe que pour $n \in \{3, 4, 6, 12\}$ on obtient une partition régulière de la sphère. En général les partitions optimales ne sont pas des *équi-partitions*, cela signifie que, les valeurs propres ne sont pas les mêmes pour toutes les cellules de la partition. Ceci nous montre que les partitions ne sont pas en fait des partitions optimales pour la fonctionnelle $\max \lambda_1^{LB}(\Omega_i)$. En faisant quelques tests numériques on observe que si au lieu de minimiser la somme on minimise le maximum

des premières valeurs propres, la topologie de la partition ne change pas, mais les sommets de la partition changent leurs positions pour que les valeurs propres de toutes les cellules soient égales.

Dans cette deuxième partie on présente aussi une méthode de calcul des valeurs propres sur la sphère en utilisant des solutions fondamentales. Elle est inspirée de la méthode présentée en chapitre 4. Au lieu de travailler avec des fonctions définies uniquement sur la surface, on considère des fonctions harmoniques en espace qui vérifient la condition de valeur propre en un nombre fini des points sur la surface. En faisant des tests numériques, on observe que cette méthode nous permet d'avoir une précision de calcul importante.

5.1 Introduction

As we have seen in previous chapters, relaxation formulations are useful in studying partitioning or multiphase problems in the plane. In this chapter we extend the previously studied methods in the case of closed surfaces in $\mathbb{R}^3$. There are two main difficulties:

- The theoretical aspect concerning the relaxations of the functionals considered;

- A numerical framework which is well adapted for these problems.

We study two partitioning problems:

1. Minimizing the sum of surface perimeters of n cells of equal areas which partition a closed three dimensional surface. This problem has been considered in the case of the sphere by Cox and Flikkema in [39]. They used the software Evolver [21] in order to study these optimal partitions. One drawback of their method is that they need to do a combinatorial optimization in order to find the topology of the optimal partition.

2. Minimizing the sum of the fundamental Laplace-Beltrami eigenvalues of the cells of a n-partition of a closed three dimensional surface. This problem was studied theoretically by [64],[63] and numerically by Elliott and Ranner in [48] for three three types of surfaces: the sphere, a torus and another closed surface. Their method is based on a penalized energy formulation presented in [33] and they used finite elements on surfaces in order to compute the eigenvalues.

We begin by the study of the equi-areal perimeter minimizing partitions. In the two dimensional case we have the Modica-Mortola theorem which provides the appropriate relaxation. This theorem extends in the three dimensional case by simply replacing the gradient by a tangential gradient with respect to the considered surface. A similar result was provided on general manifolds by Baldo and Orlandi in [12]. They did not prove that the functionals Γ-converge, but they did provide a proof for the important property which interests us: any limit of a sequence of minimizers for the relaxed formulations converges to a minimizer of the geodesic perimeter.

Of course, one needs to extend this result in the case of the partitions, and this is not trivial. We did not manage to give a complete proof of the Γ-convergence result, as the technical details of the proof are still a work in progress.

The numerical framework needs to allow us to compute all the quantities required for the computation of the relaxed formulation. Furthermore, the fixed areas constraint needs to be treated in a simple manner. A good way to address all these concerns is to consider a triangulation of the surface. On this triangulation we can construct a finite element space and this allows us to compute the value of the functional. We present an orthogonal projection algorithm which allows us to treat the constant area constraint and the partition constraint at the same time. Of course, one needs also to address the choice of the parameter ε which must be large enough in the beginning to allow the cells to move in the right position. Then, the parameter is decreased at the same time as we refine the discretization in order to have more refined results. The parameter ε is always chosen larger than the sides of the triangles. We are able to apply this method for a number of surfaces: the sphere, a torus, a double torus, etc. Any closed surface can be studied, as soon as a qualitative triangulation is found. The computation of the well behaved triangulation is made using the publicly available software DistMesh [77]. In the particular case of the sphere we can construct manually triangulations which are successive refinements starting from the icosahedron.

One further objective which we manage to achieve only in the case of the sphere is to perform a refined optimization computing exactly the perimeter of the cells. The advantage of starting with the optimization in the relaxed formulation is that there is no need to take care of the topology of the cells. In a second step we can extract the topological structure, i.e. the triple points, edge connections and faces. The results of F. Morgan [74] say that such optimal partitions exist, that the boundaries between two cells are curves of constant geodesic curvature and that at junction points boundaries meet in threes making angles of measure $2\pi/3$. This result allows us to deduce that in the case of the sphere boundaries between two cells are arcs of circles (not necessarily geodesics). Furthermore, the Gauss-Bonnet formula gives an explicit expression for the areas of the cells in this case.

The second problem we study in this chapter deals with the optimization of the sum of the first Laplace-Beltrami eigenvalues of partitions of a surface. We propose a relaxed framework inspired from [18]:

- We construct a triangulation of the surface.

- We construct a finite element space on this triangulation, which allows us to compute the mass matrix M and the stiffness matrix K.

- In order to compute the eigenvalues of a shape $\omega \subset S$ we consider the penalized formulation, inspired from the euclidean form given by Dal Maso and Mosco [40]:

$$-\Delta_\tau u + C(1-\varphi)u = \lambda u,$$

where $C >> 1$ and φ is an approximation of the characteristic function of ω, χ_ω.

- We use a gradient descent algorithm in order to find the optimal densities. In order to impose the partition condition, we use the projection operator

$$\Pi(\varphi^l) = \frac{|\varphi^l|}{\sum_{i=1}^n |\varphi^i|},$$

  which was also used in [18] and in Chapter 3.

We observe the boundaries of the optimal structure and we notice that, when the number of cells is great enough, they are close to being geodesic arcs. This behaviour was also noticed in [48]. This motivates us to perform a refined optimization procedure in the case of the sphere for the particular case when the boundaries of the cells are geodesic polygons. We do not claim that these refined partitions are optimal, but we believe that they give a reasonable upper bound for the energy, at least for a large number of cells. We provide theoretical and numerical arguments suggesting that in general the optimal cells are not geodesic polygons.

In order to do the optimization in the class of geodesic polygons we need do devise a way to compute the eigenvalues of such a subset of the sphere. We have two ways of doing this:

- using fundamental solutions.

- using a finite element approach.

In each of these two methods, a meshing procedure is needed in order to find triangulations of each such polygon. It is not hard to devise a fast triangulation algorithm, by using, for example, multiple refinements, starting from a generic configuration.

We propose a method of computing the Laplace-Beltrami eigenvalues on the three dimensional sphere using fundamental solutions. As in Chapter 4, the idea is to consider linear combinations of function which already satisfy the partial differential equation, and find the coefficients by imposing the boundary conditions. The problem here is that we only have an equation on the boundary of $\mathbb{S}^2$. In order to have a fundamental solutions framework, we consider functions which are defined in $\mathbb{R}^3$, not only on $\mathbb{S}^2$, and which are harmonic. The choice of harmonic fundamental solutions becomes evident once we write the decomposition of the Laplacian in the Laplace-Beltrami part and the normal part:

$$\Delta u = \Delta_\tau u + \mathcal{H}\partial_n u + \partial_n^2 u.$$

Thus, if u is harmonic, then the the Laplace-Beltrami operator applied to u can be computed using only normal derivatives with respect to $\mathbb{S}^2$, which can be expressed explicitly. This is a key point in the numerical computations.

We choose a family of source points outside or inside the ball determined by $\mathbb{S}^2$, and and a family of evaluation points on $\mathbb{S}^2$ where we impose the boundary condition equation. We note the following difference with respect to the Steklov problem: since we are not constrained

on considering functions which are harmonic inside or outside the unit ball, we may choose which variant we want. We prefer to work with exterior points since we observe an increase in precision. We notice that the method is precise and we study the errors in the following cases:

- We study the error made as the distance from the source points to $\mathbb{S}^2$ varies;

- We study the error made when computing eigenvalues of certain pieces of the sphere by considering certain spherical shapes for which some of the eigenvalues are known analytically.

This method of fundamental solutions has some drawbacks. If the number of points is too large or the source points are too close, then we lose precision. This is due to the poor conditioning of the matrices involved. Another aspect concerns an upper limit on the number of source points we can consider. The eigenvalue computation problem is reduced to a generalized eigenvalue matrix problem, and the matrices involved are full. Thus, beyond matrices of size 5000×5000 the algorithm becomes very slow. When the fundamental solution methods fail we turn to classical finite element methods which produce sparse matrices. Thus, in the case of partitions, when we have more than 16 cells we switch to a finite elements approach.

5.2 Perimeter minimizing equi-areal partitions

Given a partition $(\omega_i)_{i=1}^n$ of a three dimensional surface S, we associate to it the sum of the lengths of the boundaries of the cells ω_i. The problem of finding a partition of S into equal area cells which minimizes the sum of perimeters has been considered before from both numerical and theoretical points of view. The case where S is a sphere has been studied by Toth [52] and he proved that under certain hypothesis on the regularity of the partition, the regular ones are optimal for $n \in \{3, 4, 6, 12\}$ (partitions corresponding to regular polyhedra). As in the case of the study of the honeycomb conjecture the difficult part is to be able to prove the same result without convexity or connectedness assumptions. T. Hales was able to apply the method used in the proof of the honeycomb conjecture [60] to prove that in the case $n = 12$ the minimal partition corresponds to the partition generated by the dodecahedron. His method did not work for smaller n and positive results are known only for $n \in \{2, 3, 4\}$ [49]. General qualitative properties of the optimal partitions are given by F. Morgan in [74]. In particular, the cells of the optimal partition have boundaries which have piecewise constant curvature and the boundaries meet in triple points with equal angles of measure $2\pi/3$. Numerical studies of minimal perimeter partitions of the sphere were preformed by Cox and Flikkema [39] using the software Evolver [21]. They presented candidates for the optimal partitions for $n \leq 32$.

We may ask ourselves if the problem can be tackled using the same methods developed in Chapter 2 and [80]. First we need to find a suitable relaxed form for the problem. In [12] the authors present a candidate for the Γ-convergence approximation of the perimeter on surfaces.

In fact, the functional has the same structure as the Modica-Mortola theorem, but instead of a gradient term we have a tangential gradient. As the proofs in [12] involve the use of rectifiable currents instead of classical finite perimeter sets introduced in Chapter 2 we were not able generalize directly the results of [12] to the case of partitions. Nevertheless, we propose a conjectured result analogue to the partition approximation in Chapter 2. The technical details of the proof are still a work in progress.

Given a smooth, compact surface $S \subset \mathbb{R}^3$ we define $F_\varepsilon : (L^1(S))^n \to [0, \infty]$ by

$$F_\varepsilon((u_i)) = \begin{cases} \sum_{i=1}^n \left(\varepsilon \int_S |\nabla_\tau u_i|^2 + \frac{1}{\varepsilon} \int_S W(u_i) \right) & (u_i) \in X \text{ and are sufficiently regular} \\ \infty & \text{otherwise} . \end{cases}$$

where $W : \mathbb{R} \to [0, \infty)$ is a double-well potential with zeros at 0 and 1 and X is the subspace of $L^1(S)^n$ which satisfies the additional partition constraint $u_1 + ... + u_n = 1$ and the constraints $\int_S u_i = c_i$ with $\sum_{i=1}^n c_i = A$, where A is the area of S.

Define also $F : (L^1(S))^n \to [0, \infty]$ by

$$F((u_i)) = \begin{cases} \sum_{i=1}^n c \operatorname{Per}_S(\omega_i) & (u_i) \in X, u_i = \chi_{\omega_i}, (\omega_i) \text{ have finite perimeter on } S \\ \infty & \text{otherwise} . \end{cases}$$

As usual c denotes $2 \int_0^1 \sqrt{W(s)} ds$.

Conjecture. We have that $F_\varepsilon \xrightarrow{\Gamma} F$ in the $L^1(S)$ topology.

The proof of this conjecture is a work in progress. The fact that this result is a natural generalization of the two dimensional results presented in [80] and Chapter 2 and the fact that numerical computations presented in the next section give the expected results suggest the validity of the result. As in Chapter 2, in order to approximate numerically partitions into cells of equal areas of a surface, we search for minimizers of F_ε for ε small enough. The numerical algorithm and some results are presented in the next section.

5.2.1 Numerical framework and results

In order to perform numerical computations we need a framework which allows us to compute the quantity

$$\varepsilon \int_S |\nabla_\tau u|^2 + \frac{1}{\varepsilon} \int_S u^2(1-u)^2,$$

in fast, efficient way. In order to do this we triangulate the surface S and we compute the mass matrix M and the stiffness matrix K associated to this triangulation. Then, if by abuse of notation, we use the same notation u for the P_1 finite element approximation of u, we have

$$\int_S |\nabla_\tau u|^2 = u^T K u$$

and

$$\int_S u^2(1-u)^2 = v^T M v,$$

where $v = u.^2. \times (1-u).^2$. We have used the Matlab convention that adding a point before an operation means that we are doing component-wise vector computations. Note that once the matrices K, M are computed, we only have to perform matrix-vector multiplications, which is really fast. In this setting we use the discrete gradients of the above expressions given by:

$$\nabla_u u^T K u = 2Ku,$$

$$\nabla_u v^T M v = 2Mv. \times (1-2u).$$

The partition condition and the equal areas constraint are imposed by making an orthogonal projection on the linear constraints as follows. We write the discrete vectors representing P_1 discretization of the density functions in the following matrix form

$$M = (\varphi^1 \ \varphi^2 \ ... \ \varphi^n).$$

The partition constraint implies that the sum of the elements on every line of M is equal to 1 and the equal area constraint implies that for every column of the matrix M we have the relation

$$\langle v, \varphi^i \rangle = A/n, \ \text{where } v = 1_{1 \times N} \cdot M.$$

Here the constant A is the total area of the surface, N is the total number of points in the triangulation and the notation $1_{p \times q}$ represents the $p \times q$ matrix whose entries are all equal to 1. These conditions are discretizations in the finite element setting of the conditions that the integrals of the density functions u_i are all equal to A/n. Indeed, given a triangulation $\mathcal{T}$ of S and its associated mass matrix M, we have $\int_S 1 \cdot u_i = 1_{1 \times N} \cdot M \cdot \varphi^i$, where φ^i is the vector containing the values of u_i at the vertices of the triangulation. The projection routine can be found in Algorithm 4.

Once we have this discrete formulation we use an optimized LBFGS gradient descent procedure [86] in order to compute the numerical minimizers. In order to avoid local minima where one of the phases φ^l is constant, which arise often when the number of phases is greater than 5, we add a Lagrange multiplier which penalizes the constant functions. In this way, we optimize

$$\sum_{i=1}^{n} \varepsilon \int_S |\nabla_\tau \varphi^i|^2 + \frac{1}{\varepsilon} \int_S (\varphi^i)^2 (1-\varphi^i)^2 + \lambda(\text{std}(\varphi^i) - \text{starget})^2,$$

where $\text{std}(\varphi^l)$ is the standard deviation of φ^l and starget is the standard deviation of a characteristic function of area $\text{Area}(S)/n$.

In order to have a nice view of the optimal partition, we want do decrease ε so that the width of the interface is small. We notice that if we chose ε of the same order as the sides of the mesh triangles the algorithm converges. Furthermore, we cannot make ε smaller, since then the gradient term will not contain any real information, as the width of the interface is of size ε. In order to avoid this problem, we consider refined meshes associated to each ε. At each step where we decrease ε we interpolate the values of the previous optimizer on a refined mesh
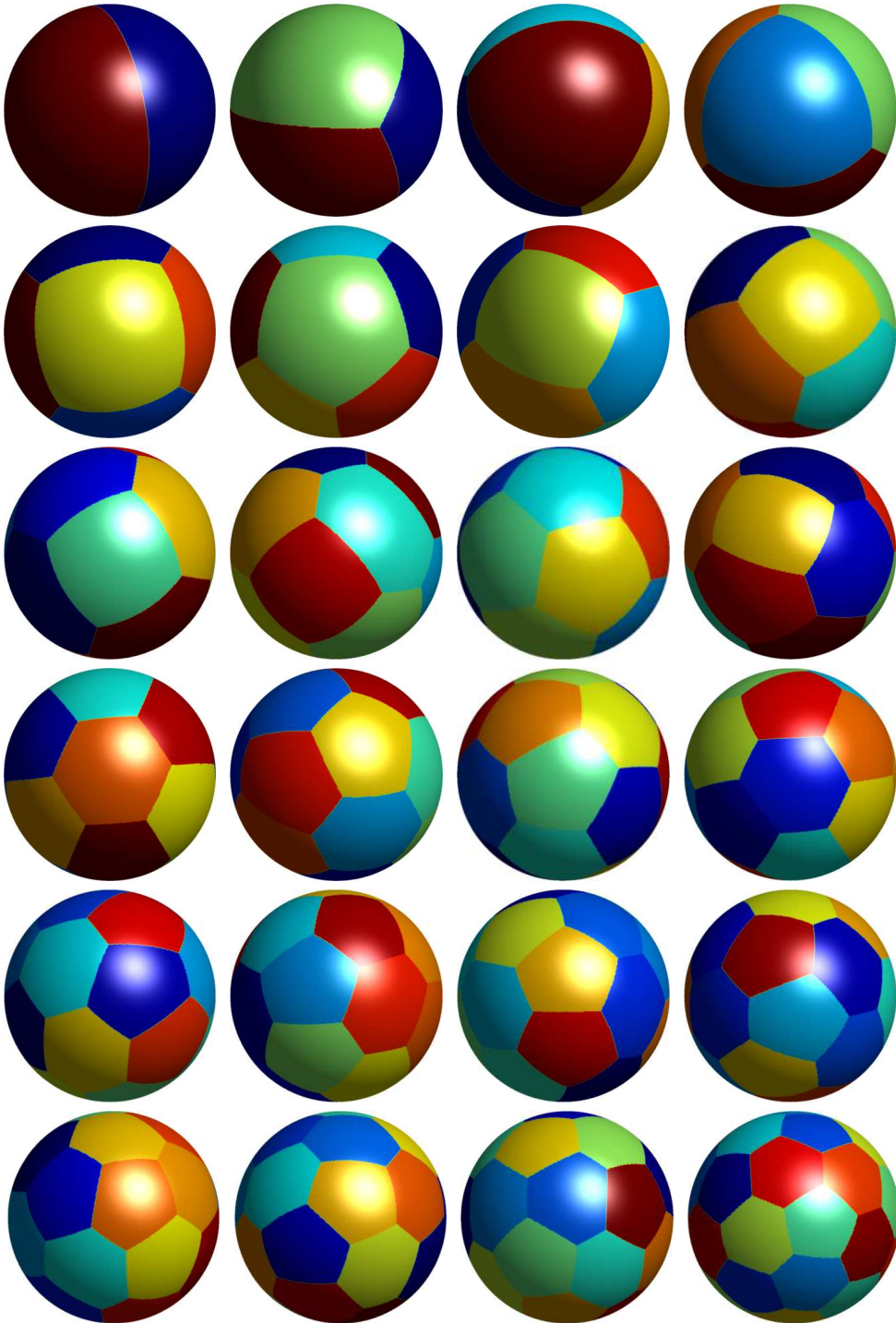
Figure 5.1: Minimal perimeter partitions on the sphere into n equal area cells for $n \in \{2, 3, ..., 24, 32\}$.
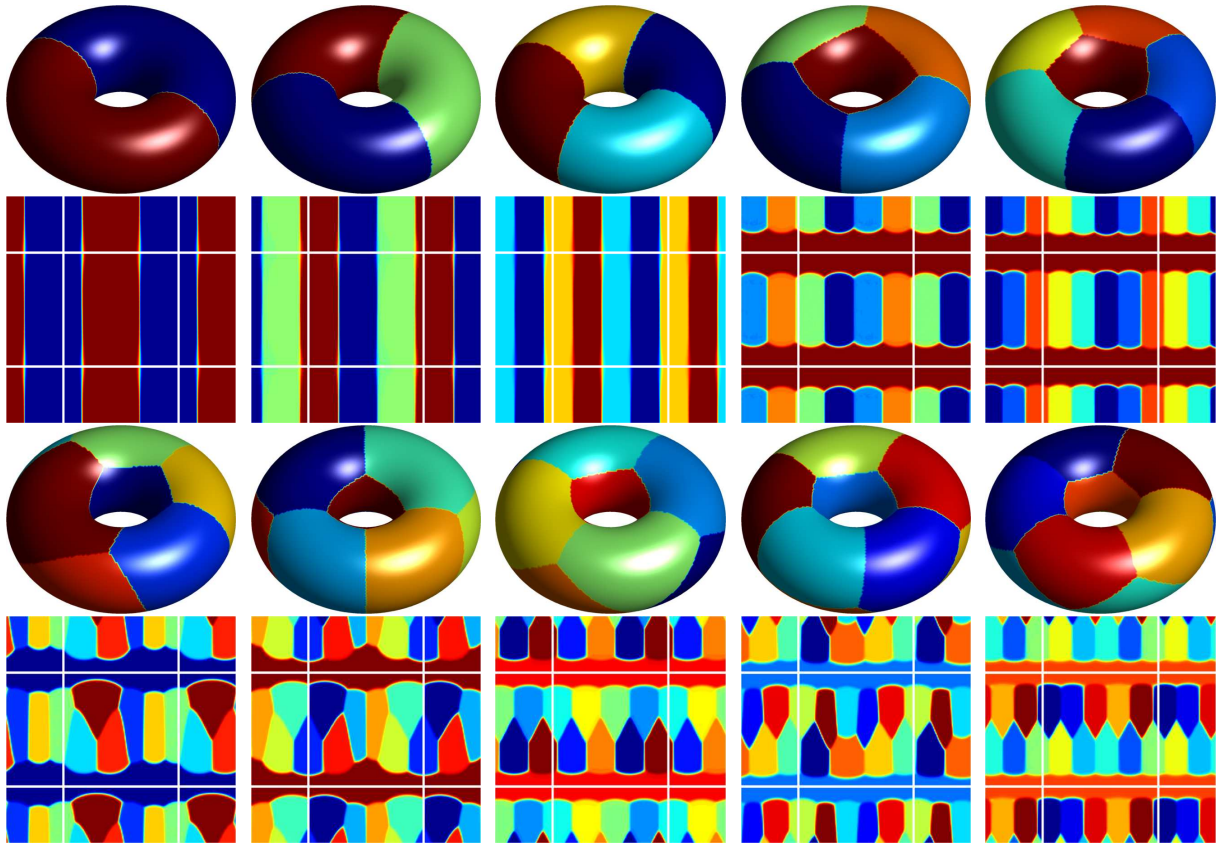
Figure 5.2: Minimal perimeter partitions on the torus with outer radius $R = 1$ and inner radius $r = 0.6$ together with their associated flattenings for $n \in [2, 11]$. The center rectangle is represents the torus, while periodic continuations are made to easily see the topological structure.
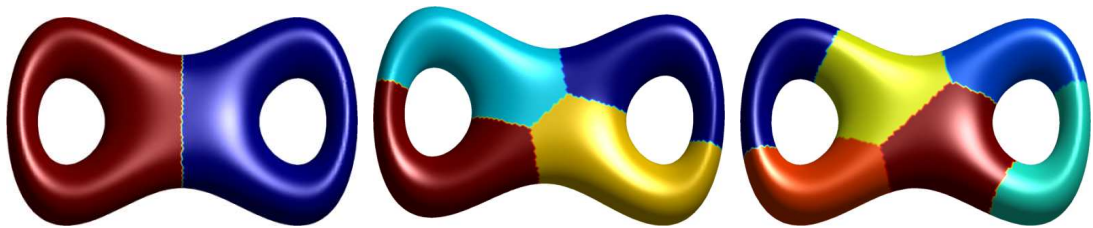
Figure 5.3: Minimal perimeter partitions on a double torus for $n \in \{2, 4, 6\}$.
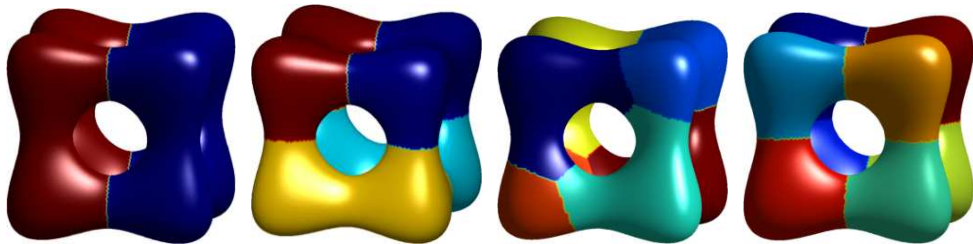
Figure 5.4: Minimal perimeter partitions on a Banchoff-Chmutov surface for $n \in \{2, 4, 6, 8\}$.

Algorithm 4 Orthogonal projection on the partition and area constraints

Require: $A = (a_{ij}) \in \mathbb{R}_{N \times n}$, $c \in \mathbb{R}_{1 \times n}$, $d \in \mathbb{R}_{N \times 1}$, v;

1: $(e_i) = \sum_j a_{ij} - c_i$; (line sum error; $N \times 1$ column vector)
2: $(f_i) = \sum_i v_i a_{ij} - d_j$; (column scalar product error; $n \times 1$ column vector)
3: Define the matrix C of size $n \times n$ by

$$\begin{cases} c_{kl} = \|v\|_2^2/n & \text{if } k \neq l \\ c_{kk} = \|v\|_2^2 - \|v\|_2^2/n; \end{cases}$$

4: $(q_j) = (f_j) - \langle v, e \rangle / n$; ($n \times 1$ column vector)
5: Compute $(\lambda_j) \in \mathbb{R}_{n \times 1}$ with $\lambda_n = 0$ such that $C|_{(n-1) \times (n-1)}(\lambda_j)|_{n-1} = (q_j)|_{n-1}$. The indices indicate a sub-matrix with the first $n - 1$ lines and columns, or the sub-vector formed by the first $n - 1$ components.
6: $S = \sum_j \lambda_j$;
7: $\eta_i = (e_i - S \cdot v_i)/n$; ($N \times 1$ column vector);
8: $A_{\text{orth}} = (\eta_i) \cdot 1_{1 \times n} + v \cdot (\lambda_j)^T$, where $1_{p \times q}$ is the $p \times q$ matrix with all entries equal to 1;
9: $A = A - A_{\text{orth}}$;
　　return A

---

and we consider this interpolated densities as starting point for the descent algorithm on the new mesh. In the case of the sphere we make four refinements ranging from 10000 to 160000 points. In order to keep things simple, we only used a nearest point interpolation, as this was good enough for our purposes for two reasons: it is fast and simple to implement and we only need an approximation of the optimal partition, since we re-optimize the interpolated densities. Some optimal configurations, in the case of the sphere, are presented in Figure 5.1. A detailed study of the case of the sphere along with a comparison with the known results of Cox and Flikkema [39] are presented in the next section.

As underlined before, our approach allows a direct treatment of any surface, as long as a qualitative triangulation is found. We were able to perform some numerical computations on various shapes like a torus, a double torus, and a more complex surface called Banchoff-Chmutov of order 4. A few details about the definitions of these surfaces are provided below:

- We consider a torus of outer radius $R = 1$ and inner radius 0.6 (see Figure 5.2). This torus is defined as the zero level set of the function

$$f(x, y, z) = (x^2 + y^2 + z^2 + R^2 - r^2)^2 - 4R^2(x^2 + y^2).$$

- The double torus used in the computation (see Figure 5.3 is given by the zero level set of the function
$$f(x, y, z) = (x(x-1)^2(x-2) + y^2)^2 + z^2 - 0.03.$$

- The complex Banchoff-Chmutov surface (see Figure 5.4) is given by the zero level set of the function
$$f(x, y, z) = T_4(x) + T_4(y) + T_4(z),$$

where $T_4(X) = 8X^4 - 8X^2 + 1$ is the Tchebychev polynomial of order 4.

5.2.2 Refined optimization in the case of the sphere

The method described in the previous section can be used on general surfaces but has the drawback that the value of the relaxed cost functional is close to the real value of the perimeter only when the parameter ε is very small, which means that the discretization needs to be fine enough. In the case of the sphere we can surpass this difficulty by noting that the results of [74] allow us to deduce that cell boundaries are arcs of circles. This follows at once from the fact that cell boundaries are curves of constant geodesic curvature and cf. for example [85, Exercise 2.4.9] in the case of the sphere the only such curves are portions of circles. The results of Cox and Flikkema [39] show that optimal configurations are not made of geodesic polygons. In order to perform an optimization procedure which captures this effect they chose to make an initial optimization in the class of geodesic polygons and then divide each geodesic arc into 16 smaller arcs and restart the procedure with more variable points. They manage to approximate well enough the general optimal structure but they still work in the class of geodesic polygons with additional vertices. Our approach presented below is different in the sense that we consider general circle arcs (not necessarily geodesics) which connect the points.

The first step is to extract the topology from the previous density results, i.e. locate the triple points, the edge connections and construct the faces. In order to perform the refined optimization procedure we need to be able to compute the areas of portions of the sphere determined by arcs of circles. This is possible using the Gauss-Bonnet formula. If M is a smooth subset of a surface then

$$\int_M K dA + \int_{\partial M} k_g = 2\pi\chi(M), \tag{5.2.1}$$

where K is the curvature of the surface, k_g is the geodesic curvature and $\chi(M)$ is the Euler characteristic of M. This result extends to piecewise smooth curves and in this case we have

$$\int_M K dA + \int_{\partial M} k_g + \sum \theta_i = 2\pi\chi(M), \tag{5.2.2}$$

where θ_i are the *turning angles* between two consecutive smooth parts of the boundary. In the case of a polygon the turning angles are the external angles of the polygon. The formula (5.2.2) allows the computation of the area of a piece of the sphere bounded by arcs of circle. In this case the Euler characteristic is equal to 1, the curvature of the unit sphere is $K = 1$ and the geodesic curvature is piecewise constant. For more details we refer to [45, Chapter 4].

A first consequence of the Gauss-Bonnet theorem in connection to our problem is noting the fact that, apart from cases where we have a certain symmetry like $n \in \{3, 4, 6, 12\}$ the optimal cells are not geodesic polygons. This is made clear in cases where we have a hexagonal cell. If the arcs forming the boundary of such a hexagonal cell would be geodesic polygons then its area would be equal to $6 \cdot 2\pi/3 - 4\pi = 0$. Thus a spherical shape bounded by six arcs of circle can never be a geodesic polygon without being degenerate.

In order to perform the optimization we take the vertices as variables and we add one supplementary vertex for each edge. This is enough to contain all the necessary information since an arc of circle is well defined by three distinct points on the sphere. In the sequel we denote $\mathcal{P}_n$ the set of partitions of the sphere into n cells and with $\mathcal{A}_n$ the partitions in $\mathcal{P}_n$ having equal areas. In order to have a simpler numerical treatment of the problem we can incorporate the area constraints in the functional by defining for every partition $(\omega_i) \in \mathcal{P}_n$ the quantity defined for every $\varepsilon > 0$ by

$$G_\varepsilon((\omega_i)) = \sum_{i=1}^n \operatorname{Per}(\omega_i) + \frac{1}{\varepsilon} \sum_{i=1}^{n-1} \sum_{j=i+1}^n (\operatorname{Area}(\omega_i) - \operatorname{Area}(\omega_j))^2.$$

If we denote

$$G((\omega_i)) = \begin{cases} \sum_{i=1}^n \operatorname{Per}(\omega_i) & \text{if } (\omega_i) \in \mathcal{A}_n \\ \infty & \text{if } (\omega_i) \in \mathcal{P}_n \setminus \mathcal{A}_n. \end{cases}$$

then we have the following Γ-convergence result.

Theorem 5.2.1. *We have that $G_\varepsilon \xrightarrow{\Gamma} G$ for the $L^1(\mathbb{S}^2)$ convergence of sets.*

Proof: For the (LI) property consider a sequence $(\omega_i^\varepsilon) \subset \mathcal{P}_n$ which convergence in $L^1(\mathbb{S}^2)$ to (ω_i). It is clear that we have $\operatorname{Area}(\omega_i^\varepsilon) \to \operatorname{Area}(\omega_i)$ and the perimeter is lower semicontinuous for the L^1 convergence. Thus we have two situations. If $(\omega_i) \in \mathcal{P}_n \setminus \mathcal{A}_n$ then $\lim_{\varepsilon \to 0} G_\varepsilon((u_i^\varepsilon)) = \infty$. If $(\omega_i) \in \mathcal{A}_n$ then the lower semicontinuity of the perimeter implies that $\liminf_{\varepsilon \to 0} G_\varepsilon((\omega_i^\varepsilon)) \geq G((\omega_i))$.

The (LS) property is immediate in this case. Choose $(\omega_i) \in \mathcal{A}_n$, or else there is nothing to prove. We may choose the recovery sequence equal to (ω_i) for every $\varepsilon > 0$. Thus the property is verified immediately. $\qquad\square$

Remark 5.2.2. We note that in the above proof the simplicity of the proof of the (LS) property is due to the fact that the functionals G_ε are well defined on the space $\{G < \infty\}$, which makes possible the choice of constant recovery sequences. This is not the case in the Modica-Mortola theorem and in the results proved in Chapters 1 and 2.

This Γ-convergence result proves that minimizers of G_ε converge to minimizers of G. As a consequence, in the numerical computations, we minimize G_ε for ε smaller and smaller in order to approach the minimizers of G, which are in fact the desired solutions to our problem.

Since the parameters are of two types: triple points and edge points, we prefer to use an optimization algorithm which is not based on the gradient. The algorithm is described below.

- For each point P consider a family of m tangential directions $(v_i)_{i=1}^m$ chosen as follows: the first direction is chosen randomly and the rest are chosen so that the angles between consecutive directions are $2\pi/m$.
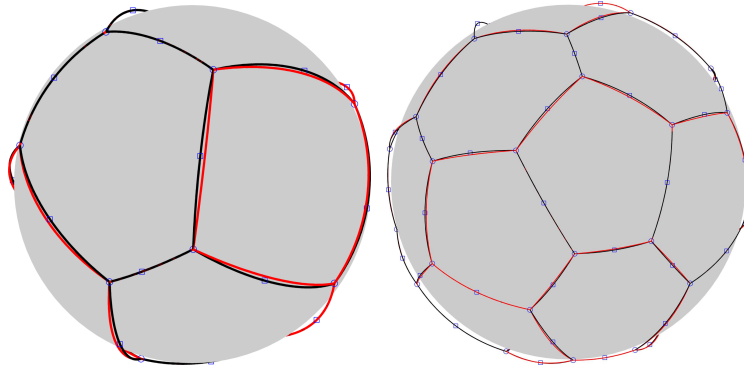
Figure 5.5: The difference between optimal configuration (black) and the geodesics connecting the points (red). Notice that the difference is really small when the number of cells is large.

- Evaluate the cost function for the new partition obtained by perturbing the point P in each of the directions v_i according to a parameter ε.

- Choose the direction which has the largest decrease and update the partition accordingly.

- Do the same procedure for each edge point by performing the two possible orthogonal perturbations of the point with respect to the edge.

- If there is no decrease for each of the points of the partition, then decrease ε.

This algorithm converges in each of the test cases and the results are presented in Table 5.1. In the optimization procedure we start with $\varepsilon = 1$ and we reiterate the optimization decreasing ε by a factor of 10 at each step until we reach the desired precision on the area constraints. We are able to recover the same results as Cox and Flikkema for $n \in [4, 32]$. Furthermore, unlike in the case of geodesic polygons, all triple points consist of boundaries which meet at equal angles of measure $2\pi/3$. In Figure 5.5 you can see the results for $n = 9$ and $n = 20$. The red arcs are geodesic connecting the points and are drawn to visually see that not all the boundaries of the optimal structure are geodesic arcs.

Thus we can conclude that the relaxed formulation presented in the previous section is able to match the best known configurations in the literature. Furthermore for $n \in [5, 25] \cup \{32\}$ the algorithm finds the good configuration without much effort, while for $n \in [26, 31]$ multiple tries with different initial conditions were needed in order to find the best configuration.

	our results		Cox-Flikkema	our results		Cox-Flikkema
N	geodesics	area tol.	geodesics	non-geo.	area tol.	non-geo.
4	11.4637	2×10^{-6}	11.464	11.4637	5×10^{-7}	11.464
5	13.4518	4×10^{-6}	13.452	13.4304	2×10^{-7}	13.430
6	14.7715	2×10^{-6}	14.772	14.7715	2×10^{-7}	14.772
7	16.3604	8×10^{-6}	16.360	16.3519	3×10^{-7}	16.352
8	17.7108	6×10^{-7}	17.710	17.6927	3×10^{-7}	17.692
9	18.8672	6×10^{-6}	18.867	18.8504	2×10^{-7}	18.850
10	20.0152	8×10^{-6}	20.015	19.9997	4×10^{-7}	20.000
11	21.1629	6×10^{-6}	21.163	21.1398	4×10^{-7}	21.140
12	21.8918	4×10^{-7}	21.892	21.8918	5×10^{-7}	21.892
13	23.1117	1×10^{-6}	23.112	23.0953	4×10^{-7}	23.095
14	23.9644	8×10^{-7}	23.964	23.9581	3×10^{-7}	23.958
15	24.8908	7×10^{-7}	24.891	24.8821	2×10^{-7}	24.882
16	25.7359	1×10^{-6}	25.736	25.7269	2×10^{-7}	25.727
17	26.6488	2×10^{-6}	26.649	26.6365	3×10^{-7}	26.637
18	27.4783	6×10^{-6}	27.478	27.4647	2×10^{-7}	27.465
19	28.2901	5×10^{-6}	28.290	28.2735	2×10^{-7}	28.274
20	29.0154	6×10^{-6}	29.015	28.9992	1×10^{-7}	28.999
21	29.7924	5×10^{-6}	29.792	29.7748	2×10^{-7}	29.775
22	30.5282	2×10^{-6}	30.528	30.5094	2×10^{-7}	30.509
23	31.2462	5×10^{-6}	31.246	31.2260	2×10^{-7}	31.226
24	31.9326	4×10^{-6}	31.933	31.9117	3×10^{-7}	31.912
25	32.6392	4×10^{-6}	32.639	32.6172	8×10^{-8}	32.617
26	33.2897	4×10^{-6}	33.290	33.2675	2×10^{-7}	33.268
27	33.9185	4×10^{-6}	33.918	33.8968	9×10^{-8}	33.897
28	34.5746	4×10^{-6}	34.575	34.5521	4×10^{-7}	34.552
29	35.2303	4×10^{-6}	35.230	35.2065	6×10^{-7}	35.207
30	35.8436	4×10^{-6}	35.844	35.8199	5×10^{-7}	35.820
31	36.4167	5×10^{-6}	36.417	36.3941	4×10^{-6}	36.394
32	36.9514	3×10^{-6}	36.951	36.9310	4×10^{-6}	36.931

Table 5.1: Comparison between our results and the results of Cox and Flikkema in the case of the sphere. The left part of the table presents the optimal costs in the class of geodesic polygons, while the right part deals with the general case where the boundaries of partition cells are not necessarily geodesics.

5.3 Spectral optimal partitions

In the following sections we present a numerical study of the partitions $(\omega_i)_{i=1}^n$ of a compact surface S without boundary which solve the problem

$$\min \lambda_1^{LB}(\omega_1) + ... + \lambda_1^{LB}(\omega_n).$$

We denote by $\lambda_k^{LB}(\omega)$ the k-th Laplace-Beltrami eigenvalue of a set ω contained in S. The existence and the regularity of such optimal partitions has been studied before (see, for example [38], [63], [64], [27]). Here we deal mainly with the problem of finding numerically candidates for the optimal configurations. Such a numerical study has been performed by Elliott and Ranner in [48]. They made computations for $n \in \{3, 4, 5, 6, 7, 8, 16, 32\}$ using a method based on finite elements and a penalized formulation of the partitioning problem which can be found in [35],[33]. The method presented in the following is based on a relaxed formulation inspired from [18]. The optimization procedure has two steps: first we find the optimizers in the relaxed form and secondly we extract the structure and continue the optimization procedure by meshing each cell of the partition and optimizing the cost function with respect to the position of the vertices. We are able to perform optimizations using the relaxed formulation on general surfaces, but the refinement procedure is only applied in the case of the sphere. Based on fundamental solutions methods used in Chapter 4 we provide an algorithm for computing the Laplace-Beltrami eigenvalues on the sphere or on portions of the sphere. This algorithm seems to be very efficient and precise when the domains we consider are not small relative to the surface of the sphere.

5.3.1 Laplace-Beltrami eigenvalues on the sphere

Motivated by the fact that the Laplace-Beltrami eigenvalues of a closed curve in $\mathbb{R}^2$ can be found using fundamental solutions, as noted in Chapter 4, we extend the method to the case of the unit sphere in $\mathbb{R}^3$. In order to do this we consider the extended problem

$$\begin{cases} -\Delta_\tau u = \lambda u & \text{on } \mathbb{S}^2 \\ -\Delta u = 0 & \text{in a neighborhood of } \mathbb{S}^2. \end{cases} \tag{5.3.1}$$

The motivation behind this consideration is the following decomposition of the Laplacian

$$\Delta u = \Delta_\tau u + \mathcal{H}\frac{\partial u}{\partial n} + \frac{\partial^2 u}{\partial n^2}. \tag{5.3.2}$$

For a proof of (5.3.2) and more details we refer to [66]. As usual, $\mathcal{H}$ denotes the mean curvature of the surface. We denote $\frac{\partial^2 u}{\partial n^2} = (D^2 n.u).u.$

As before, we seek u as a linear combination of radial harmonic functions in $\mathbb{R}^3$ which do not have singularities on $\mathbb{S}^2$. We consider the fundamental solution of the Laplace equation in three dimensions given by $\phi(x) = 1/|x|$. We choose a family of N evaluation points (x_i) on $\mathbb{S}^2$ which are uniformly distributed. We can do an explicit construction starting from a dodecahedron in
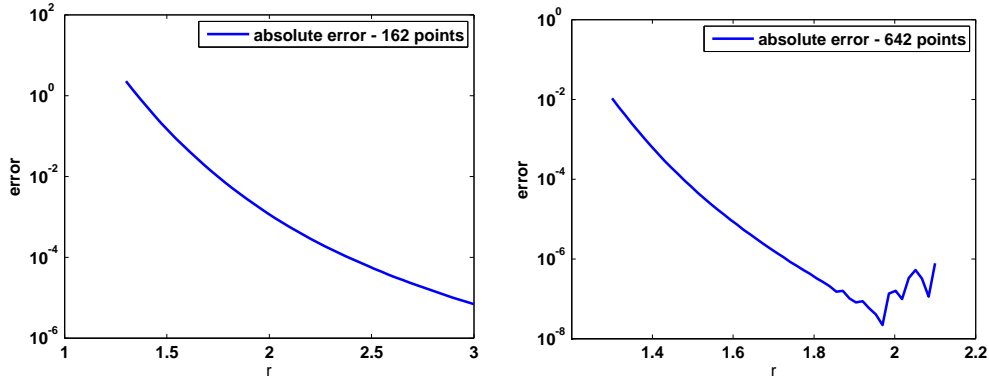
Figure 5.6: Absolute errors - approximation of the first 10 Laplace-Beltrami eigenvalues of $\mathbb{S}^2$.

the case of the sphere, or we can use DistMesh [77] in general situations. The source points (y_i) are chosen on the normals at $\mathbb{S}^2$ in x_i at a fixed distance r. As we will see below, the behaviour of the error depends on r and N. These parameters must be chosen such that the matrices involved in the computations are well conditioned, in order to have meaningful results. For each y_i we consider the fundamental solution centered in y_i defined by $\psi_i(x) = \phi(|x - y_i|)$. We seek u in the form

$$u = \alpha_1 \psi_{y_1} + ... + \alpha_N \psi_{y_N}.$$

We impose the eigenvalue condition in each of the points (x_i) and we obtain the equations

$$-\Delta_\tau(\alpha_1 \psi_{y_1}(x_i) + ... + \alpha_N \psi_{y_N}(x_i)) = \lambda^{LB}(\mathbb{S}^2)(\alpha_1 \psi_{y_1}(x_i) + ... + \alpha_N \psi_{y_N}(x_i)), \; i = 1...N. \tag{5.3.3}$$

Solving this generalized eigenvalues problem we expect to find the values of the Laplace Beltrami eigenvalues on the unit sphere. The explicit eigenvalues are of the form $\ell(\ell + 1)$ with multiplicity $2\ell + 1$, with $\ell \geq 0$. We recall that r is the distance from the exterior points (y_i) to the boundary of the sphere. The choice of the sample points (x_i) is not random. As noted in [8], the sample points should be distributed evenly across the surface in order to obtain meaningful results. We tried multiple choices for the points (x_i):

- Uniform sphere mesh found with Distmesh [77].

- The layer method described in [8]

- A uniformly refined mesh of the sphere starting from an icosahedron.

For all these choices of points we observe that the values obtained with our algorithm are very close to the analytical ones. An analysis of the dependence of the absolute error of the parameter r and on the number of sample points is given in Figure 5.6. We can see that the error decreases drastically with r. We also observe that when we have a large number of points and large r the computation is not stable anymore. These estimates are valid for the first 10 eigenvalues.

We can use the method of fundamental solutions in order to compute the Laplace-Beltrami eigenvalues with Dirichlet boundary conditions of a shape $\omega \subset \mathbb{S}^2$. In order to do this we

consider only sample points $x_i \in \omega$ and approximate $\lambda^{LB}(\omega)$ using a variation of equation (5.3.3). Indeed, let $(x_i)_{i=1}^{N-M}$ be points in the interior of ω (relative to $\mathbb{S}^2$) and $(z_i)_{i=1}^M$ be points on $\partial\omega$ (relative to $\mathbb{S}^2$). Using the same method of fundamental solutions, the eigenvalue condition is exactly (5.3.3). The boundary conditions can be written as

$$\alpha_1 \psi_{y_1}(z_j) + ... + \alpha_N \psi_{y_N}(z_j) = 0, \ \ j = 1...M. \tag{5.3.4}$$

It is possible to couple the systems (5.3.3) and (5.3.4) into one single generalized eigenvalue problem in the form

$$\begin{pmatrix} A \\ B \end{pmatrix} v = \lambda \begin{pmatrix} X \\ O \end{pmatrix} v \tag{5.3.5}$$

where

- $A = (-\Delta_\tau \psi_{y_j}(x_i)), \ i = 1...N - M, \ j = 1...N$

- $B = (\psi_{y_j}(z_k)), \ k = 1...M, \ j = 1...N$

- $X = (\psi_{y_j}(x_i)), \ i = 1...N - M, \ j = 1...N$

- O is the zero matrix of size $(N - M) \times N$.

- $v = (\alpha_1, ..., \alpha_N)^T$.

The points $(x_i), (z_j)$ are chosen by performing a triangulation of the set $\omega \subset S$, which in our computations will always be a geodesic polygon. In order to compute such a triangulation, we divide the polygon in to triangles and then refine this triangulation multiple times by considering the classical midpoint refinement.

In order to test our computational method, we consider some particular subsets of the sphere for which some of the eigenvalues are known explicitly. In the following we call *lens* of angle θ, a portion of the sphere contained between two half-meridians which make angle θ. We denote the first eigenvalue of a lens of angle θ by $L(\theta)$. We call a *double-right triangle* of angle θ a half (divided by the ecuatorial circle) of a lens of angle θ. We denote the first eigenvalue of a double-right-triangle of angle θ by $R(\theta)$. The following analytical values are known for $R(\theta), L(\theta)$:

- $L(\theta) = \dfrac{\pi}{\theta}\left(\dfrac{\pi}{\theta} + 1\right)$ (see [91]) - numerical example in Figure 5.7.

- $R(\pi/3) = 20, R(\pi/2) = 12, \ R(\pi) = 6$ (see [91]) - numerical examples in Figure 5.8)

Another interesting spherical triangle is the one which realizes the partition of the sphere into 4 congruent equilateral triangles. We denote one such triangle by T. The computation of the first eigenvalue of this triangle came up in [81] in the study of the expected capture time of some brownian motion predators on the line. The numerical value computed in the above reference is $\lambda_1^{LB}(T) = 5.1589$ (represented by the green line in Figure 5.9). We compute numerically its
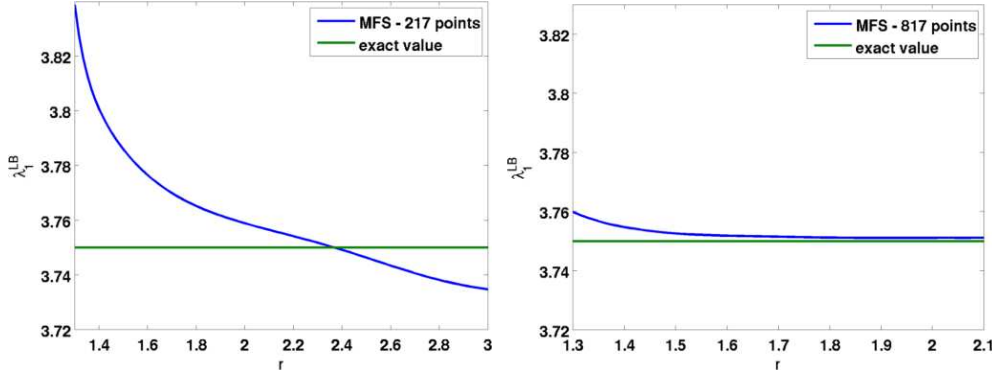
Figure 5.7: Behavior of the $L(2\pi/3)$ eigenvalue approximation with respect to the parameter r, for 217 and 817 sample points
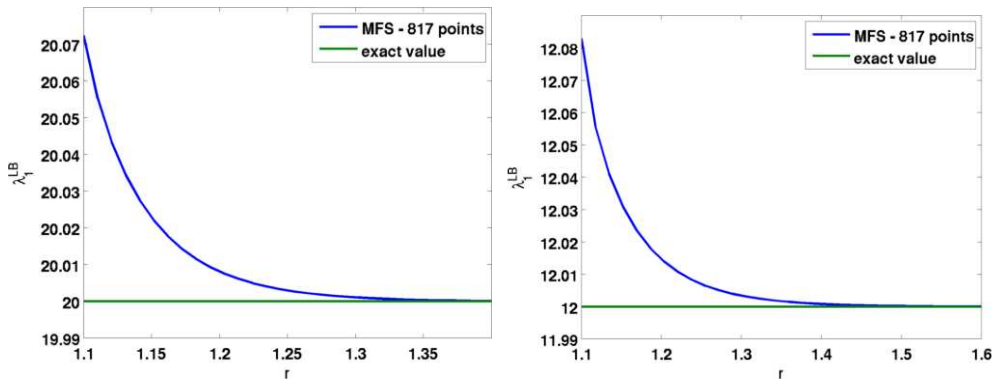
Figure 5.8: Behavior of the approximation of $R(\pi/3)$ (left) and $R(\pi/2)$ (right) with respect to r

first eigenvalue and compare it to the values presented in the cited article (see Figure 5.9). We observe that for $r \in [1.8, 1.9]$ the error made by our algorithm is really small. We see again the instability in the computation as r increases. In order to further test this numerical value, we used a finite element discretization of the triangle T, and we compute the first eigenvalue in terms of on a mesh having 98000 points. We obtain $\lambda_1^{LB}(T_{fem}) = 5.1593$, which is close to both the result of [81] and our values. We note, though, that in order to reach this precision, more than 50 times more points are needed in the discretization.

Until now we only considered exact subsets of $\mathbb{S}^2$. We can extend our method to compute the spectrum associated to an approximation φ of χ_ω. In order to do this, we use the relaxed formulation inspired from [40], [18] given by

$$-\Delta_\tau u + \mu u = \lambda u,$$

where μ is a capacitary measure which penalizes points outside ω. This relaxed formulation includes the classical case. We can compute the eigenvalues of $\omega \subset \mathbb{S}^2$ by imposing $\mu = +\infty$ in $\mathbb{S}^2 \setminus \omega$ and $\mu = 0$ in ω. The advantage is that we work on the whole sphere and the measure μ takes into account the change of shape. Using this technique, it is possible to study the partitions of the sphere which minimize the sum of their first Laplace-Beltrami eigenvalues.
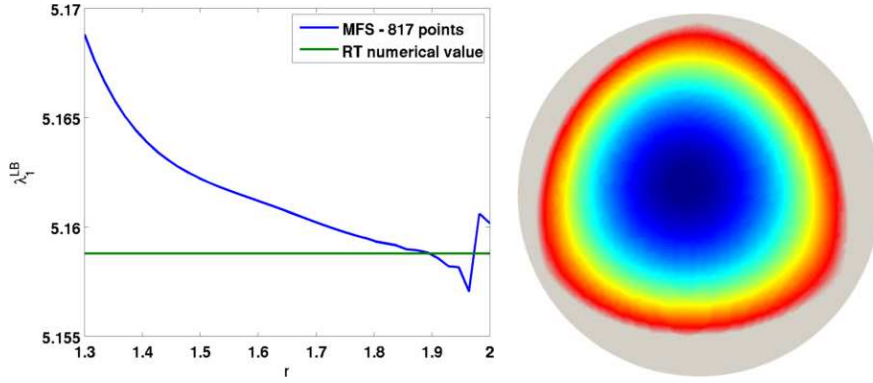
Figure 5.9: Behavior of the approximate first eigenvalue of T with respect to r (left), corresponding first eigenfunction (right)

The Euclidean case of this problem was considered by Bourdin, Bucur and Oudet in [18], while the spherical case was recently treated by Elliott and Ranner in [48] using a different method.

We choose $\mu = C(1 - \varphi)d\sigma$ and the penalized formulation becomes

$$-\Delta_\tau u + C(1 - \varphi)u = \lambda u. \tag{5.3.6}$$

This can be written in matrix form as

$$(A + C\text{diag}(1 - \varphi)B)v = \lambda Bv,$$

where

- $A = (-\Delta_\tau \psi_j(x_i)),\ i,j = 1...N$

- $B = (\psi_j(x_i)),\ i,j = 1...N$

- $v = (\alpha_1, ..., \alpha_N)^T$

- $\text{diag}(1 - \varphi)$ is the diagonal matrix with diagonal entries $1 - \varphi$.

For the generalized eigenvalues computations we use the Matlab `eigs` function. In order to be able to perform an optimization, we need to compute the gradient of the eigenvalue with respect to φ. For this we have two options:

- Compute the gradient in the analytic setting and obtain $\nabla\lambda(\varphi) = -Cv^2$ where v is the associated eigenfunction. This was proved in [18].

- Compute the gradient in the discrete setting, by differentiating the generalized eigenvalue problem. In order to do this, we need the corresponding right eigenvector v and the left eigenvector w. We obtain that

$$\nabla\lambda(\varphi) = -Cw \otimes Bv/(w^T Bv),$$

where $\otimes$ is the usual tensor product.

178

Both of the above methods work, but the second needs to perform two times the amount of computations as the first, since we need both the left and right corresponding eigenvectors. In our computations we prefer the first approach, as it is faster. The optimization is made using a standard gradient descent algorithm. We need to impose the partition condition at each iteration, and we do this by applying the following projection operator

$$\Pi(\varphi^l) = \frac{|\varphi^l|}{\sum_{i=1}^{n} |\varphi^i|}.$$

5.3.2   Numerical optimal partitions

There is an interest in computing numerically the spectral optimal partitions on the sphere. This interest is motivated by the fact that problems that are simple to state regarding these optimal partitions are still open. Bishop proved that the partition of $\mathbb{S}^2$ into two parts ω_1, ω_2 which minimizes $\lambda_1^{LB}(\omega_1) + \lambda_1^{LB}(\omega_2)$ consists of two half-spheres. The similar problem of finding the minimizer of

$$\lambda_1^{LB}(\omega_1) + \lambda_1^{LB}(\omega_2) + \lambda_1^{LB}(\omega_3), \ (\omega_1, \omega_2, \omega_3) \text{ partition of } \mathbb{S}^2,$$

is still open. In the same article [17] it is conjectured that the optimal partition in the case $n = 3$ is made of three $2\pi/3$-lens. A similar problem, which is a consequence of Bishop's conjecture, was treated by Helffer et al. in [64]. They proved that the partition of the sphere into three $2\pi/3$-lens minimizes the quantity

$$\max_{i=1,2,3} \lambda_1^{LB}(\omega_i), \ (\omega_1, \omega_2, \omega_3) \text{ partition of } \mathbb{S}^2.$$

Initial numerical computations of optimal spectral partitions on $\mathbb{S}^2$ were computed by Elliott and Ranner in [48]. They confirmed numerically Bishop's conjecture, and they made computations for $n = 3, 4, 5, 6, 7, 8, 16, 32$. Their method is based on a penalized energy formulation of the partitioning problem introduced in [33].

In the following, we propose a different approach, inspired by the two dimensional case studied by Bourdin, Bucur and Oudet [18]. We represent each phase ω_i of the partition by a density function $\varphi_i : \mathbb{S}^2 \rightarrow [0, 1]$. The partition condition then translates to $\sum_{i=1}^{n} \varphi_i = 1$. Given φ, a density function approximating ω, we consider the problem

$$-\Delta_\tau u + C(1 - \varphi)u = \lambda_1^{LB}(C, \varphi)u \text{ on } \mathbb{S}^2 \tag{5.3.7}$$

with $C >> 1$. As in [18], it can be proved that the mapping $\varphi \mapsto \lambda_1^{LB}(C, \varphi)$ is concave and as $C \rightarrow \infty$ we have $\lambda_1^{LB}(C, \chi_\omega) \rightarrow \lambda_1^{LB}(\omega)$.

We were able to compute numerically the optimal partitions for

$$\sum_{i=1}^{n} \lambda_1^{LB}(\omega_i), \ (\omega_1, ..., \omega_n) \text{ partition of } \mathbb{S}^2,$$

179
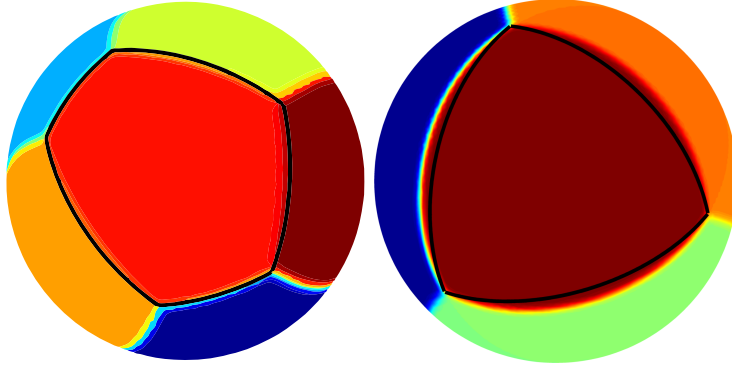
Figure 5.10: The optimal configuration for $n = 8$ (left) and $n = 5$(right). The black lines are geodesic arcs connecting the vertices of a face.

for $n \in [3, 24] \cup \{32\}$, using about 5000 sample points. It is interesting to note that for $n \in \{3, 4, 6, 12\}$ we obtain the regular tiling of the sphere. For $n \in \{5, 7, 8, 32\}$ we obtain the same results as Elliott and Ranner. For $n = 16$ we obtain something slightly different: they obtained a configuration of 4 equal hexagons, 4 equal pentagons and another 8 equal pentagons. We obtain 4 equal hexagons and 12 equal pentagons, which is plausible, since this is the most regular 16 tiling of the sphere.

In [48] it is conjectured that the common boundary of two adjacent cells is a geodesic arc. This fact can be can be seen for he case $n = 8$ in Figure 5.10, where we plotted some geodesic arcs on top of the results obtained using density functions. In our density results we can observe that for $n \geq 8$ the common boundary of any two cells is really close to being a geodesic arc. This motivated us to search for the optimal partitions among geodesic polygons which is a problem depending only on a low number of parameters. We discuss later the fact that even if for large n the optimal partition cells are close to being geodesic polygons, this is not true for $n \in \{5, 7\}$. Moreover Gauss-Bonnet theorem (5.2.2) implies that as soon as we have a hexagonal cell, its boundary cannot be made of geodesic arcs. Indeed, regularity results proved in [38] imply that at singularity points the boundaries meet with equal angles. Thus, if we have a hexagonal cell whose boundaries are geodesic arcs and whose angles are all equal to $2\pi/3$, Gauss-Bonnet formula implies that the area of this cell is zero, which is a contradiction.

A first step in the optimization procedure in the class of geodesic polygons is to extract the topological structure from the optimal densities. For each polygon in the partition we compute the corresponding first eigenvalue using the method presented in equation (5.3.5). In order to optimize the position of the vertices it is possible to write derivatives with respect to each coordinate of the vertices. Instead of doing this we use a simpler algorithm, which avoids the computation of numerical integrals on the surface of the sphere. We use the following discrete algorithm with a probabilistic touch, which is similar to the one used to study the first problem presented in this chapter:

- For each point P consider a family of q tangential directions $(v_i)_{i=1}^q$ chosen as follows:

the first direction is chosen randomly and the rest are chosen so that the angles between consecutive directions are $2\pi/q$.

- Evaluate the cost function for the new partition obtained by perturbing the point P in each of the directions v_i according to a parameter ε.

- Choose the direction which has the largest decrease and update the partition.

- If there is no decrease for each of the points of the partition then decrease ε.

This algorithm converges and it has been tested by choosing different starting configurations and observing the convergence. The optimal densities and the optimal partitions consisting of geodesic polygons are presented in the following figures. We present the results obtained in the cases corresponding to $n \in [3, 24] \cup \{32\}$. We remark the fact that for $n \geq 14$ optimal partitions seem to consist of 12 pentagons and $n - 12$ hexagons. The same argument based on Gauss-Bonnet formula implies that for $n = 11$ and $n \geq 13$, cases in which we observe the appearance of hexagonal cells, the boundaries of these hexagonal cells cannot all be geodesic arcs.

We observe that for $n \in \{4, 6, 12\}$ the optimal partition cells are regular geodesic polygons corresponding to the tetrahedron, the cube and the dodecahedron. For n large enough, the partition cells become so close to geodesic polygons that we cannot visualize the difference. However, the case $n = 5$, seen in Figure 5.10, raises some questions about the validity of the claim that boundaries are geodesics. We have devised a numerical test of this claim which is presented below.

- take the optimal partition into geodesic polygons and add supplementary variable points at the midpoint of every edge;

- perform again the optimization in this new setting.

To illustrate this better, we give more details concerning the case $n = 5$. The optimal partition into geodesic polygons consists of two triangles and four rectangles. Adding the midpoints as variables gives us a new configuration of two hexagons and three octagons. What we observed in the cases $n = 5, n = 7$ is that adding vertices at midpoints we get a new optimal partition which has a slightly lower value of the cost function. We believe that this decrease in the cost function allows us to conclude that the optimal cells do not always consist of geodesic polygons. The test cases $n = 5$ and $n = 7$ mentioned above is presented in Figure 5.11. For $n = 5$ we obtain a decrease of 0.04 in the cost function, while for $n = 7$ we obtain a decrease of 0.02. This numerical observation, together with the argument based on the Gauss-Bonnet formula suggest that it is probable that the boundaries of the cells are not geodesic curves, except for the regular cases corresponding to $n \in \{3, 4, 6, 12\}$. This observation is in accordance with the two dimensional planar case studied in Chapter 3 where numerical results show that boundaries of the cells are not always segments.
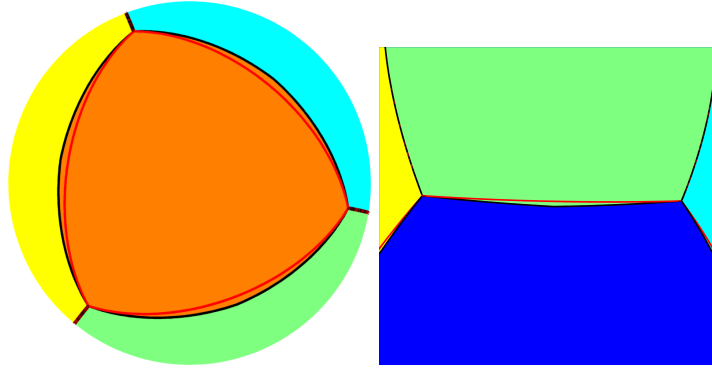
Figure 5.11: The study of the cases $n \in \{5, 7\}$; the regions correspond to the non-geodesic optimal partition and the red arcs are geodesics. Adding midpoints as variables reduces the value from 34.46 to 34.42 for $n = 5$ and from 68.99 to 68.97 for $n = 7$.

It is possible to perform similar computations for surfaces which are more complex than the sphere. The examples we considered are similar to the ones considered in the perimeter case: a torus with outer radius $R = 1$ and the inner radius $r = 0.6$ and the Banchoff-Chmutov surface of order 4. Using the proposed algorithm, we can deal with any surface, as soon as we have a qualitative triangulation. On more complex surfaces only the optimization algorithm using density functions is used, since the boundaries of the cells cannot be easily characterized.

An equally interesting problem is finding the partition which minimizes the greatest eigenvalue among $\lambda_1^{LB}(\omega_i)$. Theoretical aspects of the problem as well as a complete analysis of the case $n = 3$ were given in [64]. It is known that if the solution of the problem corresponding to the sum consists of cells with the same eigenvalue, then this is also a solution of the maximum problem. In our computations, only the regular partitions corresponding to $n \in \{3, 4, 6, 12\}$ have this property, and thus they are solutions for the maximum problem as well. In all remaining cases we obtained at least two cells with different eigenvalues, which means that our partitions are not optimal for the maximum. Optimizing the maximum is not straightforward since we are dealing with a non-differentiable functional. We may expect that minimizing a p-norm for high p will get us close to the optimal partition for the maximum. Some experiments done in this direction indicate that the topology of the optimal partition for the maximum is the same as the one for the sum, but the boundaries are just slightly moved in order to have the same eigenvalue for every one of the cells.

| $n = 3$: three $120°$ lens. This is a conjecture proposed by Bishop [17]. optimal cost $= 45/4$ lens eigenvalue $= 15/4$. | | |

$n = 4$: the optimal partition consists of the tiling generated by a regular tetrahedron inscribed in the sphere. optimal cost = 20.635 triangle eigenvalue = 5.1588			
$n = 5$: two equal equilateral triangles and three equal rectangles. optimal cost = 34.44. triangle eigenvalue = 7.26 rectangle eigenvalue = 6.57.			
$n = 6$: regular tiling generated by the cube optimal cost = 48.6. square eigenvalue = 8.10			
$n = 7$: two regular pentagons triangles and 5 equal rectangles. optimal cost = 69. pentagon eigenvalue = 8.62 rectangle eigenvalue = 10.35.			
$n = 8$: four equal quadrilaterals and four equal pentagons. optimal cost = 91.01. pentagon eigenvalue = 10.82 quadrilateral eigenvalue = 11.93.			
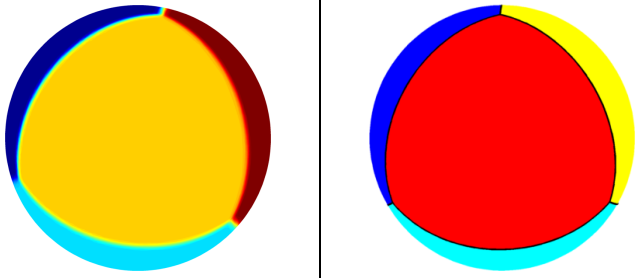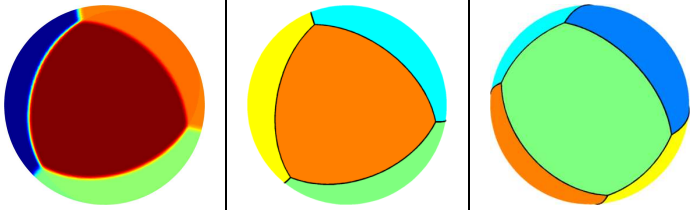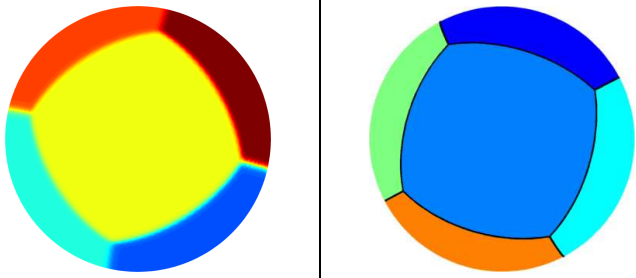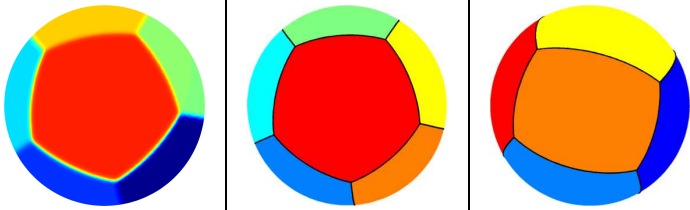
$n = 9$: 3 equal squares and 6 equal pentagons. optimal cost = 115.9. square eigenvalue = 13.64 pentagon eigenvalue = 12.38.			
$n = 10$: two equal squares and 8 equal pentagons optimal cost = 142.33. square eigenvalue = 15.85 pentagon eigenvalue = 13.95.			
$n = 11$: one hexagon, two equal quadrilaterals, eight pentagons of three types optimal cost = 175.38.			
$n = 12$: regular tiling generated by the dodecahedron optimal cost = 203.84. pentagon eigenvalue = 16.99			
$n = 13$: one rectangle, two equal hexagons, 10 pentagons of three types optimal cost = 245.55.			
$n = 14$: two equal hexagons and 12 equal pentagons optimal cost = 283.93. hexagon eigenvalue = 17.47 pentagon eigenvalue = 20.75.			
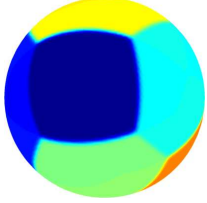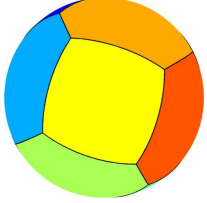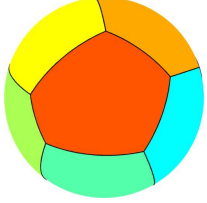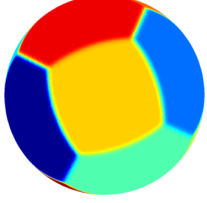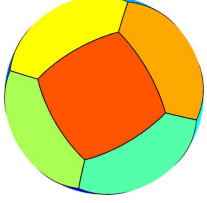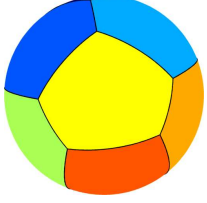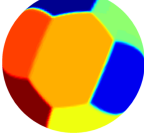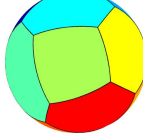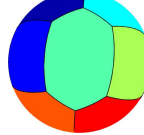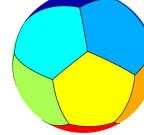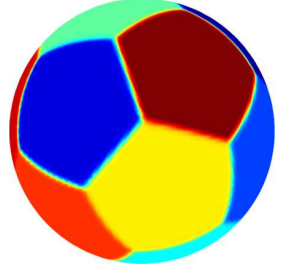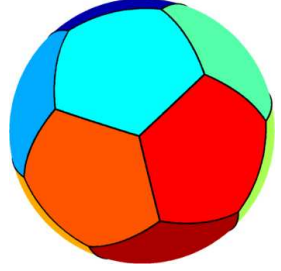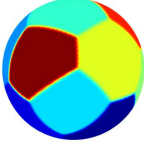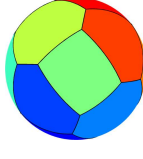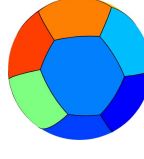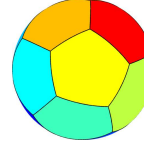
$n = 15$: 3 equal hexagons and 12 pentagons of two types optimal cost = 327.21.	
$n = 16$: 4 equal hexagons and 12 equal pentagons optimal cost = 371.76.	
$n = 17$: 5 hexagons and 12 pentagons optimal cost = 422.77.	
$n = 18$: 6 hexagons and 12 pentagons optimal cost = 475.08.	
$n = 19$: 7 hexagons and 12 pentagons optimal cost = 530.5.	
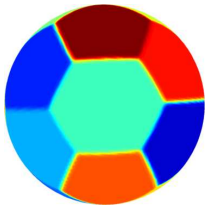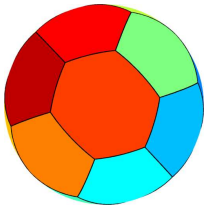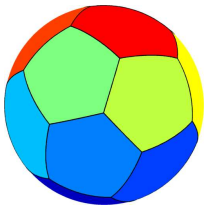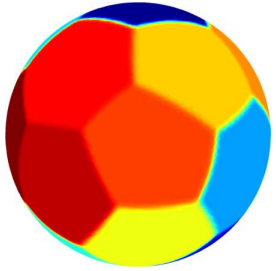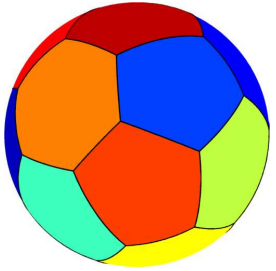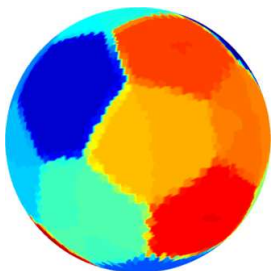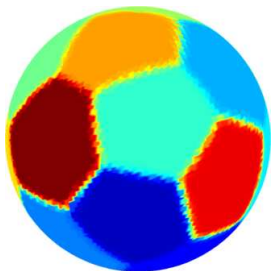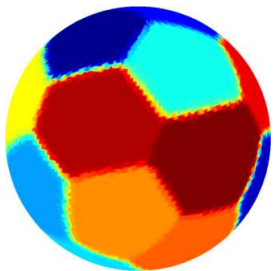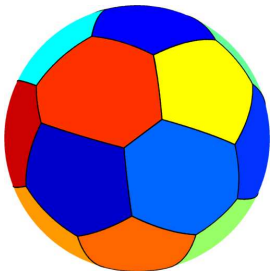
$n = 20$: 8 hexagons and 12 pentagons optimal cost = 585.98.		
$n = 21$: 9 hexagons and 12 pentagons optimal cost = 648.05.		
$n = 22$: 10 hexagons and 12 pentagons optimal cost = 711.96.		
$n = 23$: 11 hexagons and 12 pentagons optimal cost = 779.1.		
$n = 24$: 12 hexagons and 12 pentagons optimal cost = 847.39.		
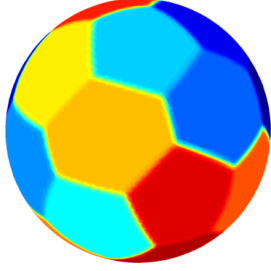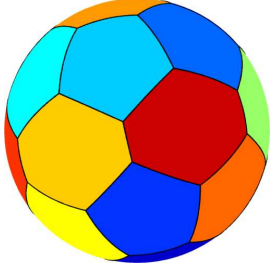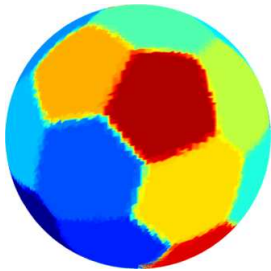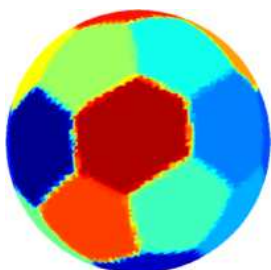
$n = 32$: 20 equal hexagons and 12 equal pentagons optimal cost = 1504.71.		
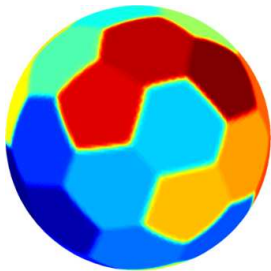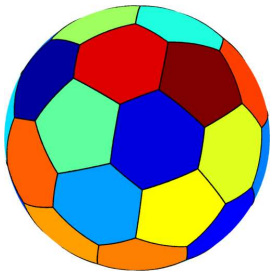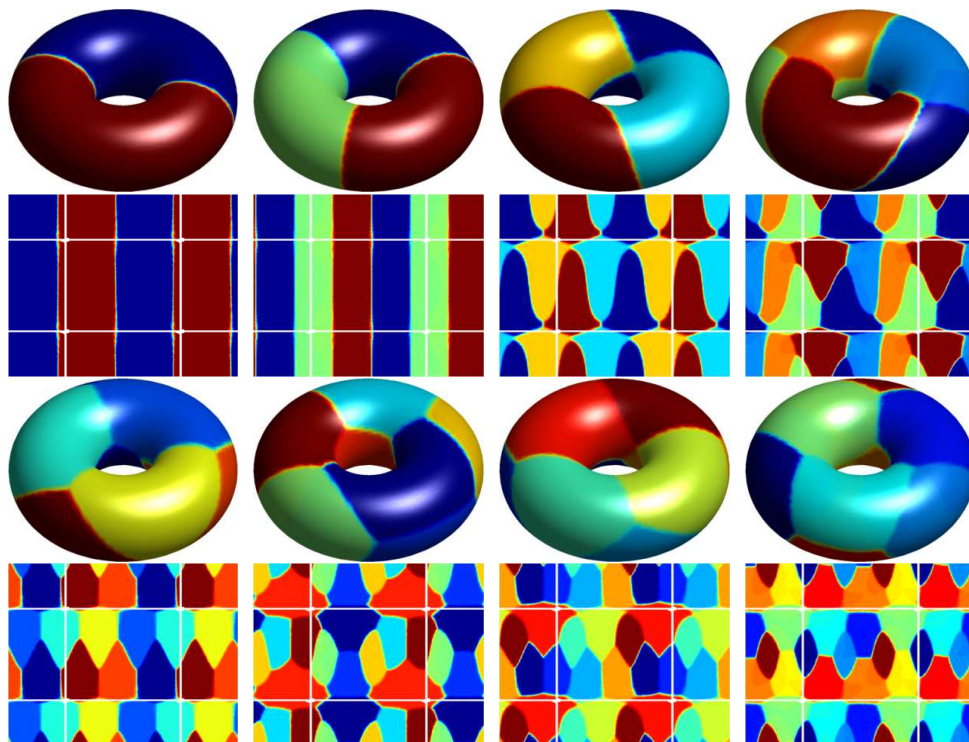


Figure 5.12: Minimal spectral partitions on a torus for $n \in [2, 9]$. The two dimensional pictures represent flattenings of the torus
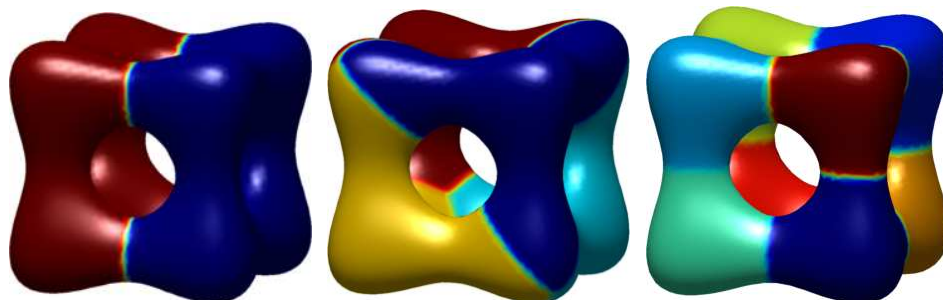

Figure 5.13: Minimal spectral partition on the Banchoff-Chmutov surface of order 4 for $n \in \{2, 4, 8\}$

Bibliography

[1] Giovanni Alberti. Variational models for phase transitions, an approach via gamma-convergence. 1998.

[2] H. W. Alt and L. A. Caffarelli. Existence and regularity for a minimum problem with free boundary. *J. Reine Angew. Math.*, 325:105–144, 1981.

[3] Hans Wilhelm Alt, Luis A. Caffarelli, and Avner Friedman. Variational problems with two phases and their free boundaries. *Trans. Amer. Math. Soc.*, 282(2):431–461, 1984.

[4] Carlos J. S. Alves and Pedro R. S. Antunes. The method of fundamental solutions applied to the calculation of eigensolutions for 2D plates. *Internat. J. Numer. Methods Engrg.*, 77(2):177–194, 2009.

[5] Carlos J. S. Alves and Pedro R. S. Antunes. The method of fundamental solutions applied to some inverse eigenproblems. *SIAM J. Sci. Comput.*, 35(3):A1689–A1708, 2013.

[6] Luigi Ambrosio, Piero Colli Franzone, and Giuseppe Savaré. On the asymptotic behaviour of anisotropic energies arising in the cardiac bidomain model. *Interfaces Free Bound.*, 2(3):213–266, 2000.

[7] Luigi Ambrosio, Nicola Fusco, and Diego Pallara. *Functions of bounded variation and free discontinuity problems*. Oxford Mathematical Monographs. The Clarendon Press, Oxford University Press, New York, 2000.

[8] Pedro R. S. Antunes. Numerical calculation of eigensolutions of 3D shapes using the method of fundamental solutions. *Numer. Methods Partial Differential Equations*, 27(6):1525–1550, 2011.

[9] Pedro R. S. Antunes and Pedro Freitas. Numerical optimization of low eigenvalues of the Dirichlet and Neumann Laplacians. *J. Optim. Theory Appl.*, 154(1):235–257, 2012.

[10] Pedro R. S. Antunes and Pedro Freitas. Optimisation of eigenvalues of the Dirichlet Laplacian with a surface area restriction. 2014.

[11] Sisto Baldo. Minimal Interface Criterion for Phase Transitions in Mixtures of Cahn-Hilliard fluids. *Annales de l'I.H.P., section C, Tome 7, No. 2*, pages 67–90, 1990.

[12] Sisto Baldo and Giandomenico Orlandi. Cycles of least mass in a Riemannian manifold, described through the "phase transition" energy of the sections of a line bundle. *Math. Z.*, 225(4):639–655, 1997.

[13] Catherine Bandle. *Isoperimetric inequalities and applications*, volume 7 of *Monographs and Studies in Mathematics*. Pitman (Advanced Publishing Program), Boston, Mass.-London, 1980.

[14] A. H. Barnett and T. Betcke. Stability and convergence of the method of fundamental solutions for Helmholtz problems on analytic domains. *J. Comput. Phys.*, 227(14):7003–7026, 2008.

[15] Carlos Alberto Berenstein. An inverse spectral theorem and its relation to the Pompeiu problem. *J. Analyse Math.*, 37:128–144, 1980.

[16] Amandine Berger. The eigenvalues of the Laplacian with Dirichlet boundary condition in $\mathbb{R}^2$ are almost never minimized by disks. *Ann. Global Anal. Geom.*, 47(3):285–304, 2015.

[17] Christopher J. Bishop. Some questions concerning harmonic measure. In *Partial differential equations with minimal smoothness and applications (Chicago, IL, 1990)*, volume 42 of *IMA Vol. Math. Appl.*, pages 89–97. Springer, New York, 1992.

[18] Blaise Bourdin, Dorin Bucur, and Édouard Oudet. Optimal partitions for eigenvalues. *SIAM J. Sci. Comput.*, 31(6):4100–4114, 2009/10.

[19] Andrea Braides. *Approximation of Free-Discontinuity Problems*. Springer, 1998.

[20] Andrea Braides. *Gamma-Convergence for beginners*. Oxford University Press, 2002.

[21] Kenneth A. Brakke. The surface evolver. *Experiment. Math.*, 1(2):141–165, 1992.

[22] Haim Brezis. *Functional analysis, Sobolev spaces and partial differential equations*. Universitext. Springer, New York, 2011.

[23] Tanguy Briançon and Jimmy Lamboley. Regularity of the optimal shape for the first eigenvalue of the Laplacian with volume and inclusion constraints. *Ann. Inst. H. Poincaré Anal. Non Linéaire*, 26(4):1149–1163, 2009.

[24] F. Brock. An isoperimetric inequality for eigenvalues of the Stekloff problem. *ZAMM Z. Angew. Math. Mech.*, 81(1):69–71, 2001.

[25] Dorin Bucur. How to prove existence in shape optimization. *Control Cybernet.*, 34(1):103–116, 2005.

[26] Dorin Bucur. Minimization of the k-th eigenvalue of the Dirichlet Laplacian. *Arch. Ration. Mech. Anal.*, 206(3):1073–1083, 2012.

[27] Dorin Bucur and Giuseppe Buttazzo. *Variational methods in shape optimization problems*. Progress in Nonlinear Differential Equations and their Applications, 65. Birkhäuser Boston, Inc., Boston, MA, 2005.

[28] Dorin Bucur, Giuseppe Buttazzo, and Antoine Henrot. Minimization of $\lambda_2(\Omega)$ with a perimeter constraint. *Indiana Univ. Math. J.*, 58(6):2709–2728, 2009.

[29] Dorin Bucur, Giuseppe Buttazzo, and Bozhidar Velichkov. Spectral optimization problems for potentials and measures. *SIAM J. Math. Anal.*, 46(4):2956–2986, 2014.

[30] Dorin Bucur and Filippo Gazzola. The first biharmonic Steklov eigenvalue: positivity preserving and shape optimization. *Milan J. Math.*, 79(1):247–258, 2011.

[31] Dorin Bucur and Bozhidar Velichkov. Multiphase shape optimization problems. *SIAM J. Control Optim.*, 52(6):3556–3591, 2014.

[32] Giuseppe Buttazzo. Gamma-convergence and its Applications to Some Problems in the Calculus of Variations. *School on Homogenization ICTP, Trieste, September 6-17*, 1993.

[33] L. A. Caffarelli and Fang-Hua Lin. Singularly perturbed elliptic systems and multi-valued harmonic functions with free boundaries. *J. Amer. Math. Soc.*, 21(3):847–862, 2008.

[34] Luis A. Caffarelli, David Jerison, and Carlos E. Kenig. Some new monotonicity theorems with applications to free boundary problems. *Ann. of Math. (2)*, 155(2):369–404, 2002.

[35] L. A. Cafferelli and Fang Hua Lin. An optimal partition problem for eigenvalues. *J. Sci. Comput.*, 31(1-2):5–18, 2007.

[36] Shu-Ming Chang, Chang-Shou Lin, Tai-Chia Lin, and Wen-Wei Lin. Segregated nodal domains of two-dimensional multispecies Bose-Einstein condensates. *Phys. D*, 196(3-4):341–361, 2004.

[37] Bruno Colbois, Ahmad El Soufi, and Alexandre Girouard. Isoperimetric control of the Steklov spectrum. *J. Funct. Anal.*, 261(5):1384–1399, 2011.

[38] M. Conti, S. Terracini, and G. Verzini. An optimal partition problem related to nonlinear eigenvalues. *J. Funct. Anal.*, 198(1):160–196, 2003.

[39] S. J. Cox and E. Flikkema. The minimal perimeter for N confined deformable bubbles of equal area. *Electron. J. Combin.*, 17(1):Research Paper 45, 23, 2010.

[40] Gianni Dal Maso and Umberto Mosco. Wiener's criterion and Γ-convergence. *Appl. Math. Optim.*, 15(1):15–63, 1987.

[41] Gianni Dal Maso and François Murat. Asymptotic behaviour and correctors for Dirichlet problems in perforated domains with homogeneous monotone operators. *Ann. Scuola Norm. Sup. Pisa Cl. Sci. (4)*, 24(2):239–290, 1997.

[42] M. Dambrine, D. Kateb, and J. Lamboley. An extremal eigenvalue problem for the Wentzell-Laplace operator. *ArXiv e-prints*, January 2014.

[43] E. B. Davies. *Heat kernels and spectral theory*, volume 92 of *Cambridge Tracts in Mathematics*. Cambridge University Press, Cambridge, 1989.

[44] Guido De Philippis and Bozhidar Velichkov. Existence and regularity of minimizers for some spectral functionals with perimeter constraint. *Appl. Math. Optim.*, 69(2):199–231, 2014.

[45] Manfredo P. do Carmo. *Differential geometry of curves and surfaces*. Prentice-Hall, Inc., Englewood Cliffs, N.J., 1976. Translated from the Portuguese.

[46] Ahmad El Soufi and Saïd Ilias. Riemannian manifolds admitting isometric immersions by their first eigenfunctions. *Pacific J. Math.*, 195(1):91–99, 2000.

[47] Ahmad El Soufi and Saïd Ilias. Domain deformations and eigenvalues of the Dirichlet Laplacian in a Riemannian manifold. *Illinois J. Math.*, 51(2):645–666 (electronic), 2007.

[48] Charles M. Elliott and Thomas Ranner. A computational approach to an optimal partition problem on surfaces, 2014.

[49] Max Engelstein. The least-perimeter partition of a sphere into four equal areas. *Discrete Comput. Geom.*, 44(3):645–653, 2010.

[50] Lawrence C. Evans. *Weak convergence methods for nonlinear partial differential equations*, volume 74 of *CBMS Regional Conference Series in Mathematics*. Published for the Conference Board of the Mathematical Sciences, Washington, DC; by the American Mathematical Society, Providence, RI, 1990.

[51] Lawrence C. Evans and Ronald F. Gariepy. *Measure theory and fine properties of functions*. Studies in Advanced Mathematics. CRC Press, Boca Raton, FL, 1992.

[52] L. Fejes Tóth. *Regular figures*. A Pergamon Press Book. The Macmillan Co., New York, 1964.

[53] G. Dal Maso G. Buttazzo. An existence result for a class of shape optimization problems. *Arch. Rational Mech. Anal.*, 122:183–195, 1993.

[54] A. Girouard, R. S. Laugesen, and B. A. Siudeja. Steklov eigenvalues and quasiconformal maps of simply connected planar domains, 2014.

[55] A. Girouard and I. Polterovich. On the Hersch-Payne-Schiffer estimates for the eigenvalues of the Steklov problem. *Funktsional. Anal. i Prilozhen.*, 44(2):33–47, 2010.

[56] Alexandre Girouard and Iosif Polterovich. Shape optimization for low Neumann and Steklov eigenvalues. *Math. Methods Appl. Sci.*, 33(4):501–516, 2010.

[57] Alexandre Girouard and Iosif Polterovich. Spectral geometry of the steklov problem, 2014.

[58] Enrico Giusti. *Minimal surfaces and functions of bounded variation*, volume 80 of *Monographs in Mathematics*. Birkhäuser Verlag, Basel, 1984.

[59] P. Grisvard. *Elliptic problems in nonsmooth domains*, volume 24 of *Monographs and Studies in Mathematics*. Pitman (Advanced Publishing Program), Boston, MA, 1985.

[60] Thomas C. Hales. The honeycomb conjecture. *Discrete & Computational Geometry*, 25(1):1–22, 2001.

[61] F. Hecht. New development in FreeFem++. *J. Numer. Math.*, 20(3-4):251–265, 2012.

[62] B. Helffer, T. Hoffmann-Ostenhof, and S. Terracini. Nodal domains and spectral minimal partitions. *Ann. Inst. H. Poincaré Anal. Non Linéaire*, 26(1):101–138, 2009.

[63] Bernard Helffer, Thomas Hoffmann-Ostenhof, and Susanna Terracini. Nodal minimal partitions in dimension 3. *Discrete Contin. Dyn. Syst.*, 28(2):617–635, 2010.

[64] Bernard Helffer, Thomas Hoffmann-Ostenhof, and Susanna Terracini. On spectral minimal partitions: the case of the sphere. In *Around the research of Vladimir Maz'ya. III*, volume 13 of *Int. Math. Ser. (N. Y.)*, pages 153–178. Springer, New York, 2010.

[65] Antoine Henrot. *Extremum problems for eigenvalues of elliptic operators*. Frontiers in Mathematics. Birkhäuser Verlag, Basel, 2006.

[66] Antoine Henrot and Michel Pierre. *Variation et optimisation de formes*, volume 48 of *Mathématiques & Applications (Berlin) [Mathematics & Applications]*. Springer, Berlin, 2005. Une analyse géométrique. [A geometric analysis].

[67] J. Hersch, L. E. Payne, and M. M. Schiffer. Some inequalities for Stekloff eigenvalues. *Arch. Rational Mech. Anal.*, 57:99–114, 1975.

[68] T. Y. Kong, David M. Mount, and Michael Werman. The decomposition of a square into rectangles of minimal perimeter. *Discrete Appl. Math.*, 16(3):239–243, 1987.

[69] V. D. Kupradze and M. A. Aleksidze. The method of functional equations for the approximate solution of certain boundary-value problems. *Ž. Vyčisl. Mat. i Mat. Fiz.*, 4:683–715, 1964.

[70] Francesco Maggi. *Sets of finite perimeter and geometric variational problems*, volume 135 of *Cambridge Studies in Advanced Mathematics*. Cambridge University Press, Cambridge, 2012. An introduction to geometric measure theory.

[71] Luciano Modica. Gradient Theory of Phase Transitions with Boundary Contact Energy. *Ann. Inst. H. Poincaré Anal. Non Linéaire*, 4(5):487–512, 1987.

[72] Luciano Modica and Stefano Mortola. Un esempio di Γ^--convergenza. *Boll. Un. Mat. Ital. B (5)*, 14(1):285–299, 1977.

[73] C. B. Moler and L. E. Payne. Bounds for eigenvalues and eigenvectors of symmetric operators. *SIAM J. Numer. Anal.*, 5:64–70, 1968.

[74] Frank Morgan. Soap bubbles in $\mathbf{R}^2$ and in surfaces. *Pacific J. Math.*, 165(2):347–361, 1994.

[75] N. Nadirashvili. Berger's isoperimetric problem and minimal immersions of surfaces. *Geom. Funct. Anal.*, 6(5):877–897, 1996.

[76] Antonio André Novotny and Jan Sokołowski. *Topological derivatives in shape optimization*. Interaction of Mechanics and Mathematics. Springer, Heidelberg, 2013.

[77] Per olof Persson and Gilbert Strang. A simple mesh generator in matlab. *SIAM Review*, 46, 2004.

[78] Braxton Osting. Optimization of spectral functions of Dirichlet-Laplacian eigenvalues. *J. Comput. Phys.*, 229(22):8578–8590, 2010.

[79] Édouard Oudet. Numerical minimization of eigenmodes of a membrane with respect to the domain. *ESAIM Control Optim. Calc. Var.*, 10(3):315–330 (electronic), 2004.

[80] Édouard Oudet. Approximation of partitions of least perimeter by Γ-convergence: around Kelvin's conjecture. *Exp. Math.*, 20(3):260–270, 2011.

[81] Jesse Ratzkin and Andrejs Treibergs. A capture problem in Brownian motion and eigenvalues of spherical domains. *Trans. Amer. Math. Soc.*, 361(1):391–405, 2009.

[82] John William Strutt Rayleigh, Baron. *The Theory of Sound*. Dover Publications, New York, N. Y., 1945. 2d ed.

[83] H. L. Royden. *Real analysis*. The Macmillan Co., New York; Collier-Macmillan Ltd., London, 1963.

[84] Mark Schmidt. minfunc, 2012. http://www.cs.ubc.ca/ schmidtm/Software/minFunc.html.

[85] Theodore Shifrin. Differential geometry - a first course in curves and surfaces.

[86] Liam Stewart. Matlab lbfgs wrapper. http://www.cs.toronto.edu/ liam/software.shtml.

[87] Axel Thue. *Selected mathematical papers*. Universitetsforlaget, Oslo, 1977. With an introduction by Carl Ludwig Siegel and a biography by Viggo Brun, Edited by Trygve Nagell, Atle Selberg, Sigmund Selberg, and Knut Thalberg.

[88] Dan Tiba. A property of Sobolev spaces and existence in optimal design. *Appl. Math. Optim.*, 47(1):45–58, 2003.

[89] B. Velichkov. *Existence and regularity results for some shape optimization problems*. PhD thesis, Scuola Normale Superiore di Pisa, Université Joseph Fourier, 2013.

[90] Bozhidar Velichkov. A note on the monotonicity formula of Caffarelli-Jerison-Kenig. *Atti Accad. Naz. Lincei Rend. Lincei Mat. Appl.*, 25(2):165–189, 2014.

[91] H. Walden and R. B. Kellogg. Numerical determination of the fundamental eigenvalue for the Laplace operator on a spherical domain. *J. Engrg. Math.*, 11(4):299–318, 1977.

[92] D. Weaire and R. Phelan. A counter-example to Kelvin's conjecture on minimal surfaces. *Forma*, 11(3):209–213, 1996. Reprint of Philos. Mag. Lett. 69 (1994), no. 2, 107–110.

[93] Robert Weinstock. Inequalities for a classical eigenvalue problem. *J. Rational Mech. Anal.*, 3:745–753, 1954.

[94] Stephen A. Williams. Boundary regularity for a family of overdetermined problems for the Helmholtz equation. *J. Math. Anal. Appl.*, 274(1):296–304, 2002.